MODELING, CONTROL AND MONITORING OF SMART STRUCTURES UNDER HIGH IMPACT LOADS

by

Kemal Sarp Arsava

A Dissertation

Submitted to the Faculty

of the

WORCESTER POLYTECHNIC INSTITUTE

in partial fulfillment of the requirements for the

Degree of Doctor of Philosophy

in

Civil and Environmental Engineering

May 2014

APPROVED:

Asst. Prof. Yeesock Kim, Advisor

Prof. Tahar El-Korchi, Co-Advisor and Head of Department

Prof. Leonard D. Albano

Asst. Prof. Jo Woon Chong

Abstract

In recent years, response analysis of complex structures under impact loads has attracted a great deal of attention. For example, a collision or an accident that produces impact loads that exceed the design load can cause severe damage on the structural components. Although the AASHTO specification is used for impact-resistant bridge design, it has many limitations. The AASHTO specification does not incorporate complex and uncertain factors. Thus, a well-designed structure that can survive a collision under specific conditions in one region may be severely damaged if it were impacted by a different vessel, or if it were located elsewhere with different in-situ conditions.

With these limitations in mind, we propose different solutions that use smart control technology to mitigate impact hazard on structures. However, it is challenging to develop an accurate mathematical model of the integrated structure-smart control systems. The reason is due to the complicated nonlinear behavior of the integrated nonlinear systems and uncertainties of high impact forces. In this context, novel algorithms are developed for identification, control and monitoring of nonlinear responses of smart structures under high impact forces.

To evaluate the proposed approaches, a smart aluminum and two smart reinforced concrete beam structures were designed, manufactured, and tested in the High Impact Engineering Laboratory of Civil and Environmental Engineering at WPI. High-speed impact force and structural responses such as strain, deflection and acceleration were measured in the experimental tests. It has been demonstrated from the analytical and experimental study that: 1) the proposed system identification model predicts nonlinear behavior of smart structures under a variety of high impact forces, 2) the developed structural health monitoring algorithm is effective in identifying damage in time-varying nonlinear dynamic systems under ambient excitations, and 3) the proposed controller is effective in mitigating high impact responses of the smart structures.

Acknowledgements

I wish to express my deepest gratitude to my supervisor Prof. Yeesock Kim for his kind and friendly guidance and continuous help, support and encouragement. It has been a privilege working with him.

I would also like to thank to Prof. Tahar El-Korchi and Prof. Leonard D. Albano from Civil Engineering Department and Prof. Jo Woon Chong from Biomedical Engineering Department for their advice and help in steps throughout the study.

I would also like to thank Don Pellegrino and Russ Lang for their help with equipment and technical assistance. I would also like to thank the rest of the faculty for allowing me to have a great experience.

Finally, I would like to offer my special thanks to my wife and my family for their unyielding patience and endless support throughout my life.

I would like to dedicate my thesis to my beloved cousin Ozgur Elif Ertan

Table of Contents

Abstract i
Acknowledgements ii
Table of Contents iv
List of Tables viii
List of Figures ix
1. Overview 1
2. Nonlinear System Identification of Smart Structures under High Impact Loads 5
2.1. Introduction 5
2.2. Time-delayed adaptive neuro fuzzy inference system (TANFIS) 7
2.2.1. Adaptive neuro fuzzy inference system (ANFIS) 7
2.2.2. Time-delayed ANFIS (TANFIS) 10
2.3. Experimental setup 11
2.3.1. Drop tower test facility 11
2.3.2. Aluminum plate beam equipped with MR dampers 12
2.3.3. Data acquisition 14
2.3.4. Test details 15
2.4. System identification results 17
2.4.1. Parameter setting 17
2.4.2. ANFIS modeling 21
2.4.3. TANFIS modeling 25
2.4.4. Evaluation of results 44
2.5. Conclusion 45
3. Nonlinear System Identification of Smart Reinforced Concrete Structures under Impact Loads 47
3.1. Introduction 47
3.2. Wavelet-based time delayed adaptive neuro fuzzy inference system (W-TANFIS) 52
3.2.1. Wavelet transform 52
3.2.2. Adaptive neuro fuzzy inference system (ANFIS) 53
3.2.3. Time delayed adaptive neuro fuzzy inference system (TANFIS) 54
3.2.4. Wavelet-based TANFIS (W-TANFIS) 57

3.3. Experimental setup 58
3.3.1. Drop tower test facility 58
3.3.2. Reinforced concrete beam equipped with MR dampers 59
3.3.3. Data acquisition 60
3.3.4. Test details 61
3.4. System identification results 63
3.4.1. Parameter setting 63
3.4.2. Benchmark ANFIS model 66
3.4.3. TANFIS model 69
3.4.4. W-TANFIS modeling 71
3.4.5. Evaluation of results 76
3.5. Conclusion 81
4. Modeling of Magnetorheological Dampers under Various Impact Loads 82
4.1. Introduction 82
4.1.1. Collision load 82
4.1.2. Impact response mitigation: structural controls 82
4.1.3. Smart control strategies 83
4.1.4. System identification 84
4.1.5. Neuro-fuzzy modeling 85
4.2. System identification 87
4.2.1. Bouc-Wen model 87
4.2.2. Bingham model 90
4.2.3. Neuro-fuzzy model 90
4.2.4. Output feedback (OF)-based neuro-fuzzy model 93
4.3. Experimental setup 95
4.3.1. Drop tower test facility 95
4.3.2. Magnetorheological (MR) dampers 95
4.3.3. Data acquisition 97
4.3.4. Test details 98
4.4. System identification results 101
4.4.1. Parameter Setting 101
4.4.1.1. Bouc-Wen model 101
4.4.1.2. Bingham model 102

4.4.1.3. Neuro-fuzzy model 102
4.4.1.4. The OF neuro-fuzzy model 106
4.4.2. System identification results 106
4.4.2.1. Bouc-Wen model 106
4.4.2.2. Bingham model 108
4.4.2.3. Neuro-fuzzy modeling 109
4.4.2.4. The OF neuro-fuzzy modeling 111
4.4.3. Evaluation of results 119
4.5. Conclusion 120
5. Smart Fuzzy Control for Impact Response Mitigation of Reinforced Concrete Structures 122
5.1. Introduction 122
5.2. Smart impact response mitigation 124
5.2.1. Smart control systems 124
5.2.2. Time-delayed fuzzy logic 127
5.2.3. Smart fuzzy controller 129
5.2.4. Proportional integral derivative controller (PID) 130
5.3. Experimental studies 131
5.3.1. Drop tower test facility 131
5.3.2. Reinforced concrete beam equipped with MR dampers 132
5.3.3. Data acquisition 133
5.3.4. Test details 134
5.4. Results 135
5.4.1. Fuzzy controller design 135
5.4.2. Evaluation of results 141
5.5. Conclusion 144
6. Smart Control of Reinforced Concrete Bridge Piers under a Variety of Impact Loads 145
6.1. Introduction 145
6.2. Experimental studies 147
6.2.1 Drop tower test facility 147
6.2.2 Reinforced concrete bridge pier equipped with MR dampers 148
6.2.3 Data acquisition 149
6.2.4 Test details 150

6.3. Impact Response Mitigation 151
6.3.1. Passive Control 152
6.3.2. PID Control 154
6.3.3. Fuzzy Logic Control 157
6.4. Evaluation of results 161
6.5. Conclusion 166
7. A Novel Health Monitoring Scheme for Smart Structures 167
7.1. Introduction 167
7.2. Multiclass nonlinear relevance vector machine (MNRVM) 169
7.2.1. Support vector machine (SVM) 171
7.2.2. Relevance vector machine (RVM) 172
7.2.3. Discrete wavelet transforms (DWT) 174
7.2.4. Autoregressive (AR) model 175
7.2.5. Wavelet-based AR model (WAR) 177
7.2.6. Pole location identification 177
7.2.7. Damage-sensitive feature extraction 178
7.3. Case study: smart structures 179
7.3.1. Magnetorheological (MR) damper 179
7.3.2. A building equipped with an MR damper 180
7.3.3. Damage scenario 183
7.4. Classification results 184
7.4.1. Two-class classification 185
7.4.2. Multi-class classification 187
7.5. Conclusion 194
8. Summary 196
8.1. Summary and concluding remarks 196
8.2. Future research 199
9. References 200

List of Tables

Table 2-1. Experimental Test Details....16
Table 2-2. Simulation parameter studies....20
Table 2-3. Error Quantities of the ANFIS and TANFIS Models....45
Table 3-1. Experimental Test Details....62
Table 3-2. Error Quantities of the ANFIS, TANFIS and W-TANFIS: constant currents....78
Table 3-3. Error Quantities of the ANFIS, TANFIS and W-TANFIS: random currents....79
Table 4-1. Experimental Test Details....99
Table 4-2. Parameters of Bouc-Wen model....102
Table 4-3. Parameters of Bingham model....102
Table 4-4. Simulation parameter studies....103
Table 4-5. Simulation parameter studies for neuro-fuzzy models....104
Table 4-6. Simulation parameter studies for the OF neuro-fuzzy models....106
Table 4-7. Error Quantities of the SI Models....120
Table 5-1. Experimental Test Details....135
Table 5-2. Evaluation of Fuzzy Controller....142
Table 5-3. Evaluation of Percentage Reduction in Impact Response....143
Table 6-1. Experimental Test Details....151
Table 6-2. Evaluation of Fuzzy Controller....162
Table 6-3. Evaluation of Control Models in Terms of Uncontrolled Impact Response Mitigation 165
Table 7-1. The structural properties of a three-story building structure....182
Table 7-2. Parameters for SD-1000 MR damper model....183
Table 7-3. Damage scenarios....184
Table 7-4. Evaluation indexes of SVM and RVM binary classification....187
Table 7-5. Evaluation of SVM and RVM multi-class classification....193

List of Figures

Figure 2-1. Nonlinear behavior of the structure equipped with MR dampers.....6
Figure 2-2. Typical ANFIS architecture.....8
Figure 2-3. TANFIS architecture showing three input and one output model.....11
Figure 2-4. Drop-tower testing facility with a capacity of 22,500 kg.....12
Figure 2-5. Details of cantilever aluminum plate beam: (a) CAD drawing and illustration of impact point (b) Location of two MR dampers, accelerometers and LVDT 13
Figure 2-6. (a) Schematic of MR damper (Dyke, 1996), (b) RD-8040-1 MR damper.....14
Figure 2-7. Configuration of the data acquisition system 14
Figure 2-8. Input-output data sets to train the model to predict acceleration: constant currents...17
Figure 2-9. Input-output data sets to train the model to predict acceleration: random currents..18
Figure 2-10. Input-output data sets to train the model to predict deflection: constant currents..18
Figure 2-11. Input-output data sets to train the model to predict deflection: random currents..19
Figure 2-12. The type of MF: (a) Gaussian 1 (b) Gaussian 2 (c) Gaussian 3 19
Figure 2-13. ANFIS (I)-CC: Acceleration training- constant currents and different drop release heights 21
Figure 2-14. ANFIS (II)-CC: Deflection training- constant currents and different drop release heights 22
Figure 2-15. ANFIS (I)-RC: Acceleration training-random currents and different drop release heights 23
Figure 2-16. ANFIS (II)-RC: Deflection training-random currents and different drop release heights 24
Figure 2-17. Configuration of the proposed TANFIS (I): Impact acceleration prediction 25
Figure 2-18. Configuration of the proposed TANFIS (II): Impact deflection prediction 25
Figure 2-19. Initial and final membership functions: TANFIS (I) 26
Figure 2-20. Initial and final membership functions: TANFIS (II).....26
Figure 2-21. Step size and iteration: TANFIS (I) 27
Figure 2-22. Step size and iteration: TANFIS (II).....27
Figure 2-23. Acceleration training- constant current (1.4 A) and different drop release heights..28
Figure 2-24. Acceleration training- constant current (1.4 A) and different drop release heights..29

Figure 2-25. TANFIS (I)-CC: Acceleration training- constant currents and different drop release heights 30
Figure 2-26. TANFIS (II)-CC: Deflection training- constant currents and different drop release heights 31
Figure 2-27. TANFIS (I)-RC: Acceleration training-random currents and different drop release heights 32
Figure 2-28. TANFIS (II)-RC: Deflection training-random currents and different drop release heights 33
Figure 2-29. TANFIS (I)-CC-1 Acceleration-1st validation: Constant currents.....34
Figure 2-30. TANFIS (I)-CC-2 Acceleration-2nd validation: Constant currents.....35
Figure 2-31. TANFIS (I)-RC-1 Acceleration-1st validation: Random currents 36
Figure 2-32. TANFIS (I)-RC-2 Acceleration-2nd validation: Random currents.....37
Figure 2-33. TANFIS (II)-CC-1 Deflection-1st validation: Constant currents.....38
Figure 2-34. TANFIS (II)-CC-2 Deflection-2nd validation: Constant currents.....39
Figure 2-35. TANFIS (II)-RC-1 Deflection-1st validation: Random currents.....40
Figure 2-36. TANFIS (II)-RC-2 Deflection-2nd validation: Random currents.....41
Figure 2-37. TANFIS (I)-RC-3 Acceleration-3rd validation: Random currents.....42
Figure 2-38. TANFIS (II)-RC-3 Deflection-3rd validation: Random currents 43
Figure 3-1. Collision-induced impact forces of waterway vessel - Sunshine Skyway Bridge in Florida 48
Figure 3-2. Comparison of the acceleration response measurements with WANFIS model for various currents and drop release heights.....51
Figure 3-3. Typical ANFIS architecture.....54
Figure 3-4. TANFIS architecture showing three input and one output model 55
Figure 3-5. Configuration of W-TANFIS architecture 57
Figure 3-6. Configuration of reinforcement 59
Figure 3-7. (a) Schematic of MR damper (b) RD-8040-1 MR damper 60
Figure 3-8. Configuration of the sensors and data acquisition system 61
Figure 3-9. Architecture of the proposed mathematical modeling 64
Figure 3-10. Input-output data sets to train the W-TANFIS models 66
Figure 3-11. Configuration of the ANFIS model.....67
Figure 3-12. ANFIS training - random currents and different drop release heights.....68
Figure 3-13. Configuration of the TANFIS model 69
Figure 3-14. TANFIS training - random currents and different drop release heights 70

Figure 3-15. Configuration of the proposed W-TANFIS: Impact response prediction 71
Figure 3-16. Initial and final membership functions: W-TANFIS 72
Figure 3-17. W-TANFIS training - random currents and different drop release heights 74
Figure 3-18. W-TANFIS validation - random currents and different drop release heights 75
Figure 4-1. Nonlinear behavior of an MR damper under high impact loads 84
Figure 4-2. Typical neuro-fuzzy architecture 91
Figure 4-3. OF neuro-fuzzy architecture showing four input and one output model 94
Figure 4-4. Schematic of RD-8040-1 MR damper 96
Figure 4-5. Details of the test framework.....97
Figure 4-6. Configuration of the data acquisition system 98
Figure 4-7. The type of MF: (a) Gaussian MF (b) Bell MF (c) Triangular MF (d) Sigmoidal MF (e) Trapezoidal MF 103
Figure 4-8. Input-output data sets to train the neuro-fuzzy models.....105
Figure 4-9. Comparison of the impact load measurements with the Bouc-Wen model for various currents and drop release heights.....107
Figure 4-10. Comparison of the impact load measurements with Bingham plastic model for various currents and drop release heights.....108
Figure 4-11. Configuration of the neuro-fuzzy model: Impact load prediction 109
Figure 4-12. Neuro-fuzzy training results: constant, sinusoidal and random currents for different drop release heights.....110
Figure 4-13. Configuration of the OF neuro-fuzzy model: Impact load prediction 111
Figure 4-14. Initial and final membership functions.....112
Figure 4-15. Iteration 113
Figure 4-16. OF neuro-fuzzy training results: constant, sinusoidal and random currents for different drop release heights.....113
Figure 4-17. 1st validation.....114
Figure 4-18. 2nd validation.....115
Figure 4-19. Impact Load-Displacement and Impact Load-Velocity curves: Different drop release heights and sinusoidal current signal.....116
Figure 4-20. Impact Load-Displacement and Impact Load-Velocity curves: Different drop release heights and random current signal 117
Figure 4-21. Impact Load-Displacement and Impact Load-Velocity curves: Different drop release heights and constant current signal 118
Figure 5-1. Integrated building structure-MR damper system 125

Figure 5-2. Deflection response- Various currents and different drop release heights.....126
Figure 5-3. Acceleration response- Various currents and different drop release heights 126
Figure 5-4. Proposed fuzzy-neuro controller.....127
Figure 5-5. Configuration of fuzzy controller 130
Figure 5-6. Drop-tower testing facility and experimental test setup 132
Figure 5-7. Preparation of concrete beams.....133
Figure 5-8. Schematic of RD-8040-1 MR damper 133
Figure 5-9. Configuration of the sensors and data acquisition system 134
Figure 5-10. Configuration of the fuzzy controller.....136
Figure 5-11. Input–output data sets to train the fuzzy controller 137
Figure 5-12. Comparison of structural responses for 80 mm drop release height.....138
Figure 5-13. Comparison of structural responses for 100 mm drop release height.....139
Figure 5-14. Comparison of structural responses for 120 mm drop release height.....140
Figure 6-1. Drop-tower testing facility and experimental test setup 148
Figure 6-2. Reinforced concrete bridge pier.....149
Figure 6-3. Schematic of RD-8040-1 MR damper 149
Figure 6-4. Configuration of the sensors and data acquisition system 150
Figure 6-5. Input-output data set - Passive controlled 152
Figure 6-6. Acceleration responses – passive control and different drop release heights 153
Figure 6-7. Deflection responses – passive control and different drop release heights.....153
Figure 6-8. Input-output data set – PID controlled.....155
Figure 6-9. Acceleration responses – PID control and different drop release heights.....156
Figure 6-10. Deflection responses – PID control and different drop release heights.....156
Figure 6-11. Configuration of the TANFIS model.....157
Figure 6-12. Input-output data set – Fuzzy logic controlled 159
Figure 6-13. Acceleration responses – Fuzzy logic control and different drop release heights..160
Figure 6-14. Deflection responses – Fuzzy logic control and different drop release heights 160
Figure 6-15. Comparison of controllers – Acceleration.....163
Figure 6-16. Comparison of controllers – Deflection 164
Figure 7-1. Architecture of the proposed RVM scheme for smart structures 170
Figure 7-2. Schematic of MR damper.....179
Figure 7-3. Smart building equipped with MR dampers.....180
Figure 7-4. Integrated structure-MR damper system 181
Figure 7-5. Training of RVM and SVM: case 0 through case 5.....186

Figure 7-6. Training of RVM and SVM: case 6 through case 10.....186
Figure 7-7. Validation of RVM and SVM binary classifications: case 0 through case 5.....186
Figure 7-8. Validation of RVM and SVM binary classifications: case 6 through case 10.....187
Figure 7-9. Training of SVM multi-class classification: case 0 through case 5.....188
Figure 7-10. Training of SVM multi-class classification: case 6 through case 10.....188
Figure 7-11. Validation of SVM multi-class classification: case 0 through case 5.....189
Figure 7-12. Validation of SVM multi-class classification: case 6 through case 10.....189
Figure 7-13. Training of RVM multi-class classification: case 0 through case 5 189
Figure 7-14. Training of RVM multi-class classification: case 6 through case 10 190
Figure 7-15. Validation of RVM multi-class classification: case 0 through case 5 190
Figure 7-16. Validation of RVM multi-class classification: case 6 through case 10 190
Figure 7-17. Comparison of number of support and relevance vectors for each damage statuses 191
Figure 7-18. Comparison of training errors vectors for each damage statuses 191
Figure 7-19. Comparison of validation errors vectors for each damage statuses.....192

1. Overview

A collision-induced impact on a high-rise building or a bridge will affect the structural integrity of the members. Several such incidents have occurred on major buildings, interstate highways, beltways, bridges and overpasses in the US. In such scenarios, the impact led to a weakening, by reducing the stiffness of structural girders and beams and possibly resulting in the collapse of structures. However, such damage mechanisms of structures can be significantly reduced through high impact force attenuations, using smart control systems (Kim et al. 2009). The reduced damage results in delayed stress increase within the structural components. In addition, improved dynamic behavior will result in reduced maintenance and an extended service life of the structures.

However, there are significant uncertainties associated with the use of smart control systems in actual practice, as well as limitations in our knowledge. The two main sources of uncertainties in practical situations result from the definition of the dynamic excitation itself and from our lack of adequate knowledge and characterization of the structures' properties. For important structures, it is common to perform detailed risk analyses, and it would be normally required to also use more sophisticated models, but the validity of doing so will depend on the quantity and quality of the available information. However, it is very difficult to estimate the physical properties when highly nonlinear hysteretic control devices are equipped with structural systems. The reason is that the behavior of controlled structures is nonlinear although it is assumed that the structure itself remains linear due to the interaction effects between the structure and control devices (Kim et al. 2011). There is no available approach in the literature about how to model an integrated structure-magnetorheological (MR) damper system under high impact loads (including the interaction effects between a structure and MR dampers). In this context, the research outlined in the following dissertation presents novel algorithms that can be used for system identification (SI), control and health monitoring of the smart structures equipped with MR dampers subjected high impact loads.

The challenge of developing an accurate mathematical model of the integrated structure-MR damper system can be addressed by applying nonlinear system identification (SI) methodologies The SI methodologies can be categorized into two parts: parametric and nonparametric SI approaches. A parametric SI method is effective to directly identify physical quantities such as the stiffness and damping of structural systems. However, it is difficult to apply the parametric approach to complex nonlinear problems, in general. A nonparametric SI

method is to train the input-output map of the structural systems. In particular, the nonparametric SI approach is effective for the complex nonlinear problems of large civil infrastructures. One of the nonparametric nonlinear SI methodologies that have been widely used in the field of large civil structures is a neural network (NN). A NN is normally more readily useful than the parametric SI approach to identify incomplete and incoherent measurements of large civil structures, although conventional NN models have drawbacks of the slow convergence rate and the potential to local minima due to the characteristics of the black-box model. Another popular nonparametric SI method for modeling complex nonlinear dynamic systems is fuzzy logic theory because it is effective to represent complex nonlinearities and uncertainties of dynamic systems in a more transparent way. Fuzzy SI model provides an effective representation of nonlinear systems with the aid of fuzzy sets, fuzzy rules, and a set of local linear models. Thus, an adaptive neuro-fuzzy inference system (ANFIS) model is used to identify the integrated structure-MR damper system under high impact loads.

The good performance of ANFIS in the SI of smart structures subjected to seismic loads was demonstrated by Mitchell et al. (2012). They performed a numerical study on a three-story smart structure equipped with an MR damper under various seismic loads. It was demonstrated from the simulation that the proposed ANFIS model is effective in identifying the nonlinear behavior of the seismically excited building-MR damper system. The second and the third chapters of this dissertation evaluate the performance of the ANFIS model in the SI of smart structures subjected to high impact. The results demonstrated that although the ANFIS model is effective in identifying the nonlinear behavior of the seismically excited building-MR damper system, it is not effective for high impact load cases. The main source of the phenomenon is the low sensitivity of ANFIS to high frequency responses. Most earthquake waves have a frequency of less than 20 Hz (USGS, 2014), while collision loads can reach up to 250–1500 Hz (Yan and Zhou, 2009). An excessively high computational complexity occurs when training ANFIS for high frequency signals. The main problems to face here are that when the input frequency increases, the computational complexity and memory requirements of the ANFIS increase. Training of the model becomes more difficult with high variance inputs. High frequency variables act as noise, which deteriorates the generalization capability of the model. In this context, this study proposes time-delayed adaptive neuro-fuzzy inference system (TANFIS) and wavelet-based TANFIS (W-TANFIS) models. The models combine aspects of neural networks, time-delay, fuzzy logic theory, and wavelet transforms to create a framework that is new in the field of civil engineering structures. The time-delay approach is used to obtain a subset of variables that are truly relevant or the most influential to high frequency output. The proposed

models preserve the time sequence of the input vectors and memorize the past of the time series sensor data (Adeli and Jiang, 2006). The additional time-delayed input data, which involves the important features of the output data, increases the sensitivity of the SI model. It is observe that the proposed TANFIS and WTANFIS models are effective in identifying the nonlinear impact behavior of the structure-MR damper system while shortening the training time of ANFIS model. Then, the models are used in the development of the control algorithm to optimize the impact energy dissipation.

The objective of the control algorithm is to improve the impact performance of a building or a bridge by optimizing the damping force of MR dampers. This is essential, as being able to limit the responses of a structure can maintain the strength and integrity of the building or bridge, allowing for a safer structure over the course of the design life (Mitchell et al. 2012). In this context, by using the previously developed TANFIS model a fuzzy logic control algorithm is developed to improve the impact performance of control system used on high-rise buildings and highway bridge structures. To train the proposed fuzzy logic controller, test specimens equipped with MR dampers are tested under different impact loads and different current levels. Structural responses are used as the inputs to predict the optimized current signal. Then the test specimens are subjected to impact forces from a variety of drop release heights, and the effectiveness of the fuzzy controller is obtained in real time. Both analytical and experimental studies demonstrated that the proposed fuzzy controller is effective in mitigating high impact responses of smart structures.

The last study is performed on the structural health monitoring systems that assist engineers to detect structural damage proactively with non-destructive testing by providing real-time monitoring systems. As a preliminary study, a support vector machine (SVM) framework is used in the damage classification of a three story smart structure equipped with MR damper subjected to random excitations. It is seen that the accuracy of the SVM classification decreases when it is trained using small data sets. With this in mind, a new relevance vector machine (RVM) approach is proposed, which does not require slack parameters and can accurately classify the data with less data points. Both binary and multi-class classification demonstrated that RVM is very effective in classifying various levels of damage status.

This dissertation combines six journal papers. The first two papers outline the performance of the proposed TANFIS and W-TANFIS models as a means for system identification of a structure employing a smart damper. The third paper discusses system identification models of MR dampers that will be used to predict and analyze the nonlinear impact behavior of MR damping systems under high impact loads. The fourth paper details the

use of the TANFIS model as a control algorithm to improve the structural performance of an integrated structure-MR damper system subjected high impact loads. The application of the TANFIS control algorithm to a scaled down smart bridge pier equipped with MR damper is presented in the fifth paper. The last paper focuses on the structural health monitoring of smart structures equipped with MR dampers.

2. Nonlinear System Identification of Smart Structures under High Impact Loads

2.1. Introduction

The complexity of predicting the response of structures under high impact loads such as non-linear material behaviors, extreme structural responses and structural instabilities has attracted a great deal of attention in various engineering fields. (Wang and Li, 2006; Ahmadian and Norris, 2008; Hongsheng and Suxiang, 2009; Wiklo and Holnicki-Szulc, 2009 a,b; Consolazio et al., 2010). For example, when a structure is excited by an impact load such as an aircraft or ship collision, key components of the infrastructure can be severely damaged. Such events often cause a shutdown of critical life safety systems (Consolazio et al., 2010). Hence the use of shock absorbers to mitigate such hazards has been proposed by some researchers (Wang and Li, 2006; Ostrowski et al., 2007; Ahmadian and Norris, 2008; Graczykowski and Holnicki-Szulc, 2009, Holnicki-Szulc et al., 2009).

One of the most promising strategies to absorb and dissipate the external energy would be to use a smart control mechanism that adjusts the force levels of mechanical devices within the infrastructure in real time. In recent years, with the increase of smart structure applications in many engineering fields, usage of smart control systems in the improvement of the dynamic behavior of complex structural systems has become a topic of major concern (Spencer and Nagarajajah, 2003; Jung et al., 2006). In particular, magnetorheological (MR) dampers have received great attention for use in large-scale civil infrastructural systems since they combine the best features of both the passive and active control strategies (Spencer et al., 1997b). Many investigators have demonstrated that this technology shows great deal of promise for engineering applications in recent years (Dyke et al., 1996a, 1998, 2001; Yi et al., 1998, 1999; Mikułowski and Holnicki-Szulc, 2007; Kim et al., 2009, 2010). However, most of the studies on MR damper technology has focused on nonlinear behavior under low velocity environments while relatively few studies have been carried out on the performance of MR dampers under high impact forces (Wang and Li, 2006; Mao et al., 2007; Mikułowski and Holnicki-Szulc, 2007; Ahmadian and Norris, 2008; Graczykowski and Holnicki-Szulc, 2009). The main focus of these studies was on the behavior of the MR damper itself under impact loads, not specifically a large structure employing MR dampers: review of the literature suggests that an integrated model to predict

nonlinear behavior of large structure-MR damper systems under high impact loads has not been proposed or realized.

It is quite challenging to develop an accurate mathematical model of the integrated structure-MR control systems due to the complicated nonlinear behavior of integrated systems and uncertainties of high impact forces. For example, when highly nonlinear hysteretic actuators/dampers are installed in structures for efficient energy dissipation, the structure employing the nonlinear control devices behaves nonlinearly while the structure itself is usually assumed to behave linearly (Kim et al., 2011). Moreover, this nonlinear problem becomes more complex with the application of unexpected high impact loads. Hence, developing an appropriate mathematical model considering the interaction effects between the structural system and the nonlinear control device under high impact loads becomes more complex and challenging. Figure 2-1 represents the highly nonlinear hysteretic behavior between the high impact force and the structural velocity responses under high impact loads due to nonlinear MR dampers, high speed impact forces and nonlinear contact between structure and MR damper. This issue can be addressed by applying nonlinear system identification (SI) methodologies to a set of input and output data in order to derive a nonlinear input-output mapping function.

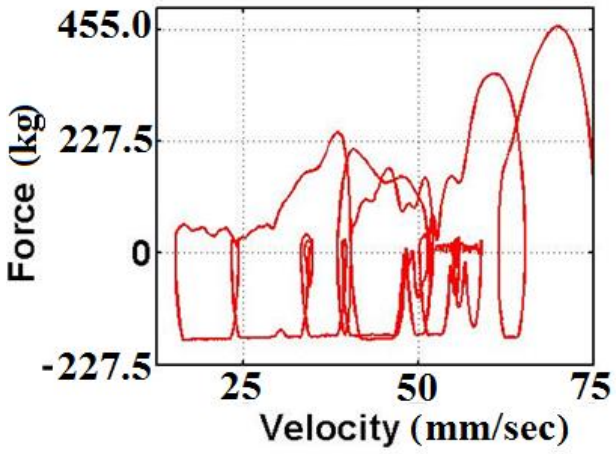

Figure 2-1. Nonlinear behavior of the structure equipped with MR dampers under high impact loads

In general, the SI methodologies can be categorized into two parts: parametric and nonparametric SI approaches (Bani-Hani et al., 1999; Suresh et al., 2008). In the parametric approach, the architecture of the mathematical model is directly dependent on the physical quantities of structural system such as stiffness, damping and mass (Lin et al., 2001; Lin and Batti, 2004; Yang and Lin, 2004). On the other hand, to identify the given system model, the

nonparametric SI method trains the input-output map of the structural system (Hung et al., 2003; Kim et al., 2011). The nonparametric SI approaches have been widely used in the field of large civil structures because of their proven usefulness to estimate incomplete and incoherent measurements of large-scale infrastructural systems (Allison and Chase, 1994; Marsri et al., 2000; Hung et al., 2003; Suresh et al., 2008). However, no studies were found on SI for predicting high impact nonlinear behavior of smart structures equipped with highly nonlinear hysteretic devices.

With this in mind, a nonlinear SI framework is proposed for estimating complex behavior response of structure-MR control systems under high impact loads in this paper. The approach is developed through the introduction of time-delayed components to adaptive neuro-fuzzy inference system (ANFIS) modeling framework, which is an integrated learning model of fuzzy logic and neural network.

This paper is organized as follows. Section 2.2 discusses the time-delayed ANFIS (TANFIS). In Section 2.3, the experimental setup and procedures are described. The modeling results, including training and validations are given in Section 2.4. Concluding remarks are given in Section 2.5.

2.2. Time-delayed adaptive neuro fuzzy inference system (TANFIS)

2.2.1. Adaptive neuro fuzzy inference system (ANFIS)

ANFIS can be simply defined as a set of fuzzy ‘if-then’ rules with appropriate membership functions to generate the stipulated input-output pairs in the solution of uncertain and ill-defined systems (Jang, 1993). The application of ANFIS models in the SI of complex civil engineering structures is a relatively new topic (Mitchell et al., 2012). Although the application of the ANFIS system has been commonly used (Faravelli and Yao, 1996; Alhanafy, 2007; Gopalakrisnan and Khaitan, 2010; Wang, 2010; Jang et al, 1997), minimizing the output error to maximize the performance of the SI is still a challenging issue.

ANFIS is a hybrid system that is able to integrate fuzzy inference system and adaptive learning tools from neural networks to get more accurate results (Mitchell et al., 2012). By using a backpropagation neural network learning algorithm, the parameters of the Takagi-Sugeno (TS) fuzzy model are updated until they reach the optimal solution (Tahmasebi and Hezarkhani, 2010). A typical ANFIS system with three inputs and one output is presented in the Figure 2-2.

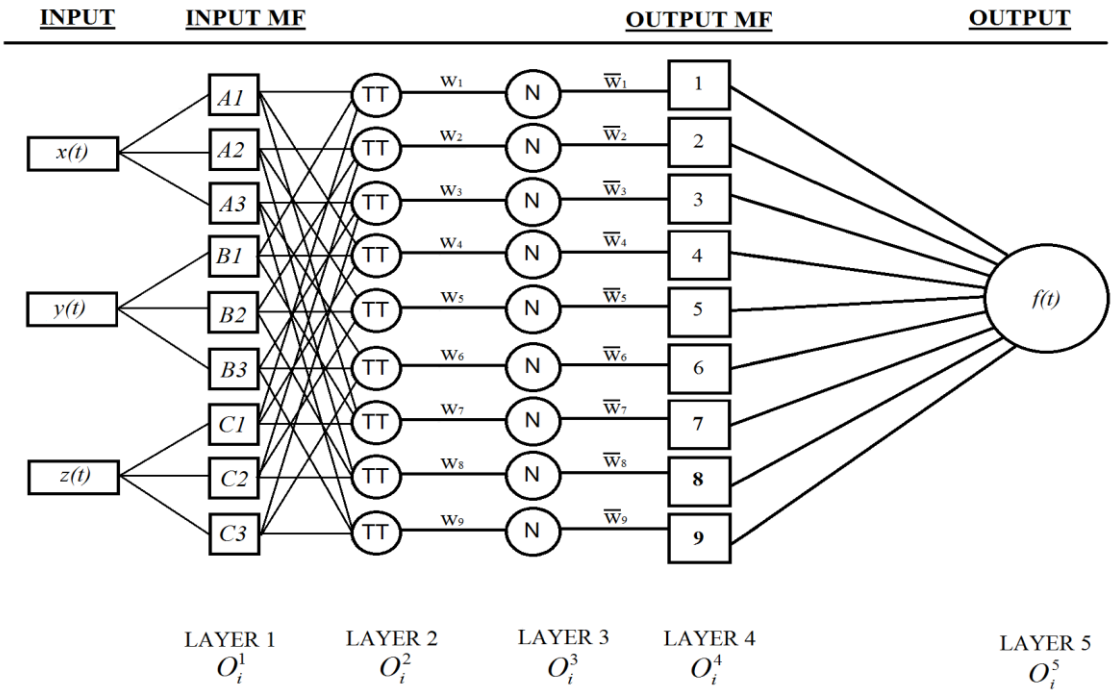

Figure 2-2. Typical ANFIS architecture

After the data is processed in the current layer, it moves forward to the next layer. The process stops when each layer completes its task. A typical three-rule ANFIS fuzzy model (Jang, 1993) is as follows

Rule 1: If x is A_1, y is B_1 and z is C_1, then $f_1 = p_1 x + q_1 y + k_1 z + r_1$ (2-1)

Rule 2: If x is A_2, y is B_2 and z is C_2, then $f_2 = p_2 x + q_2 y + k_2 z + r_2$ (2-2)

Rule 3: If x is A_3, y is B_3 and z is C_3, then $f_3 = p_3 x + q_3 y + k_3 z + r_3$ (2-3)

where x, y and z are the inputs and f is the output of the TS fuzzy system, while p_i, q_i, k_i and r_i are defined as consequent parameters. The function of Layer 1 is presented as

$$O_i^1 = \mu A_i(x) \quad (2\text{-}4)$$

where μ is the appropriate parameterized membership function (MF), and O_i^1 (i = 1,2,3) is the output that specifies the degree to which the given input x satisfies the quantifier A.

After the application of MFs to each input, data moves to the second layer to combine all the inputs. Output of the Layer 2 is the product of all incoming inputs which is also defined as the 'firing strength' of a fuzzy control rule

$$w_i = \mu A_i(x) \times \mu B_i(y) \times \mu C_i(z),\ i = 1,2,3 \tag{2-5}$$

In order to normalize the output of Layer 2, the ratio of the firing strength is taken in Layer 3

$$\overline{w}_i = \frac{w_i}{w_1 + w_2 + w_3},\ i = 1,2,3 \tag{2-6}$$

In Layer 4, node functions ($f_i = p_i x + q_i y + k_i z + r_i, i = 1,2,3$) are applied to output of Layer 3

$$O_i^4 = \overline{w}_i \times f_i = \overline{w}_i \times \left(p_i x + q_i y + k_i z + r_i\right),\ i = 1,2,3 \tag{2-7}$$

As a last step, Layer 5 summates the layer inputs

$$O_i^5 = overall\ \ output + \sum_i \overline{w}_i \times f_i = \frac{\sum_i w_i \times f_i}{\sum_i w_i},\ i = 1,2,3 \tag{2-8}$$

To obtain the optimum solution, ANFIS creates a nonlinear mapping by using adjustable parameters such as MF type, number of MFs, step size and number of iterations. The change of output results in the variation of adjustable parameters is demonstrated by Filev (1991).

At the end of the research, it is observed that ANFIS predictions are not in agreement with the actual high impact responses. Only 20% to 40% of the actual acceleration and deflection values are predicted correctly by ANFIS. Although the ANFIS model is very effective in the SI of smart structures under seismic loads, it is not effective in the prediction of structural responses under high frequency loads. Statistical variance in high frequency input, avoid ANFIS to identify the features high impact signals. High frequency variables act as noise, which increases the computational complexity and memory requirements of the ANFIS model. In order to increase the accuracy between the trained and the actual high impact test data, TANFIS, which uses the outputs of the previous steps to predict the features of the following output, is used. The time-delay approach preserves the input data order from distortion and frequency changes. The new

TANFIS method, which is defined below, increased the accuracy of the trained model significantly.

2.2.2. Time-delayed ANFIS (TANFIS)

The objective of the method is to estimate the output by using the observations from previous steps. In general, a dynamic input-output mapping (Adeli and Jiang 2006) can be expresed as follows

$$f_j(t) = f\left(x^{t-d}, f^{t-d}, e^{t-d}\right) + e(t) \tag{2-9}$$

where x^t, f^t, and e^t represent the input, output and error for time *t*, respectively. The time delay term is represented by the term *d*. In this research, impact loading, the electrical current applied to the MR damper and the responses are assigned as input. The fuzzy model is then trained to identify the features of acceleration and deflection responses. In the research, time delay term *d* is assigned as 1, which means that model uses the observations from previous step (*t-1)* to estimate the output at time *t*. By the integration of Eq. (2-8) and Eq. (2-9), the proposed TANFIS model is as follows

$$O_j^5 = overall \quad output + \sum_j \overline{w}_j \times f_j = \frac{\sum_j w_j \times f_j}{\sum_j w_j} \tag{2-10}$$

The architecture of the TANFIS model is depicted in Figure 2-3.

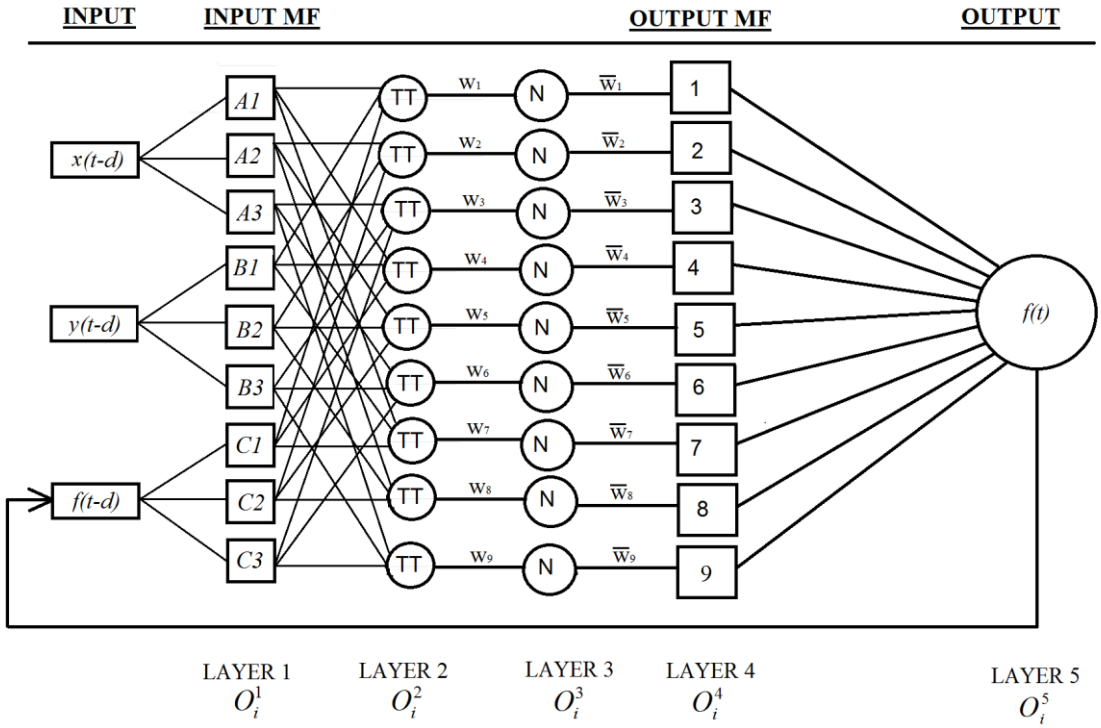

Figure 2-3. TANFIS architecture showing three input and one output model

In order to obtain input-output data for training and validating the TANFIS models, experimental studies are performed. Impact load, current on MR damper, acceleration and deflection values are measured, and models are trained to predict the noninear behavior of the smart structure. Results are used in the evaluation of the accuracy of ANFIS and TANFIS to predict the actual test data.

2.3. Experimental setup

To investigate the effectiveness of smart control systems on the high impact response attenuations of the structure, an experimental test framework is proposed that includes drop tower tests, an aluminum cantilever beam, two MR dampers, data acquisition system, sensors and a high speed camera.

2.3.1. Drop tower test facility

Drop-tower testing is an effective way of investigating the dynamic response and energy dissipation of structure-MR damper systems under impulse loads. In this study, the high impact load test facility in Structural Mechanics and Impact Laboratory in the Civil and Environmental

Engineering Department at Worcester Polytechnic Institute was used as shown in (Figure 2-4). The maximum capacity to apply impulse load of the used mechanism is 22,500 kilogram. In the study, impact loads were applied with a 6.8 kg free falling drop-mass. The applied load was adjusted by changing the drop release heights.

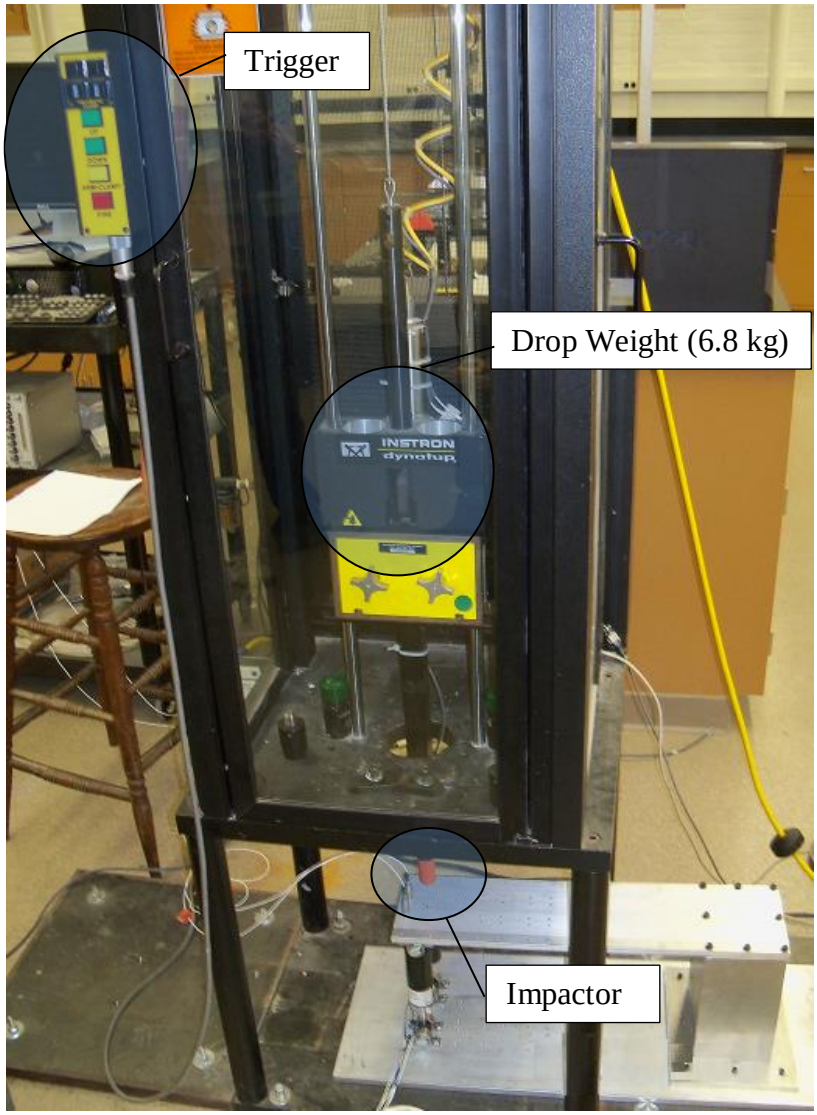

Figure 2-4. Drop-tower testing facility with a capacity of 22,500 kg

2.3.2. Aluminum plate beam equipped with MR dampers

As the structure used to measure the dynamic response, a cantilever aluminum plate beam with dimensions of 615×155×10 mm is used. The aluminum beam is fixed to the ground to prevent it from shifting during the application of high impact loading. For consistency in each test, the load is applied to the free end of the cantilever beam. The CAD drawing of the beam, placement

of the actuators/sensors (MR dampers, accelerometers and LVDT) and location of the impact load are presented in Figure 2-5.

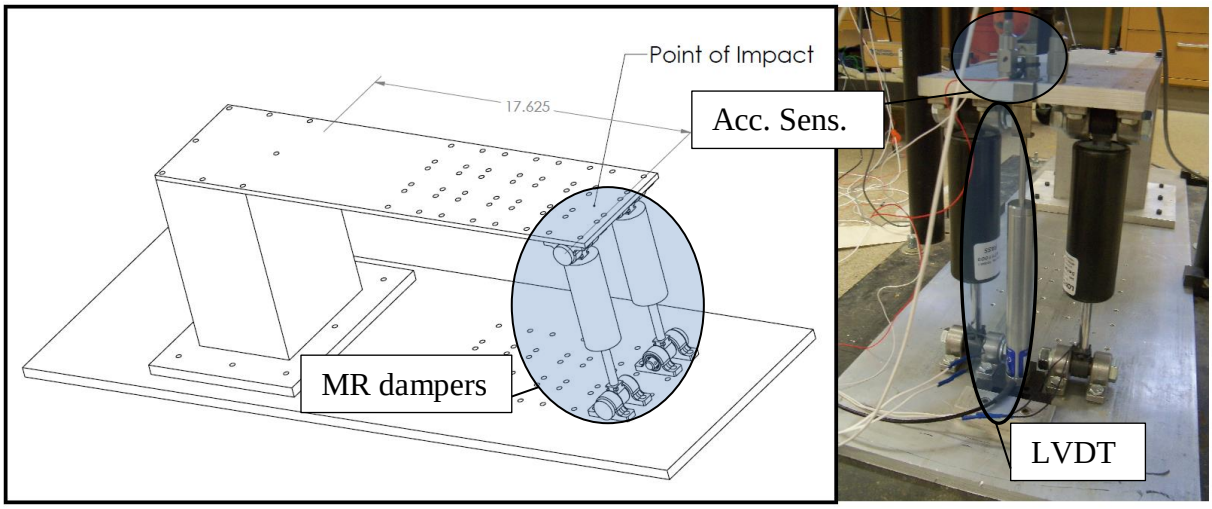

(a) (b)

Figure 2-5. Details of cantilever aluminum plate beam: (a) CAD drawing and illustration of impact point (b) Location of two MR dampers, accelerometers and LVDT

The smart control system includes the two MR dampers placed under the cantilever beam and the control system (Figure 2-6). The MR dampers consist of the hydraulic cylinders, the magnetic coils and MR fluid. The MR fluid consists of micron sized magnetically polarized particles within an oil-type fluid (Spencer et al. 1997b). The feature, which makes the MR dampers so attractive, is that they can be both operated as passive or active dampers. In the active system, the application of a measured magnetic field to the MR fluid affects its rheological and flow properties that cause it to absorb and dissipate energy effectively. The MR energy dissipation function is adjusted based on feedback of current signals associated with structural response gained through sensors monitoring the structure. In contrast to active systems, MR dampers can still operate as a passive damper if some control feedback component, e.g., wires and sensors, are damaged for some reason (Mitchell et al., 2012).

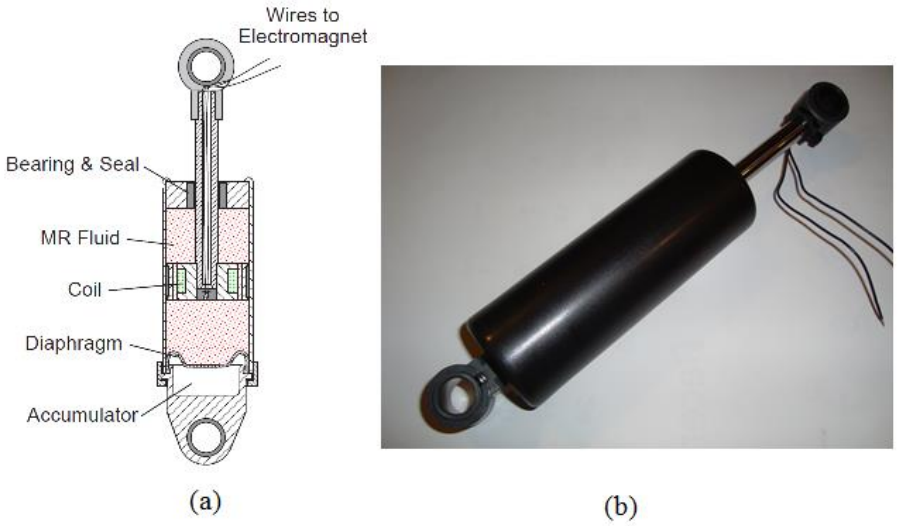

Figure 2-6. (a) Schematic of MR damper (Dyke, 1996), (b) RD-8040-1 MR damper

2.3.3. Data acquisition

During the impact tests, acceleration, velocity and impact forces are collected with three sensors connected to a National Instrument (NI) LabView data acquisition system. Displacement, acceleration and impact force are measured using the data acquisition system as shown in Figure 2-7. In the measurement of the displacement data, R.D.P product ACT1000A type LVDT is used. A 500 g capacity PCB type 302A accelerometer and a 4,500 kg capacity Central HTC-10K type load cells are used in the acceleration and impact force measurements respectively. The sampling rate of the data acquisition system is 10000 data points per second.

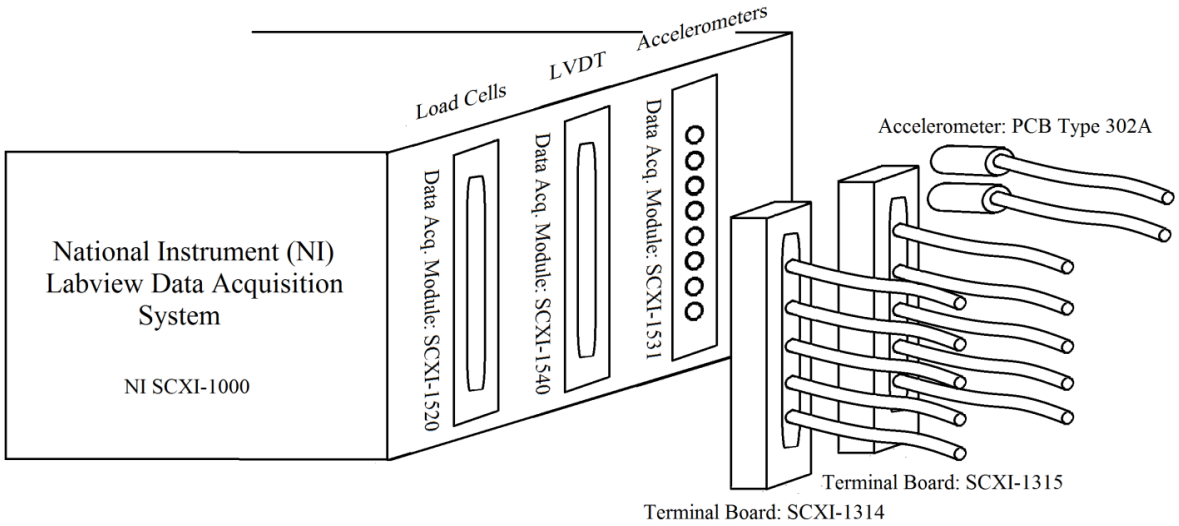

Figure 2-7. Configuration of the data acquisition system

2.3.4. Test details

The goal of the experimental testing is to measure the dynamic response of the smart structure under different impact loads and different scenarios including with and without the MR dampers. A series of experimental tests are performed by changing the drop release height and the current level applied to the MR damper. For each drop release height and current on the MR damper, the drop release test is performed three times to train and validate the proposed models. Details of the performed tests can be found in Table 2-1.

A total of 120 impact tests were performed to investigate the responses of the structure with and without MR dampers. The applications of both constant and random current signals to the MR dampers were examined in the tests. The high impact test was repeated for each current level.

Table 2-1. Experimental Test Details

Case Studies			Current on MR Damper	Drop Release Height (mm)	Impact Velocity (mm/s)
Trained Data	Validated Data				
	1st Set	2nd Set			
Case 1	Case 2	Case 3	Uncontrolled	25	700
Case 4	Case 5	Case 6	0	25	
Case 7	Case 8	Case 9	0.3	25	
Case 10	Case 11	Case 12	0.6	25	
Case 13	Case 14	Case 15	1	25	
Case 16	Case 17	Case 18	1.4	25	
Case 19	Case 20	Case 21	1.9	25	
Case 22	Case 23	Case 24	Random	25	
Case 25	Case 26	Case 27	Uncontrolled	35	828
Case 28	Case 29	Case 30	0	35	
Case 31	Case 32	Case 33	0.3	35	
Case 34	Case 35	Case 36	0.6	35	
Case 37	Case 38	Case 39	1	35	
Case 40	Case 41	Case 42	1.4	35	
Case 43	Case 44	Case 45	1.9	35	
Case 46	Case 47	Case 48	Random	35	
Case 49	Case 50	Case 51	Uncontrolled	40	885
Case 52	Case 53	Case 54	0	40	
Case 55	Case 56	Case 57	0.3	40	
Case 58	Case 59	Case 60	0.6	40	
Case 61	Case 62	Case 63	1	40	
Case 64	Case 65	Case 66	1.4	40	
Case 67	Case 68	Case 69	1.9	40	
Case 70	Case 71	Case 72	Random	40	
Case 73	Case 74	Case 75	Uncontrolled	65	1129
Case 76	Case 77	Case 78	0	65	
Case 79	Case 80	Case 81	0.3	65	
Case 82	Case 83	Case 84	0.6	65	
Case 85	Case 86	Case 87	1	65	
Case 88	Case 89	Case 90	1.4	65	
Case 91	Case 92	Case 93	1.9	65	
Case 94	Case 95	Case 96	Random	65	
Case 97	Case 98	Case 99	Uncontrolled	80	1253
Case 100	Case 101	Case 102	0	80	
Case 103	Case 104	Case 105	0.3	80	
Case 106	Case 107	Case 108	0.6	80	
Case 109	Case 110	Case 111	1	80	
Case 112	Case 113	Case 114	1.4	80	
Case 115	Case 116	Case 117	1.9	80	
Case 118	Case 119	Case 120	Random	80	

2.4. System identification results

2.4.1. Parameter setting

To develop the proposed models, sets of input and output data are collected and prepared for training and validation. Figure 2-8 and Figure 2-9 shows the set of input-output signals for training the TANFIS (I): impact loads and current signals are used as the inputs while the acceleration response is used as an output signal. Figure 2-10 and Figure 2-11 shows the input-output data sets for training the TANFIS (II). In this modeling, deflection is used as the output while currents and impact loads are the 1st and 2nd input signals. Same input-output data sets are also used in the ANFIS model and results are discussed later in the evaluation section.

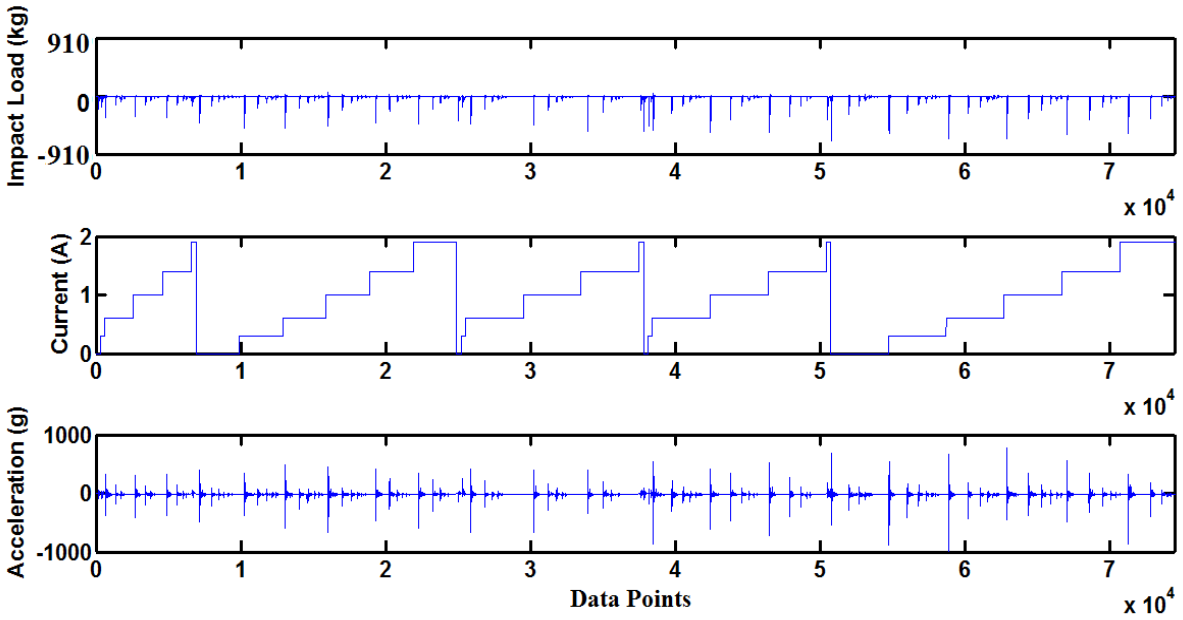

Figure 2-8. Input-output data sets to train the model to predict acceleration: constant currents

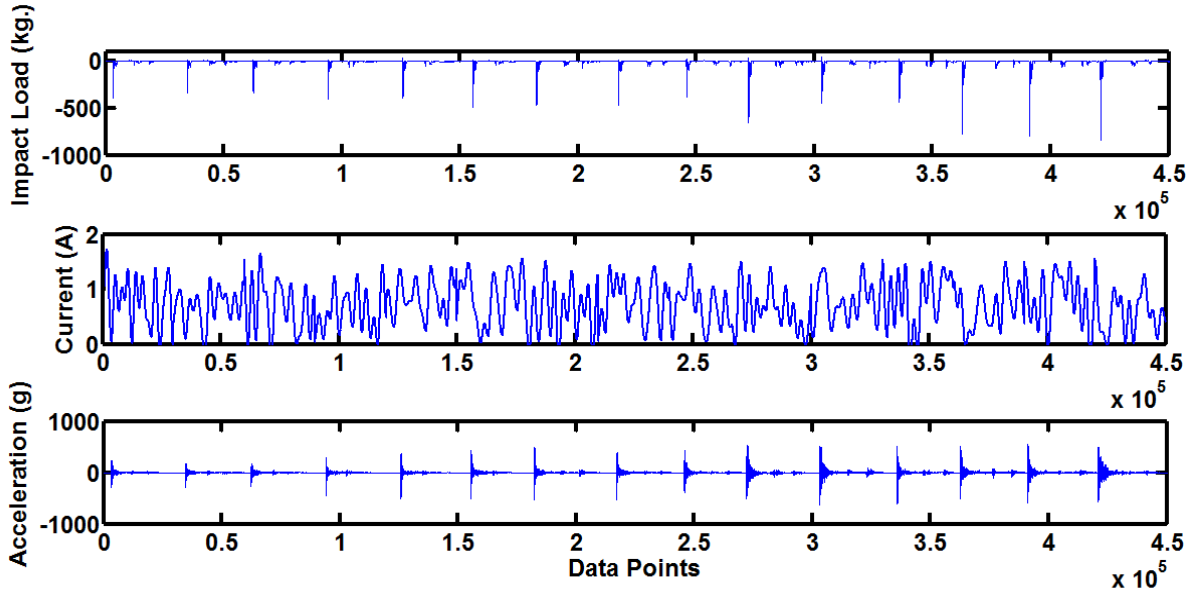

Figure 2-9. Input-output data sets to train the model to predict acceleration: random currents

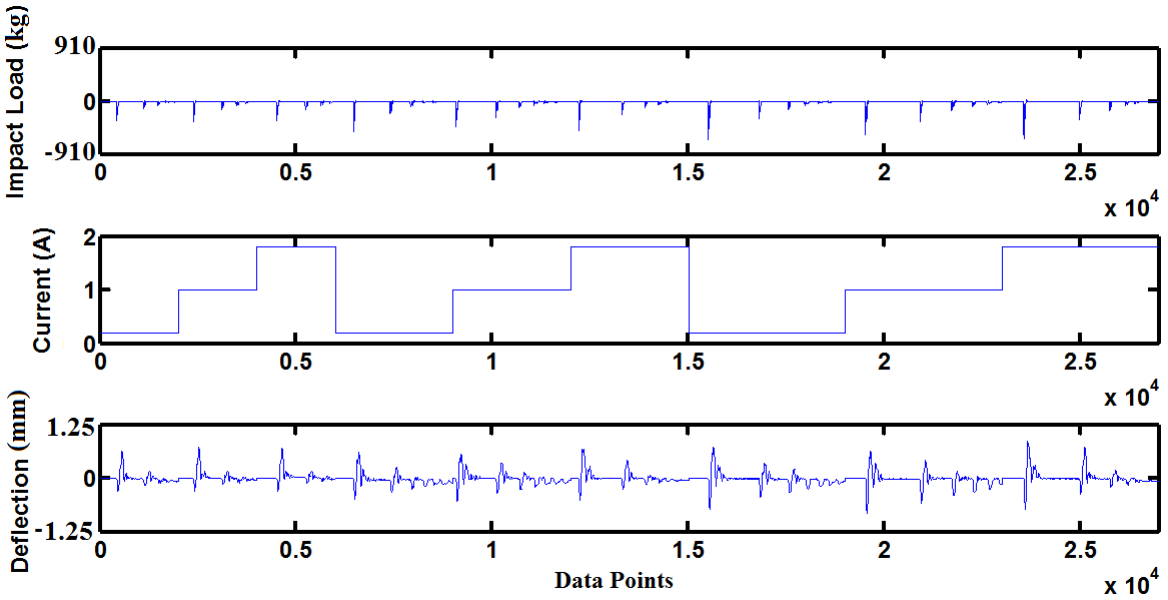

Figure 2-10. Input-output data sets to train the model to predict deflection: constant currents

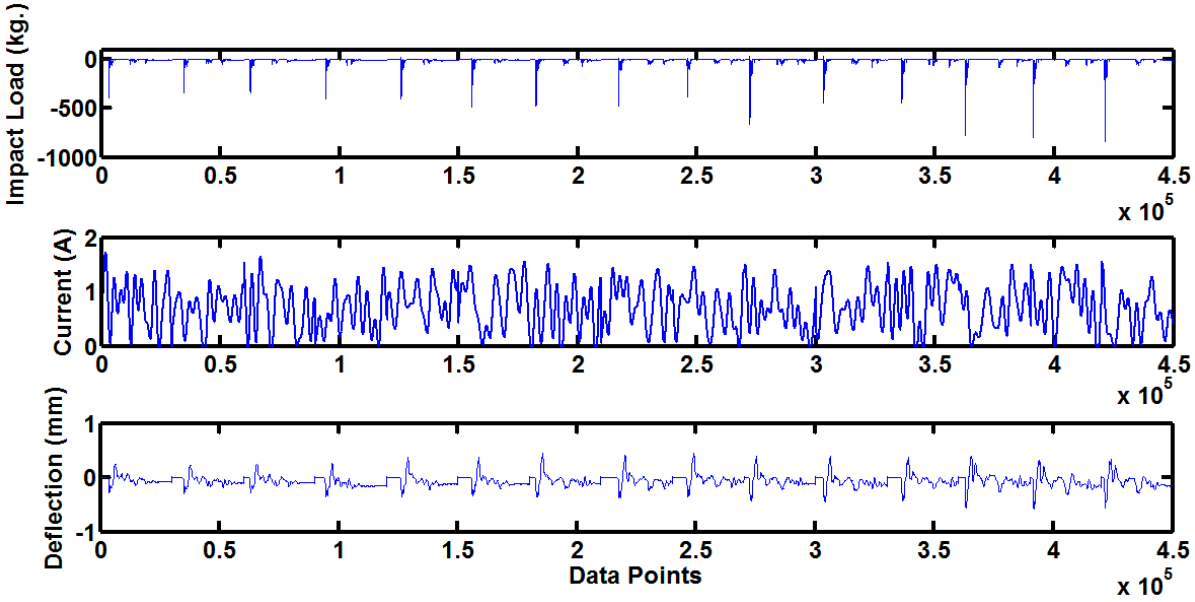

Figure 2-11. Input-output data sets to train the model to predict deflection: random currents

In the simulation process, to get the best match, an iterative method is used by changing the training iteration, step size, type and quantity of MFs. Figure 2-12 shows the type of MFs used and Table 2-2 represents the details of the 39 parameter studies. After performing simulations, it is observed that changing iteration and step sizes does not have a significant effect on the given data set since the error tolerance level reaches the training error goal before reaching the assigned iteration.

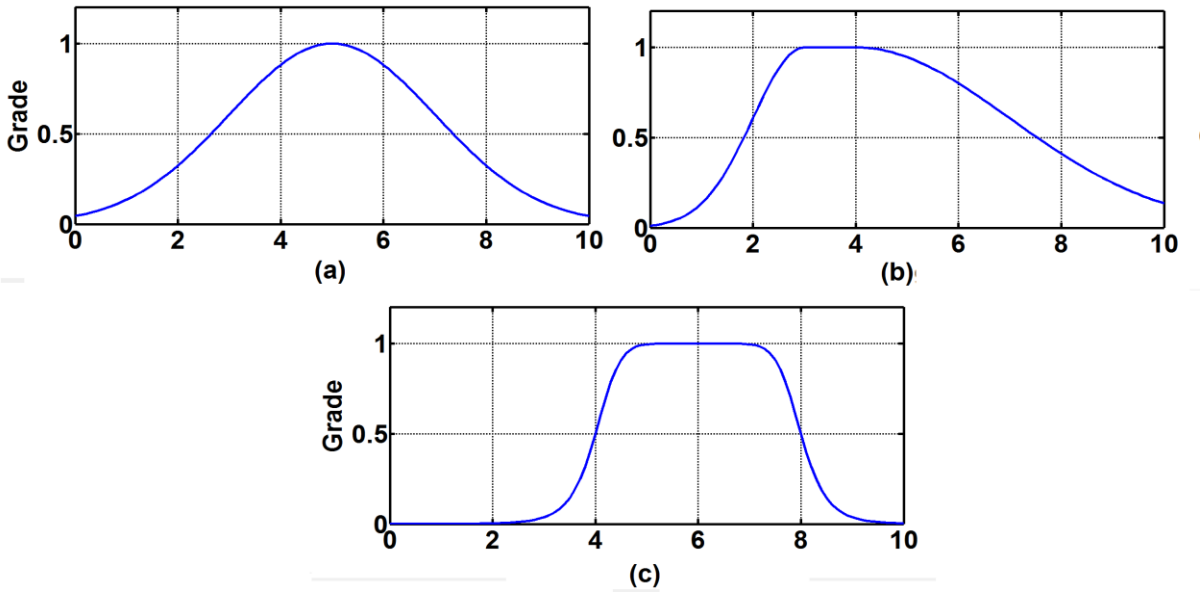

Figure 2-12. The type of MF: (a) Gaussian 1 (b) Gaussian 2 (c) Gaussian 3

Table 2-2. Simulation parameter studies

TRY	MF	ss	Iteration	Membership Function		Error (Unit)	
1	Gaussian 3	0.4	400	2	2	301.175	-174.0575
2	Gaussian 3	0.4	400	2	3	294.8257	-151.7968
3	Gaussian 3	0.4	400	2	4	294.465	-149.3413
4	Gaussian 3	0.4	400	2	5	296.2641	-181.6892
5	Gaussian 3	0.4	400	3	2	263.8354	-110.6075
6	Gaussian 3	0.4	400	4	2	290.1787	-129.336
7	Gaussian 3	0.4	400	5	2	242.2016	-104.2576
8	Gaussian 3	0.4	400	3	3	238.454	-128.9931
9	Gaussian 3	0.4	400	3	4	258.1606	-115.1826
10	Gaussian 3	0.4	400	3	5	254.3344	-117.6737
11	Gaussian 3	0.4	400	4	3	262.3171	-82.0911
12	Gaussian 3	0.4	400	5	3	227.5869	-107.6931
13	Gaussian 3	0.4	400	4	4	262.9816	-81.2276
14	Gaussian 3	0.4	400	4	5	262.6796	-81.6742
15	Gaussian 3	0.4	400	5	4	238.6476	-104.2439
16	Gaussian 3	0.4	400	5	5	238.1985	-104.3979
17	Gaussian 3	0.4	600	4	5	262.2278	-83.0477
18	Gaussian 3	0.2	500	5	4	238.8043	-104.0616
19	Gaussian 3	0.2	600	5	5	240.0591	-103.0386
20	Gaussian 1	0.4	400	2	2	309.676	-181.8678
21	Gaussian 1	0.4	400	2	3	315.8973	-181.2744
22	Gaussian 1	0.4	400	2	4	293.5166	-144.3133
23	Gaussian 1	0.4	400	2	5	294.0135	-185.2934
24	Gaussian 1	0.4	400	3	2	293.6066	-99.4267
25	Gaussian 1	0.4	400	4	2	273.2148	-149.667
26	Gaussian 1	0.4	400	5	2	285.5391	-101.8039
27	Gaussian 1	0.4	400	3	3	280.8643	-114.843
28	Gaussian 1	0.4	400	3	4	276.1538	-111.6044
29	Gaussian 1	0.4	400	3	5	260.1134	-116.312
30	Gaussian 1	0.4	400	4	3	270.2851	-123.514
31	Gaussian 1	0.4	400	5	3	251.7693	-114.6532
32	Gaussian 1	0.4	400	4	4	270.2643	-125.0717
33	Gaussian 1	0.4	400	4	5	270.2644	-125.993
34	Gaussian 1	0.4	400	5	4	245.7084	-113.7196
35	Gaussian 1	0.4	400	5	5	248.6173	-114.7212
36	Gaussian 2	0.4	400	2	2	310.9469	-198.9278
37	Gaussian 2	0.4	400	3	2	390.4772	-91.6052
38	Gaussian 2	0.4	400	4	2	289.1871	-123.2061
39	Gaussian 2	0.4	400	5	2	263.8774	-117.1053

2.4.2. ANFIS modeling

In the modeling of ANFIS, best match is obtained from the MF type of Gaussian 3. The time history responses of the proposed system employing constant currents and different drop release heights are depicted in Figure 2-13 and Figure 2-14.

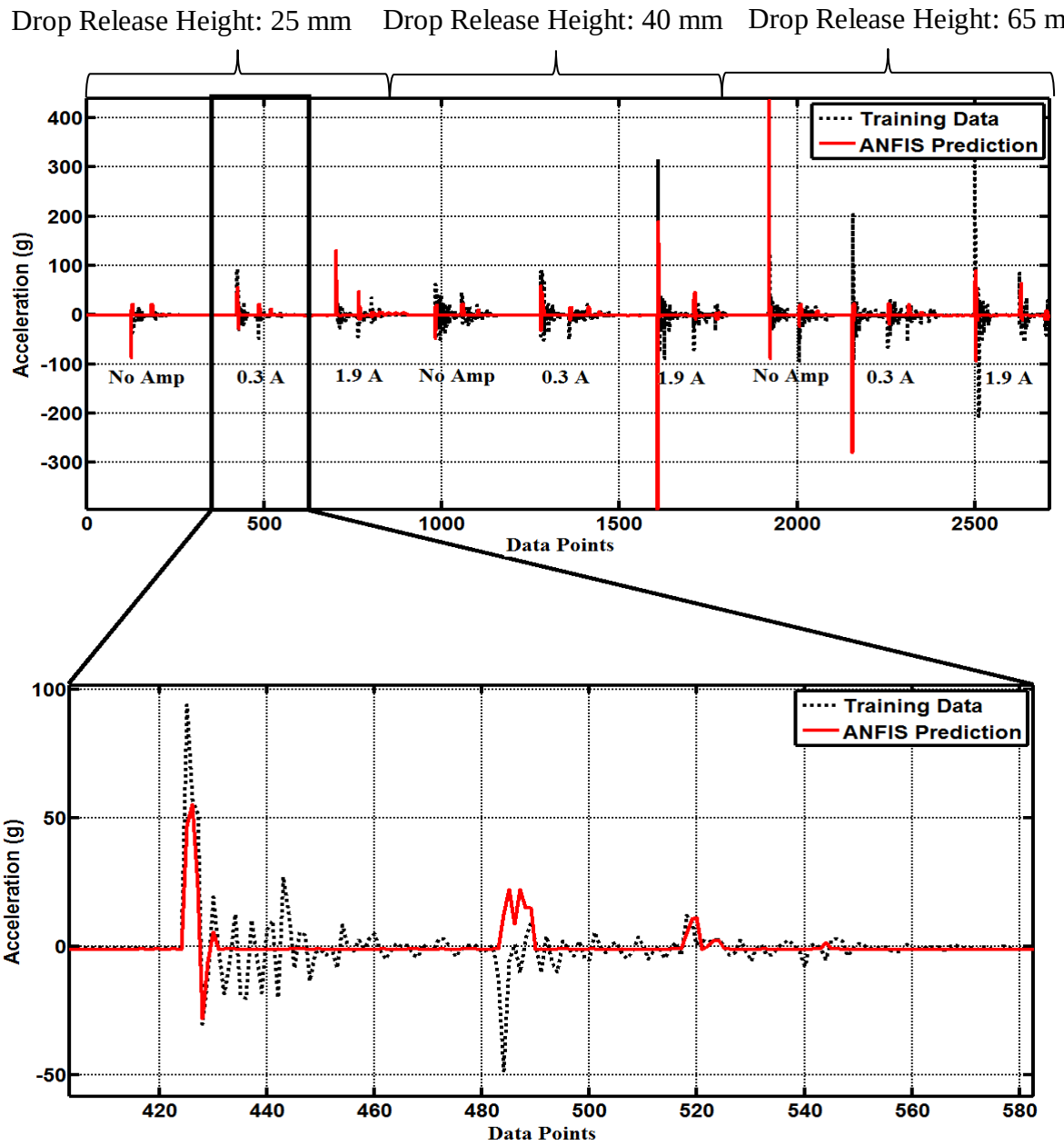

Figure 2-13. ANFIS (I)-CC: Acceleration training- constant currents and different drop release heights

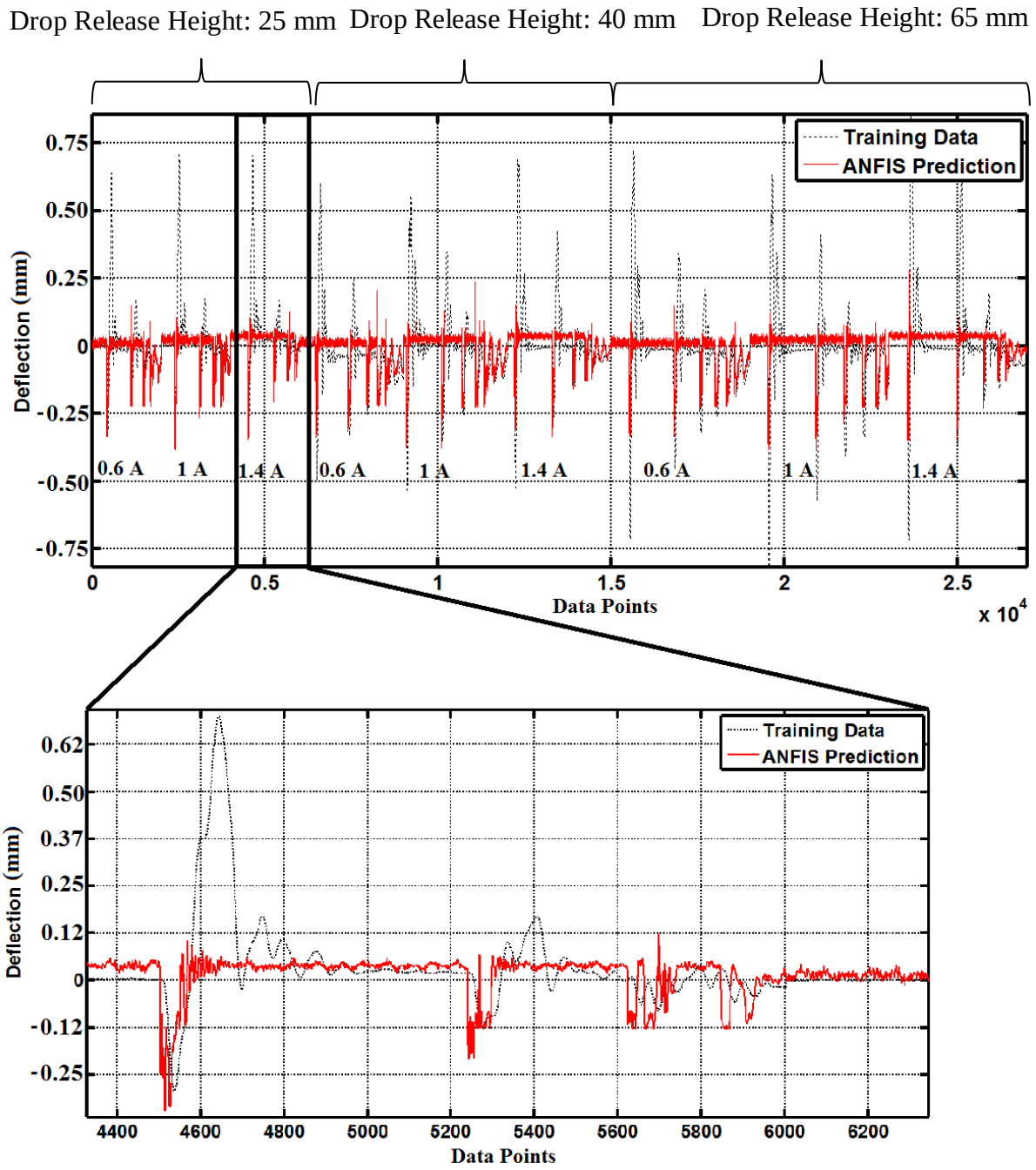

Figure 2-14. ANFIS (II)-CC: Deflection training- constant currents and different drop release heights

Figure 2-15 and Figure 2-16 depict the time history responses of the ANFIS system employing random currents and various drop release heights.

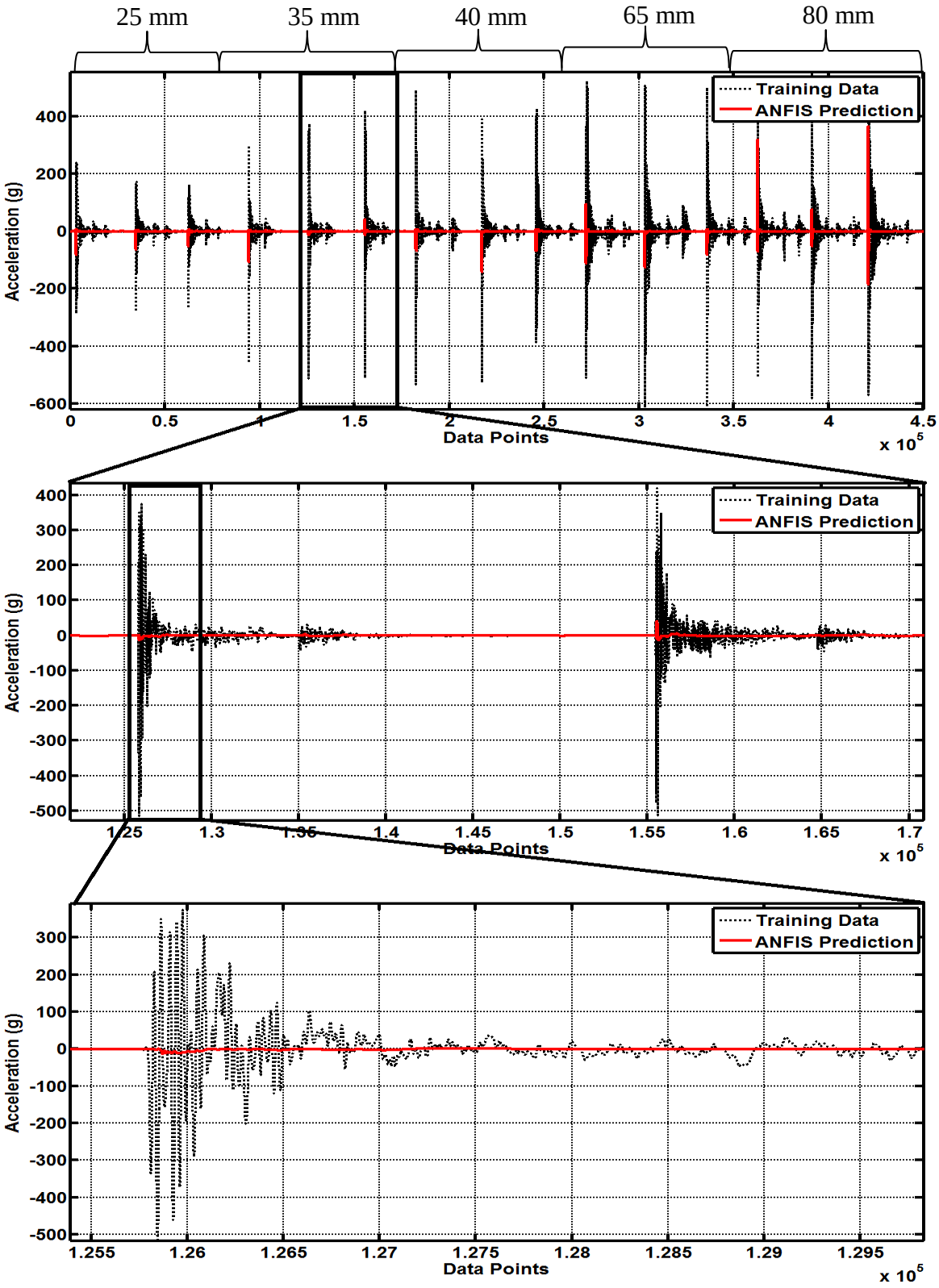

Figure 2-15. ANFIS (I)-RC: Acceleration training-random currents and different drop release heights

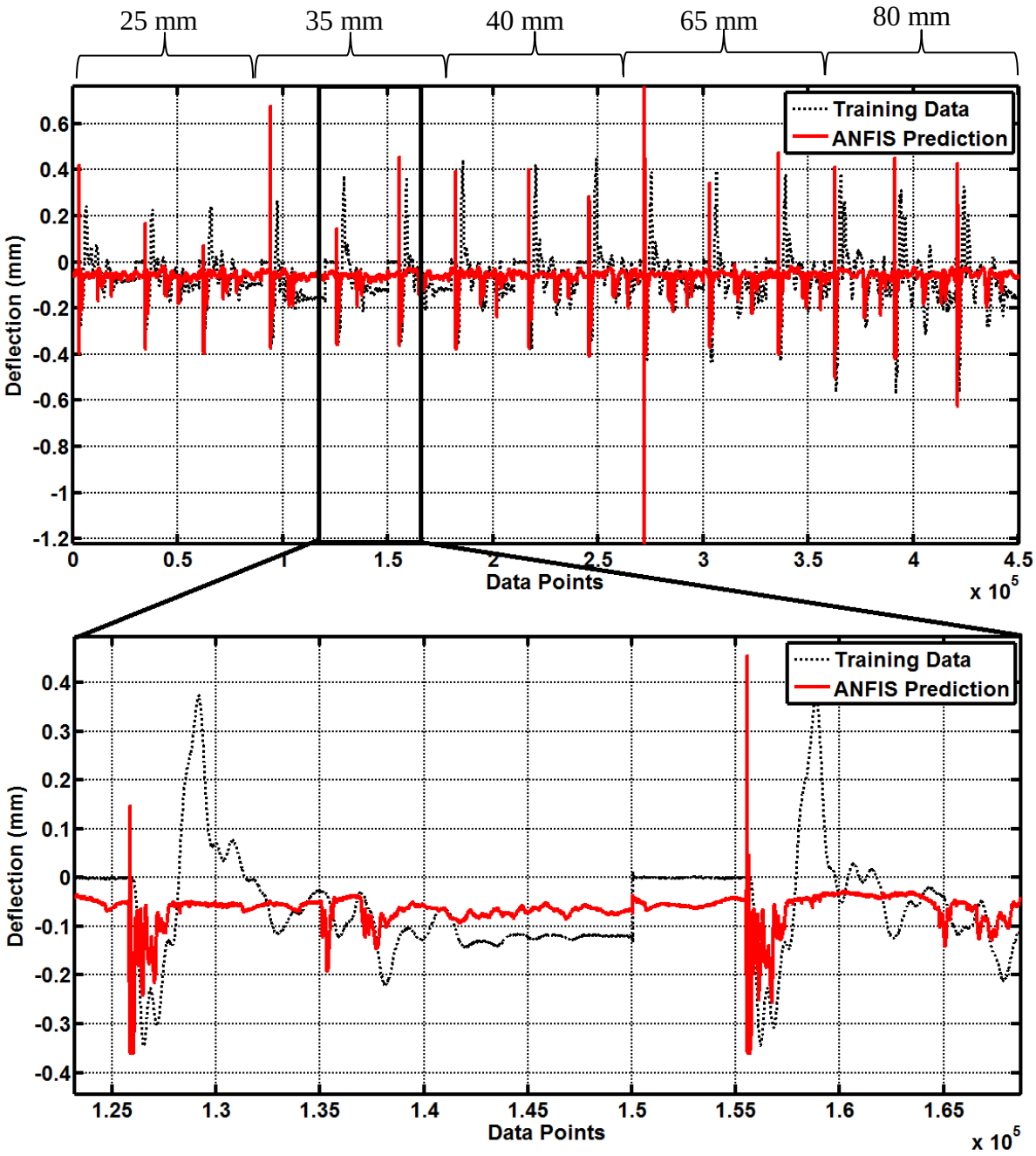

Figure 2-16. ANFIS (II)-RC: Deflection training-random currents and different drop release heights

It is shown from figures that for some cases there are no significant difference in structural responses for different current levels. It is discussed from Ahmadian and Norris (2008) that fluid inertia due to the initial impact prevents the MR fluid from traveling fast enough. As a result, the MR fluid does not accommodate the rapid displacement, resulting in traveling of the damper piston and accumulator piston at the same time.

For each different MR damper current and impact load case, ANFIS predictions are not in an agreement with the actual deflection and acceleration measurements. For this reason, a novel modeling framework is proposed by introducing a TANFIS model.

2.4.3. TANFIS modeling

Figure 2-17 and Figure 2-18 represents the conceptual configuration of the propsed TANFIS models. Figure 2-17 configures the training of the acceleration data (TANFIS (I)) while Figure 2-18 presents the training of deflection data (TANFIS (II)).

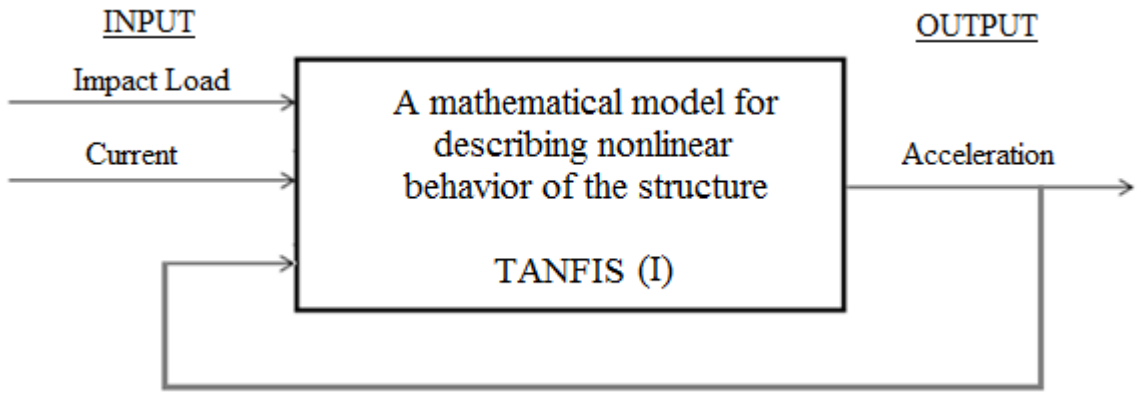

Figure 2-17. Configuration of the proposed TANFIS (I): Impact acceleration prediction

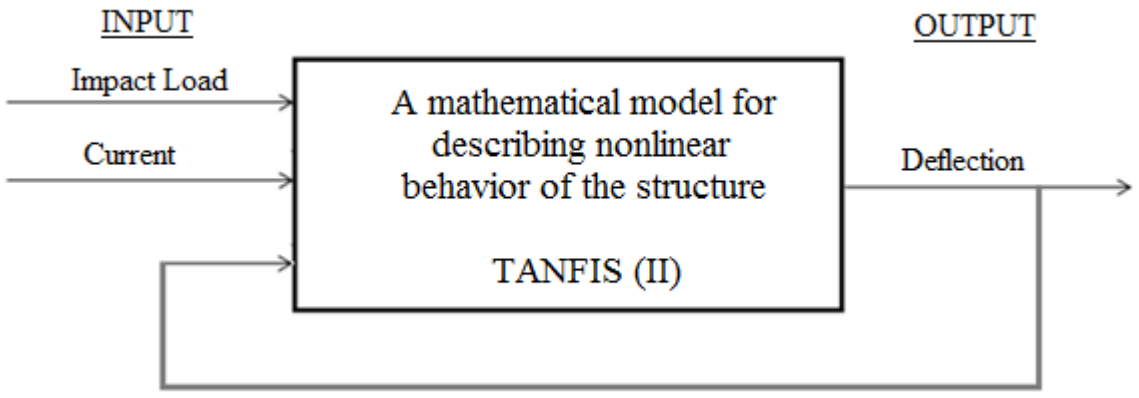

Figure 2-18. Configuration of the proposed TANFIS (II): Impact deflection prediction

Each input variable uses two MFs. The MFs of TANFIS (I) and TANFIS (II) are presented in Figure 2-19 and Figure 2-20. The left column shows the initial MFs values, while the right column represents the optimally tuned MFs.

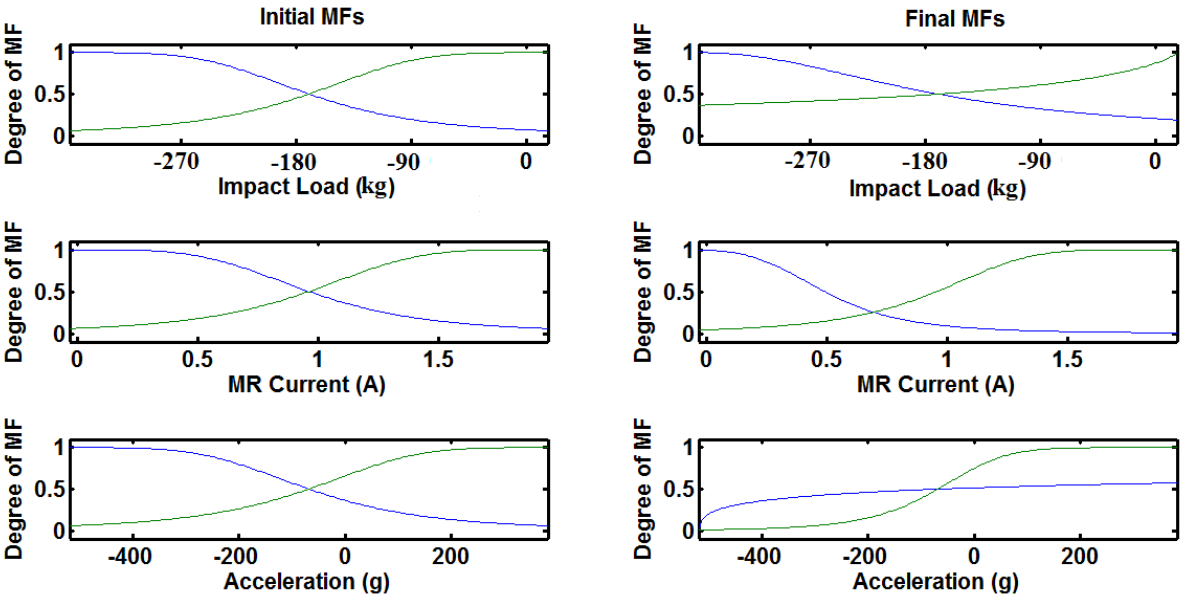

Figure 2-19. Initial and final membership functions: TANFIS (I)

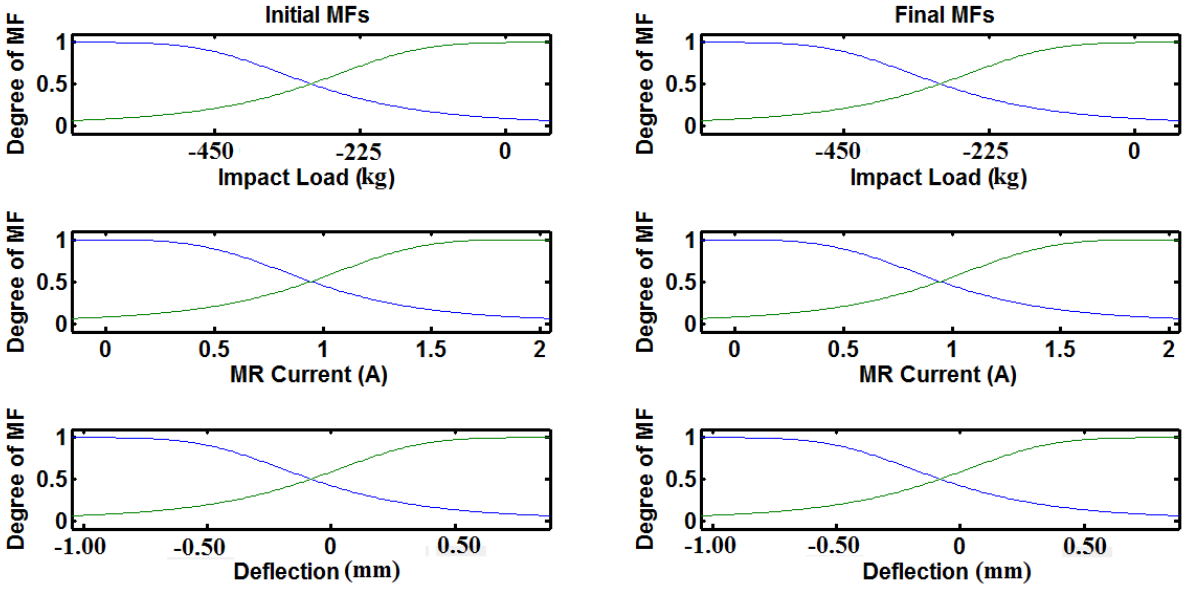

Figure 2-20. Initial and final membership functions: TANFIS (II)

Time steps and iterations of the TANFIS (I) and TANFIS (II) are presented in Figure 2-21 and Figure 2-22. For the TANFIS (I), both step size and iteration reached the training error goal at step 7 before reaching the assigned iteration, which means that iterations after step 7 do not have any contribution to the model accuracy. For the TANFIS (II), although the training error goal is not reached, 10 iteration is assumed enough since the predictions of the model have good performances.

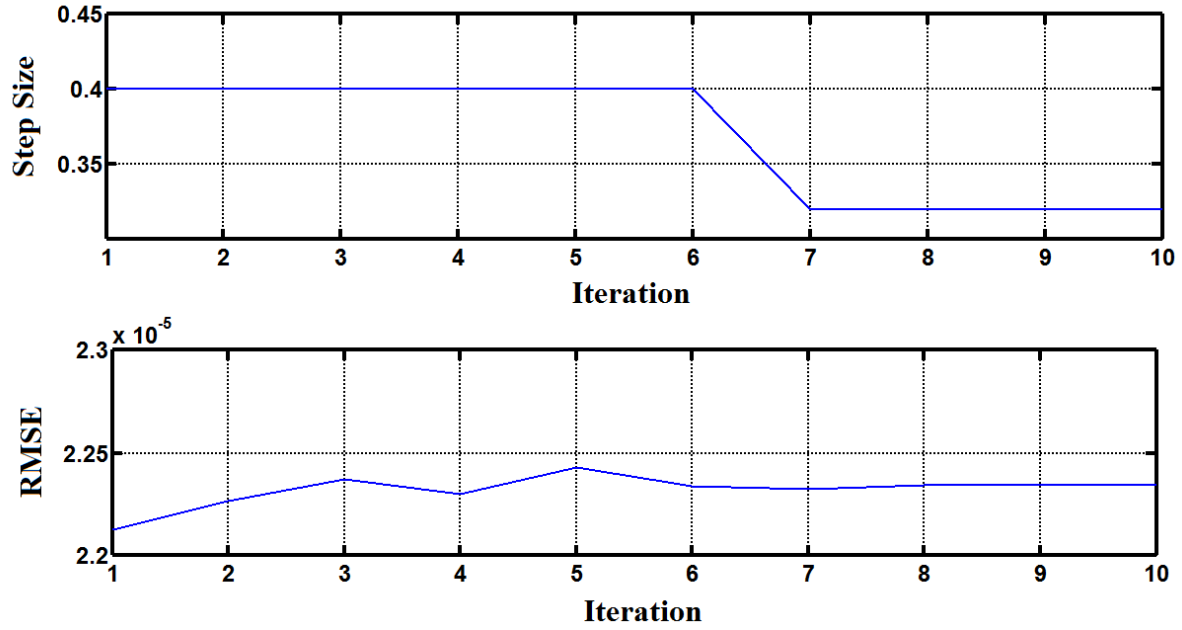

Figure 2-21. Step size and iteration: TANFIS (I)

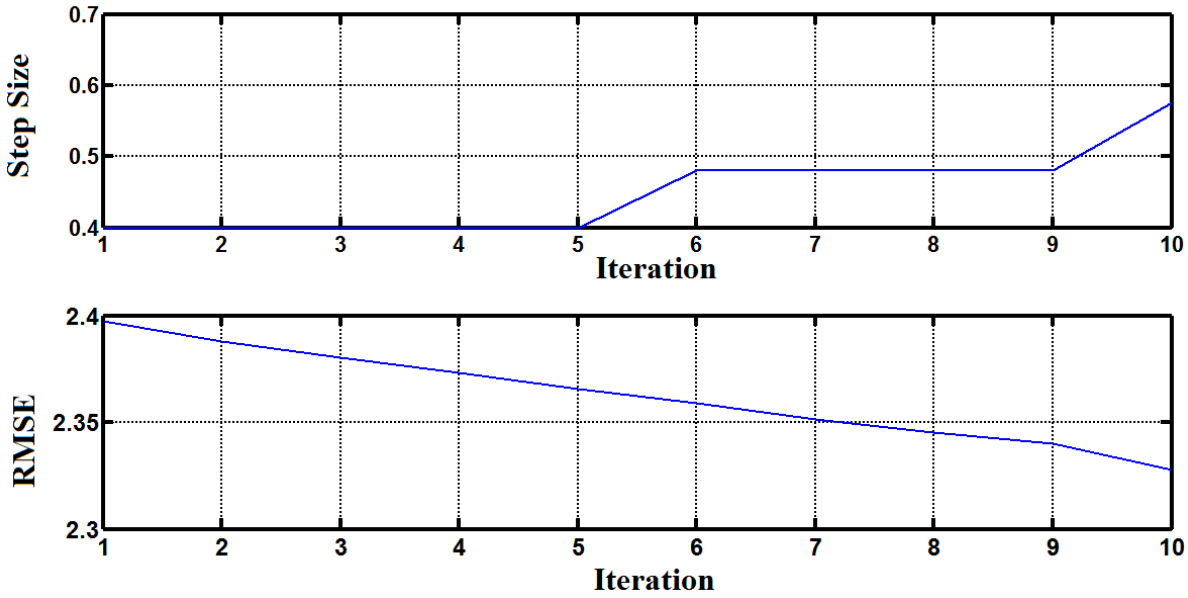

Figure 2-22. Step size and iteration: TANFIS (II)

With these parameter settings, Figure 2-23 and Figure 2-24 compare the real measured acceleration and deflection responses with the estimates from the proposed models for different drop release heights with a current level of 1.4 A. Figure 2-25 and Figure 2-26 depict the same comparison for various current levels: 0.6, 1, and 1.4. The response measurements, which are collected under random currents, are compared with TANFIS in Figure 2-27 and Figure 2-28.

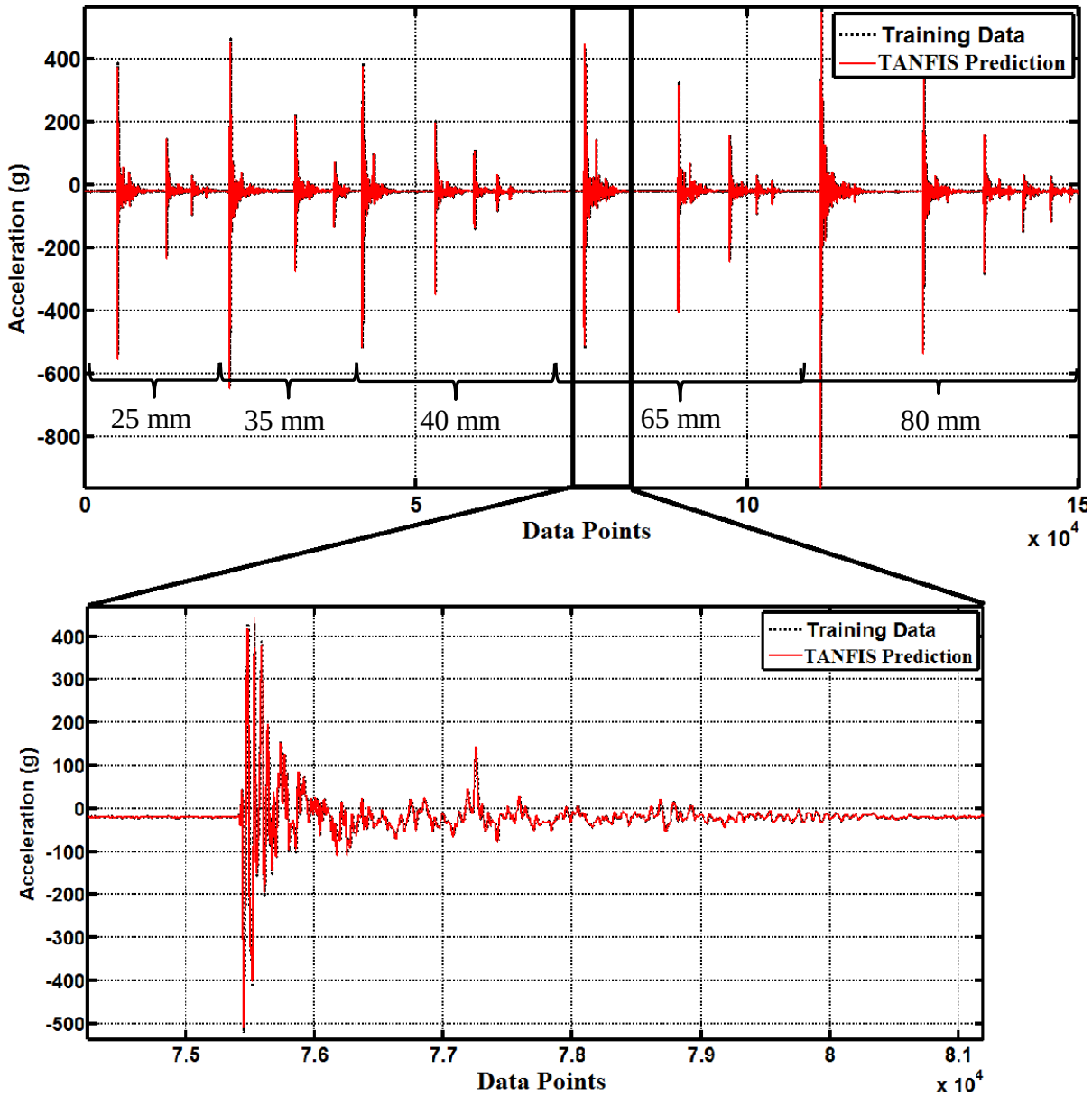

Figure 2-23. Acceleration training- constant current (1.4 A) and different drop release heights

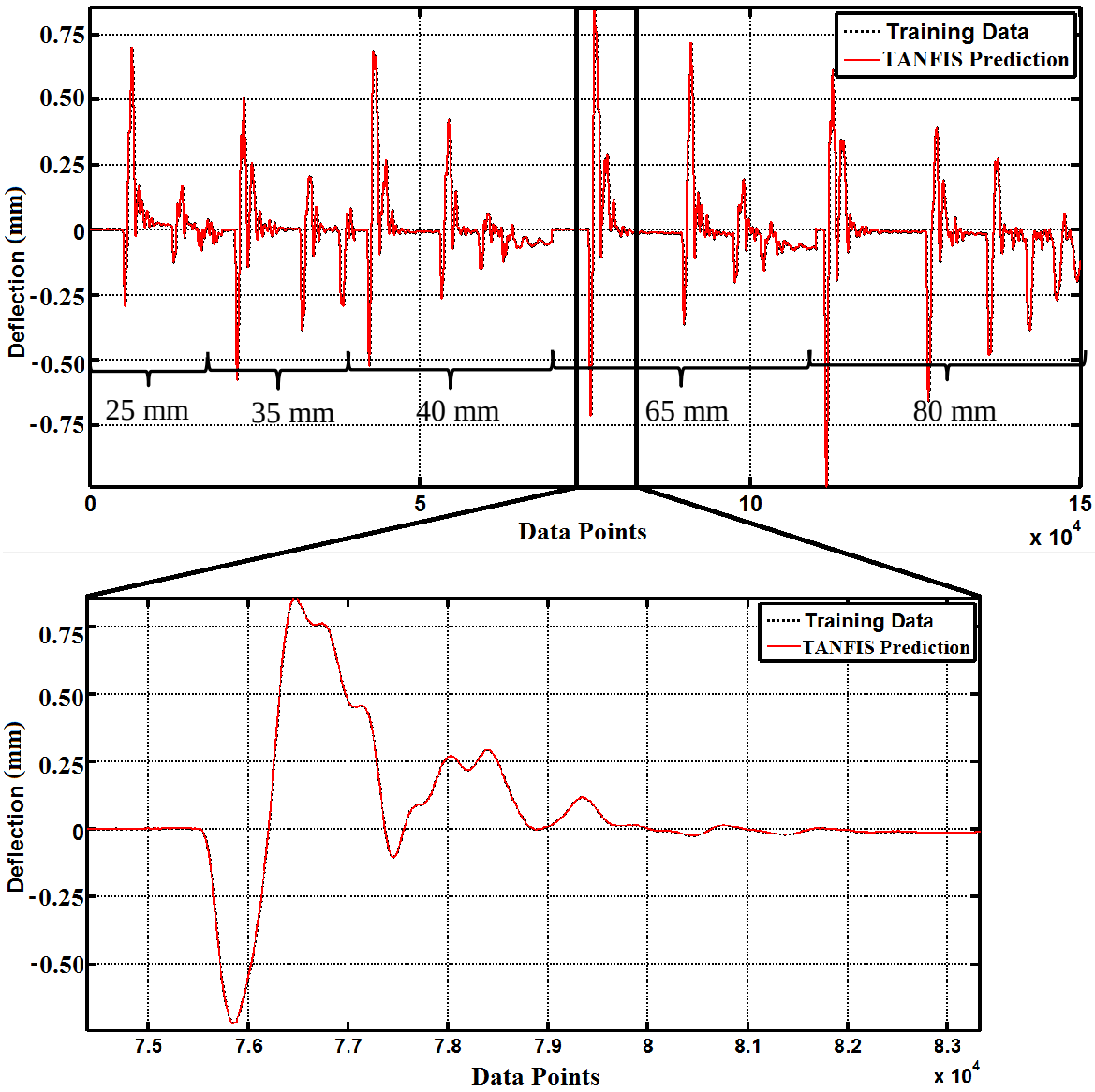

Figure 2-24. Acceleration training- constant current (1.4 A) and different drop release heights

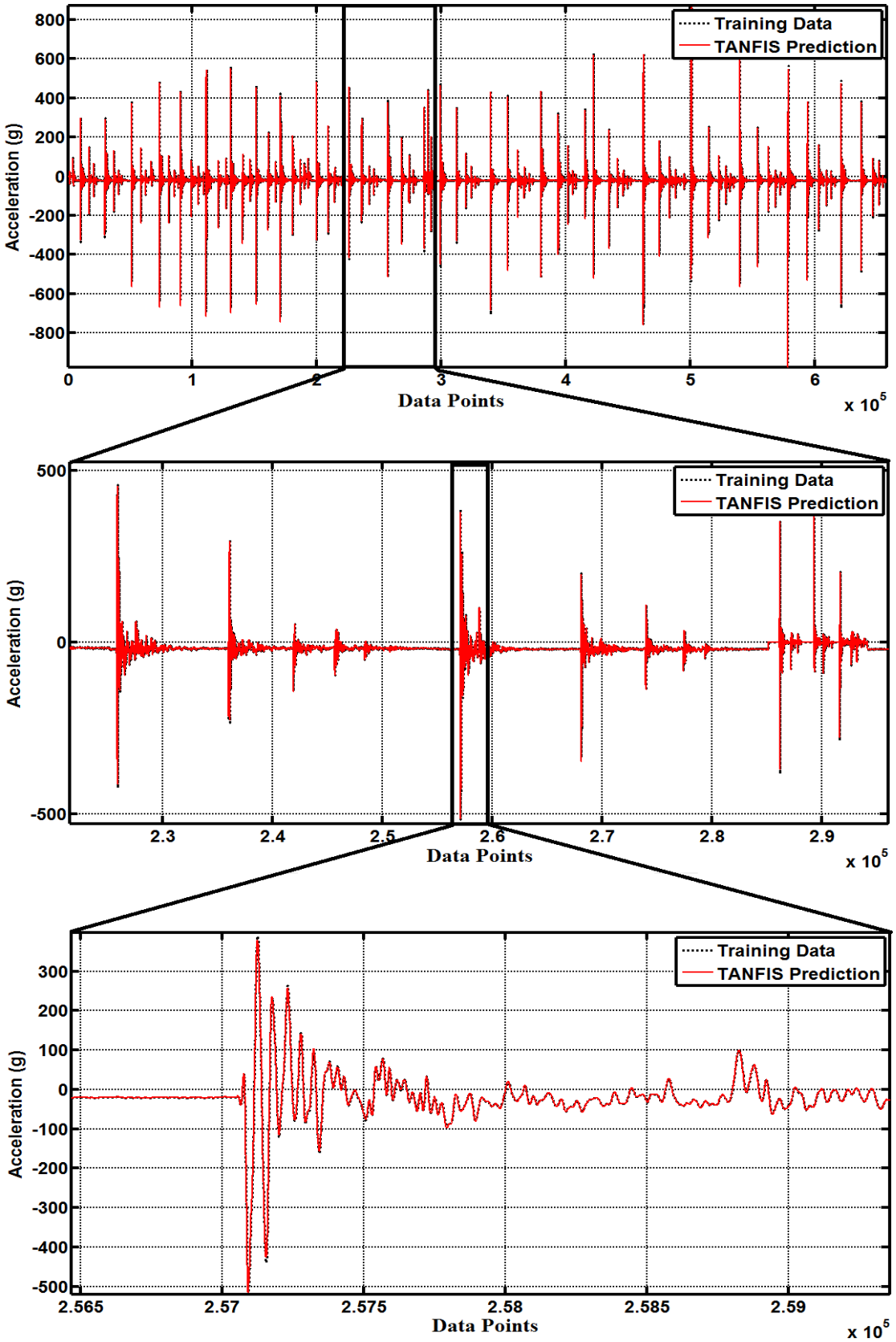

Figure 2-25. TANFIS (I)-CC: Acceleration training- constant currents and different drop release heights

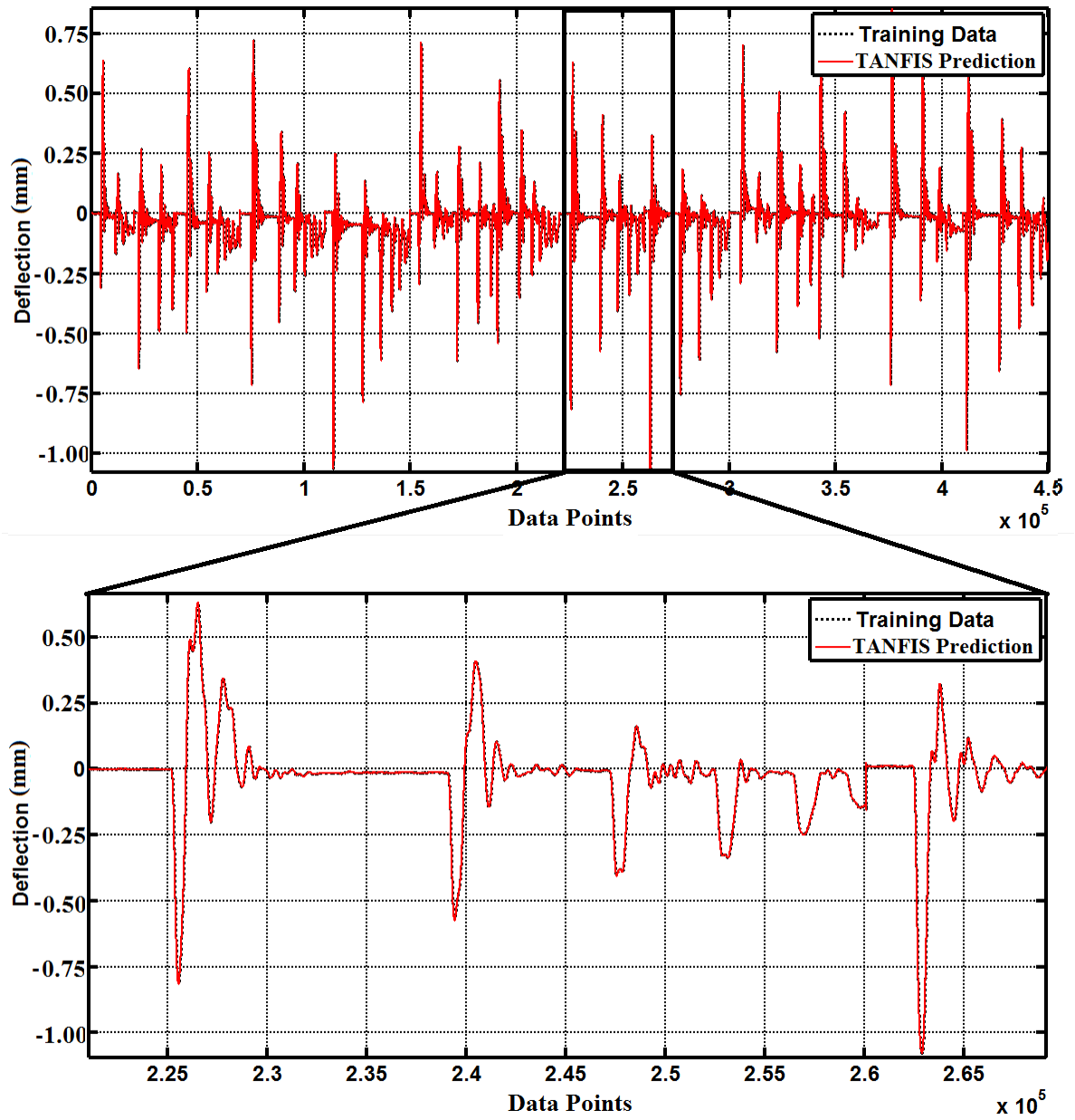

Figure 2-26. TANFIS (II)-CC: Deflection training- constant currents and different drop release heights

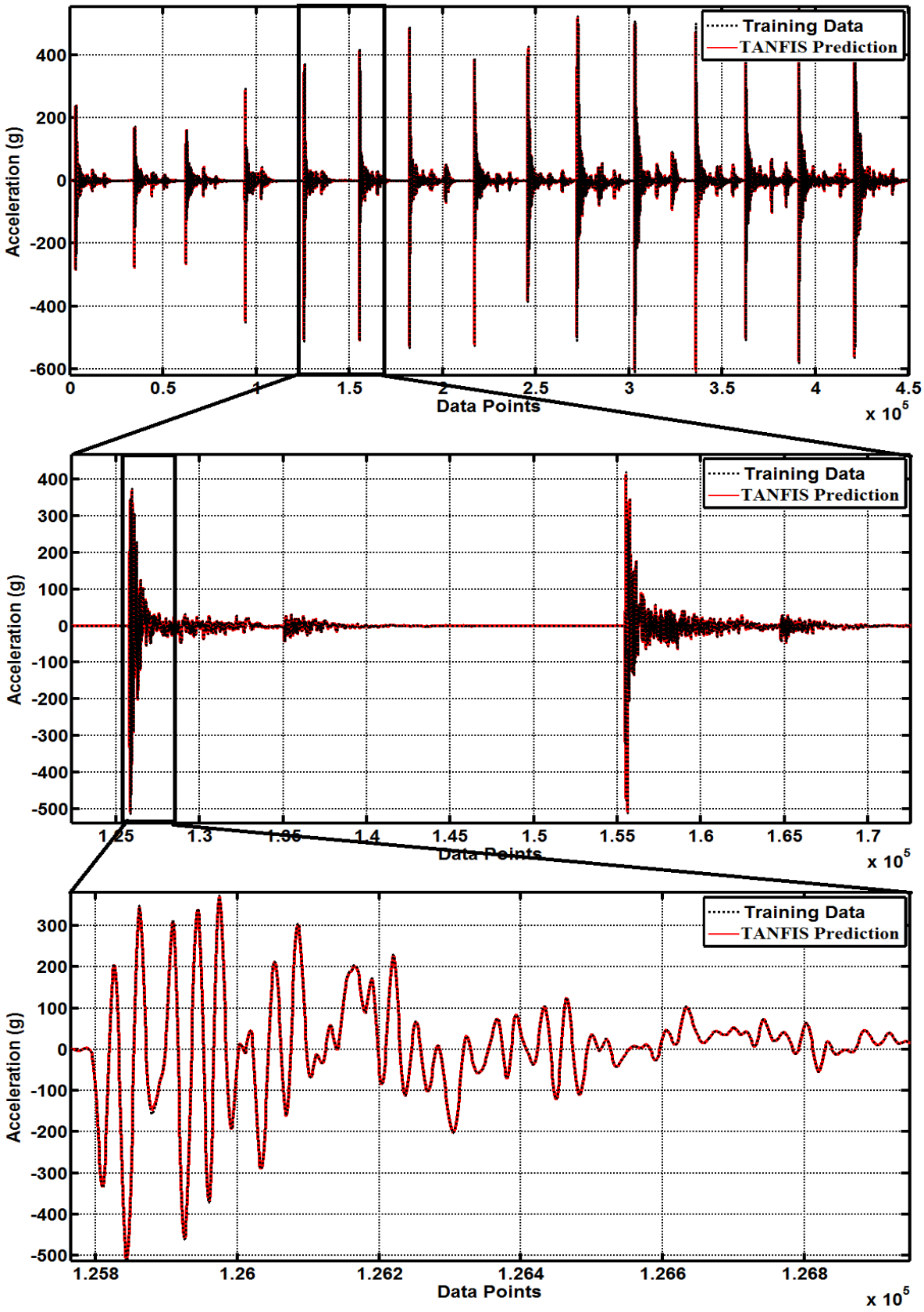

Figure 2-27. TANFIS (I)-RC: Acceleration training-random currents and different drop release heights

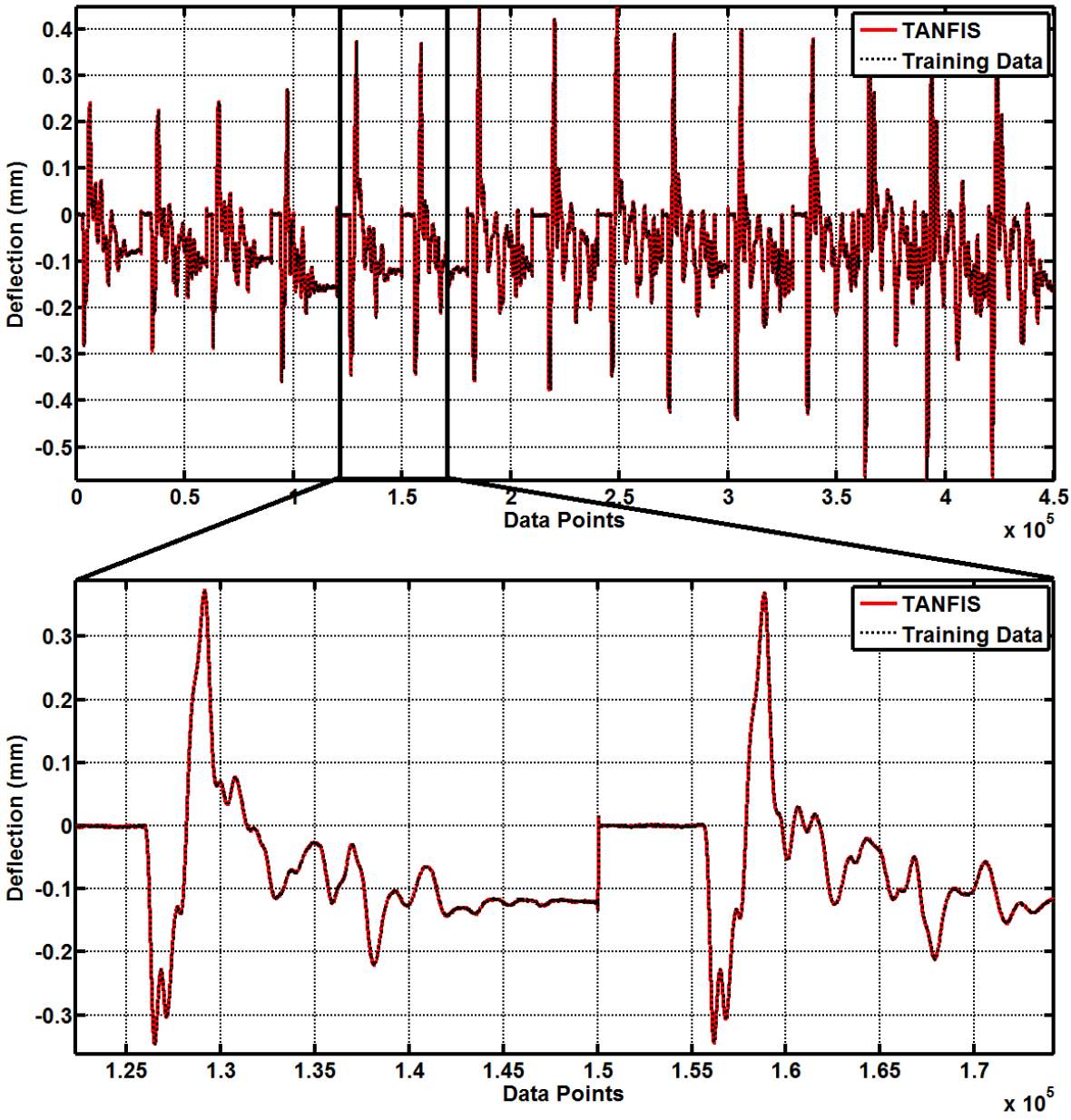

Figure 2-28. TANFIS (II)-RC: Deflection training-random currents and different drop release heights

There is a great agreement between the estimates and measurements. It is observed from the simulations that using TANFIS models increased the accuracy of the trained data significantly, compared to the ANFIS models. Based on this identified model using either random or constant current signals, an effective control system can be designed such that the impact responses of the structure are mitigated. The use of an adaptive control system makes the impact energy dissipation more effective (Mikułowski and Holnicki-Szulc, 2007).

To generalize the trained models, they are validated using different data sets that are not used in the training process. Figure 2-29 to Figure 2-36 exhibit the graphs of validated data sets.

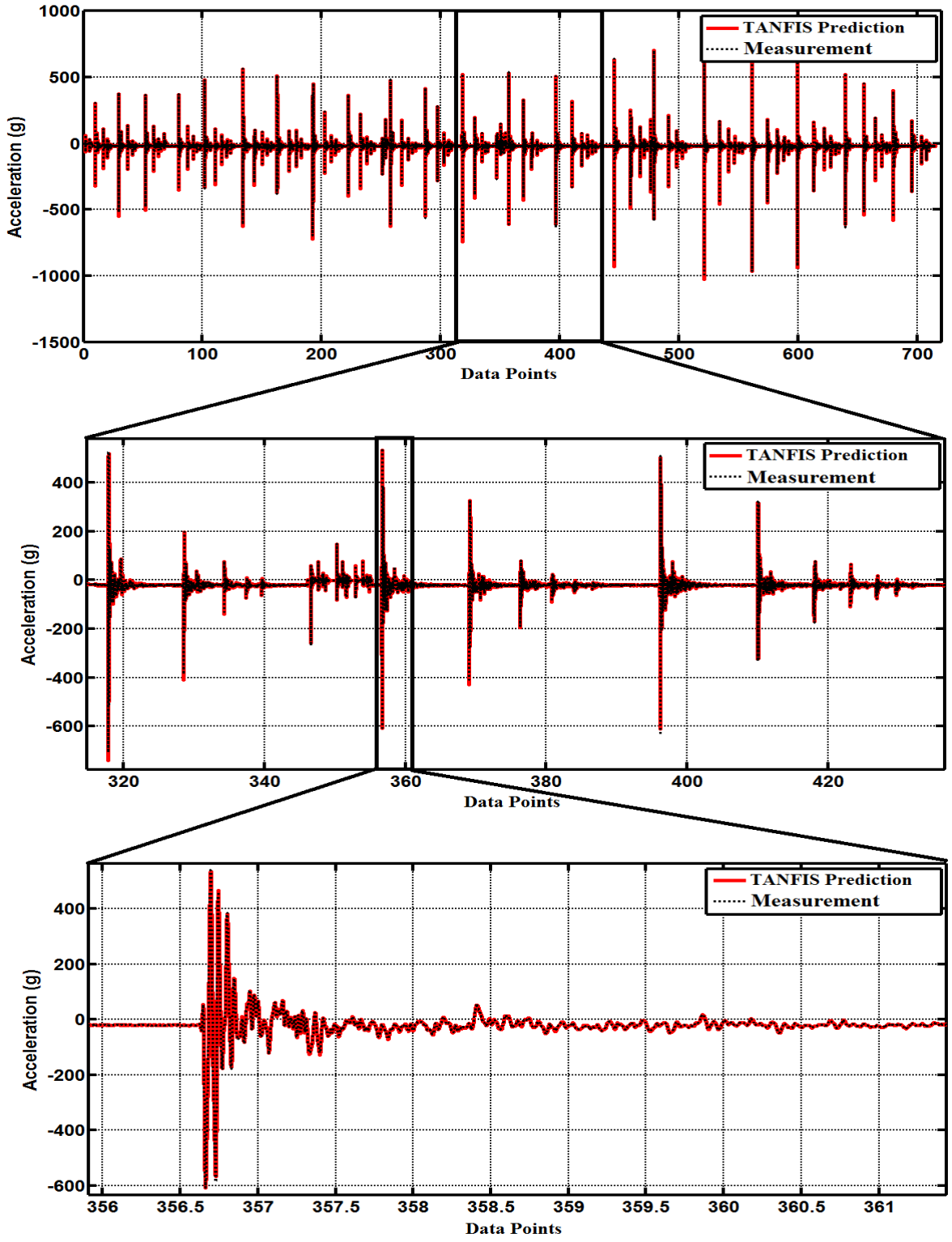

Figure 2-29. TANFIS (I)-CC-1 Acceleration-1st validation: Constant currents

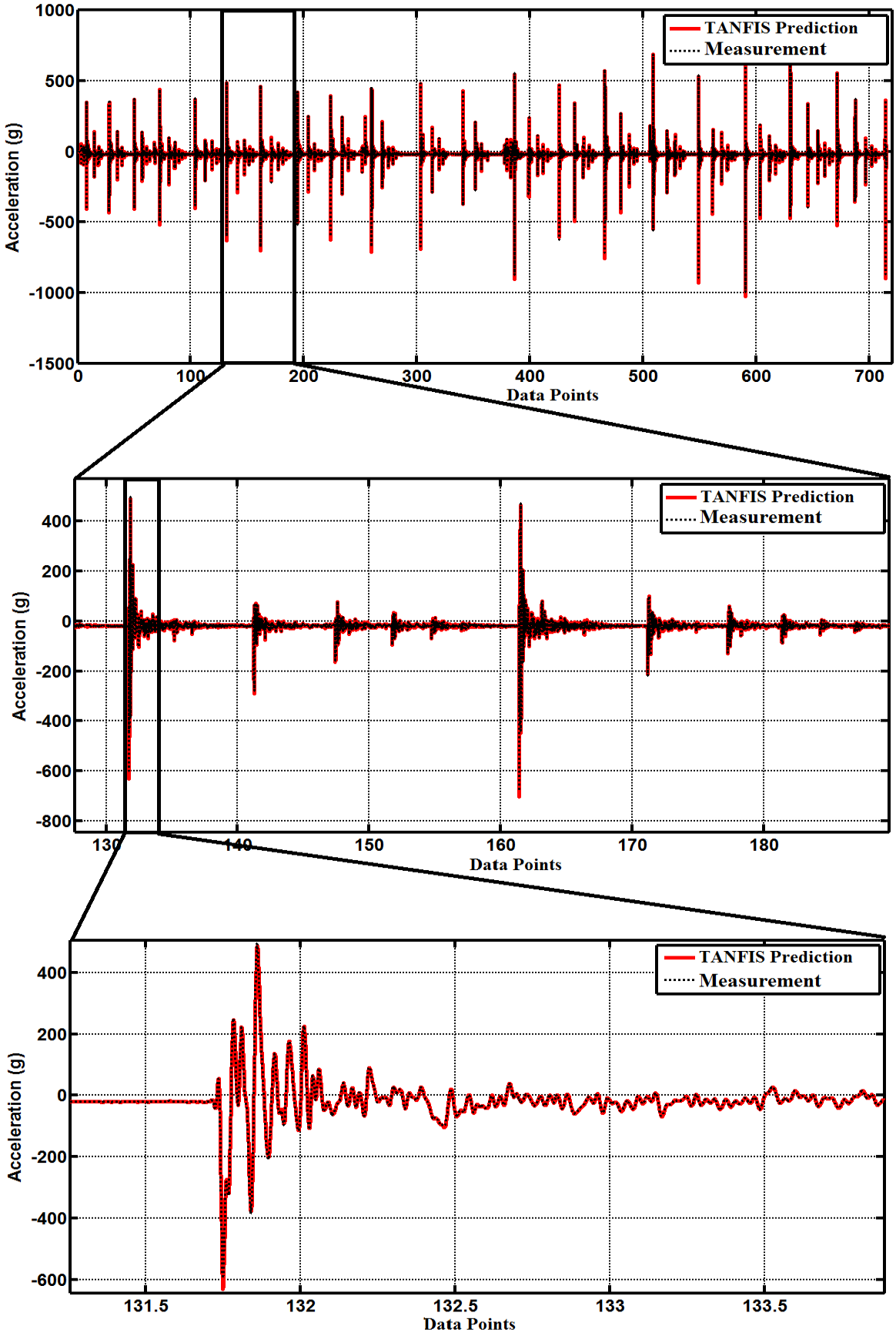

Figure 2-30. TANFIS (I)-CC-2 Acceleration-2nd validation: Constant currents

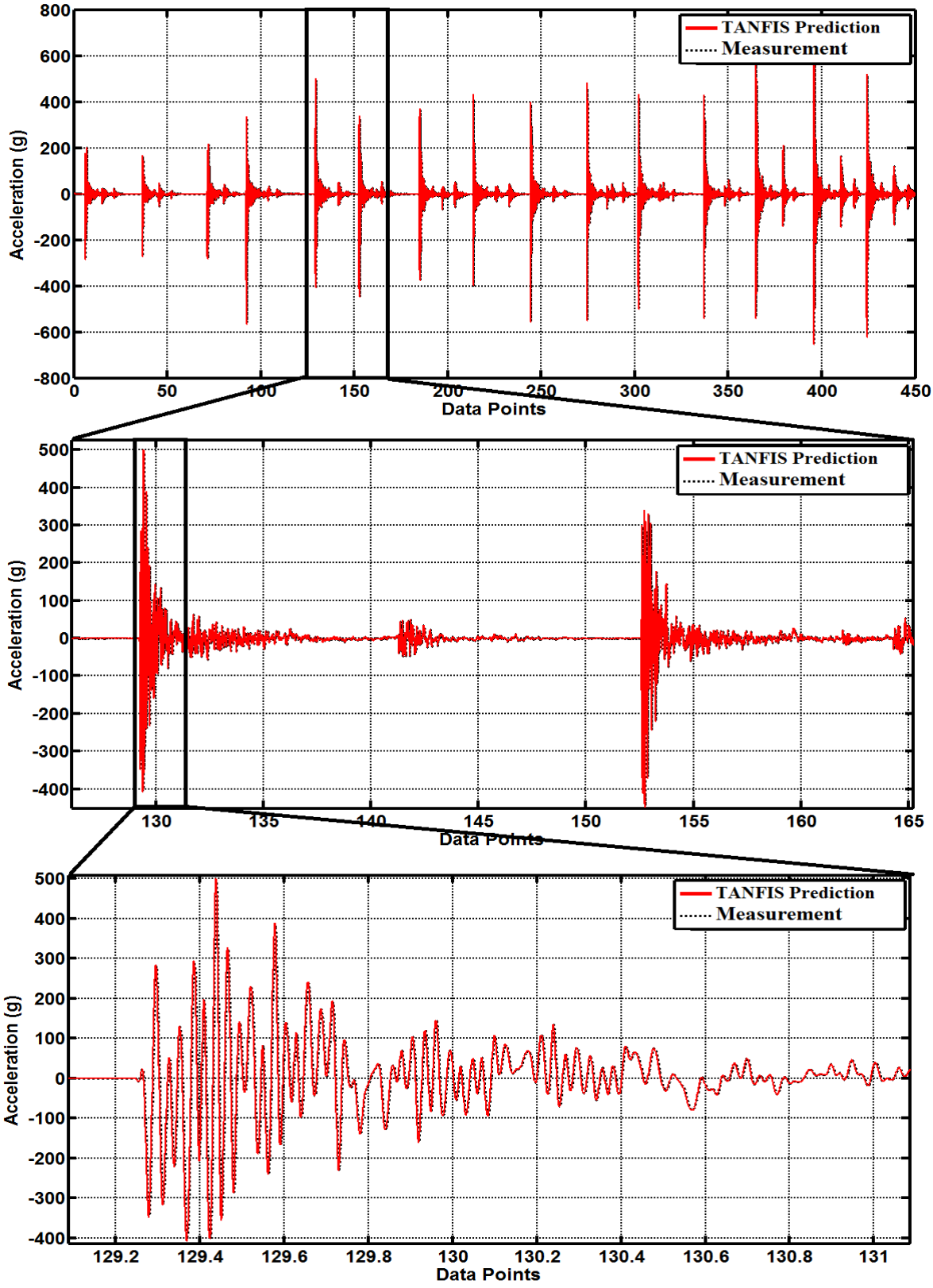

Figure 2-31. TANFIS (I)-RC-1 Acceleration-1st validation: Random currents

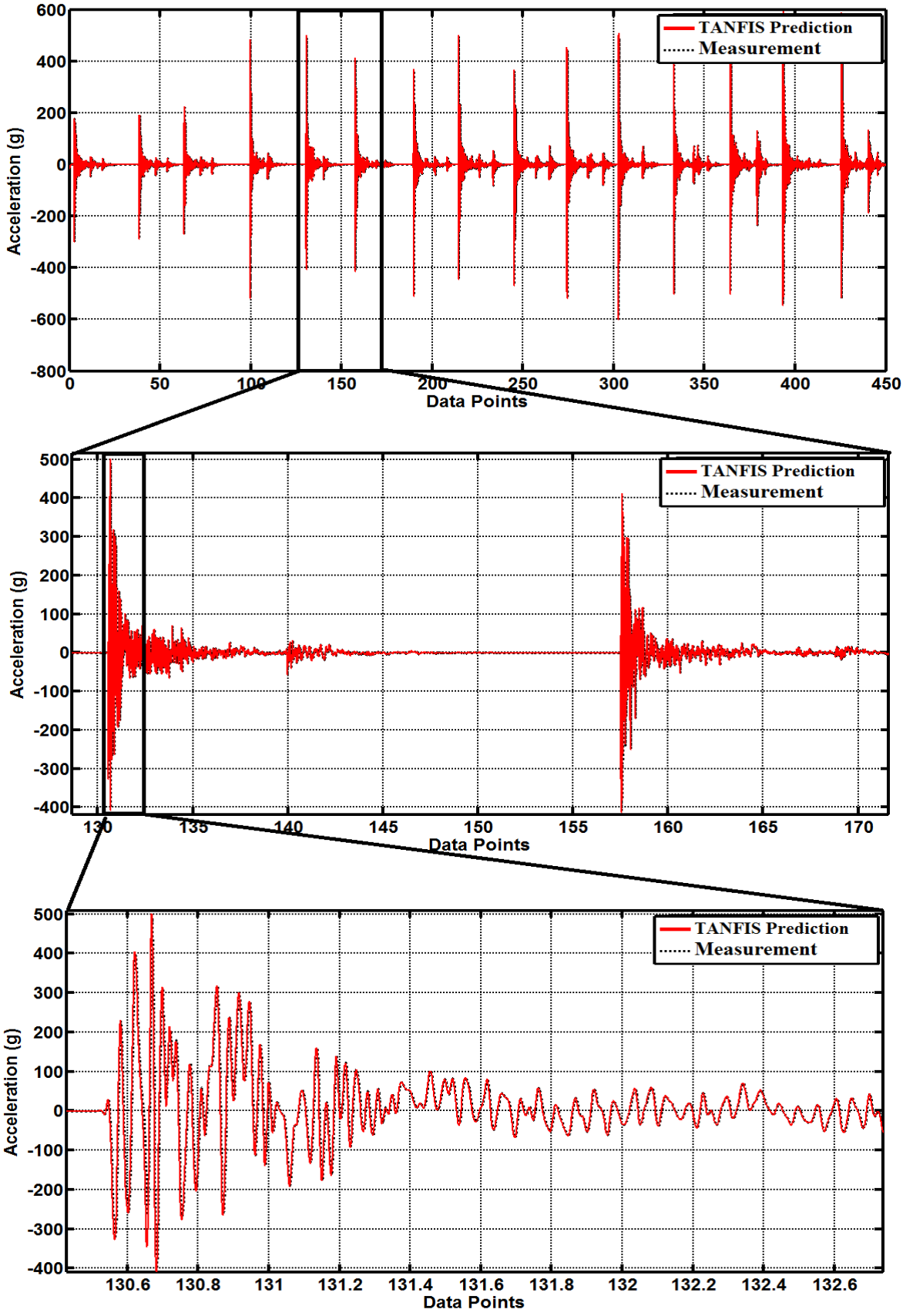

Figure 2-32. TANFIS (I)-RC-2 Acceleration-2nd validation: Random currents

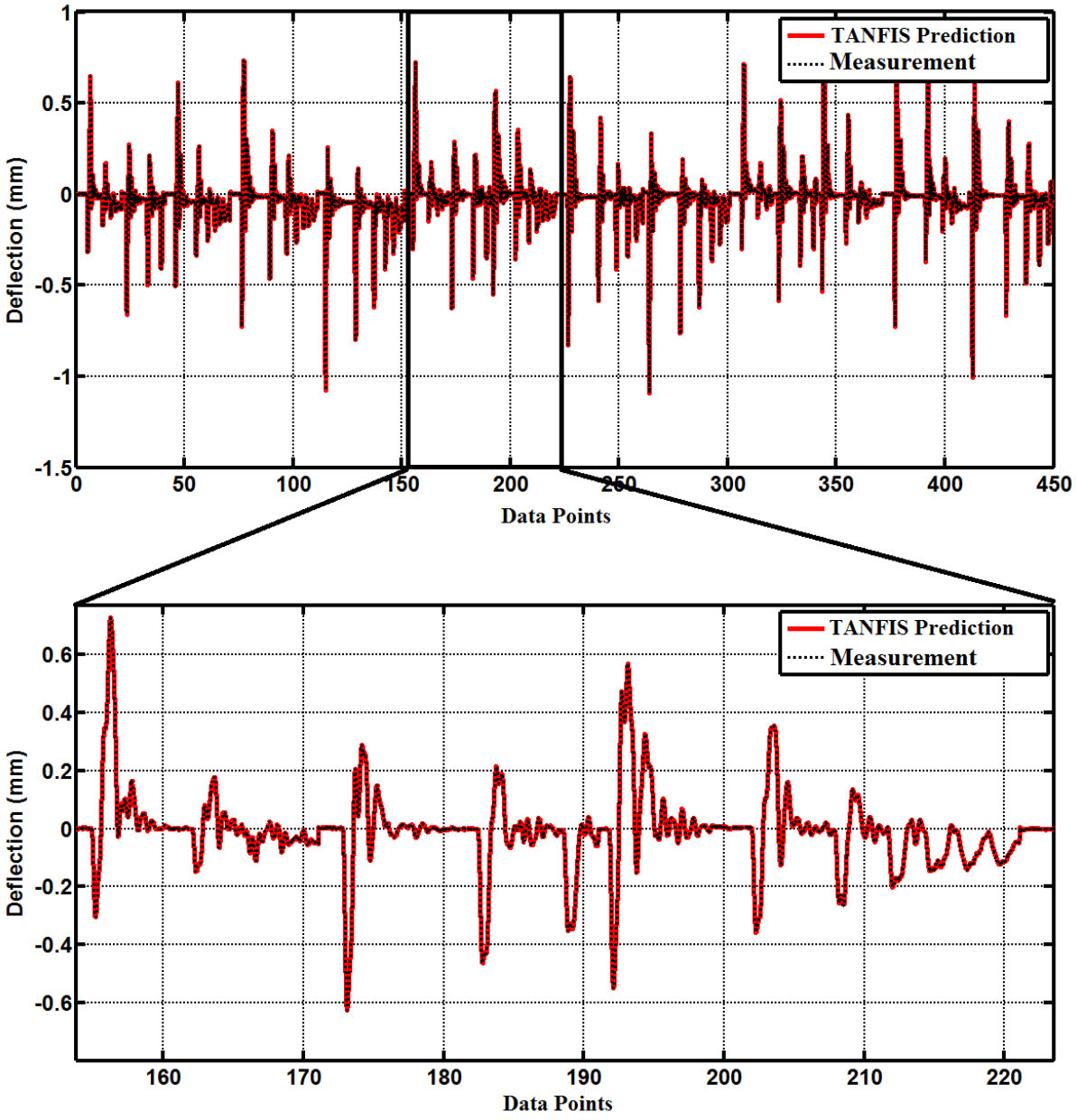

Figure 2-33. TANFIS (II)-CC-1 Deflection-1st validation: Constant currents

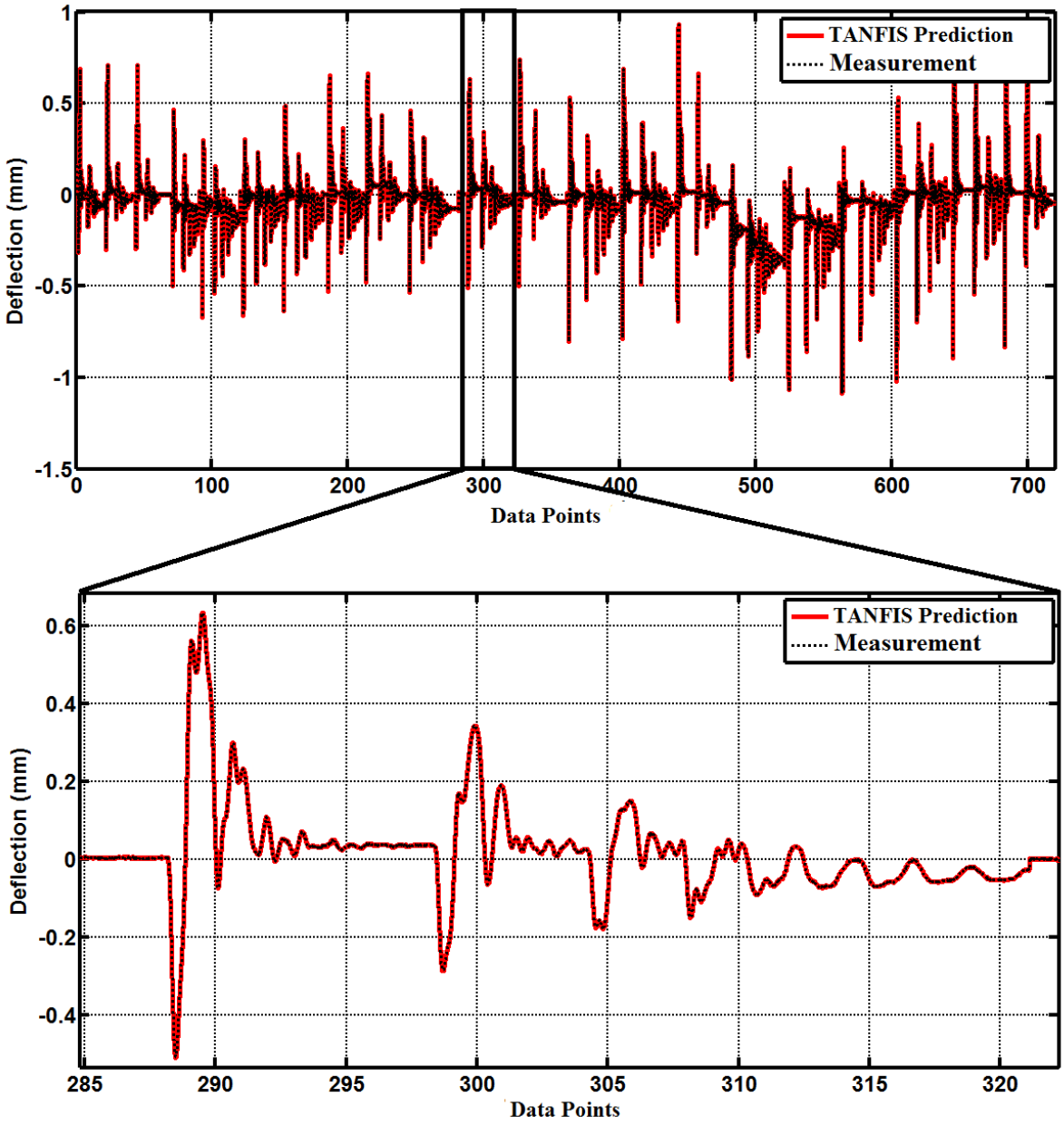

Figure 2-34. TANFIS (II)-CC-2 Deflection-2nd validation: Constant currents

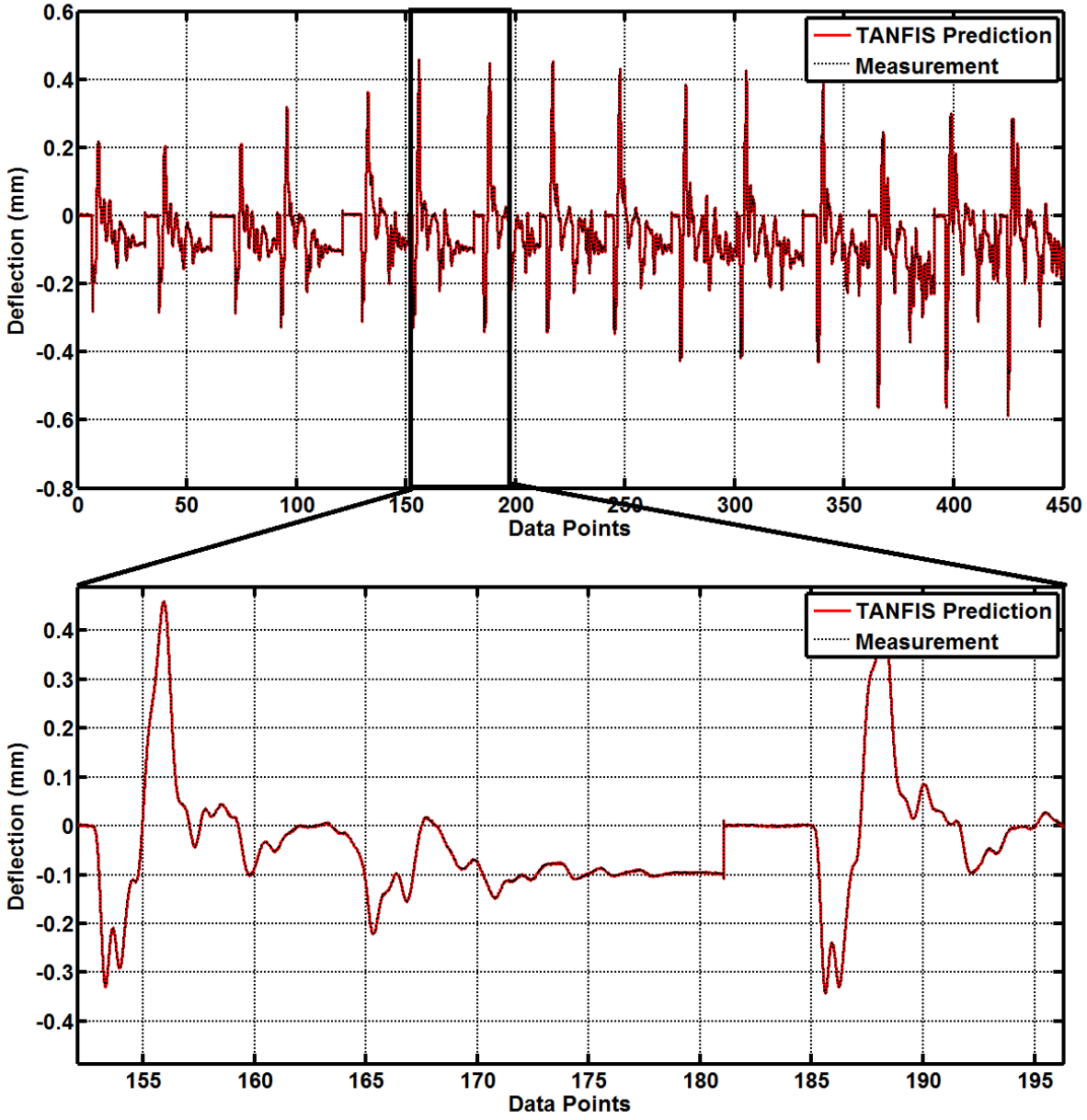

Figure 2-35. TANFIS (II)-RC-1 Deflection-1st validation: Random currents

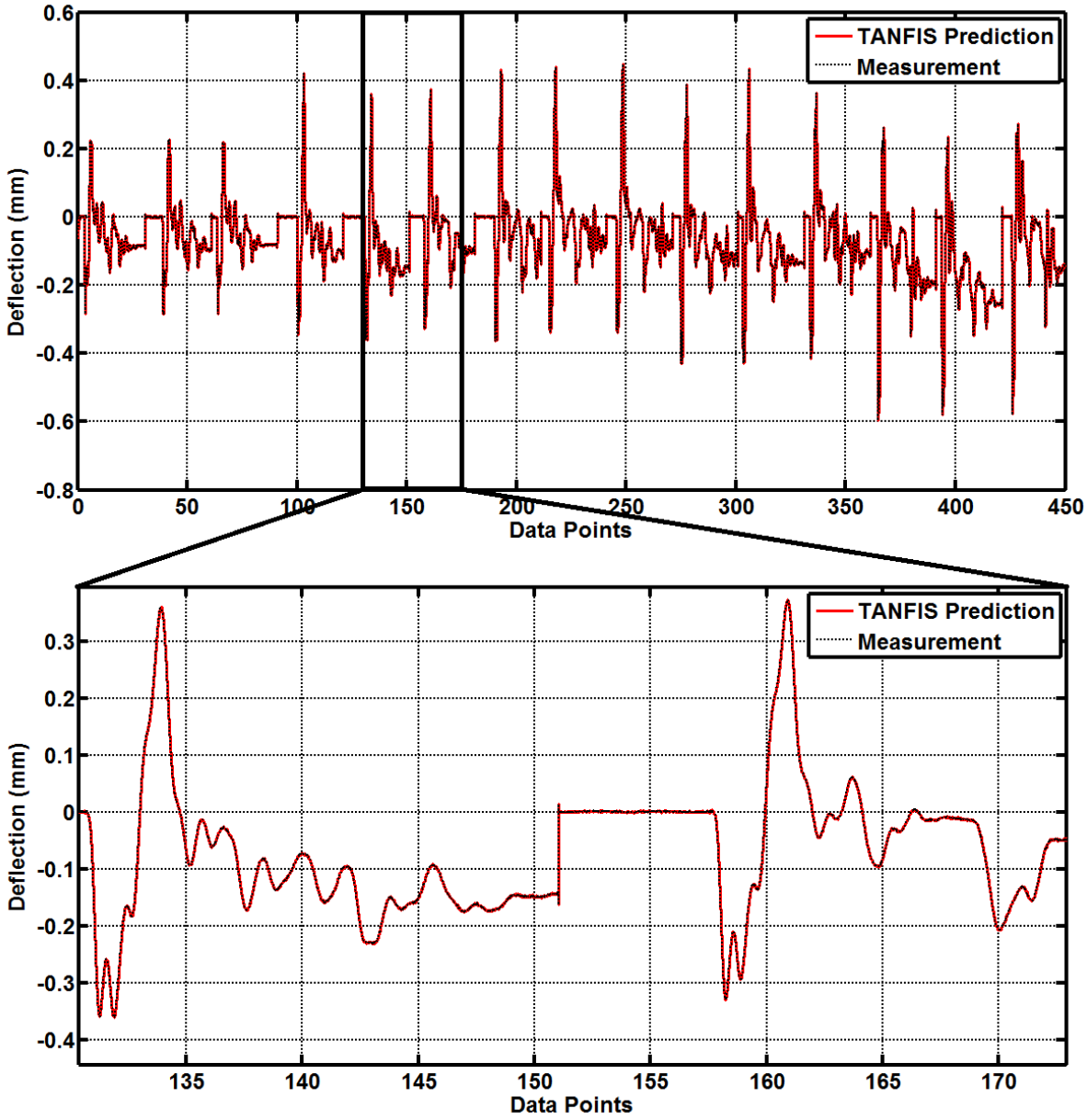

Figure 2-36. TANFIS (II)-RC-2 Deflection-2nd validation: Random currents

Trained model with random current signals are also validated by the data sets obtained from the beam employing MR damper with constant currents. Figure 2-37 to Figure 2-38 represents the graphs of validated data sets.

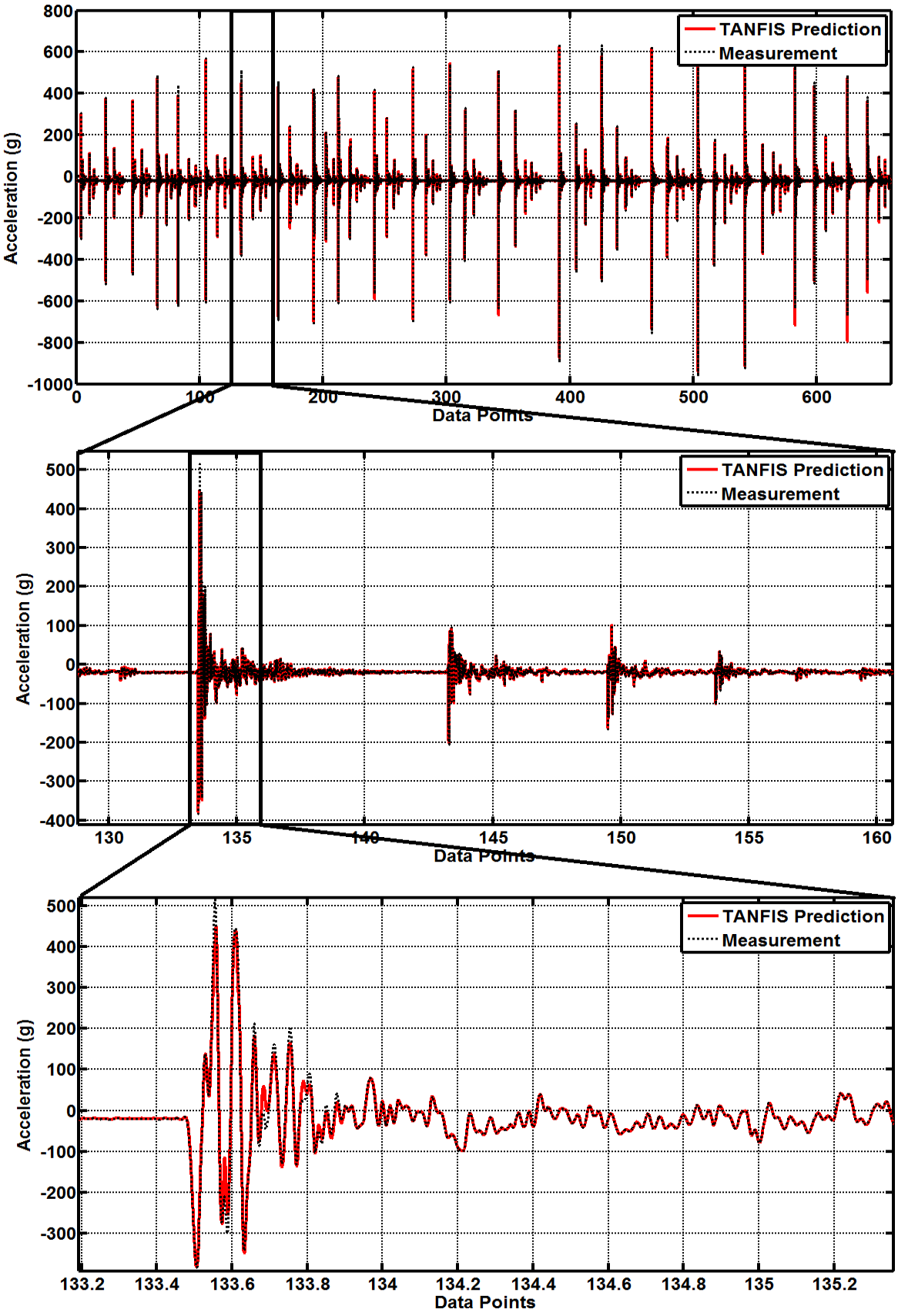

Figure 2-37. TANFIS (I)-RC-3 Acceleration-3rd validation: Random currents

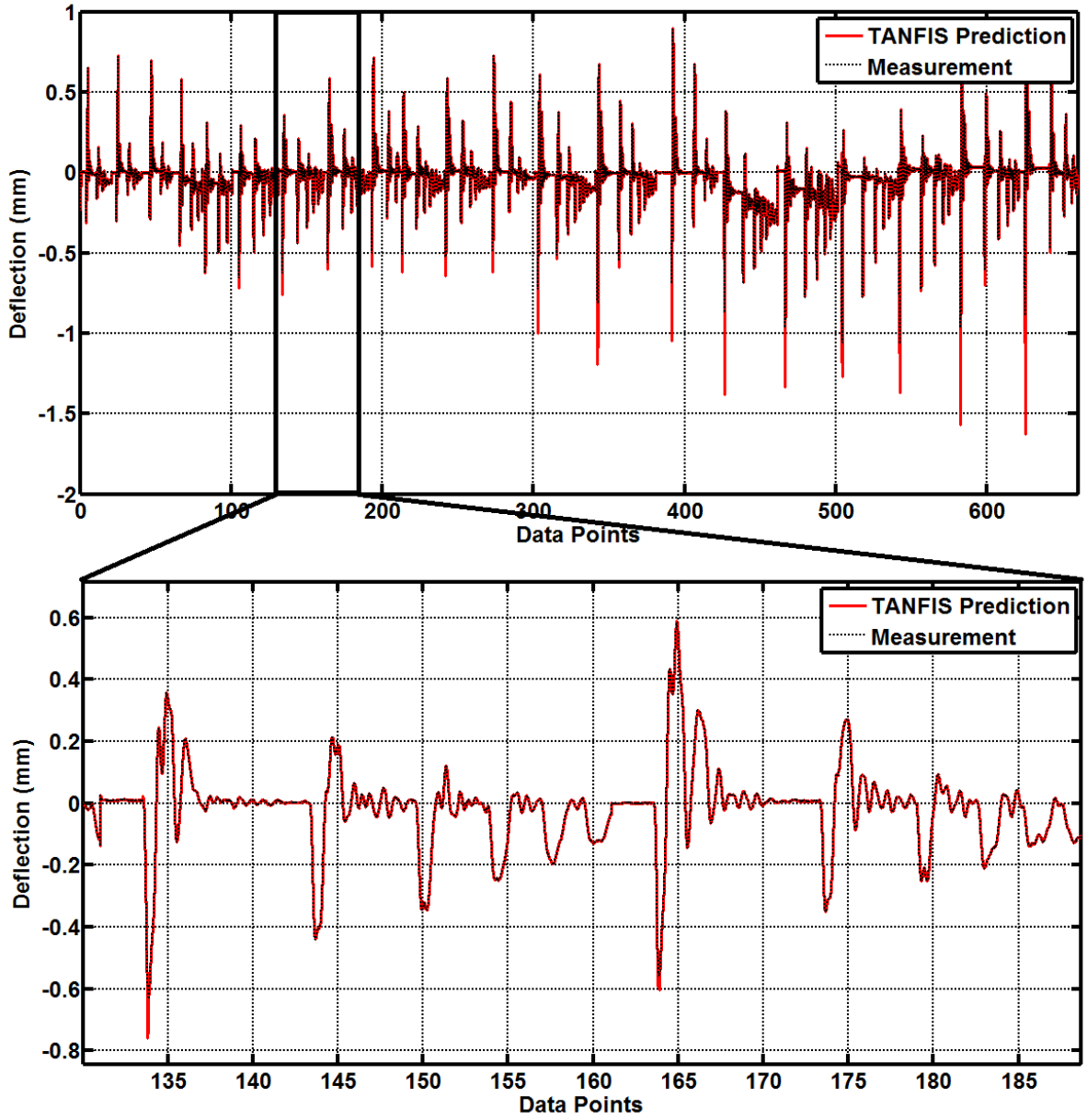

Figure 2-38. TANFIS (II)-RC-3 Deflection-3rd validation: Random currents

2.4.4. Evaluation of results

To demonstrate the effectiveness of the proposed TANFIS models, several evaluation indices are used. In the quantification of errors, first maximum absolute error is calculated as

$$J_1 = \max|\hat{y} - \tilde{y}| \tag{2-11}$$

where $\hat{y}$ is the trained data and $\tilde{y}$ is the actual measurements. Second evaluation criterion is defined as the mean of absolute error

$$J_2 = \text{mean}|\hat{y} - \tilde{y}| \tag{2-12}$$

Third criterion index is minimum absolute error

$$J_3 = \min|\hat{y} - \tilde{y}| \tag{2-13}$$

Formulation of the fourth evaluation index is as follows

$$J_4 = \left[1 - \frac{\text{var}(\hat{y} - \tilde{y})}{\text{var}(\hat{y})}\right] \times 100 \tag{2-14}$$

where var represents the variance of data. The better the trained model predicts the measurement results accuratly, the more the fitting rate of index J_4 will become close to 100. The last evaluation index J_5 is assigned as the CPU time to evaluate the duration of the training and validation time. Table 2-3 shows the results of the error between the trained and actual data.

Table 2-3. Error Quantities of the ANFIS and TANFIS Models

		J_1 (Unit)	J_2 (Unit)	J_3 (Unit)	J_4 %	J_5 (Sec.)
Training	ANFIS (I)- CC	499.306	6.3334	4.181e-5	21.617	2,868.830
	ANFIS (II)- CC	0.0431	0.0029	2.115e-9	37.951	21,674.932
	ANFIS (I)- RC	626.233	9.8950	5.524e-6	1.8233	3,800.837
	ANFIS (II)- RC	0.0218	0.0013	5.517e-10	13.669	3612.199
	TANFIS (I)- CC	39.512	0.2113	7.973e-7	**99.328**	**55.545**
	TANFIS (II)- CC	2.348e-4	3.974e-6	3.330e-12	**99.999**	**4,238.564**
	TANFIS (I)- RC	50.605	0.1127	5.908e-10	**98.835**	**1,567.908**
	TANFIS (II)- RC	2.283e-5	7.008e-13	1.328e-13	**99.999**	**1,509.422**
Validation	TANFIS (I)-CC-1	112.135	0.771	1.073e-6	**98.658**	
	TANFIS (I)-CC-2	74.249	0.736	8.569e-9	**98.841**	
	TANFIS (I)-RC-1	133.977	1.053	7.013e-8	**97.248**	
	TANFIS (I)-RC-2	220.743	0.959	4.729e-8	**97.305**	
	TANFIS (I)-RC-3	478.462	1.205	5.786e-8	**95.518**	
	TANFIS (II)-CC-1	6.768e-4	1.168e-5	2.738e-12	**99.991**	
	TANFIS (II)-CC-2	0.001	1.130e-5	1.809e-11	**99.992**	
	TANFIS (II)-RC-1	4.141e-4	2.953e-6	5.203e-12	**99.996**	
	TANFIS (II)-RC-2	4.892e-4	3.0897e-6	3.971e-12	**99.985**	
	TANFIS (II)-RC-3	0.753	0.001	2.582e-11	**97.903**	

It is observed that although the TANFIS and ANFIS use the same input-output data, the performance of the TANFIS models are much better than the ANFIS with dramatically reduced computational loads. For the TANFIS models, the J_4 is almost 100, which means that the proposed TANFIS model is very effective in predicting the dynamic responses of the smart systems under high impact loading. It is also noted that the duration required to train the TANFIS model is significantly less than the ANFIS model.

2.5. Conclusion

In this paper, a new time-delayed adaptive neuro fuzzy inference system (TANFIS) model is proposed for modeling nonlinear impact responses of smart structures equipped with highly nonlinear hysteretic control devices under high impact loadings. To demonstrate the effectiveness of the proposed system, an aluminum beam structure is investigated. The beam employs two MR dampers whose fluids are controlled with either constant or random currents, while the beam without any MR damper is used as a baseline. To train the proposed TANFIS models, high impact loads and current signals are used as input signals while the acceleration and deflection responses are used as output signals. Importance of the current level selection on the effectiveness of magnetorheological (MR) damper performance is confirmed with the test

results. As a baseline model, a traditional adaptive neuro fuzzy inference system (ANFIS) is trained using the same sets of the input and output signals; it does not give the reasonable match between the trained and actual test data, while the proposed TANFIS model is effective in predicting both deflection and acceleration responses of smart structures. Also, the trained TANFIS models are validated using different data sets that are not used in the training process. It is demonstrated from both the training and validation results that the proposed TANFIS is very effective in estimating nonlinear behaviors of structures equipped with highly nonlinear hysteretic MR damper systems under a variety of high impact loads.

3. Nonlinear System Identification of Smart Reinforced Concrete Structures under Impact Loads

3.1. Introduction

In recent years, response analysis of complex structures under impact loads has attracted a great deal of attention. For example, a collision or an accident that produces impact loads that exceed the design load can cause severe damage to the structural components. It may affect the structural integrity of the members (Sharma et al. 2008, 2012; Consolazio et al., 2010), as shown in Figure 3-1. However, such damage on structures can be significantly reduced through impact force attenuations, using optimized smart control systems. The use of smart control systems in the field of civil engineering has become an attractive topic due to its effectiveness to absorb and dissipate the external energy in real time. Specifically, magnetorheological (MR) dampers, which are used as both passive and active controllers, have received great attention for use in complex structural systems (Spencer et al., 1997; Hurlebaus and Gaul 2006). The effectiveness of this technology in civil engineering applications has been demonstrated by many investigations (Dyke et al. 1996, 1998, 2001; Yi et al. 1998, 1999; and Kim et al. 2009, 2010).

On the other hand, the performance of MR dampers under impact forces has been studied relatively less. One of these studies was performed by Wang and Li (2006). The purpose of their study was to investigate the behavior of MR shock absorbers under impact loads. MR dampers subjected to impact loading was modeled by using the Herschel-Bulkley model. Experimental studies were performed on the long-stroke MR shock absorber under impact loads, and the results were compared with the Herschel-Bulkley model. Comparison of the experimental test and the model showed that the results are similar to each other in nature, but not quantitatively. Another study was performed by Ahmadian and Norris (2008). In the study, force-displacement characteristics of MR dampers were investigated for different impact velocities with various current signals. A drop-tower setup was developed to apply impulse loads to the MR dampers. Two MR damper configurations were tested: a damper with a single-stage, double-ended piston and a mono-tube damper with a two-stage piston. To investigate the flow behavior of MR fluid under impact loads, a theoretical model of the accumulator was derived. Results demonstrated that the fluid inertia due to the initial impact prevents the MR fluid from accommodating rapid displacement. Initial impact was absorbed by the pre-loaded spring effect, which is created by the compression of the accumulator. The comparison of the theoretical and experimental study

showed that the forces associated with shearing the MR fluid resulted in a difference between the theoretical accumulator force and the experimental force. Hongsheng and Suxiang (2009) developed a dynamic model for MR dampers and developed a fuzzy controller to increase the effectiveness of the MR absorber under impact loads. Herschel-Bulkley model was used to define the important parameters of an MR damper. The model was integrated into fuzzy and fuzzy PID control models. Experiments were performed and the results showed that the designed MR damper can effectively reduce the shock vibration. Mao et al. (2007) focused on the theoretical analysis, design, and laboratory implementation of MR dampers under shock and impact loads.

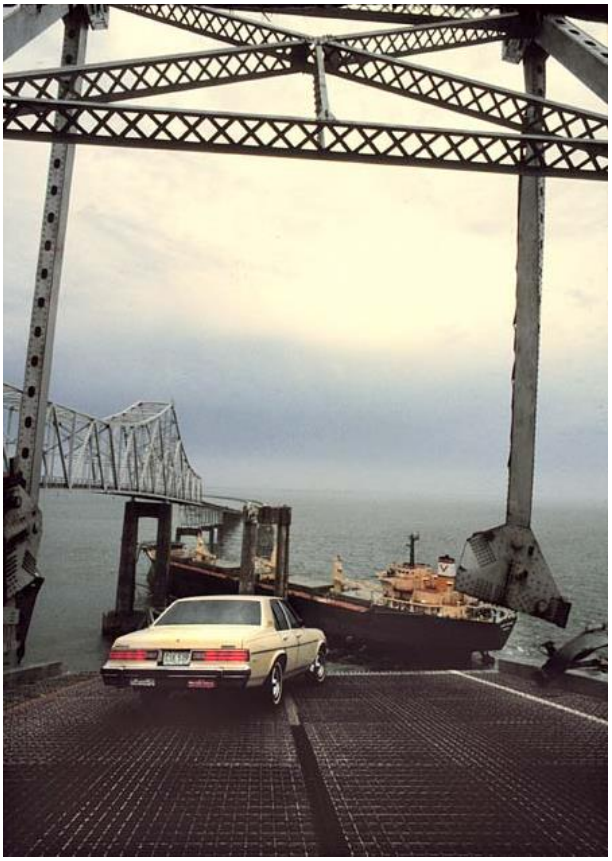

Figure 3-1. Collision-induced impact forces of waterway vessel - Sunshine Skyway Bridge in Florida

Although the aforementioned studies focused on the dynamic response of the MR damper under impact loads, there has been minimal research regarding highly complicated behavior of structural systems employing MR dampers. The reason is the usage of a smart control mechanism in the improvement of the complex structural systems, introduces new concerns about the complicated nonlinear behavior of integrated structure-smart control systems (Spencer

and Nagarajajah, 2003; Jung et al., 2006). As an example, when a linear structure employing smart dampers is excited by a load, the responses can be nonlinear (Kim et al., 2011). This nonlinear problem becomes more complex with the installation of highly nonlinear hysteretic actuators/dampers into non-homogeneous reinforced concrete system under a variety of impact loads. Hence, developing an appropriate mathematical model for the integrated nonlinear system including the interaction effects between the structural system and the nonlinear control device becomes more challenging. With this in mind, this study aims to develop a new nonlinear system identification (SI) framework for estimating nonlinear behavior of smart reinforced concrete structures-MR damper systems under impact loads. This paper represents the first study in literature that focuses on the SI of smart reinforced concrete structure-MR damper systems subjected to a variety of impact loads.

In general, SI uses a set of input and output data in order to derive a nonlinear input-output mapping function. SI methodologies can be categorized into two parts that are parametric and nonparametric SI approaches (Bani-Hani et al., 1999; Suresh et al., 2008). The parametric approach defines the architecture of the mathematical model based on the physical quantities of structures such as stiffness, damping, and mass (Lin et al., 2001; Lin and Betti, 2004; Yang and Lin, 2004), while the nonparametric SI method trains the input-output map of the structural system (Allison and Chase, 1994; Hung et al., 2003; Suresh et al., 2008; Kim et al., 2011). As one of such parametric SI approaches, neuro-fuzzy model has been widely used to represent the nonlinear systems by using fuzzy sets and fuzzy rules (Faravelli and Yao, 1996; Alhanafy, 2007; Gopalakrisnan and Khaitan, 2010; Wang, 2010; Jang et al, 1997). In particular, the application of neuro-fuzzy models in the field of civil engineering has become an attractive topic. Abdulkadir et al. (2006) proposed an adaptive neuro-fuzzy inference system (ANFIS) for predicting the elastic modulus of normal and high-strength concrete. The results showed that the ANFIS approach accurately predicts the elastic modulus of the concretes. Tesfamariam and Najjaran (2007) tried to estimate the concrete strength of a given mix proportioning by using neuro-fuzzy models. The slump, water-cement, admixture, and the fine and coarse aggregate ratio were used as inputs to train the proposed ANFIS model. At the end of the study, the effectiveness of the proposed method was verified by using actual concrete mix proportioning datasets. Another study was performed by Fonseca et al. (2008). In this study, a neuro-fuzzy model was used to investigate the behavior of steel beam web panels subjected to concentrated loads. The results obtained by the proposed model were compatible with the experimental data. Ozbulut and Hurlebaus (2010) applied the ANFIS strategy to modeling of temperature- and

strain-rate-dependent behavior of nickel titanium (NiTi) shape memory alloys for seismic response mitigation applications.

In literature, there were multiple studies that used neuro-fuzzy models for identification and control of the smart control devices, especially on MR dampers (Schurter and Roschke, 2000; Hongsheng and Suxiang 2009; Wang, H. 2009, 2010). Schurter and Roschke (2000) proposed an ANFIS model to describe the behavior of the SD-l000 model MR damper subjected to various wave forms such as sine, step, triangle, and pseudorandom. Wang and Hu (2009) proposed a novel way to describe the direct and inverse model of the MR damper. They developed the direct and inverse ANFIS models for the identification and control of MR damper, respectively. The numerical simulation demonstrated that the neuro-fuzzy systems can precisely describe the direct model and inverse model of the MR damper. However, there is little study that focused on the system identification of integrated structure-MR damper systems by using neuro-fuzzy models (Mitchell et al. 2012; Arsava et al. 2013). Mitchell et al. (2012) developed an ANFIS to model the integrated linear structure-MR damper system under earthquake loads. A linear three-story building employing an MR damper under various earthquake signals was investigated. Acceleration responses were trained to be predicted by using an artificial earthquake signal and an MR damper force signal. It has been demonstrated from extensive simulations that the ANFIS model was very effective in modeling the complex seismic responses of structure-MR damper systems. However, the results of the authors showed that the approach of Mitchell et al. (2012) is not effective in predicting the structural impact responses of smart structural systems, although Mitchell's ANFIS modeling framework is very effective in predicting seismic responses of smart structures. Figure 3-2 represents the structural impact response of an integrated structure-MR damper system under different impact loads. As shown in Figure 3-2, the predictions of the Mitchell's model (WANFIS) are not in agreement with the experimental data. To address such an issue, Arsava et al. (2013a) proposed a modification of Mitchell's approach by integrating the ANFIS modeling framework with a time-delay term. They demonstrated the effectiveness of the proposed approach using a cantilever-type aluminum beam equipped with MR dampers under impact loads. However, the high computational load is still challenging to implement the modeling approach into structural control system design. With this in mind, a wavelet-based time delayed adaptive neuro-fuzzy inference system (W-TANFIS) is proposed to reduce the computational load while the performance on structural impact response prediction is improved. The effectiveness of the proposed W-TANFIS model is demonstrated using experimental data obtained from a smart reinforced concrete structure under a variety of impact loads. The tested data include accelerations, displacements, and strains. The

proposed SI framework integrates autoregressive fuzzy rules and backpropagation neural network with discrete wavelet transform (WT).

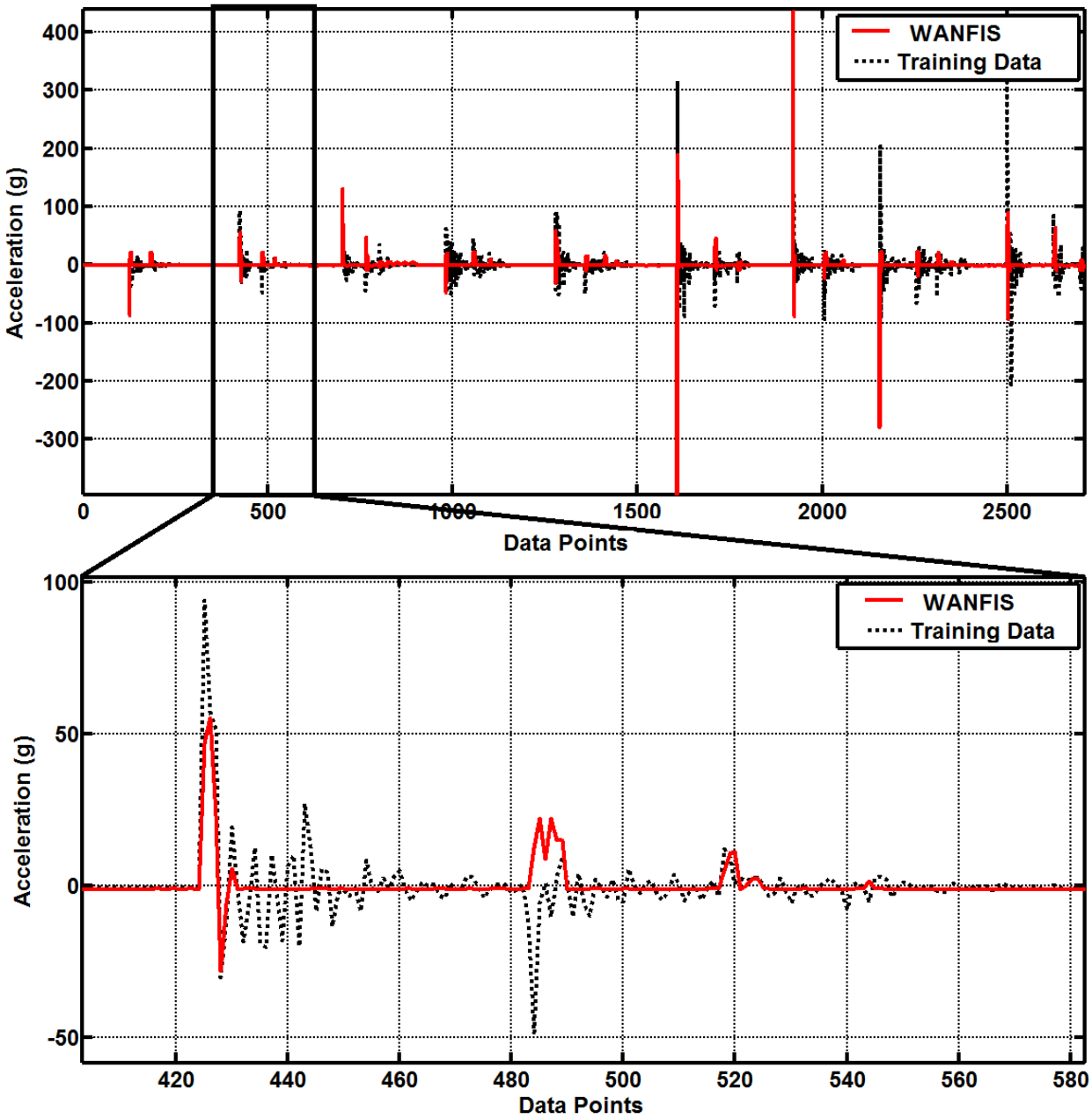

Figure 3-2. Comparison of the acceleration response measurements with WANFIS model for various currents and drop release heights

Wavelet transform, adaptive neuro-fuzzy inference system (ANFIS) and wavelet-based time delayed ANFIS (W-TANFIS) are described in Section 3.2. Section 3.3 gives information about the experimental setup, equipment and procedures. In Section 3.4, results of the proposed model including training and validation are presented. Evaluation of results and concluding remarks are presented in Section 3.5.

3.2. Wavelet-based time delayed adaptive neuro fuzzy inference system (W-TANFIS)

3.2.1. Wavelet transform

The WT provides a time-frequency representation of the signal using time and scale window functions. WT decomposes the given signal into sub-signals and then reconstruct them into to the original signal to compress the data and reduce the noise (Thuillard, 2001). A continuous WT can be represented as

$$W_\psi f(a,b) = 1/\sqrt{a} \int_{-\infty}^{\infty} f(t)\psi\left(\frac{t-b}{a}\right)dt \tag{3-1}$$

where a and b are the scaling factor and translation parameter respectively, while ψ is the wavelet function. The derived discrete WT is

$$\begin{bmatrix} X_i \\ Y_i \\ Z_i \end{bmatrix} = 2^{\frac{s}{2}} \sum_n x_i(os)\phi\left(2^s t - l\right) \ , \tag{3-2}$$

where $x_i(os)$ is defined as the original signal, while X_i , Y_i and Z_i are premise variables. The reorganized format of the equation (2) is given as

$$x_i(os) = \sum_l \sum_s \begin{bmatrix} X_i \\ Y_i \\ Z_i \end{bmatrix} \psi_{l,s}(os) \ , \tag{3-3}$$

where l, s and ϕ are the location index, scale index and the mother function respectively. The discrete WT isolates the high frequency components from the original signal. In order to investigate the both high and low frequency signals, multi-resolution analysis (MRA), which divides the signal into segments, is used. MRA reduces the required total number of data points by dicretizing the function using the step size (Mitchell et al., 2012). The mother function ϕ and the corresponding wavelt ψ are defined such that it represents the original signals as follows

$$\phi_{l,s} := 2^{\frac{s}{2}} \phi\left(2^s t - l\right) \ , \tag{3-4}$$

$$\psi_{l,s} := 2^{\frac{s}{2}} \psi\left(2^s t - l\right) \tag{3-5}$$

The mother function allows filtering high frequencies from the data, while the corresponding wavelet filters the low frequencies. As a useful tool to filter the data and decompose the time series in terms of time and frequency, WT is applied to TANFIS model in order to reduce the computation time.

3.2.2. Adaptive neuro fuzzy inference system (ANFIS)

In general, ANFIS generates input-output maps by using sets of fuzzy 'if-then' rules with appropriate membership functions to solve the complex nonlinear problems. As a hybrid system, ANFIS integrates fuzzy inference systems and adaptive learning tools to increase the accuracy of the results. Figure 3-3 shows a typical ANFIS system with three inputs and one output.

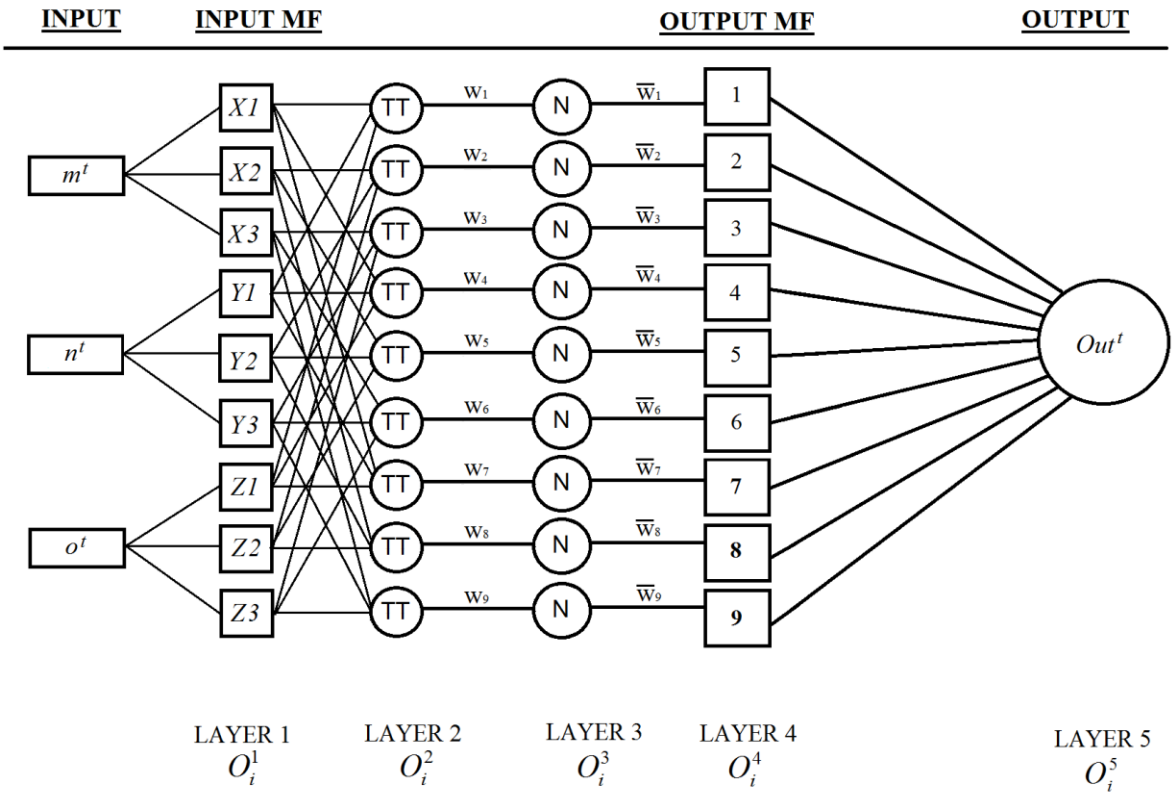

Figure 3-3. Typical ANFIS architecture

The process starts in the current layer with the entry of the input data (*m, n* and *o*). After the current layer completes its task, the processed data moves forward to the next layer. The process ends when each layer completes its task and produces an output signal (*Out)*. The algorithm proceeds until the parameters of the Takagi-Sugeno (TS) fuzzy model reach optimal solution (Tahmasebi and Hezarkhani, 2010).

3.2.3. Time delayed adaptive neuro fuzzy inference system (TANFIS)

As previously discussed, an existing modeling framework (Mitchell et al. 2012) is not effective in predicting structural impact responses of smart concrete structures under various impact loads. Hence it is proposed the use of an output feedback to the ANFIS framework called TANFIS. The TANFIS estimates the following output by using observations from previous steps. The TANFIS system with three inputs and one output is presented in Figure 3-4.

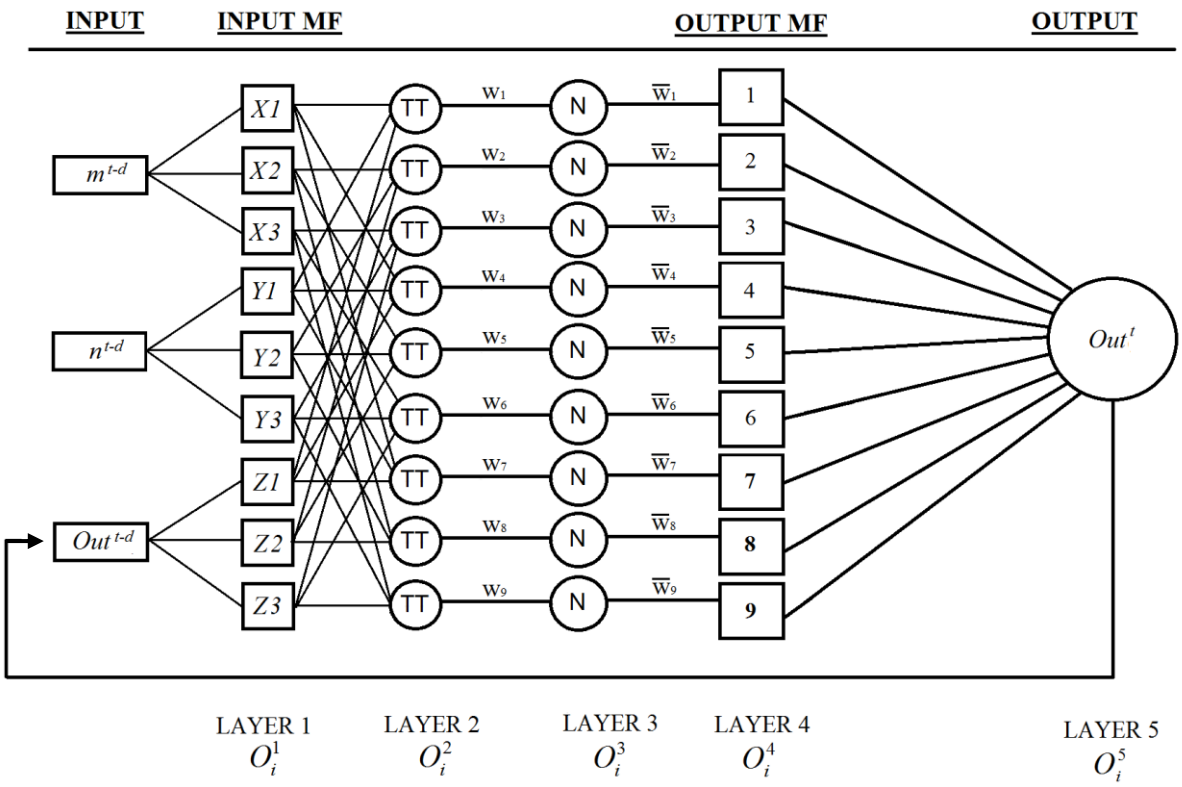

Figure 3-4. TANFIS architecture showing three input and one output model

In the study impact load and current signals are used to train the fuzzy model to estimate the displacement, acceleration and strain responses. A three rule TANFIS fuzzy model is as follows

Rule 1: If m is X_1, n is Y_1 and o is Z_1, then $Out_1^{\ t} = p_1 m_1^{t-d} + q_1 n_1^{t-d} + k_1 Out_1^{\ t-d} + re_1$ (3-6)

Rule 2: If m is X_2, n is Y_2 and o is Z_2, then $Out_2^{\ t} = p_2 m_2^{t-d} + q_2 n_2^{t-d} + k_2 Out_2^{\ t-d} + re_2$ (3-7)

Rule 3: If m is X_3, n is Y_3 and o is Z_3, then $Out_3^{\ t} = p_3 m_3^{t-d} + q_3 n_3^{t-d} + k_3 Out_3^{\ t-d} + re_3$ (3-8)

where m^{t-d}, n^{t-d} are inputs at time t-d and Out^{t-d} is the input from the previous iteration while Out^t is the output at time t of the fuzzy system. The delay term is represented by d. In the model consequent parameters are represented as p_i, q_i, k_i and re_i. The functions of Layer 1 is presented as

$$O_i^1 = \mu\begin{bmatrix} X_i\left(m^{t-d}\right) \\ Y_i\left(n^{t-d}\right) \\ Z_i\left(Out^{t-d}\right) \end{bmatrix} \tag{3-9}$$

where μ is the appropriate parameterized membership function (MF), and O_i^1 (i = 1,2,3) is the output that specifies the degree to which the given input m^{t-d} satisfies the quantifier X.

In Layer 1 MFs are applied to each input and send to the second layer, which combines all the inputs. The product of Layer 2 is the combination of all incoming outputs that is called 'firing strength' of a fuzzy control rule

$$w_i^t = \mu X_i(m^{t-d}) \times \mu Y_i(n^{t-d}) \times \mu Z_i(Out^{t-d}),\ i = 1,2,3 \tag{3-10}$$

In Layer 3 the output of Layer 2 is normalized by taking the ratio of the firing strength

$$\overline{w}_i^t = \frac{w_i^t}{w_1^t + w_2^t + w_3^t},\ i = 1,2,3 \tag{3-11}$$

As a next step, node functions ($Out_i^t = p_i m^{t-d} + q_i n^{t-d} + k_i Out^{t-d} + re_i, i = 1,2,3$) are applied to output of Layer 3

$$O_i^4 = \overline{w}_i^t \times Out_i^t = \overline{w}_i \times \left(p_i m^{t-d} + q_i n^{t-d} + k_i Out^{t-d} + re_i\right),\ i = 1,2,3 \tag{3-12}$$

In the last step, Layer 5 summates the layer inputs

$$O_i^5 = overall\ \ output + \sum_i \overline{w}_i^t \times Out_i^t = \frac{\sum_i w_i^t \times Out_i^t}{\sum_i w_i^t},\ i = 1,2,3 \tag{3-13}$$

In the optimization of the results, TANFIS uses adjustable parameters such as number of MF, type of MF, iteration and size of the step.

However, it is challenging to develop the TANFIS model when many design variables are considered due to high cost of computation. In order to decrease the computation time, WT,

which compresses the data and reduces the noise, is used. It is shown that the new W-TANFIS model decreases the computation time while accuracy of the trained model increases.

3.2.4. Wavelet-based TANFIS (W-TANFIS)

The proposed approach incorporates WT to the TANFIS model to reduce the computation time while preserving the good performance of training and validation process. By the application of the WT, the response data gathered from the acutal tests are scretched and filtered to optimize the output signal. The architecture of the proposed W-TANFIS model is presented in Figure 3-5.

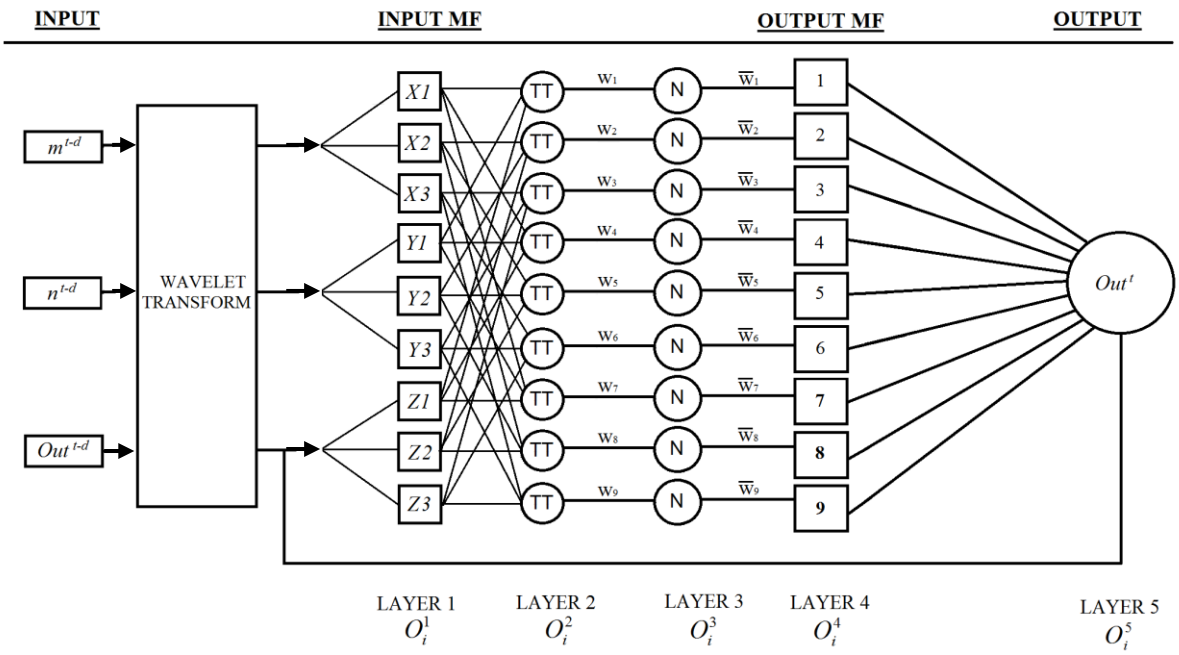

Figure 3-5. Configuration of W-TANFIS architecture

Sets of experimental studies are performed to obtain the input-output data for training and validation of the W-TANFIS model. Structural responses such as acceleration, deflection and strain are obtained for different impact loads and various currents. By using the impact load and current on MR damper values as input, the W-TANFIS model is trained to predict the noninear behavior of the smart structure. Accuracy and computation time of the W-TANFIS and TANFIS modesl are compared.

3.3. Experimental setup

The proposed experimental program in order to obtain a set of input-output data includes a drop tower impact testing facility, a reinforced concrete beam, one MR damper, a data acquisition system, sensors and a high speed camera. Various impact forces (i.e. a number of drop release heights) and numerous counter acting control forces (i.e. a variety of levels of current signals) are used in the experimental study. A computer algorithm is developed in Labview such that several structural responses are collected and control force command signals are sent to the MR damper at the same time. In other words, when the impact testing machine starts the testing (i.e. the release of the drop mass), the program starts to send the previously defined current signals to the MR damper, while collecting the structural responses. Then the collected data set is processed and evaluated by using MATLAB software.

In practice, creating a SI model that incorporate all the scenarios is very challenging since the location and the magnitude of impact loads are unknown. With this in mind, the main objective of this research is to develop effective algorithms for system identification of smart structures under a variety of impact loadings and control inputs. There is no doubt that full scale testing will produce valuable and more realistic results but it is not readily feasible to construct even a full scaled concrete structural member equipped with high capacity sensors (e.g. Load cells). Moreover, the capacity of the impact test facility is not adequate to perform full-scale experiments. Thus, a scaled testing framework is proposed due to the restrictions of resources. The proposed test setup for structural impact testing makes it possible to study the nonlinear interaction between structures and MR damper systems under a variety of impact loads and control signals. Furthermore, the developed mathematical model can be used to create a robust control model to fully use MR damper technology in mitigating the impact response of the structure under impact loads. In near future, the authors of this paper plan to design controllers based on the SI model. If facility and/or budget are allowed, it is suggested to perform full-scale test to deeply investigate the structure-MR damper interaction under high impact loads.

3.3.1. Drop tower test facility

The impact load test facility in Structural Mechanics and Impact Laboratory in the Civil and Environmental Engineering Department at Worcester Polytechnic Institute is used in the experimental studies. To perform the tests, a drop tower test facility with a capacity of 22,500 kilogram is used in the investigation of the dynamic response of the smart structure under impact

loads. Impact load was applied with a 6.8 kg free falling drop-mass. By changing the drop release height and drop mass, several impact scenarios can be evalauted.

3.3.2. Reinforced concrete beam equipped with MR dampers

To demonstrate the effectiveness of the W-TANFIS model, a reinforced concrete beam structure equipped with an MR damper is investigated. The test beam is designed with a maximum 2000 kg load capacity, which is the maximum impact load that is used in the experimental study. The research team plan to conduct the larger (scaled-up) testing in near future.

A total of 6 longitudinal reinforcement bars having a tensile yield strength of 248 MPa with 0.75 cm in diameter are placed in to concrete beams (Figure 3-6). Stirrups consisting of 0.25 cm steel wire are placed with 7.5 cm spacings. Portland cement concrete mixtures with a maximum aggregate size of 6.5 mm are used and the concrete beams were cured in a curing room for over three weeks. At the time of testing, the compressive strength of the concrete was 26 MPa and the modulus of elasticity *E* was 15 GPa.

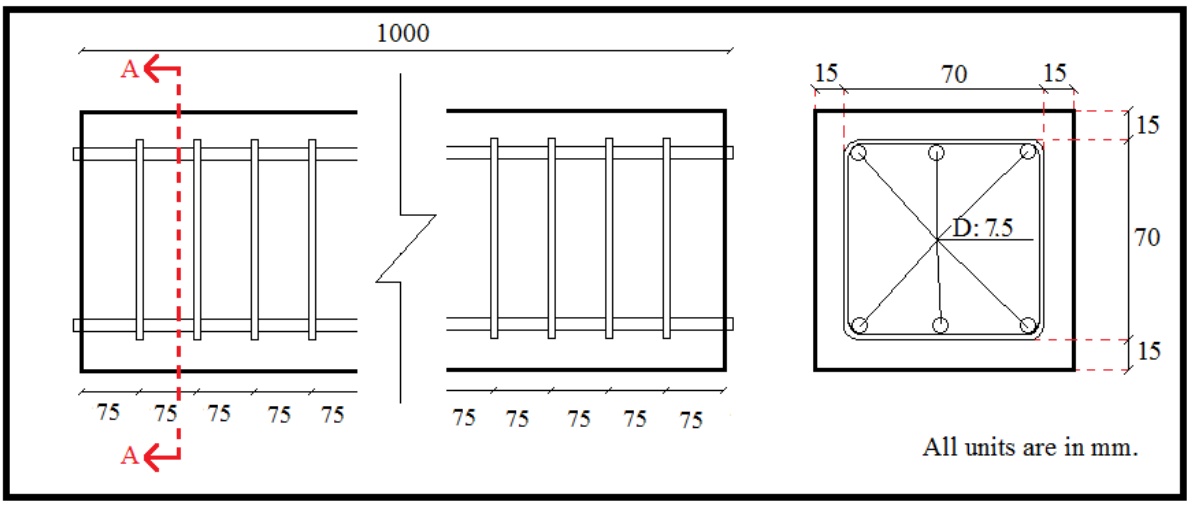

Figure 3-6. Configuration of reinforcement

In order to mitigate the effect of impact load on the reinforced concrete beam, an MR damper is placed under mid-span of the simply supported beam (Figure 3-7). An MR damper comprises a hydraulic cylinder, magnetic coils and MR fluids that consist of micron sized magnetically polarized particles within an oil-type fluid (Spencer et al., 1997b, Kim et al., 2009). As an effective smart control system, MR dampers can be both operated as passive or active system. In active systems, by changing the current on magnetic field on the MR fluid, flow of

the MR fluids can be adjusted to absorb and dissipate the energy in a most effective way. In opposition to active systems, MR dampers are still operable as a passive damper if some control feedback components, e.g., wires and sensors, are broken for some reasons (Mitchell et al., 2012). The control command current of the used RD-8040-1 MR damper is between 0 to 1.9 A.

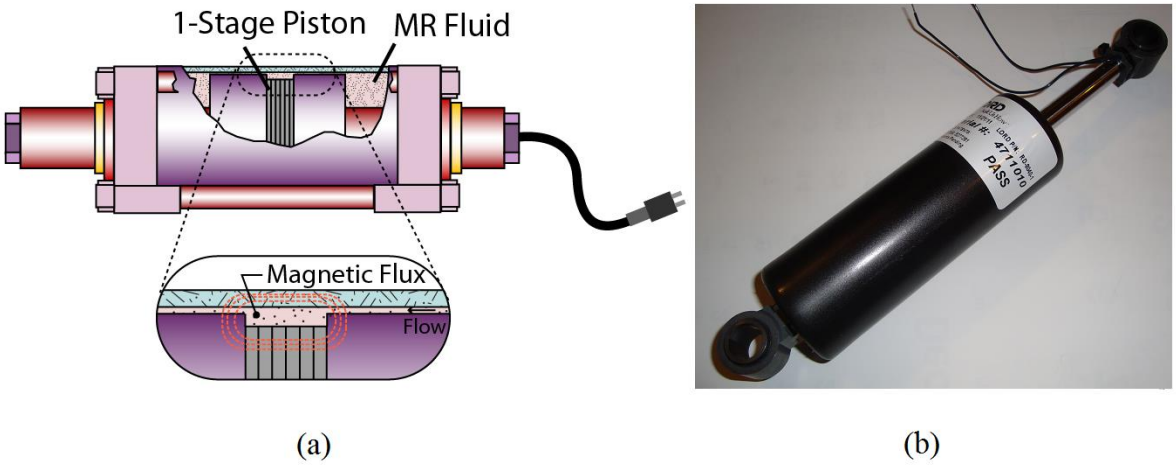

Figure 3-7. (a) Schematic of MR damper (b) RD-8040-1 MR damper

3.3.3. Data acquisition

In the tests, five sensors, which are connected to National Instrument (NI) labview data acquisition system, are used to obtain the acceleration, deflection, strain and impact force data. The displacement data is measured by R.D.P product ACT1000A type LVDT that is placed at the middle of the beam. Two PCB type 302A accelerometers with a capacity of 500 g and one M.M product N2A series strain gauge are used in the acceleration and strain measurements, respectively. As a last sensor, a 4,500 kg capacity Central HTC-10K type load cell is used to measure the applied impact force. Drop tower test facility and placement of the sensors is depicted in Figure 3-8. As a sampling rate of the data acquisition system, 10,000 data points per second is selected.

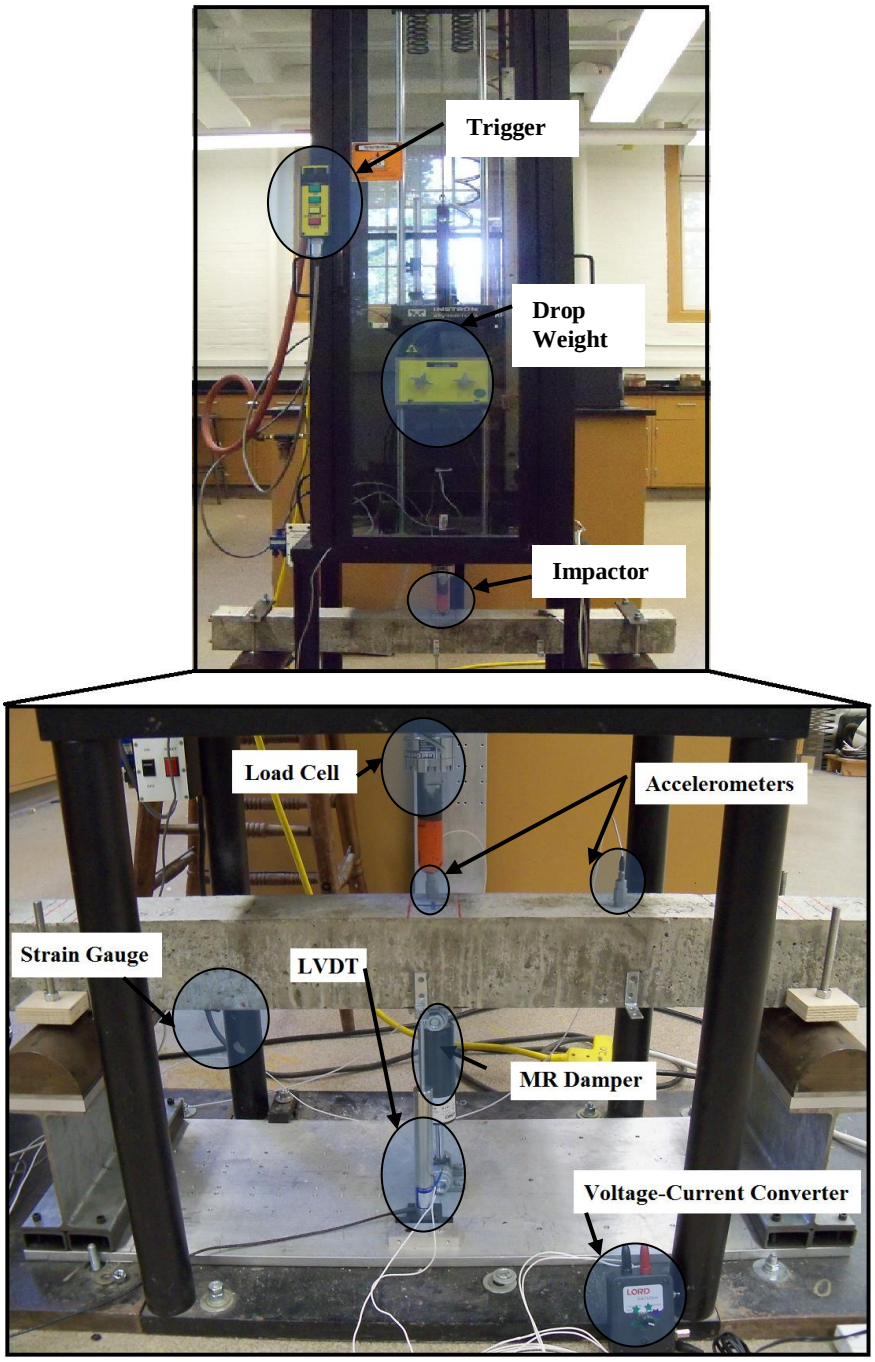

Figure 3-8. Configuration of the sensors and data acquisition system

3.3.4. Test details

The goal of the experimental testing is to measure the dynamic response of the smart structure under different impact loads and different scenarios including with and without the MR damper. For each drop release height and current on the MR damper, the impact test is performed five times to train and validate the proposed models. Details of the performed tests can be found in Table 3-1.

Table 3-1. Experimental Test Details

Case Studies					Current on MR Damper	Drop Release Height (mm)	Impact Velocity (mm/s)
Trained Data	Validated Data						
	1st Set	2nd Set	3th Set	4th Set			
Case 1	Case 2	Case 3	Case 4	Case 5	Uncontrolled	20	775
Case 6	Case 7	Case 8	Case 9	Case 10	0	20	
Case 11	Case 12	Case 13	Case 14	Case 15	0.3	20	
Case 16	Case 17	Case 18	Case 19	Case 20	0.6	20	
Case 21	Case 22	Case 23	Case 24	Case 25	1	20	
Case 26	Case 27	Case 28	Case 29	Case 30	1.4	20	
Case 31	Case 32	Case 33	Case 34	Case 35	1.9	20	
Case 36	Case 37	Case 38	Case 39	Case 40	Random	20	
Case 41	Case 42	Case 43	Case 44	Case 45	Uncontrolled	40	885
Case 46	Case 47	Case 48	Case 49	Case 50	0	40	
Case 51	Case 52	Case 53	Case 54	Case 55	0.3	40	
Case 56	Case 57	Case 58	Case 59	Case 60	0.6	40	
Case 61	Case 62	Case 63	Case 64	Case 65	1	40	
Case 66	Case 67	Case 68	Case 69	Case 70	1.4	40	
Case 71	Case 72	Case 73	Case 74	Case 75	1.9	40	
Case 76	Case 77	Case 78	Case 79	Case 80	Random	40	
Case 81	Case 82	Case 83	Case 84	Case 85	Uncontrolled	55	990
Case 86	Case 87	Case 88	Case 89	Case 90	0	55	
Case 91	Case 92	Case 93	Case 94	Case 95	0.3	55	
Case 96	Case 97	Case 98	Case 99	Case 100	0.6	55	
Case 101	Case 102	Case 103	Case 104	Case 105	1	55	
Case 106	Case 107	Case 108	Case 109	Case 110	1.4	55	
Case 111	Case 112	Case 113	Case 114	Case 115	1.9	55	
Case 116	Case 117	Case 118	Case 119	Case 120	Random	55	
Case 121	Case 122	Case 123	Case 124	Case 125	Uncontrolled	70	1175
Case 126	Case 127	Case 128	Case 129	Case 130	0	70	
Case 131	Case 132	Case 133	Case 134	Case 135	0.3	70	
Case 136	Case 137	Case 138	Case 139	Case 140	0.6	70	
Case 141	Case 142	Case 143	Case 144	Case 145	1	70	
Case 146	Case 147	Case 148	Case 149	Case 150	1.4	70	
Case 151	Case 152	Case 153	Case 154	Case 155	1.9	70	
Case 156	Case 157	Case 158	Case 159	Case 160	Random	70	

Experimental study contains a total of 160 impact tests that investigate the structure with and without an MR damper. Four different impact force levels were applied to structure-MR damper system. To evaluate the performance of the MR damper under different current cases, various random (0-1.9 A) signals as well as six constant (0, 0.3, 0.6, 1, 1.4, and 1.9A) signals are examined.

3.4. System identification results

3.4.1. Parameter setting

The data generation, training and validation process of the proposed models are depicted in Figure 3-9.

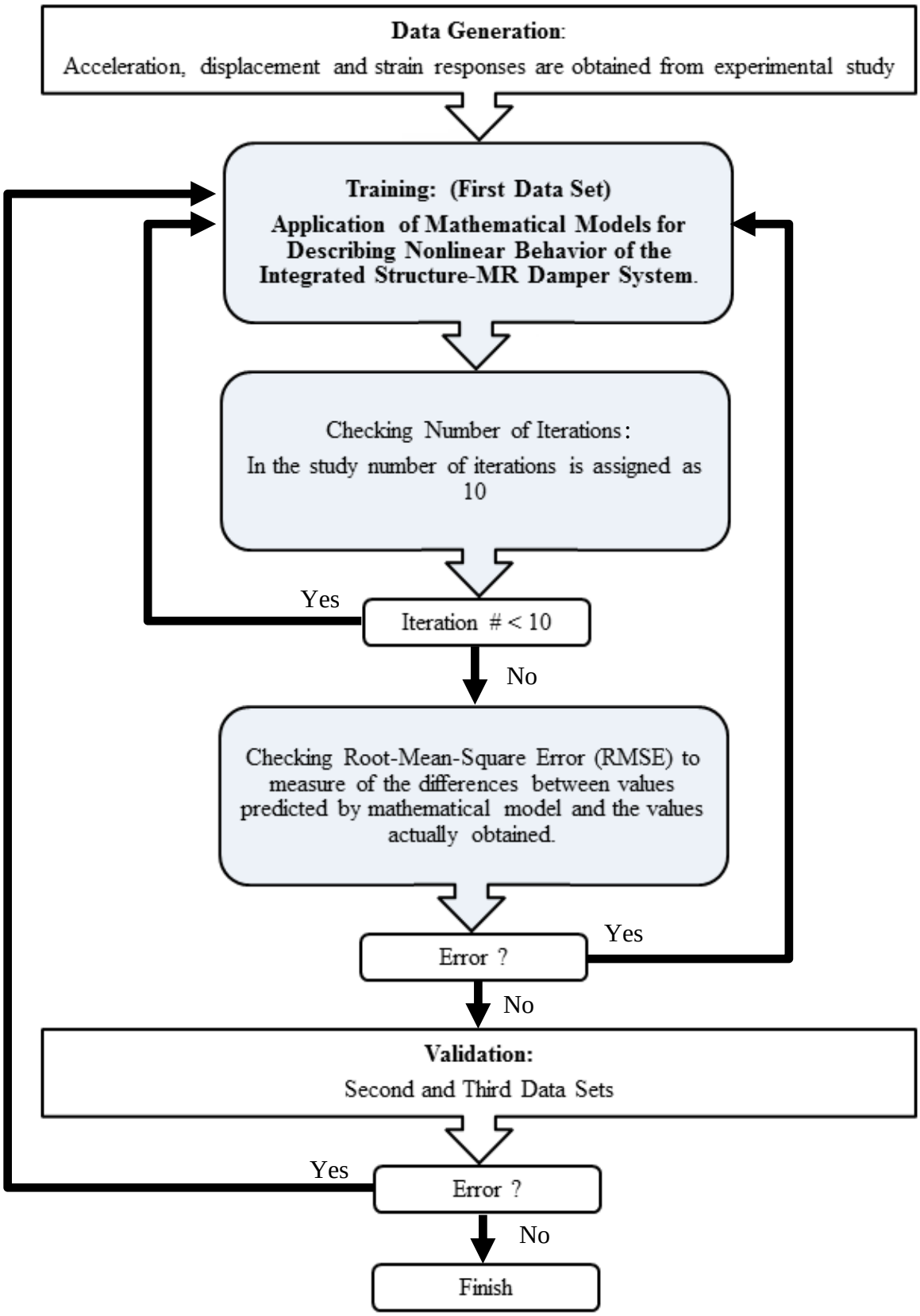

Figure 3-9. Architecture of the proposed mathematical modeling

To train and test the ANFIS, TANFIS and W-TANFIS models, sets of input and output data are collected from the proposed experimental setup. A variety of impact loads and current signals are used as the input while strain, deflection and acceleration responses are used as output signals. In the training process, the number of iterations is assigned as 10 and then the RMSE values are checked. It is observed that both TANFIS and W-TANFIS predicted the dynamic responses accurately. Thus, an iteration of 10 is set as default because the performance improve rate is small after the 10 iterations.

Figure 3-10 shows the input-output data set for training the W-TANFIS for both constant and random current signals. In the training of W-TANFIS, impact loads and current signals are used as the input while strain, deflection and acceleration responses are used as an output signal. Same input-output data sets are also used in the ANFIS and TANFIS models and results are discussed later in the evaluation section.

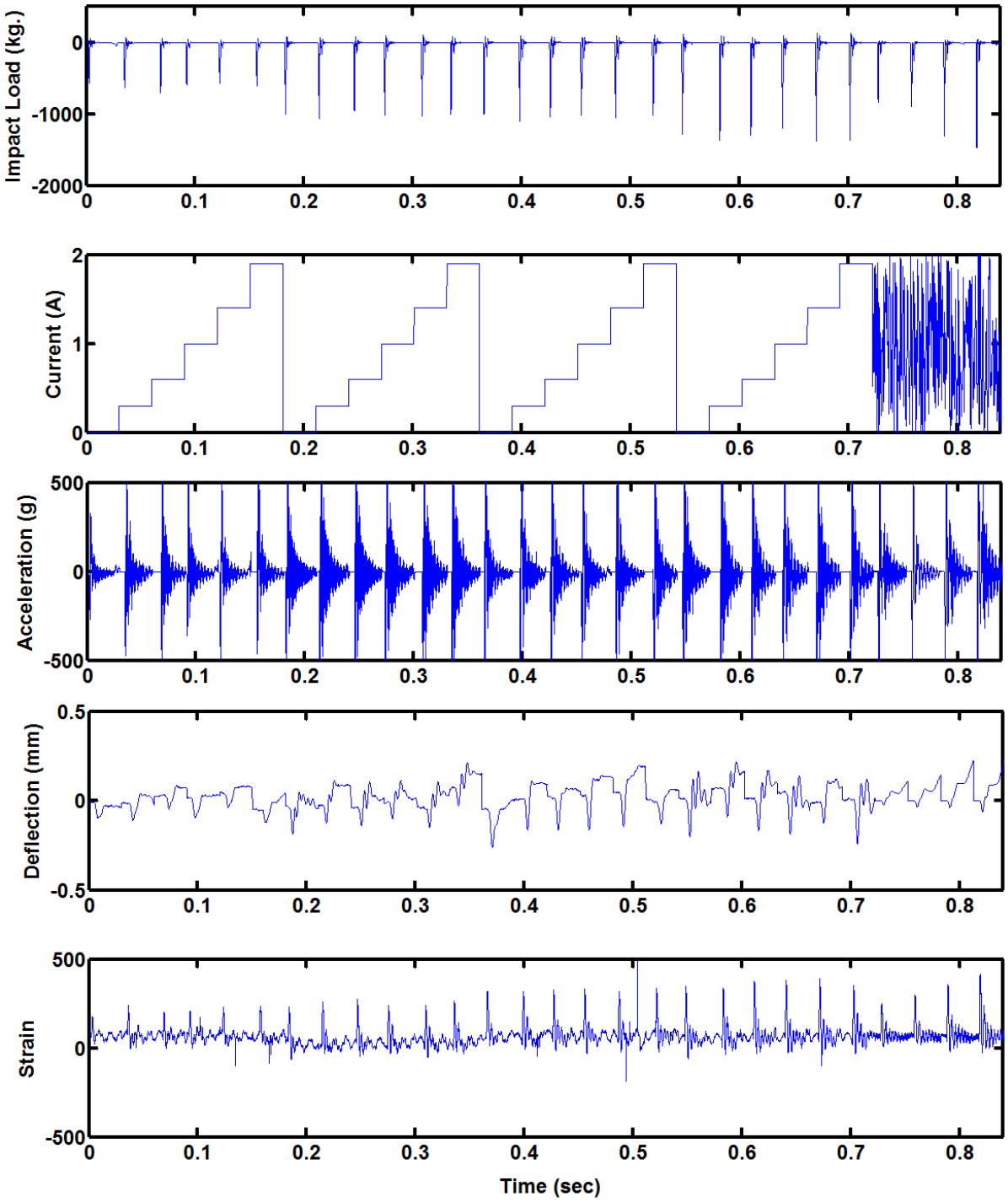

Figure 3-10. Input-output data sets to train the W-TANFIS models

3.4.2. Benchmark ANFIS model

To demonstrate the effectiveness of the proposed W-TANFIS model, an ANFIS model is selected as a first benchmark. The structure of the ANFIS models is configured in Figure 3-11.

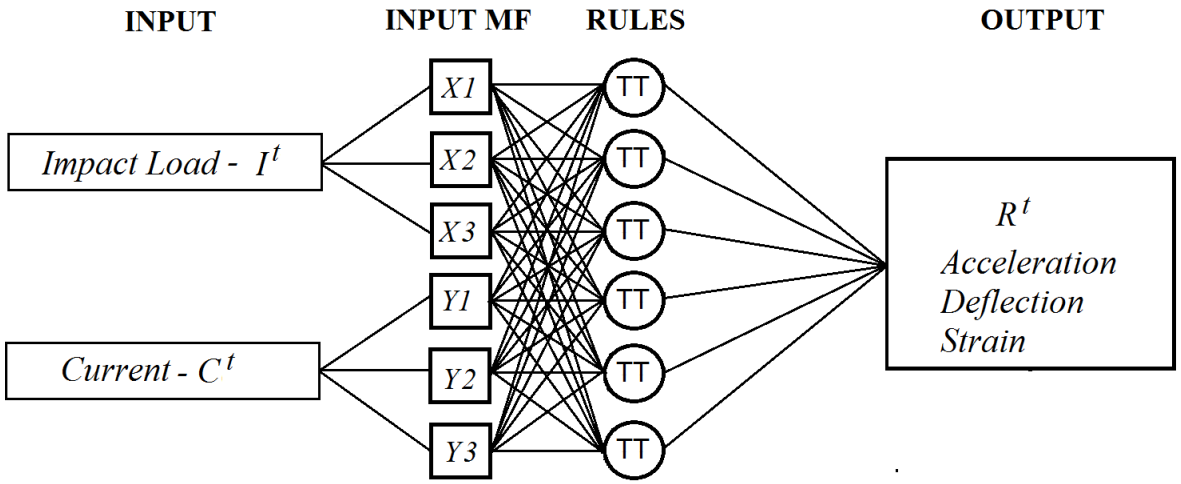

Figure 3-11. Configuration of the ANFIS model

Rule *c*: If $I^t(u)$ is X_{c1}, $I^t(u\text{-}1)$ is X_{c2}, $I^t(u\text{-}2)$ is X_{c3}, …, and $I^t(u\text{-}h+1)$ is X_{ch} then

$$\tilde{I}^t(u+1) = A_c \tilde{I}^t(u) + B_c g(u) \tag{3-14}$$

where

$$\tilde{I}^t(u) = \left[I^t(u) \;\; I^t(u-1) \;\; I^t(u-2) \;\; I^t(u-h+1) \right]^T \tag{3-15}$$

and $g(u)$ denotes the input variable. c= 1,2,…,h and h is the number of rules. $\tilde{I}^t(k+1)$ is the output of the c'th rule, while A_c and B_c are the state and input matrices of the system as correlated with the c'th rule. The behavior of the ANFIS system can be described as

$$\tilde{R}^t(u+1) = \frac{\sum_{c=1}^{h} w_c^t(u)\left(A_c \tilde{I}^t(u) + B_c g(u)\right) + \sum_{c=1}^{h} w_c^t(u)\left(D_c \tilde{C}^t(u) + E_c g(u)\right)}{\sum_{c}^{h} w_c^t(u)} \tag{3-16}$$

Figure 3-12 compares the predictions of ANFIS model with the actual test data that performed by random current signal. Detailed results of the tests with constant and random currents can be found in Table 3-2 and Table 3-3. It is seen that ANFIS does not give the reasonable match between the trained and actual test data.

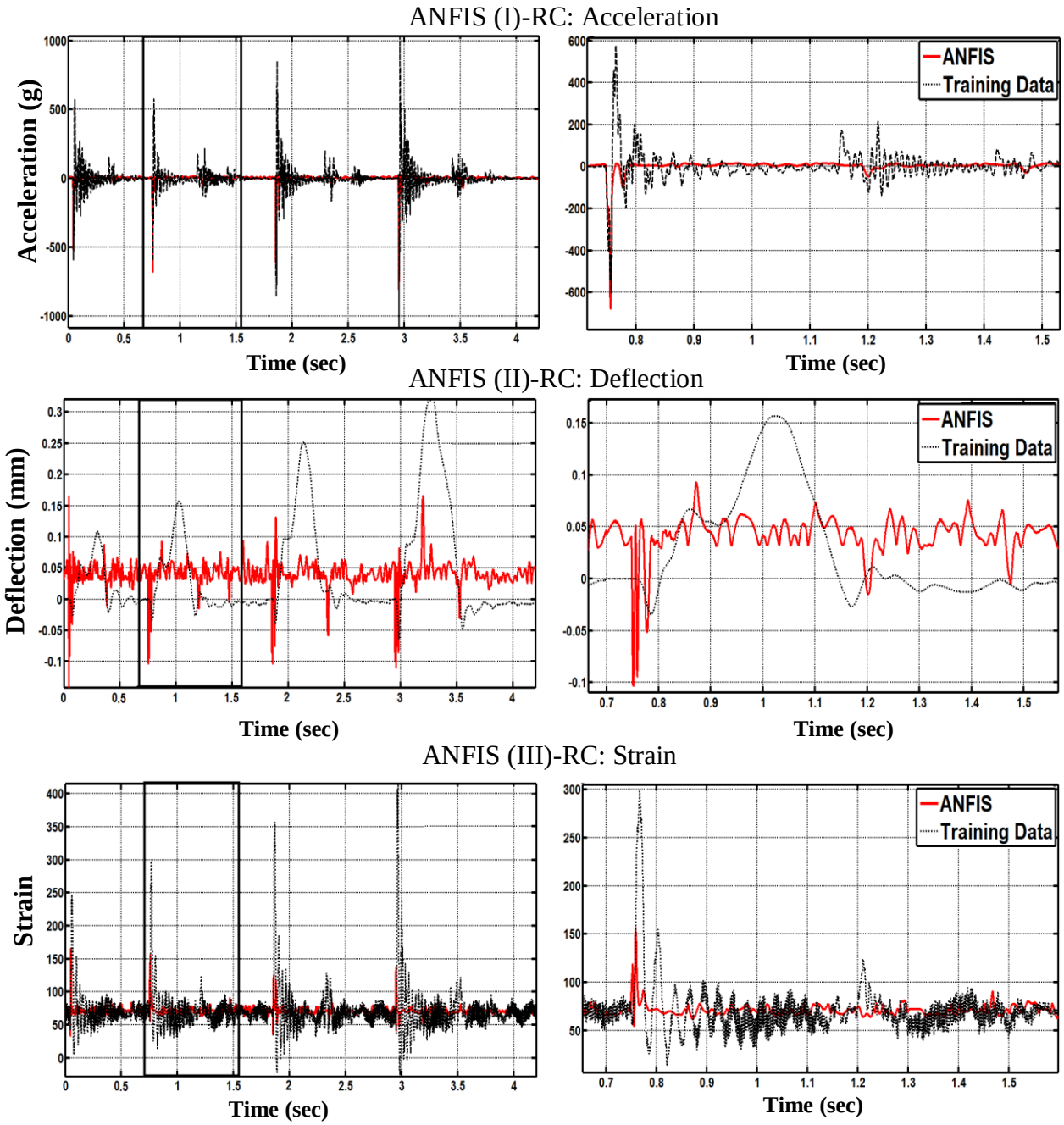

Figure 3-12. ANFIS training - random currents and different drop release heights

It is observed that ANFIS predictions are not in agreement with the actual impact responses. Only 1% to 21% of the actual acceleration, deflection and strain values are predicted correctly by the ANFIS. A detailed evaluation is performed in Section 3.4.5. In order to increase the accuracy between the trained and the actual impact test data, the TANFIS model is used.

3.4.3. TANFIS model

The conceptual configuration of the TANFIS models is shown in Figure 3-13. In the taining and validation process of the TANFIS model, structural responses obtained from the sensors are directly used without compressing and filtering.

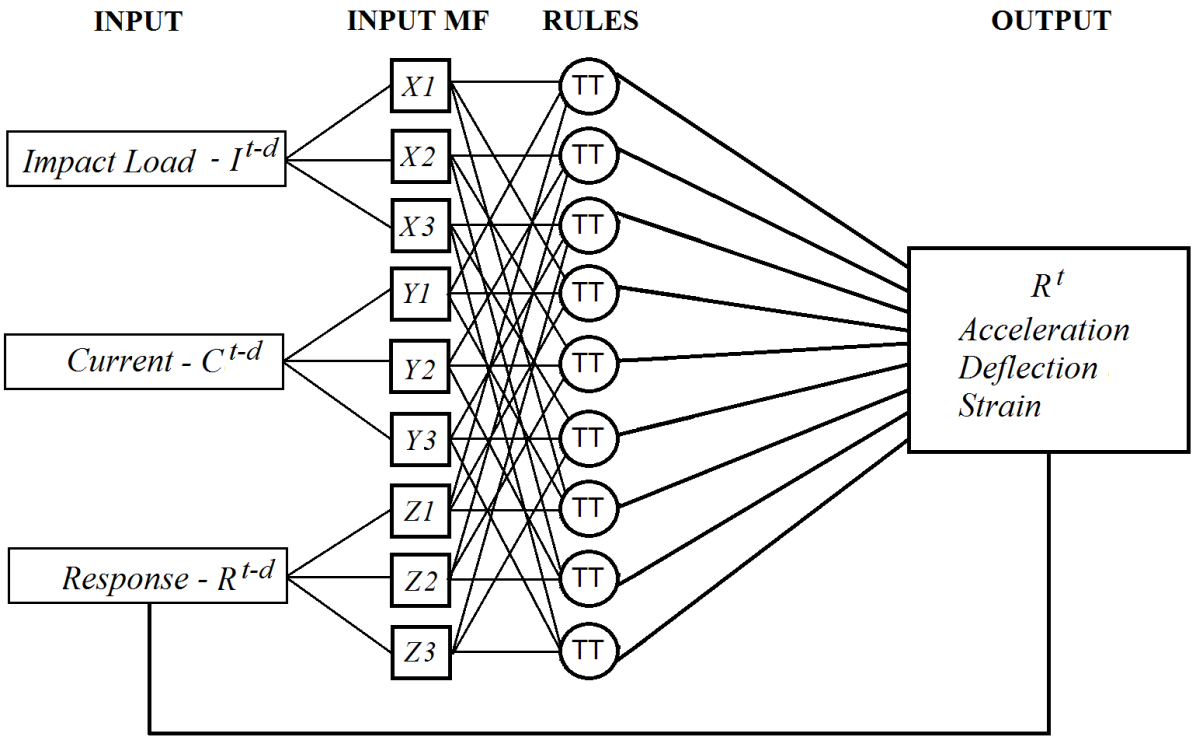

Figure 3-13. Configuration of the TANFIS model

The mathematical model of the TANFIS system is

$$\tilde{R}^t(u+1)=\left[\frac{\sum_{c=1}^{h} w_c^{t-d}(u)\left(A_c\tilde{I}^{t-d}(u)+B_c g(u)\right)+\sum_{c=1}^{h} w_c^{t-d}(u)\left(D_c\tilde{C}^{t-d}(u)+E_c g(u)\right)}{\sum_{c}^{h} w_c^{t-d}(u)} + \frac{\sum_{c=1}^{h} w_c^{t-d}(u)\left(F_c\tilde{R}^{t-d}(u)+G_c g(u)\right)}{\sum_{c}^{h} w_c^{t-d}(u)}\right] \quad (3\text{-}17)$$

Figure 3-14 compares the real measured acceleration, deflection and strain responses with the estimates from the TANFIS models for different drop release heights with random current

levels. It is observed that TANFIS is very effective in the estimation of the highly nonlinear structural responses under impact loads. There is a great agreement between the estimates and measurements.

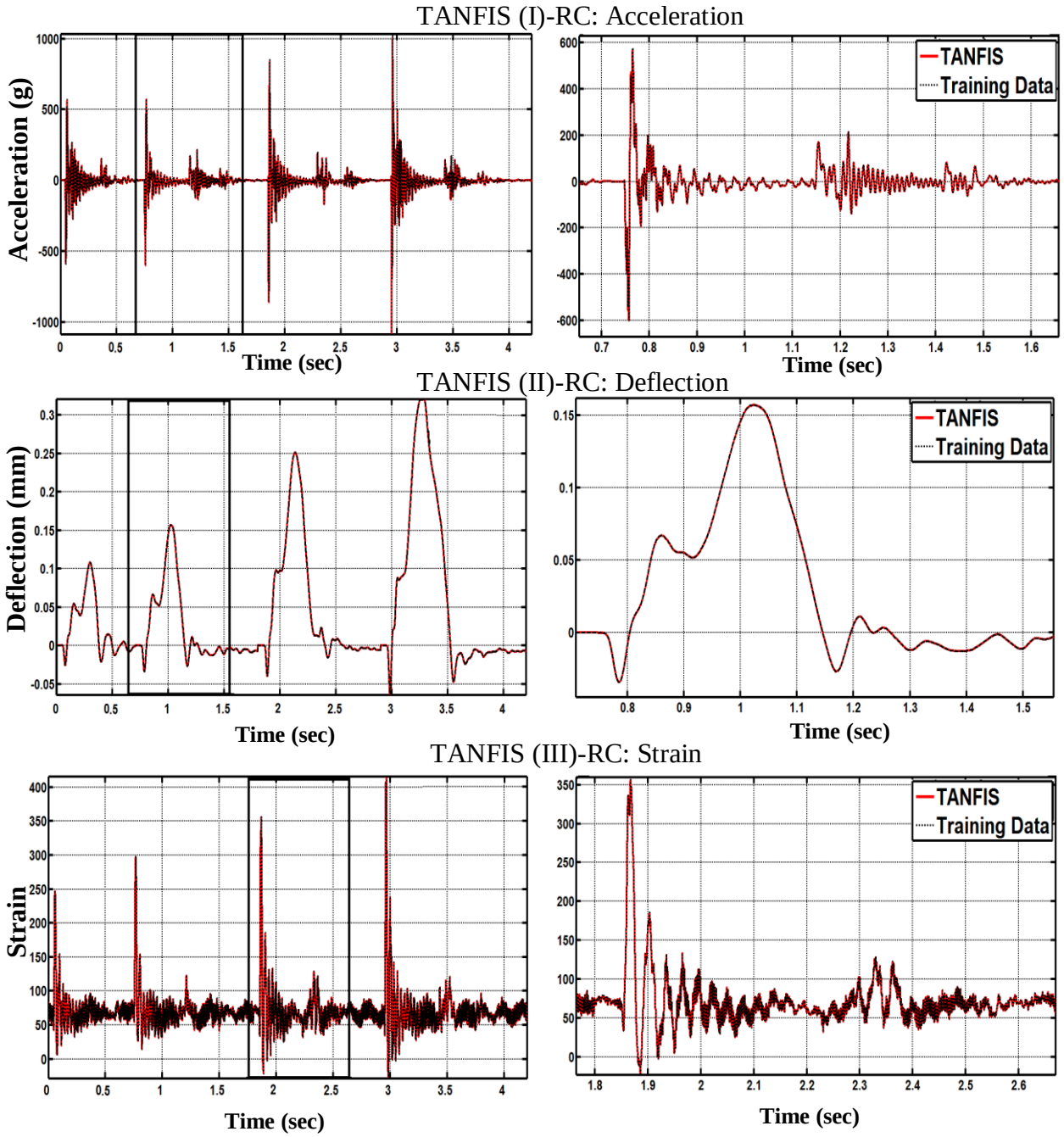

Figure 3-14. TANFIS training - random currents and different drop release heights

Results show that both the training and validation results are in a match with the actual impact responses. This demonstartes that the TANFIS model is very effective in the estimation of actual acceleration, deflection and strain values. For example, the maximum errors of the TANFIS model in predicting the structural impact responses are 10.3 for strains, $0.803e^{-3}$ mm for

deflections, and 61.8 g for accelerations, which represent less than 2.57%, 0.26%, and 8.24% errors compared to the collected data. In order to improve the modeling efficiency of the TANFIS model in terms of computation time, a new novel modeling framework is proposed by the integration of the WT with the TANFIS process.

3.4.4. W-TANFIS modeling

Figure 3-15 represents the configuration of the W-TANFIS for training the acceleration, deflection and strain data.

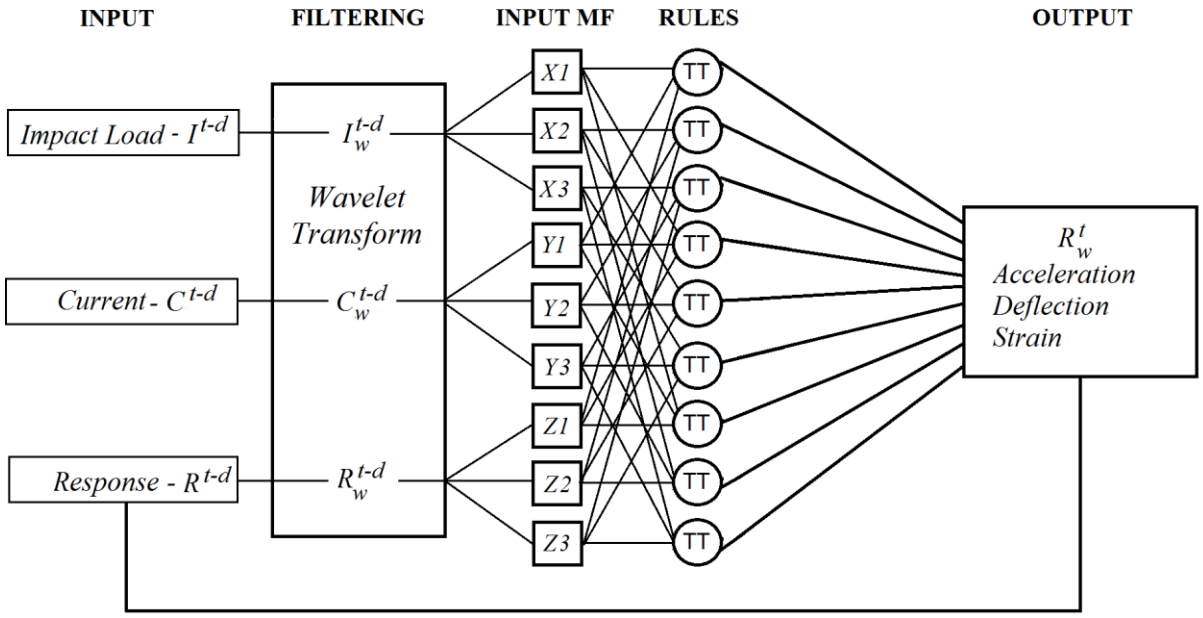

Figure 3-15. Configuration of the proposed W-TANFIS: Impact response prediction

The behavior of the proposed W-TANFIS system is as follows

$$\tilde{R}_w^t(u+1)=\left[\begin{array}{l}\dfrac{\sum_{c=1}^{h} w_c^{t-d}(u)\left(A_c\tilde{I}_w^{t-d}(u)+B_c g(u)\right)+\sum_{c=1}^{h} w_c^{t-d}(u)\left(D_c\tilde{C}_w^{t-d}(u)+E_c g(u)\right)}{\sum_{c}^{h} w_i^{t-d}(u)} \\ +\dfrac{\sum_{c=1}^{h} w_c^{t-d}(u)\left(F_c\tilde{R}_w^{t-d}(u)+G_c g(u)\right)}{\sum_{c}^{h} w_c^{t-d}(u)}\end{array}\right] \tag{3-18}$$

In the training, the type of the membership functions (MFs) of the input data are assigned as a gaussian bell. The selected MFs of the W-TANFIS are presented in Figure 3-16. Left column shows the initial MFs values while right column represents the optimally tuned MFs.

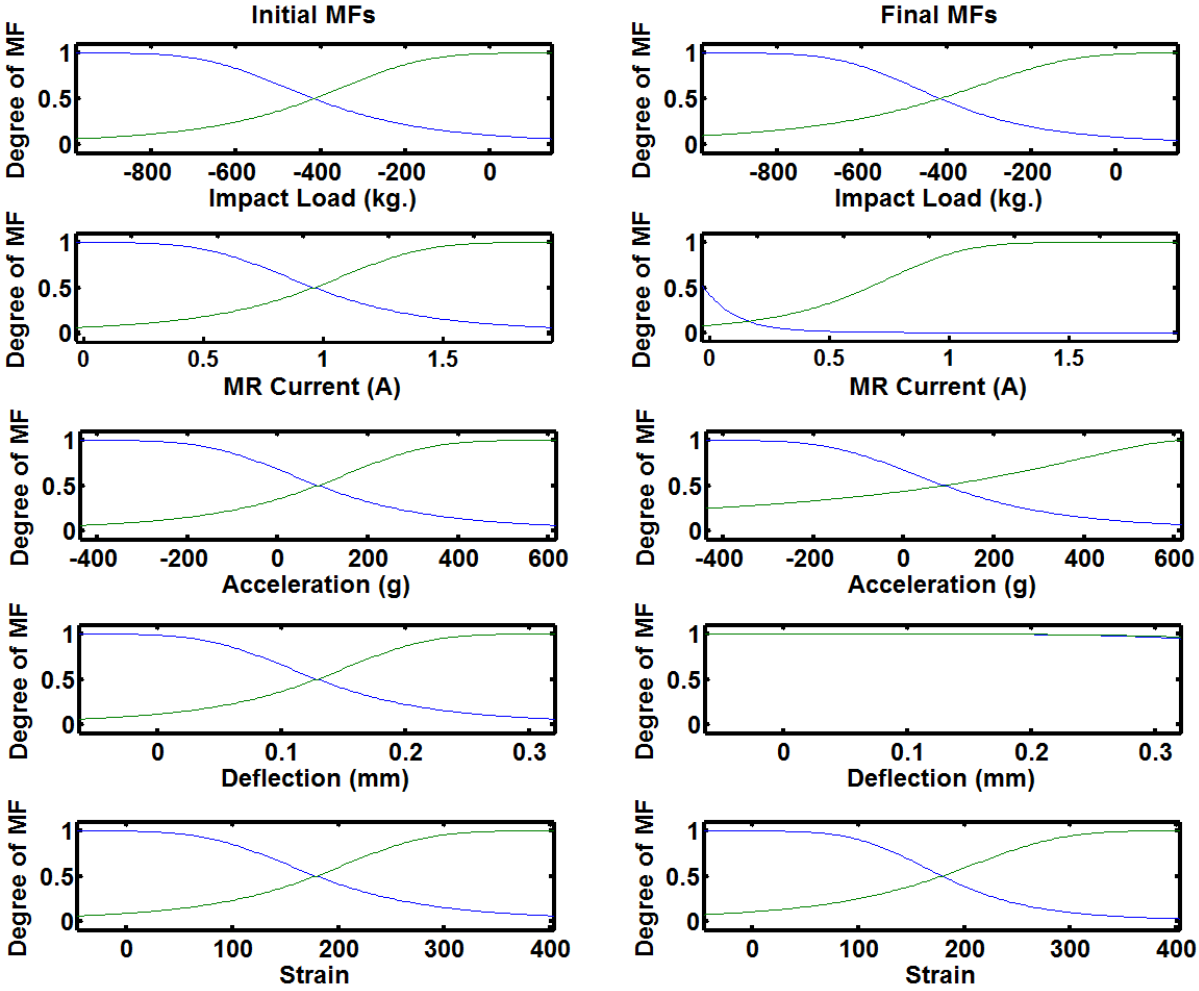

Figure 3-16. Initial and final membership functions: W-TANFIS

In the training of W-TANFIS models, time step is optimally adjusted to obtain the best performance. The step size can be simply defined as the length of each gradient transition during the optimization process. Based on the error obtained after each iteration, the neural network model adjusts the step size in order to optimize the training. In our case, the initial step size is assigned as 0.4. If the error increases after the iteration, the neural network model is assigned to divide the current step size by 1.25. When the error measure surface is smooth in other steps, the model multiplies the step size by 1.2.

As an evaluation index to identify the modelling accuracy, root mean square error (RMSE) values are used. In general, high correlation values relate to low RMSEs. The low values and/or decreasing trend in RMSE implies that the proposed W-TANFIS model has a good performance in predicting the dynamic responses. It is oserved that all W-TANFIS models have low RMSE values with a decrasing trend. After the $10^{'th}$ iteration, decrease in RMSE values becomes insignificant that means the performance improve rate is small after the $10^{'th}$ iteration.

Figure 3-17 compares the predictions of W-TANFIS model for four different force levels and random current levels. The results of tests with the constant current are presented in Table 3-2. It is seen that W-TANFIS estimates the highly nonlinear structural responses accurately and much faster than TANFIS model.

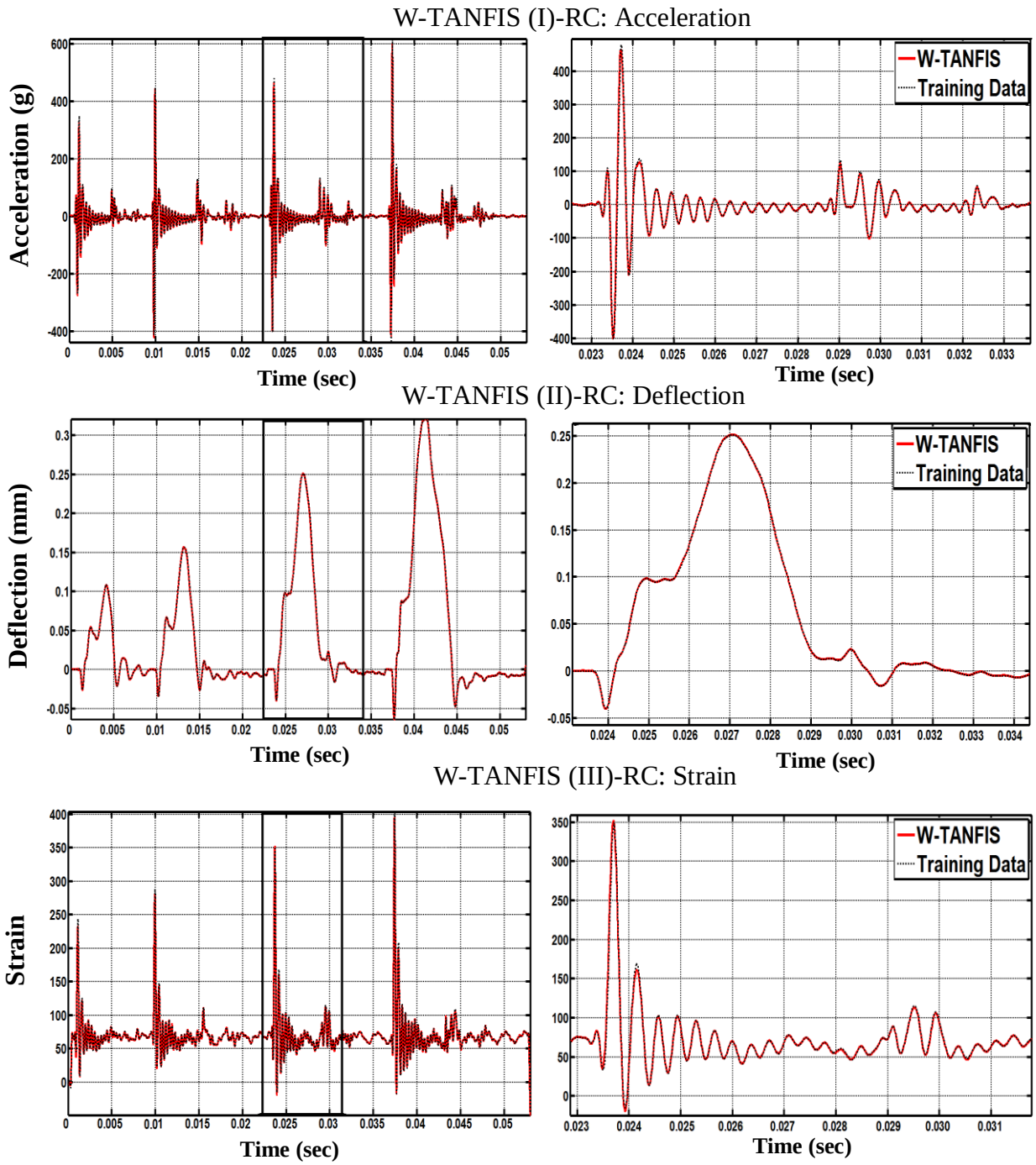

Figure 3-17. W-TANFIS training - random currents and different drop release heights

It is shown from the figures that the training responses correlate well with the actual responses. The proposed W-TANFIS model is effective in modeling the nonlinear dynamic response of a structure employing an MR damper under impact loads. For example, the maximum errors of the W-TANFIS model in predicting the structural impact responses are 3.2 for the strains, $0.376e^{-4}$ mm for deflections, and 119 g for accelerations, which represent less than 2.57%, 0.01%, and 15% error compared to the collected data. It was also estimated that the

W-TANFIS model has the RMSE errors of 2.4 for strains, $3e^{-4}$ mm for deflections and 7.4 g for acceleration. To generalize the trained models, they are validated using different data sets that are not used in the training process. Figure 3-18 exhibits the graphs of validated data sets.

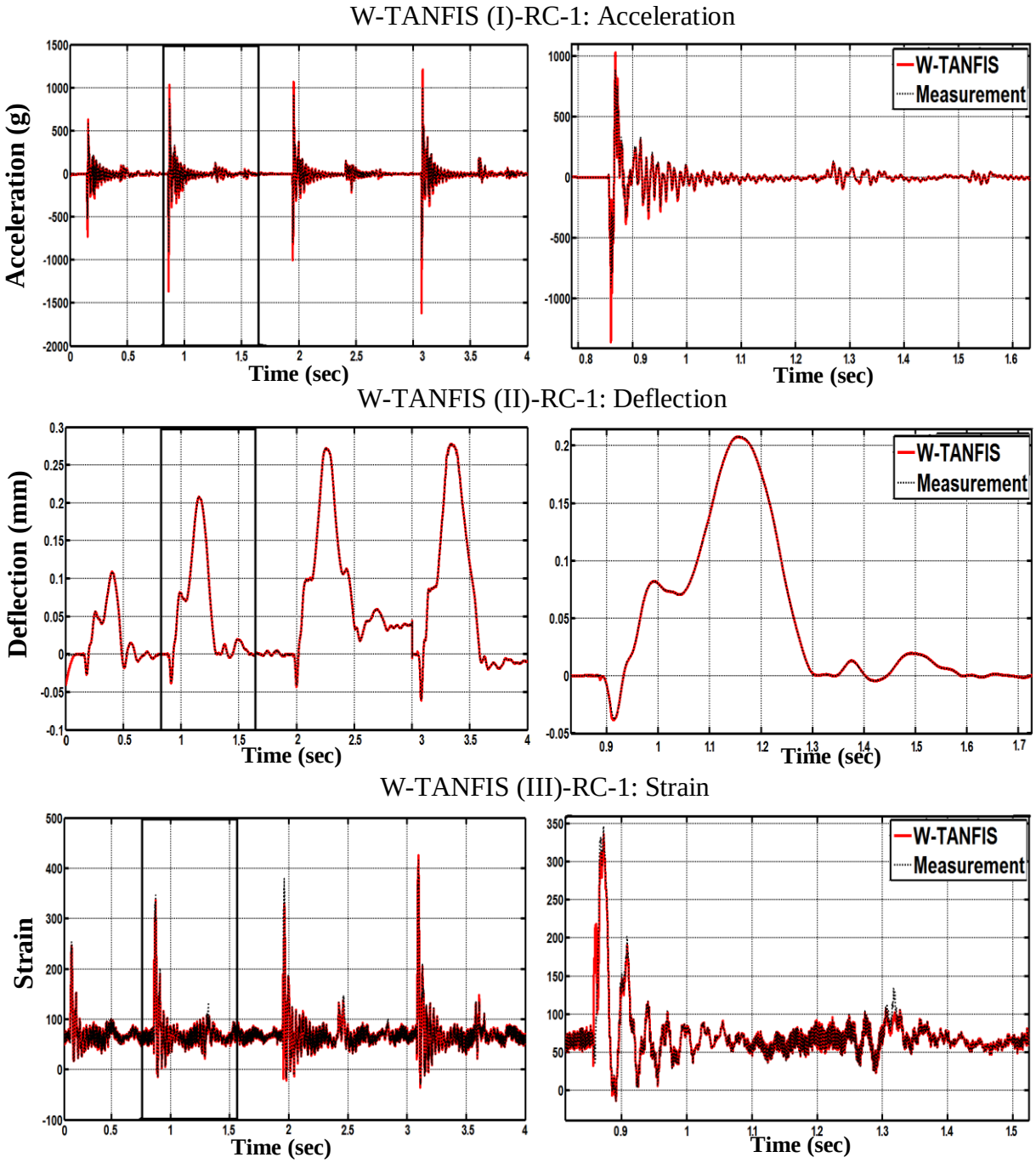

Figure 3-18. W-TANFIS validation - random currents and different drop release heights

The validation results show that the W-TANFIS predicts the dynamic impact responses of the concrete beam very accurately. The maximum errors of the W-TANFIS model in testing the

structural impact responses are 19 for the strains, 0.04 mm for deflections, and 195 g for accelerations, which represent less than 5%, 14%, and 18% errors compared to the testing data. It was also estimated that the W-TANFIS model has the RMSE errors of 18 for strains, $2e^{-3}$ mm for deflections and 49 g for acceleration. The fitting rates of both models are about over 90 %. On the other hand, the performance of the W-TANFIS in terms of computation load is significantly better than the ANFIS and TANFIS model. The quantitative evaluation of the proposed model is presented in detail in the Section 3.4.5.

Trained model with random current signals are also validated by the data sets obtained from the beam employing MR damper with constant currents. A detailed numerical evaluation is presented in Table 3-3.

3.4.5. Evaluation of results

Demonstration of the proposed W-TANFIS model is provided by using evaluation indices. In the quantification of errors, maximum absolute error is first calculated as

$$J_1 = \max|\hat{y} - \tilde{y}| \tag{3-19}$$

where, $\hat{y}$ is the trained data and $\tilde{y}$ is the actual measurements. Second evaluation criterion is defined as the mean of absolute error

$$J_2 = \text{mean}|\hat{y} - \tilde{y}| \tag{3-20}$$

Third criterion index is minimum absolute error

$$J_3 = \min|\hat{y} - \tilde{y}| \tag{3-21}$$

Fourth evaluation criterion is defined as root mean square error (RMSE)

$$J_4 = \text{RMSE} = \sqrt{\frac{\sum(\hat{y} - \tilde{y}|)^2}{DP}} \tag{3-22}$$

where, *DP* is the number of data points. Formulation of the fifth evaluation index is as follows

$$J_5 = \left[1 - \frac{\mathrm{var}(\hat{y} - \tilde{y})}{\mathrm{var}(\hat{y})}\right] \times 100 \tag{3-23}$$

where var represent the variance of data. As the trained model better predicts the measurements, the fitting rate of index J_5 will become close to 100. The last evaluation index J_6 is assigned as the CPU time to evaluate the duration of the training time. In other words, J_6 shows how much time the model requires completing the assigned iterations. Table 3-2 and Table 3-3 show the results of the error between the trained and actual data for the models trained with constant and random currents, respectively. Table 3-2 shows a detailed comparison between the proposed models and the actual test data with various constant current signals. The models are trained to predict acceleration (I), deflection (II) and strain (III) responses. The trained models are validated with four different data sets that were not used for the training process.

Table 3-2. Error Quantities of the ANFIS, TANFIS and W-TANFIS: **constant currents**

		J_1	J_2	J_3	J_4	J_5	J_6
Training	**ANFIS (I)**	729.644	25.475	8.696e-5	65.795	17.320	**1640.0494**
	ANFIS (II)	0.262	0.037	4.1734e-7	0.051	20.798	**2040.3765**
	ANFIS (III)	450.934	23.361	2.634e-4	34.528	1.617	**1436.7797**
	TANFIS (I)	62.079	0.176	6.387e-8	6.633	99.581	**638.7037**
	TANFIS (II)	1.891e-5	2.395e-7	2.349e-13	9.86e-4	99.998	**657.1080**
	TANFIS (III)	6.902	0.159	5.915e-8	0.928	99.962	**647.4733**
	W-TANFIS (I)	83.554	1.207	8.817e-6	12.298	98.659	**25.9174**
	W-TANFIS (II)	1.001e-5	4.255e-8	9.691e-13	3.28e-4	99.959	**22.5379**
	W-TANFIS (III)	2.616	0.144	1.261e-9	2.049	99.595	**20.9851**
Testing	ANFIS (I)-1	831.0461	22.676	2.063e-4	60.386	17.152	
	ANFIS (I)-2	765.229	20.789	2.482e-5	58.005	17.178	
	ANFIS (I)-3	701.140	20.557	7.287e-5	57.580	17.311	
	ANFIS (I)-4	686.256	21.451	1.841e-4	59.171	17.947	
	ANFIS (II)-1	0.249	0.045	2.190e-7	0.058	6.698	
	ANFIS (II)-2	0.252	0.040	1.312e-7	0.051	5.856	
	ANFIS (II)-3	0.266	0.043	1.769e-7	0.0547	4.252	
	ANFIS (II)-4	0.264	0.043	6.213e-8	0.056	6.340	
	ANFIS (III)-1	706.251	23.946	1.371e-4	41.523	0.247	
	ANFIS (III)-2	381.352	22.599	2.009e-4	33.039	1.019	
	ANFIS (III)-3	405.820	22.649	3.219e-5	33.915	0.962	
	ANFIS (III)-4	355.953	22.733	3.251e-6	34.688	1.583	
	TANFIS (I)-1	114.876	1.753	1.452e-7	5.986	99.215	
	TANFIS (I)-2	117.015	1.593	1.268e-7	5.872	99.160	
	TANFIS (I)-3	109.591	1.612	9.778e-8	5.856	99.172	
	TANFIS (I)-4	103.782	1.655	4.569e-7	5.894	99.186	
	TANFIS (II)-1	3.106e-4	5.703e-6	4.189e-11	7.06e-4	99.997	
	TANFIS (II)-2	4.872e-4	5.731e-6	1.974e-12	5.92e-4	99.940	
	TANFIS (II)-3	4.319e-4	5.674e-6	1.519e-11	6.27e-4	99.998	
	TANFIS (II)-4	6.488e-4	6.074e-6	2.634e-12	7.28e-4	99.914	
	TANFIS (III)-1	40.933	0.518	2.518e-6	1.331	98.692	
	TANFIS (III)-2	43.907	0.461	1.272e-6	0.878	99.760	
	TANFIS (III)-3	46.527	0.466	6.255e-6	0.957	99.799	
	TANFIS (III)-4	27.009	0.480	6.235e-6	0.982	99.536	
	W-TANFIS (I)-1	127.507	8.915	1.143e-5	11.004	95.266	
	W-TANFIS (I)-2	147.663	6.552	4.201e-6	11.093	95.222	
	W-TANFIS (I)-3	137.123	2.210	5.798e-6	10.672	94.790	
	W-TANFIS (I)-4	158.934	4.451	1.143e-6	10.322	94.655	
	W-TANFIS (II)-1	2.003 e-4	4.153 e-6	3.505e-12	2.86e-4	99.945	
	W-TANFIS (II)-2	2.782 e-4	4.874 e-6	2.278e-12	3.27e-4	99.957	
	W-TANFIS (II)-3	4.186 e-4	4.153 e-6	6.041e-12	2.94e-4	99.954	
	W-TANFIS (II)-4	3.144 e-4	4.674 e-6	1.167e-12	4.22e-4	99.984	
	W-TANFIS (III)-1	31.193	0.125	3.180e-6	3.986	95.874	
	W-TANFIS (III)-2	13.764	0.184	3.725e-7	1.987	98.505	
	W-TANFIS (III)-3	14.002	0.332	7.955e-6	3.141	98.771	
	W-TANFIS (III)-4	26.546	0.377	6.949e-6	2.457	99.595	

Table 3-3 shows another comparison of the proposed models with experimental datas collected under random current signals. To demonstrate the effectiveness of the proposed approach, the W-TANFIS models trained with the random current signal are validated by eight different data sets. The validations 1 to 4 were conducted under random current control command signals while the tests 5 to 8 were performed by using the data obtained from constant current case. As shown, the performance of the proposed models is robust against a variety of signals that were not used for training the models.

Table 3-3. Error Quantities of the ANFIS, TANFIS and W-TANFIS: **random currents**

		J_1	J_2	J_3	J_4	J_5	J_6
Training	**ANFIS (I)**	1.022e+3	34.028	5.414e-4	71.8872	28.185	**210.8356**
	ANFIS (II)	2.871	0.600	1.898e-5	0.790	5.788	**246.1441**
	ANFIS (III)	13.636	1.533	4.635	31.5036	3.2465	**184.4183**
	TANFIS (I)	61.842	0.387	8.962e-6	2.007	99.816	**37.2954**
	TANFIS (II)	0.803	2.152e-4	1.625e-9	3.981e-4	100.00	**35.7064**
	TANFIS (III)	10.323	0.137	5.429e-6	0.362	99.823	**29.7608**
	W-TANFIS (I)	119.289	2.038	2.916e-5	7.405	98.651	**4.8291**
	W-TANFIS (II)	0.376	1.801e-4	1.106e-7	3.017e-4	99.994	**4.3763**
	W-TANFIS (III)	3.199	0.794	1.974e-5	2.476	99.422	**5.2901**
Testing	ANFIS (I)-1	2.809e+4	74.280	6.435e-5	883.387	17.500	
	ANFIS (I)-2	1.986e+3	40.514	7.854e-4	95.786	29.502	
	ANFIS (I)-3	1.021e+3	39.044	0.001	83.127	23.585	
	ANFIS (I)-4	3.058e+3	36.263	4.590e-4	91.927	30.270	
	ANFIS (II)-1	12.576	0.073	4.855e-6	0.345	18.144	
	ANFIS (II)-2	38.616	0.124	6.277e-6	1.035	19.570	
	ANFIS (II)-3	31.960	0.113	1.345e-6	1.098	22.152	
	ANFIS (II)-4	3.780	0.062	7.940e-6	0.120	12.643	
	ANFIS (III)-1	2.565e+3	49.657	4.053e-4	238.121	1.274	
	ANFIS (III)-2	3.878e+3	65.504	2.310e-4	356.520	1.114	
	ANFIS (III)-3	2.856e+3	53.281	2.117e-4	263.349	2.570	
	ANFIS (III)-4	329.343	19.643	0.001	39.403	0.756	
	TANFIS (I)-1	153.276	2.197	4.923e-6	6.182	98.620	
	TANFIS (I)-2	136.525	2.141	6.620e-6	6.142	98.661	
	TANFIS (I)-3	170.706	2.261	3.527e-5	6.578	99.515	
	TANFIS (I)-4	164.934	1.935	5.310e-6	6.523	98.652	
	TANFIS (II)-1	0.004	7.657e-5	1.672e-9	1.314e-4	99.993	
	TANFIS (II)-2	0.004	7.070e-5	1.230e-9	1.206e-4	99.994	
	TANFIS (II)-3	5.274e-4	7.750e-5	3.034e-10	1.180e-4	99.989	
	TANFIS (II)-4	5.124e-4	7.283e-5	1.551e-10	1.123e-4	99.986	
	TANFIS (III)-1	56.765	3.775	1.474e-4	16.448	93.086	
	TANFIS (III)-2	23.458	3.173	4.199e-5	11.802	96.697	
	TANFIS (III)-3	19.964	3.609	1.062e-5	15.296	94.239	
	TANFIS (III)-4	16.923	1.613	5.811e-5	1.951	99.870	
	W-TANFIS (I)-1	195.735	6.014	1.081e-6	49.304	97.999	
	W- TANFIS (I)-2	137.437	3.871	1.631e-6	15.193	94.480	
	W- TANFIS (I)-3	182.985	4.746	5.117e-6	19.969	96.726	
	W- TANFIS (I)-4	235.798	3.752	1.022e-6	16.450	93.164	
	W- TANFIS (I)-5	260.235	4.444	7.1512e-8	64.024	98.045	
	W- TANFIS (I)-6	138.869	3.825	2.860e-7	43.016	99.906	
	W- TANFIS (I)-7	150.433	3.9412	2.693-6	49.130	99.412	
	W- TANFIS (I)-8	150.436	3.9412	2.693-6	49.130	99.412	
	W- TANFIS (II)-1	0.040	5.048e-5	6.867e-10	0.002	99.711	
	W- TANFIS (II)-2	0.046	2.910e-5	1.700e-9	0.001	99.893	
	W- TANFIS (II)-3	0.034	5.212e-5	3.213e-9	0.002	99.665	
	W- TANFIS (II)-4	0.0127	2.516e-5	1.474e-11	7.545e-4	99.860	
	W- TANFIS (II)-5	0.084	3.888e-5	7.275e-10	0.0017	99.536	
	W- TANFIS (II)-6	0.464	4.547e-5	5.130e-9	0.0054	99.582	
	W- TANFIS (II)-7	0.281	4.551e-5	2.276e-10	0.0042	99.829	
	W- TANFIS (II)-8	0.0535	4.243e-5	5.400e-11	0.0020	99.942	
	W- TANFIS (III)-1	19.917	2.9591	1.392e-4	18.348	95.943	
	W- TANFIS (III)-2	17.679	4.158	1.087e-5	45.405	94.638	
	W- TANFIS (III)-3	19.060	2.562	8.610e-5	8.964	91.423	
	W- TANFIS (III)-4	21.291	3.821	5.507e-7	31.510	89.859	
	W- TANFIS (III)-5	19.362	2.9206	1.990e-6	36.656	98.747	
	W- TANFIS (III)-6	24.986	2.649	4.102e-8	34.131	98.785	
	W- TANFIS (III)-7	27.412	2.651	1.048e-5	36.589	99.255	
	W- TANFIS (III)-8	16.267	2.824	7.394e-7	37.191	99.078	

It is observed from both training and validation processes that TANFIS and W-TANFIS achieve greater performance, while the predictions of the ANFIS are not in an agreement with actual test data.

As previously discussed, six indices are used to evaluate the simulation results. The first evalaution index, J_1, represents the maximum error between the proposed model and the actual test data. The low value in J_1 represents the good response prediction. As an example, in Table 3-3 the J_1 values in the training of the TANFIS and W-TANFIS models for acceleration responses are 61g and 119 g, which is about 6% and 11% of the ANFIS, respectively.

J_2 index shows the mean error between the test data and the proposed models. Small J_2 values imply the better performance. For instance, J_2 index of W-TANFIS in the training of deflection response is about 16% and 99.97% less than the TANFIS and ANFIS models, respectively. (Table 3-3)

When the minimum error (J_3) of the models are compared, it is seen that both TANFIS and W-TANFIS models performed better than the ANFIS models. For example, J_3 index of the ANFIS in the training of the strain responses is about $8e^5$ and $2e^4$ times higher than the ones of the TANFIS and the W-TANFIS models, respectively. (Table 3-3)

Both TANFIS and W-TANFIS models gave the J_5 index almost 100, which means that the models are very effective in predicting the dynamic responses of the smart systems under a variety of impact loadings. However, the performance of the W-TANFIS, in terms of computation time, is much better than the ANFIS and TANFIS. For the W-TANFIS models, the J_6 is almost 70 and 27 times smaller than the ones of ANFIS and TANFIS models, respectively. In other words, the computational load required to train the W-TANFIS model is significantly less than the ANFIS and TANFIS models. Although the RMSE and the accuracy of the TANFIS and W-TANFIS models are close, the W-TANFIS model is selected as the best model for identifying nonlinear behavior of reinforced concrete structure-MR damper systems in this paper due to the similar accuracy but faster computation time. It is demonstrated that the W-TANFIS model is an effective approach to understand and predict how the smart concrete structure will act under various impact loads. Based on this identified model, a smart control algorithm can be designed to optimize the current level of MR dampers for the dissipation of the structural impact energy.

3.5. Conclusion

This paper represents the application of a new wavelet-based time delayed adaptive neuro fuzzy inference system (W-TANFIS) model to the estimation of the nonlinear responses of smart reinforced concrete structures equipped with highly nonlinear hysteretic control devices under a variety of impact loads. The proposed models defines the behavior of physical systems in terms of a combination of numerics, linguistics and fuzzy rules by using input-output data without a full understanding of the complex mechansim in the high impact-induced smart concrete structure, which makes it simpler and more robust than the conventional system identification (SI) models. However, the proposed algorithm requires input-output data set to identify and test the nonlinear system model.

To obtain the necessary input-output data set and demonstrate the effectiveness of the proposed system, a simply supported reinforced concrete beam structure is investigated. The beam employs one MR damper whose fluids are controlled with either constant or random currents, while the beam without any MR damper is used as a baseline. In the training process of the proposed model, a variety of impact loads and current signals are used as input signals while the acceleration, deflection, and strain responses are used as output signals. To illustrate the effectiveness of the W-TANFIS model, an adaptive neuro fuzzy inference system (ANFIS) model and delayed ANFIS (TANFIS) model are used as baselines and the results are compared. It is demonstrated that the estimations of the ANFIS models do not give the reasonable match between the trained and actual test data. By contrast, both the W-TANFIS and TANFIS models are very effective in estimating nonlinear behaviors of structures equipped with highly nonlinear hysteretic magentorheological (MR) damper systems under a variety of impact loads. However, when the two models are evaluated in terms of computation time, the training process of W-TANFIS models is much shorter than TANFIS models. In conclusion, the study demonstrated that W-TANFIS is both fast and accurate in estimating the dynamic responses of the smart reinforced concrete structures under impact loading. The proposed models are used in understanding and predicting how the smart concrete structure will act under various levels of impact loads. Having a system that can effectively predict the nonlinear impact behavior allows us to develop a controller that can optimally dissipate the impact energy for different impact scenarios without a full understanding of complex behaviors of real infrastructural sytsems. In Chapter 5, the authors intend to develop an optimal control algorithm using the proposed model and test the performance of the controller using experimental study.

4. Modeling of Magnetorheological Dampers under Various Impact Loads

4.1. Introduction

4.1.1. Collision load

In recent years, the threat of impact or explosive loads have become an important topic to be taken into account in the design of structures (Wang and Li 2006; Ahmadian and Norris 2008; Hongsheng et al. 2009; Wiklo and Holnicki-Szulc 2009 a-b; Consolazio et al. 2010; Arsava et al 2013a). The impact and impulsive loads due to accidents, collisions, terrorist or military conditions can threaten the integrity of structures. For instance, the nonlinear material behaviors and high velocity responses, which are not considered in most of the existing structural design methods, can cause severe damage on the structural components. The partial or complete collapse of load bearing elements, and shifting or unseating failures of upper parts in structures are the most common failure mechanisms due to such impact loadings. To address such issues, structural control systems have been proposed as smart impact energy absorbers (Arsava et al 2013b). However, it is quite challenging to develop an effective structural control algorithm due to the complicated nonlinear behavior of the integrated systems and the uncertainties of high impact forces.

4.1.2. Impact response mitigation: structural controls

A control system can be implemented into a structure to adjust the stiffness or damping of the structure. Such control systems can be categorized into three main groups: passive, active and semiactive systems (Spencer et al. 1997b; Lynch 2002; Kim et al. 2009; Mitchell et al. 2012). Due to their low cost and relative easy design, passive dampers are the most widely used devices for structural control system design in the field of civil structures. Passive control systems do not require any external power source to operate the control device to damp the responses of excited structures. However, the effectiveness of the passive control systems are dependent on the design spectra of destructive environmental forces since they do not have the capability of a feedback-based parameter updating (Luca et al. 2005). On the other hand, active control systems adjust the force levels of the mechanical devices within the structure based on the structural response feedback. However, active controllers are highly dependent on a large external power suppliers to operate large actuators (Scruggs 1999; Scruggs and Lindner 1999). If there is an electricity cut

or some of the control feedback components such as wires and sensors are damaged, a malfuntion of the active controllers may occur. To address such issues, a solution could be found in semiactive control systems, which combines the best features of both passive and active control systems. Semiactive controller adjusts the level of control forces of smart control devices within structural systems in real time without requiring large power sources. (Arsava et al 2013a).

4.1.3. Smart control strategies

As a smart controller, magnetorheological (MR) damper technology has received great attention from various fields of engineering (Spencer et al. 1997b; Hurlebaus and Gaul 2006) due to the favorable features such as fast response time, reliable operation and low manufacturing cost (Dyke and Spencer 1996a; Dyke et al. 1998, 2001; Yi et al. 1998, 1999; Kim et al. 2009, 2010). MR damper is a viscous liquid damper that consists of small magnetically polarized particles whose flow rate can be adjusted according to the strength of the applied magnetic field (Schurter and Roschke 2000). To fully use the MR damper technology in implementing into high impact resistant infrastructural systems, a robust computational model that can describe the complex nonlinear behavior of the MR damper first needs to be developed.

One of the biggest challenges in semiactive control system design is the development of an accurate mathematical model of the MR damper system due to the highly nonlinear behavior of MR damping device (Bani-Hani et al 1999; Lin et al 2001; Kim and Langari, 2007; Kerber et al 2007; Kim et al 2011). Moreover, the nonlinear behavior becomes more complex when the MR damper is excited by unexpected high impact loads. Figure 4-1 represents the highly nonlinear hysteretic behavior of an MR damper between the high impact force and the corresponding strain. When a variety of impact forces and various control current signals are considered, the complex behavior will be much more complicated. Hence, it would be very challenging to develop an idealized parametric mechanical model for an MR damper under a variety of impact forces and control current control signals.

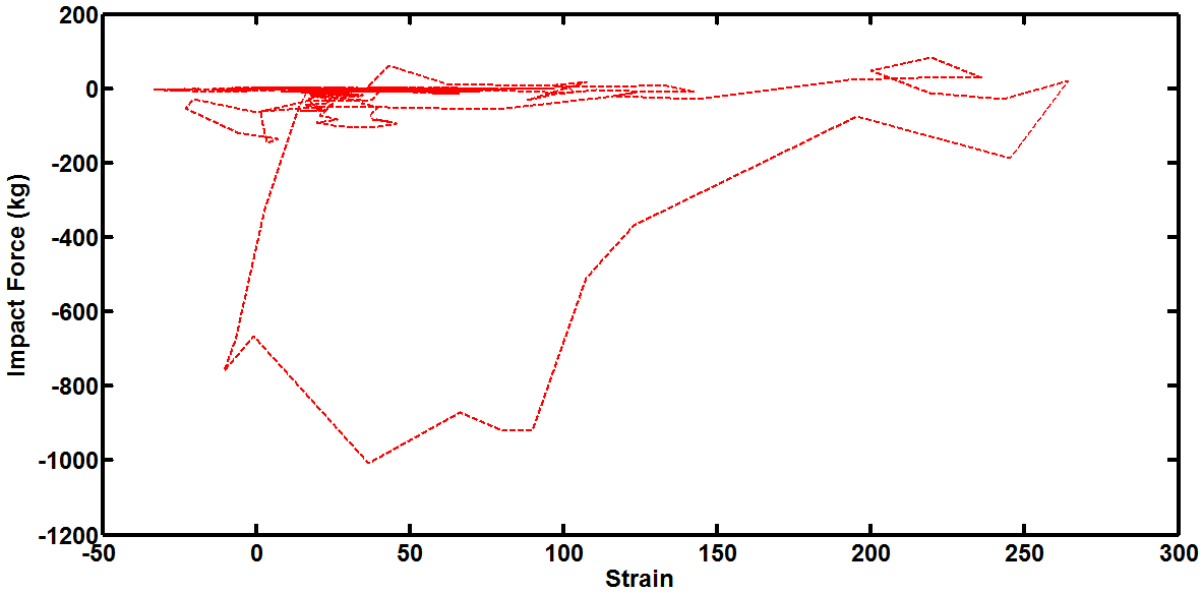

Figure 4-1. Nonlinear behavior of an MR damper under high impact loads

4.1.4. System identification

Such a challenging issue on the complex modeling can be addressed by applying nonlinear system identification (SI) methodologies. SI methodologies can be categorized into two parts: parametric and nonparametric (Bani-Hani et al. 1999; Suresh et al. 2008). The parametric approach uses the physical quantities of systems while the nonparametric SI method trains the input-output map of the system to define the architecture of the mathematical model (Lin et al. 2001; Hung et al. 2003; Lin and Betti 2004; Yang and Lin 2004). There exist few studies that performed the parametric system identification of MR dampers subjected to high impact loads (Lee et al. 2002; Hengbo et al. 2008; Hongsheng et al. 2009). Hengbo et al. (2008) presented a parametric study to predict the shock isolation performance of MR dampers under impact loads. A RD-1005-3 type MR damper was tested under impact loads at different constant current signals. The results demonstrated that the area of the hysteric response curves has a highly nonlinear relationship with the current that is applied to the MR damper. For example, the area under the force-displacement curve does not proportionally increase as the current increases. Thus, instead of using a typical Bouc-Wen model, they proposed a modified Bouc-Wen model to predict the nonlinear behavior of MR dampers under impact loads. It was demonstrated that the modified Bouc-Wen model has a good performance in predicting the impact response of MR dampers. However, the model was not tested under a variety of current signals, i.e., not random but constant current signals were investigated. Lee et al. (2002) used the Herschel-Bulkley shear model, which is a modified version of Bingham model, to evaluate the performance of ER-MR

impact damper systems. The equation of motions of the impact dampers was derived and its computer simulations were performed to analytically evaluate the characteristics of the ER-MR impact damper system under impact loads with constant current signals. The effects of flow behavior index on the performance of the impact damper system were evaluated. However, they investigated the MR damper performance under a single impact scenario using constant current signals.

As previously discussed, all of the aforementioned approaches have focused on the application of parametric models to the impact force estimation of MR dampers under constant voltages and limited impact scenarios. It is very challenging to develop a robust model for impact force prediction of an MR damper under a variety of applied voltages and impact scenarios. Note that the relationship between the collision forces and the associated MR damping forces is highly nonlinear. As previously discussed, the nonlinear relationship between the voltages and the MR damper under impact loads makes the modeling process much more difficult. With this in mind, a nonparametric approach, fuzzy models are proposed for the development of an MR damper model under a variety of impact scenarios and random current signals. The reason is that the fuzzy model is effective in modeling the complex nonlinear behavior of dynamic systems with parameter uncertainties.

4.1.5. Neuro-fuzzy modeling

The neuro-fuzzy approaches have been commonly applied to civil engineering problems (Allison and Chase 1994; Hung et al. 2003; Tesfamariam and Najjaran 2007; Faravelli and Yao 1996; Fonseca et al. 2008; Suresh et al. 2008; Kim et al. 2011). Muzzammil (2010) proposed an adaptive neuro-fuzzy inference system (ANFIS) to predict the maximum possible scour depth for bridge abutments. In the study, a regression model (RM) and artificial neural networks (ANNs) were used as baselines. It was demonstrated that the ANFIS model in predicting the scour depth outperforms over other models. Na et al. (2009) used the ANFIS to predict the compressive strength of concrete systems. The mix proportions and the results of nondestructive tests such as ultrasonic pulse velocity and rebound hammer test were used as inputs. Four different models were assessed using different inputs. The results showed that the ANFIS model can be reliably used to predict the compressive strengths of concretes without performing costly experimental investigation. Balasubramaniam et al. (2012) investigated the characteristics of glass fiber strengthened reinforced concrete beams due to corrosion damage. An experimental study was performed including 21 specimens with and without corrosion damage. The percentage of

corrosion, the type of fiber reinforced polymer (FRP) laminate and the thickness of the FRP plate were used as inputs in the ANFIS model to predict the load bearing, cracking and ductility behaviors of the concrete system. It was shown that the ANFIS is very effective to predict the defined outputs for the given system.

Because of their proven usefulness to estimate incomplete and incoherent measurements, the use of neuro-fuzzy models to identify the behavior of MR dampers has attracted a great deal of attention (Schurter and Roschke, 2000; Wang, H. 2009, 2010). Schurter and Roschke (2000) proposed the use of the ANFIS to describe the behavior of the SD-l000 MR damper subjected to sine, step, triangle, and pseudo random signals. Data for training and validating the ANFIS were obtained from the mathematical model of the MR damper proposed by Spencer et al. (1997b). Displacement, velocity and voltage were used as inputs to predict the MR damping force. The frequency content of the training data was approximately 0-3 Hz. The results showed that the proposed ANFIS model successfully represented the behavior of the MR damper. Another application was performed by Wang and Hu (2009). They proposed a novel way to describe the direct and inverse model of the MR damper. The direct and inverse ANFIS models were developed for the identification of the MR damper subjected to sinusoidal loading. In the training of the direct ANFIS model, the relative velocity, relative acceleration and the control voltage were used as inputs while the MR damping force was an output. As an inverse model of an MR damper, the MR damping forces, the relative velocity and the relative acceleration were used as input signals to predict the applied voltage. The numerical simulation demonstrated that the ANFIS systems can precisely model the direct and inverse problems of the MR damper under sinusoidal loading. Zeinali et al. (2013) proposed developing dynamic models of two MR dampers (a long stroke damper and a short stroke damper) by using ANFIS approach. MR dampers employing constant current signals (0-1 A) were tested under low frequency loads (1.9 Hz – 12.6 Hz). Current signal, displacement, and velocity data obtained from the experimental study were used as inputs to predict the force. It was demonstrated that the proposed ANFIS model have successfully predicted the behavior of MR damper.

Although all of the aforementioned approaches have successfully modeled the behavior of the MR damper under low frequency excitations, the modeling of the MR damping forces under a variety of impact scenarios and random control currents still remains far from fully answered. This paper is the first study in literature that focuses on the neuro-fuzzy system identification of an MR damper itself subjected to a variety of high impact loads and current signals. It should be noted that a dynamic load could be designated as an impact load if the magnitude is over 0.2 ton with an average of 0.5 ms peak force duration (Sekula et al. 2013;

Gencoglu and Mobasher 2007). It is indicated that the frequency of collision loads such as barge impact force can reach up to 50 Hz (Consolazio et al. 2006, 2008). Thus, the capture of the rapid and nonlinear changes in the system responses may be challenging for conventional models. In this context, a new experimental setup and a variety of numerical models are investigated for modeling the complex impact behavior of an MR damper, including a neuro-fuzzy, a modified neuro-fuzzy, a modified Bingham, and a modified Bouc-Wen models.

This paper is organized as follows. Section 4.2 discusses both parametric SI (Bouc-Wen and Bingham) as well as nonparametric (neuro-fuzzy models) approaches. The experimental setup and its procedures are described in section 4.3. In section 4.4, the results of the models including training and validation are presented. Concluding remarks are given in section 4.5.

4.2. System identification

As baselines, the Bouc-Wen model and the Bingham model are described in brief and then the neuro-fuzzy models are discussed.

4.2.1. Bouc-Wen model

A Bouc-Wen model has been commonly accepted in the field of MR damper technology (Spencer et al. 1997b; Hengbo et al. 2008). The restoring force of the MR damper is as follows;

$$f_{MR} = C_0\dot{u} + K_0(u - u_0) + \alpha_0 z \tag{4-1}$$

where evolutionary variable z is

$$\dot{z} = -\gamma|\dot{u}||z|^{na-1} - \beta\dot{u}|z|^{na} + Q\dot{u} \tag{4-2}$$

where f_{MR}, $\dot{u}$ and u are the damping force, velocity and deflection of piston rod, respectively. C_0 is damping coefficient, K_0 is elastic coefficient, α_0 , γ , β , na and Q are shape parameters

related to current signal. Although the Bouc-Wen model has been used extensively for modeling hysteretic systems, optimization of the characteristic parameters is very challenging. Generalization of the characteristic parameters for different excitations may be hard, since the parameters of traditional Bouc-Wen model are not functions of the frequency, amplitude and current signal (Dominguez et al., 2006). The estimated parameters shall be recalculated, which is a hard and computationally expensive process, if the MR damper is subjected to different excitations. In this context Dominguez et al. (2004) proposed a new methodology to determine the constant parameters of the Bouc-Wen. The following relationships were proposed.

$$f_{MR} = f_{Z0}(I) + C_0(I)\dot{u} + K_0(I)u + \alpha_0(I)z \tag{4-3}$$

$$C_0(I) = \begin{cases} C_1 + C_2\left(1 - e^{-C_3(I-I_c)}\right) & I > I_c \\ C_4 + \dfrac{C_4 - C_1}{I_c} I & I \le I_c \end{cases} \tag{4-4}$$

$$K_0(I) = -K_1 + K_2 I \tag{4-5}$$

$$\alpha_0(I) = \begin{cases} \alpha_1 + \alpha_2\left(1 - e^{-\alpha_3(I-I_c)}\right) & I > I_c \\ \alpha_1 + \dfrac{\alpha_4 - \alpha_1}{I_c} I & I \le I_c \end{cases} \tag{4-6}$$

$$\gamma_0(I) = -\gamma_1 + \gamma_2 I \tag{4-7}$$

$$f_{Z0}(I) = \begin{cases} f_{Z1} + f_{Z2}\left(1 - e^{-f_{Z3}(I-I_c)}\right) & I > I_c \\ f_{Z4} + \dfrac{f_{Z4} - f_{Z1}}{I_c} I & I \le I_c \end{cases} \tag{4-8}$$

where C_1, C_2, C_3, C_4, K_1, K_2, α_1, α_2, α_3, α_4, f_{Z1}, f_{Z2}, f_{Z3} and f_{Z4} are the constant parameters used to relate the characteristic shape paramaters to current signal, while $f_{Z0}(I)$ is defined as the offset force of MR damper. I is the current signal and I_c is the critical current in which the characteristic parameters change their linear behavior. By using the above parameters the evolutionary variable z is modified as follows;

$$z(I)=\frac{1}{\sqrt{\gamma(I)}}\tanh\left\{\sqrt{\gamma(I)}\left[\dot{u}+\frac{1}{\sqrt{\gamma(I)}}\times a\tanh\left(\frac{f_{Z0}(I)\sqrt{\gamma(I)}}{\alpha_0(I)}\right)\right]\right\} \quad \begin{matrix} for \quad (z<0,x<0) \quad or \\ for \quad (z\geq 0,x<0) \end{matrix} \qquad (4\text{-}9)$$

$$z(I)=\frac{1}{\sqrt{\gamma(I)}}\tanh\left\{\sqrt{\gamma(I)}\left[\dot{u}+\frac{1}{\sqrt{\gamma(I)}}\times a\tanh\left(-\frac{f_{Z0}(I)\sqrt{\gamma(I)}}{\alpha_0(I)}\right)\right]\right\} \quad \begin{matrix} for \quad (z\geq 0,x\geq 0) \quad or \\ for \quad (z<0,x\geq 0) \end{matrix} \qquad (4\text{-}10)$$

It was demonstrated that the proposed model was very effective to predict the behavior of MR damper subjected to different harmonic excitations (0.25, 2.5, 5.0, 7.5 and 10.0 Hz) and various constant current signals (0.0 0.25 0.50 0.75 1.00 1.25 1.50 A).

Hengbo et al (2008) updated the equations of Dominguez et al. (2006) to estimate the dynamic behaviors of MR dampers under high impact loads. Hengbo et al. (2008) modified the damping coefficient, elastic coefficient and evolutionary variable as follows;

$$C_0(I)=C_{R1}+(C_{R2}\times I) \qquad (4\text{-}11)$$

$$K_0(I)=-K_{R1}\left(e^{\frac{-I}{K_{R2}}}\right)+K_{R3} \qquad .(4\text{-}12)$$

$$z(I)=\frac{1}{\sqrt{\gamma(I)}}\tanh\left\{\sqrt{\gamma(I)}\times[\dot{u}+\dot{u}_h(I)]\right\} \qquad (4\text{-}13)$$

$$\dot{u}_h=u_{h1}-(u_{h2}\times I) \qquad (4\text{-}14)$$

where C_{R1}, C_{R2}, K_{R1}, K_{R2}, u_{h1} and u_{h2} the characteristic shape paramaters of the modified equations. In this study, the parameters of the Bouc-Wen model are adopted from Hengbo et al. (2008), which are provided in section 4.4.1.1. However, the results showed that the Bouc-Wen model is not effective in predicting various impact responses of MR damper under random

current signals although the model is very effective in a passive controlled case. The simulation results are described in section 4.4.2.1.

4.2.2. Bingham model

A Bingham model is used to understand and predict the behavior of an MR damper by modeling the viscous magnetic liquid in it. It is an effective way to investigate the flow properties and yield stress of MR fluids in liquid, quasi-solid and solid phases. The equation of the Bingham model can be expressed as (Li et al. 2012)

$$f_{MR} = c_d \dot{u} + \tau(\mathrm{sgn}(\dot{u})) \tag{4-15}$$

where c_d is the viscousity coefficient of MR fluids and τ represents the yield strength of the MR fluids. τ is formulated as follows

$$\tau = (\bar{a} \times I^3) + (\bar{b} \times I^2) + (\bar{c} \times I) + \bar{d} \tag{4-16}$$

where $\bar{a}, \bar{b}, \bar{c}$ and $\bar{d}$ are the identification parameters for the current signal between 0 A and 2 A. However, it is assumed that the Bingham model has a linear relationship between the stress and the rate of deflection when the yield stress is exceeded. Due to the assumption on the linear post yield damping, the shear thinning observed in impact damper applications cannot be accounted for in the Bingham model. The results showed that the Bingham model would not be effective in reproducing the nonlinear impact behavior of MR dampers. In this context, different nonlinear SI frameworks, which are described below, are used to improve the performance on the MR damper impact response prediction under a variety of impact loads and current signals.

4.2.3. Neuro-fuzzy model

A neuro-fuzzy model can be simply described as a system that integrates the neural network and fuzzy set theory (Mitchell et al., 2012). Neural network is used to mimic the human brain to improve the pattern recognition and the adaptability of the system, while fuzzy inference is used

in the decision making. In this study, the parameters of Takagi-Sugeno (TS) fuzzy models are determined using neural network algorithms (Tahmasebi and Hezarkhani, 2010). A typical neuro-fuzzy system with four inputs and one output is presented in Figure 4-2.

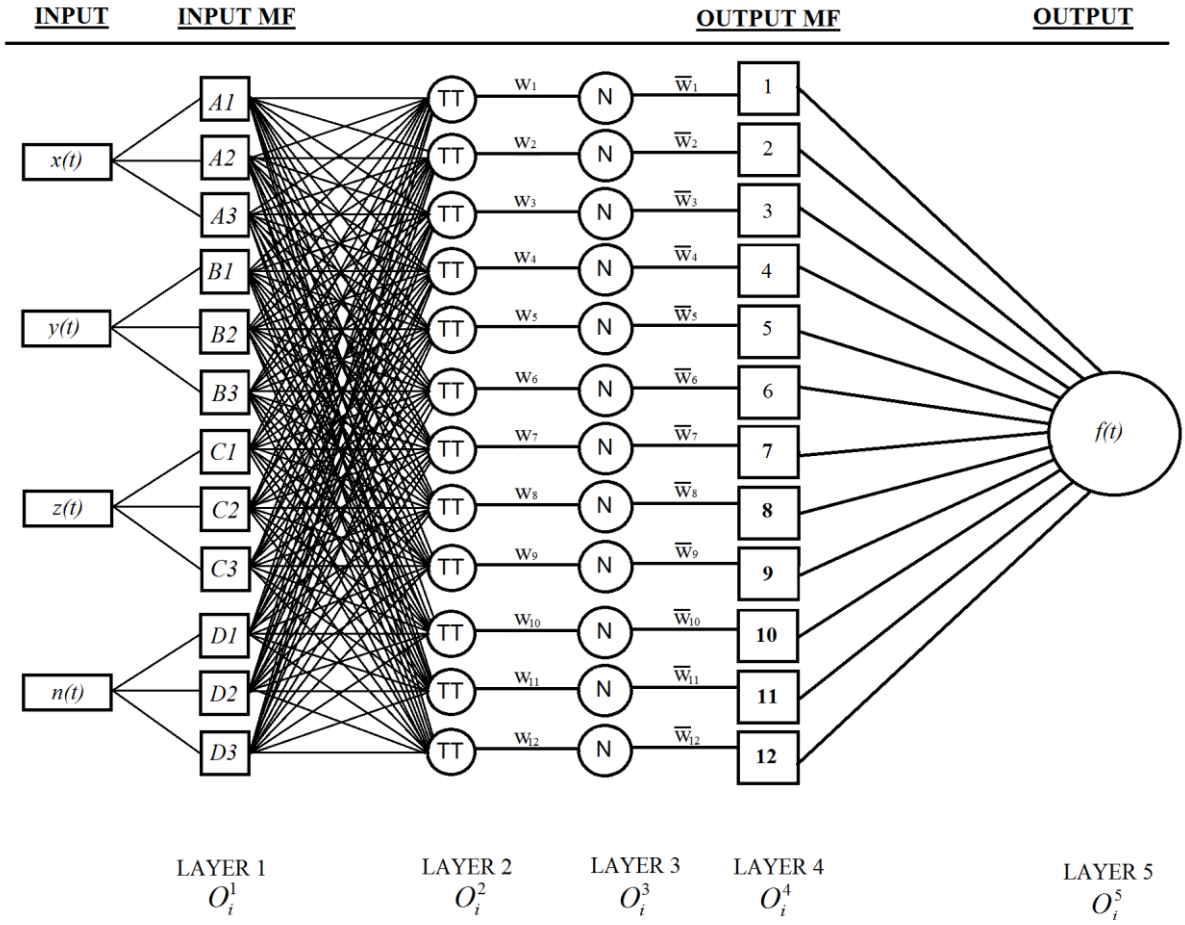

Figure 4-2. Typical neuro-fuzzy architecture

After the data is processed in the current layer, it moves forward to the next layer. The process can be described as: i) Layer 1 determine the fuzzy membership of inputs. ii) The product of all incoming inputs is colleceted in Layer 2. iii) In Layer 3, the data is normalized. iv) Node functions are applied in Layer 4 to solve the output of each fuzzy rule. v) Overall output of the fuzzy system is summated in Layer 5. A typical four rule neuro-fuzzy model is as follows

Rule 1: If x is A_1, y is B_1, z is C_1 and m is D_1, then $f_1 = p_1x + q_1y + k_1z + l_1n + r_1$ (4-17)

Rule 2: If x is A_2, y is B_2, z is C_2 and m is D_2, then $f_2 = p_2x + q_2y + k_2z + l_2n + r_2$ (4-18)

Rule 3: If x is A_3, y is B_3, z is C_3 and m is D_3, then $f_3 = p_3x + q_3y + k_3z + l_3n + r_3$ (4-19)

Rule 4: If x is A_4, y is B_4, z is C_4 and m is D_4, then $f_4 = p_4x + q_4y + k_4z + l_4n + r_4$ (4-20)

where x, y, z and n are the inputs and f is the output of the TS fuzzy system. The consequent parameters are defined as p_i, q_i, k_i, l_i and r_i. The function of Layer 1 is presented as

$$O_i^1 = \mu \begin{bmatrix} A_i(x) \\ B_i(y) \\ C_i(z) \\ D_i(n) \end{bmatrix} \tag{4-21}$$

where μ is the appropriate parameterized membership function (MF). O_i^1 (i = 1,2,3,4) is the output that specifies the degree to which the given input x satisfies the quantifier A.

After the application of MFs to each input, the data moves to the second layer. The function of Layer 1 is presented as

$$w_i = \mu A_i(x) \times \mu B_i(y) \times \mu C_i(z) \times \mu D_i(n),\ i = 1,2,3,4 \tag{4-22}$$

Output of the Layer 2 is the product of all incoming inputs. In order to normalize the output of Layer 2, the ratio of the output is taken in Layer 3

$$\overline{w}_i = \frac{w_i}{w_1 + w_2 + w_3 + w_4},\ i = 1,2,3,4 \tag{4-23}$$

In Layer 4, node functions ($f_i = p_ix + q_iy + k_iz + l_in + r_i, i$ = 1,2,3,4) are applied to output of Layer 3

$$O_i^4 = \overline{w}_i \times f_i = \overline{w}_i \times \left(p_i x + q_i y + k_i z + l_i n + r_i\right),\ i = 1,2,3,4 \tag{4-24}$$

As a last step, Layer 5 summates the layer inputs

$$O_i^5 = overall\ \ output + \sum_i \overline{w}_i \times f_i = \frac{\sum_i w_i \times f_i}{\sum_i w_i},\ i = 1,2,3,4 \tag{4-25}$$

In the optimization of the results, the neuro-fuzzy system uses adjustable parameters such as the number of MFs, types of MFs, the iteration and the step size. Various input-output data sets with different MF types are studied in this study in order to improve the effectiveness of the neuro-fuzzy model. In order to obtain input-output data for training and validating the the neuro-fuzzy model , a number of experimental studies are performed. The responses such as acceleration and deflection are obtained under a variety of combinations of the impact loads and the current signals. In this study, the displacement, acceleration, velocity and current signals are used to train the neuro-fuzzy model to model the impact force of the MR damper. At the end of the research, it is observed that about 75% of the actual impact force of the MR damper is correctly predicted by the neuro-fuzzy model. Howerer, only 44% of the peak values of impact forces are accurately predicted. It is also observed that the effectiveness of peak impact value predictions decreases as the level of the impact loads increases. In high impact scenarios, the MR damper model in the controlled structure may be effective due to the underestimated impact load when the neuro-fuzzy cannot predict the peak forces. In order to increase the accuracy between the trained and the actual high impact test data, a slightly modified fuzzy model can be used, which is defined below. It uses the outputs of the previous steps to predict the features of the following output.

4.2.4. Output feedback (OF)-based neuro-fuzzy model

The OF neuro-fuzzy model with four inputs and one output is presented in Figure 4-3.

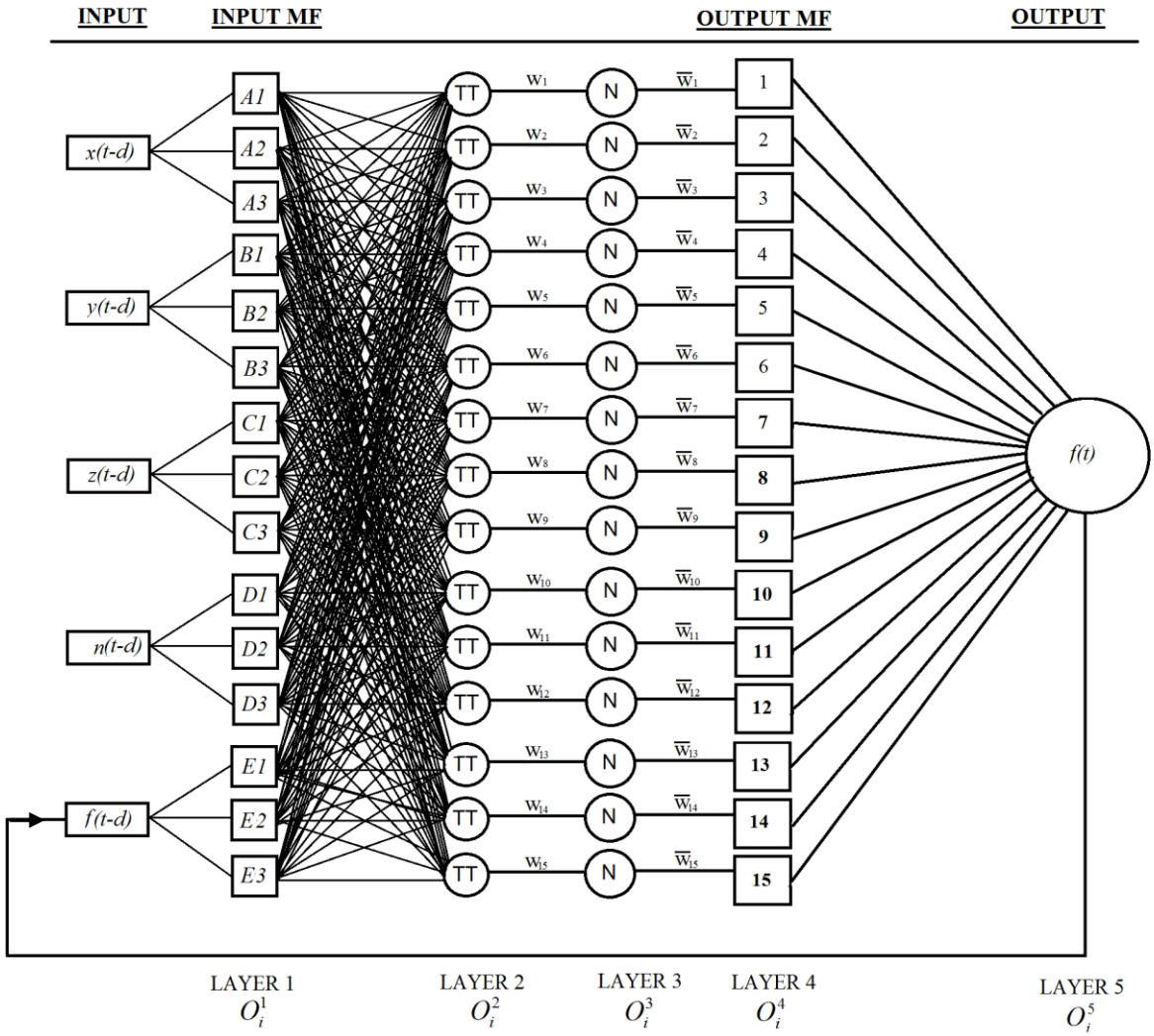

Figure 4-3. OF neuro-fuzzy architecture showing four input and one output model

Although the architectures of both neuro-fuzzy and OF neuro-fuzzy models are similar, the OF neuro-fuzzy model uses the observations obtained from the previous steps to predict the features of the following output. The input-output mapping (Adeli and Jiang 2006) can be expresed as follows

$$f_j(t) = f\left(x^{t-d}, f^{t-d}, e^{t-d}\right) + e(t) \tag{4-26}$$

where x^t represents the input, f^t is the output and and e^t is the error for time t. In this study, the time delay term d is assigned as 1, which means that the model uses the observations from the previous step (t-1) to estimate the output at time t. The OF neuro-fuzzy model is as follows

$$O_j^5 = overall \quad output + \sum_j \overline{w}_j \times f_j = \frac{\sum_j w_j \times f_j}{\sum_j w_j} \tag{4-27}$$

It is oberved that, the BP neuro-fuzzy approach increases the accuracy of the trained model significantly. The accuracy of peak response value predictions are about over 97%. The simulation results will be described in the following section.

4.3. Experimental setup

A set of experimental tests are conducted to study the effectiveness of the proposed models on anticipating the nonlinear behavior of MR dampers under a variety of high impact loads. The proposed test framework includes drop tower tests, MR dampers, a data acquisition system and sensors.

4.3.1. Drop tower test facility

The high impact load test facility in Smart Impact Mitigation and Mechanics (SIMM) Laboraotry in the Civil and Environmental Engineering Department at Worcester Polytechnic Institute (WPI) has been used to apply the controlled impact loads to the MR damper. The maximum capacity to apply the impact load of the testing facility is 22,500 kg. In this study, the impact loads are applied by releasing a falling drop-mass from different combinations of the drop release heights.

4.3.2. Magnetorheological (MR) dampers

In general, an MR damper consists of a hydraulic cylinder, the magnetic coils and MR fluids. The MR fluid consists of micron sized magnetically polarized particles within an oil-type fluid (Spencer et al., 1997b). Some of the distinguishing characteristics of MR dampers are can be listed as: (i) MR dampers require low power sources when they are operated as active controllers. (ii) The performance is stable in a broad range of temperatures. (iii) They have a very fast response time. (iv) They have a high yield stress level (Hurlebaus and Gaul, 2006; Kim et al., 2009). The RD-8040-1 type MR damper developed by Lord Corporation is used in the experimental study (Figure 4-4).

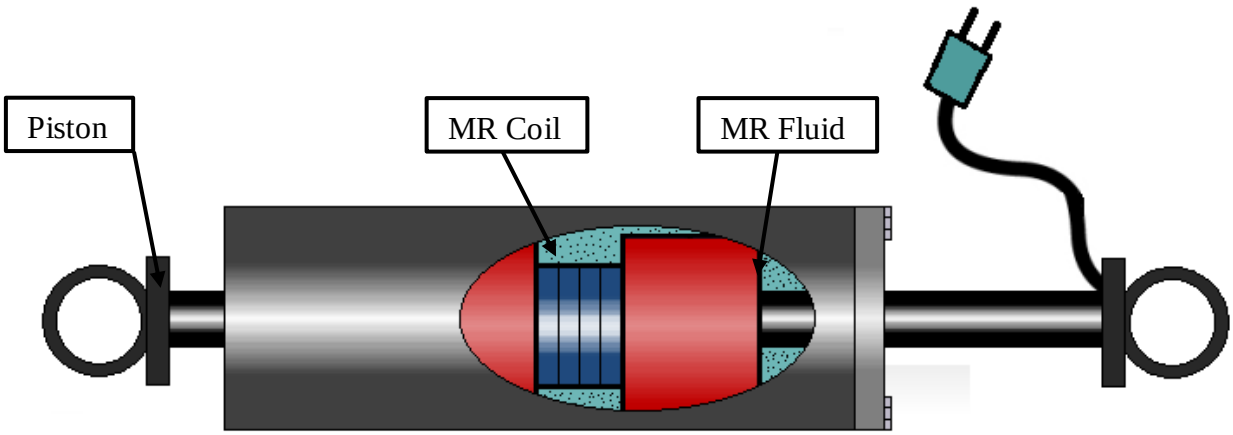

Figure 4-4. Schematic of RD-8040-1 MR damper

A test framework as depicted in Figure 4-5 is prepared. An MR damper is fixed to the ground and the lateral plates to prevent it from shifting during the application of the high impact loading. To apply the impact loads and connect the sensors, a special housing system is manufactured. The lateral plates and the impact plate are assembled with a special rail system and oiled before each test in order to minimize the friction. For the consistency, the load is applied to the center of the impact plate.

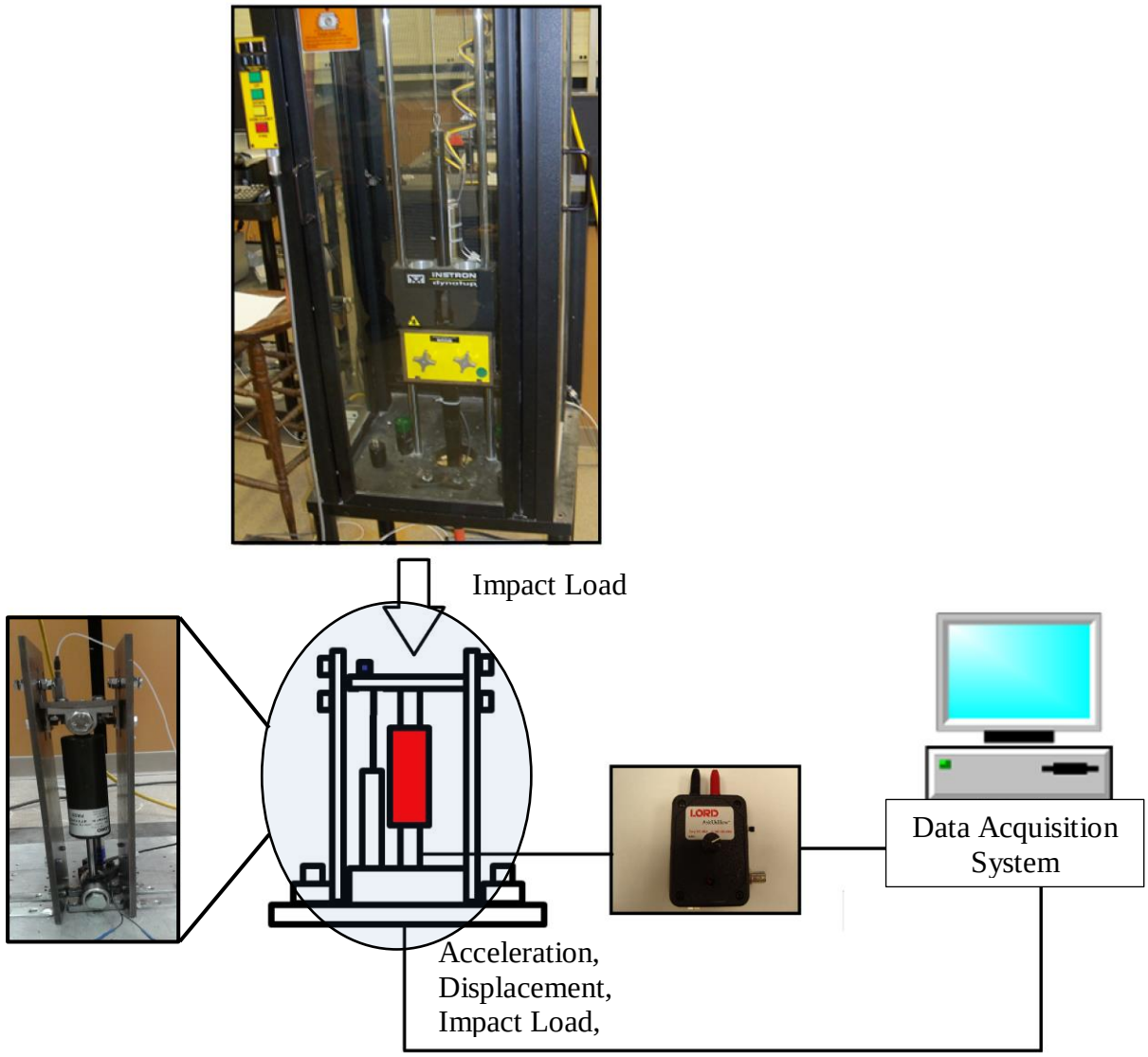

Figure 4-5. Details of the test framework

4.3.3. Data acquisition

During the impact tests, a National Instrument (NI) LabView data acquisition is used to obtain the acceleration, deflection, impact force and current signal data. The displacement data is measured by R.D.P product ACT1000A type LVDT, while a PCB type 302A accelerometer and a 4,500 kg capacity Central HTC-10K type load cells are used in the acceleration and impact force measurements, respectively. As a sampling rate of the data acquisition system, 10,000 data points per second is selected. The locations of the sensors are depicted in Figure 4-6.

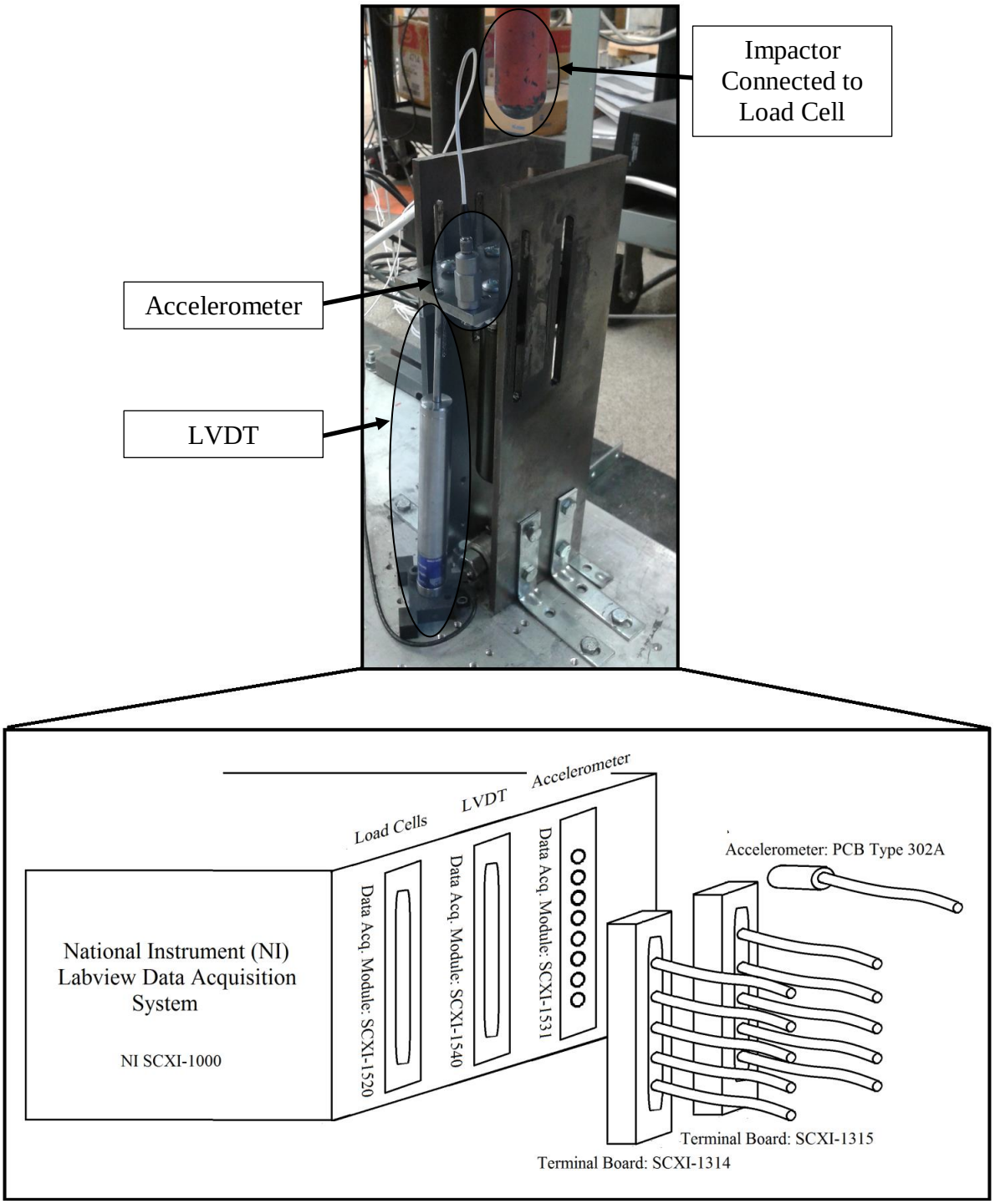

Figure 4-6. Configuration of the data acquisition system

4.3.4. Test details

A series of experimental tests are performed to measure the dynamic response of the MR damper under a variety of impact loads and various current signals. For each drop release height and

current on the MR damper, the drop release test is performed three times to train and validate the models. Details of the performed tests can be found in Table 4-1.

Table 4-1. Experimental Test Details

Case Studies			Drop Release Height (mm)	Type of Output Signal	Current on MR Damper	Impact Velocity (mm/s)
Trained Data	Validated Data 1st Set	Validated Data 2nd Set				
Case 1	Case 2	Case 3	65	Constant	0 A	1129
Case 4	Case 5	Case 6	65		0.2 A	
Case 7	Case 8	Case 9	65		0.6 A	
Case 10	Case 11	Case 12	65		1 A	
Case 13	Case 14	Case 15	65		1.5 A	
Case 16	Case 17	Case 18	65		1.9 A	
Case 19	Case 20	Case 21	65	Sinusoidal	0 A-1.9 A	
Case 22	Case 23	Case 24	65			
Case 25	Case 26	Case 27	65			
Case 28	Case 29	Case 30	65			
Case 31	Case 32	Case 33	65			
Case 34	Case 35	Case 36	65			
Case 37	Case 38	Case 39	65			
Case 40	Case 41	Case 42	65			
Case 43	Case 44	Case 45	65	Random	0 A-1.9 A	
Case 46	Case 47	Case 48	130	Constant	0 A	2258
Case 49	Case 50	Case 51	130		0.2 A	
Case 52	Case 53	Case 54	130		0.6 A	
Case 55	Case 56	Case 57	130		1 A	
Case 58	Case 59	Case 60	130		1.5 A	
Case 61	Case 62	Case 63	130		1.9 A	
Case 64	Case 65	Case 66	130	Sinusoidal	0 A-1.9 A	
Case 67	Case 68	Case 69	130			
Case 70	Case 71	Case 72	130			
Case 73	Case 74	Case 75	130			
Case 76	Case 77	Case 78	130			
Case 79	Case 80	Case 81	130			
Case 82	Case 83	Case 84	130			
Case 85	Case 86	Case 87	130			
Case 88	Case 89	Case 90	130	Random	0 A-1.9 A	

Table 4-1. Experimental Test Details (Cont.)

Case Studies			Drop Release Height (mm)	Output Signal	Current on MR Damper	Impact Velocity (mm/s)
Trained Data	Validated Data 1st Set	Validated Data 2nd Set				
Case 91	Case 92	Case 93	254	Constant	0 A	4412
Case 94	Case 95	Case 96	254		0.2 A	
Case 97	Case 98	Case 99	254		0.6 A	
Case 100	Case 101	Case 102	254		1 A	
Case 103	Case 104	Case 105	254		1.5 A	
Case 106	Case 107	Case 108	254		1.9 A	
Case 109	Case 110	Case 111	254	Sinusoidal	0 A-1.9 A	
Case 112	Case 113	Case 114	254			
Case 115	Case 116	Case 117	254			
Case 118	Case 119	Case 120	254			
Case 121	Case 122	Case 123	254			
Case 124	Case 125	Case 126	254			
Case 127	Case 128	Case 129	254			
Case 130	Case 131	Case 132	254			
Case 133	Case 134	Case 135	254	Random	0 A-1.9 A	
Case 136	Case 137	Case 138	380	Constant	0 A	6600
Case 139	Case 140	Case 141	380		0.2 A	
Case 142	Case 143	Case 144	380		0.6 A	
Case 145	Case 146	Case 147	380		1 A	
Case 148	Case 149	Case 150	380		1.5 A	
Case 151	Case 152	Case 153	380		1.9 A	
Case 154	Case 155	Case 156	380	Sinusoidal	0 A-1.9 A	
Case 157	Case 158	Case 159	380			
Case 160	Case 161	Case 162	380			
Case 163	Case 164	Case 165	380			
Case 166	Case 167	Case 168	380			
Case 169	Case 170	Case 171	380			
Case 172	Case 173	Case 174	380			
Case 175	Case 176	Case 177	380			
Case 178	Case 179	Case 180	380	Random	0 A-1.9 A	

Table 4-1. Experimental Test Details (Cont.)

Case Studies			Drop Release Height (mm)	Output Signal	Current on MR Damper	Impact Velocity (mm/s)
Trained Data	Validated Data 1st Set	Validated Data 2nd Set				
Case 181	Case 182	Case 183	500	Constant	0 A	8685
Case 184	Case 185	Case 186	500		0.2 A	
Case 187	Case 188	Case 189	500		0.6 A	
Case 190	Case 191	Case 192	500		1 A	
Case 193	Case 194	Case 195	500		1.5 A	
Case 196	Case 197	Case 198	500		1.9 A	
Case 199	Case 200	Case 201	500	Sinusoidal	0 A-1.9 A	
Case 202	Case 203	Case 204	500			
Case 205	Case 206	Case 207	500			
Case 208	Case 209	Case 210	500			
Case 211	Case 212	Case 213	500			
Case 214	Case 215	Case 216	500			
Case 217	Case 218	Case 219	500			
Case 220	Case 221	Case 222	500			
Case 223	Case 224	Case 225	500	Random	0 A-1.9 A	

Experimental study contains a total of 225 impact tests that investigate the dynamic responses of the MR damper under five different force levels by various current signals. Three types of current signals are used in the tests such as several constants, the sinusoidal signals with different frequencies (0.75, 1, 2, 1.5, 2, 3, 5, 7 and 10 Hz), and random signals. The high impact test is repeated for each current level.

4.4. System identification results

4.4.1. Parameter Setting

4.4.1.1. Bouc-Wen model

The parameters of the impact Bouc-Wen model are adopted from Hengbo et al. (2008) as shown in Table 4-2.

Table 4-2. Parameters of Bouc-Wen model

Parameter	Value	Parameter	Value
C_{R1}	1528 N.s.m^{-1}	u_{h1}	0.0345
C_{R2}	1994 N.s.m^{-1}	u_{h2}	0.0138
K_{R1}	53346 N. m^{-1}	α_1	1514 N. m^{-1}
K_{R2}	69003 N. A^{-1}	α_2	4200 N. m^{-1}
K_{R3}	0.3584	α_3	2.2 A^{-1}
γ_1	280 m^{-2}	α_4	5728 N. m^{-1}
γ_2	8.66 m^{-2}	I_c	0.25 A

The result of the Bouc-Wen model is discussed in the following section.

4.4.1.2. Bingham model

Table 4-3 shows the parameters used in the development of the impact Bingham model. The parameters come from the results of Li et al. (2012).

Table 4-3. Parameters of Bingham model

Parameter	Value	Parameter	Value
c_d	252.0898	$\bar{c}$	14.631534
$\bar{a}$	-15.821146	$\bar{d}$	2.229533
$\bar{b}$	27.469656		

4.4.1.3. Neuro-fuzzy model

To develop the neuro-fuzzy model, many sets of input and output data are collected and prepared for training and validation. In the simulation process, to get the best match, an iterative method is used by changing the training iteration, step size, type and quantity of MFs. Figure 4-7 shows the type of MFs used. Table 4-4 depicts the effect of MFs on the accuracy of the developed neuro-fuzzy models .

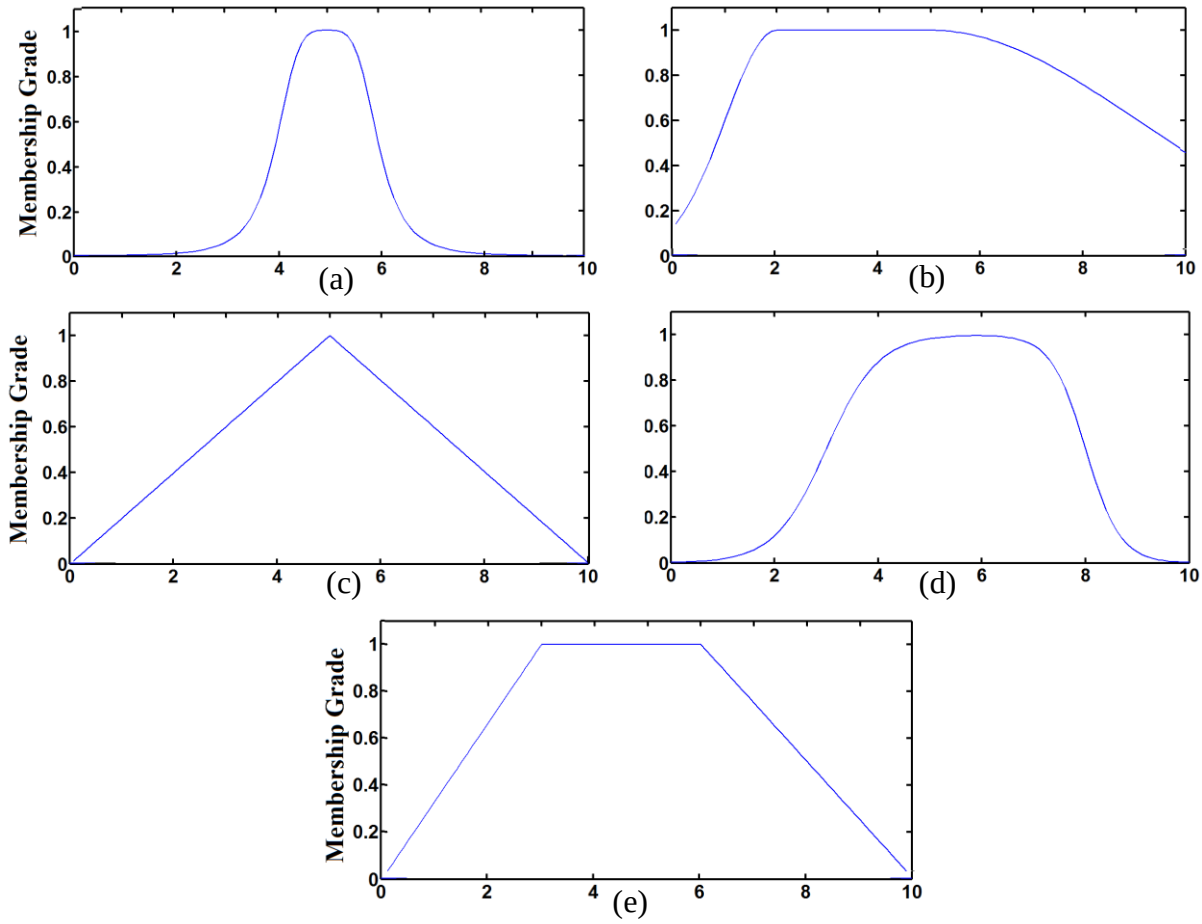

Figure 4-7. The type of MF: (a) Gaussian MF (b) Bell MF (c) Triangular MF (d) Sigmoidal MF (e) Trapezoidal MF

Table 4-4. Simulation parameter studies

Inputs				Output	MF Type	Accuracy (%)
Deflection	Acceleration	Velocity	Current	Impact Load		
Neuro-fuzzy **training (4 inputs - 1 output)**					Gaussian	**74.68**
					Bell	68.57
					Triangular	71.37
					Sigmoidal	73.75
					Trapezoidal	65.10

After performing the extensive simulations, it is observed that the best match was obtained from the Gaussian MF. Hence using the Gaussian MFs, the parametric studies on the combination of input-output data sets are conducted in this study. A total of 15 combinations are evaluated. Table 4-5 compares the performance of fuzzy models for different input data sets.

Table 4-5. Simulation parameter studies for neuro-fuzzy models

		Input				
Model #		Deflection	Acceleration	Velocity	Current	Accuracy (%)
1	1 in 1 out	+				32.52
2			+			40.34
3				+		39.72
4					+	2.09
5	2 in 1 out	+	+			60.65
6		+		+		63.4
7		+			+	37.32
8			+	+		61.74
9			+		+	41
10				+	+	41.58
11	**3 in 1 out**	+	+	+		68.23
12		+	+		+	58.34
13		+		+	+	56.55
14			+	+	+	47.45
15	**4 in 1 out**	**+**	**+**	**+**	**+**	**74.68**

It is demonstrated that the choice of input-output data set has a significant effect on the accuracy of the neuro-fuzzy model. When the MR damper is modelled using a single input and single output data set, the accuracy of the model does not reach up to 50%. To obtain a better performance, number of inputs are increased step by step. The fitting rates of the fuzzy model are about over 50% for the three input-one output data set. As seen from the above table, the fuzzy model trained using the input-output data set that was used in Wang and Hu (2009) produced around the fitting rate of 47%, which is the case of 14. The best model for identifying the nonlinear behavior of MR dampers is obtained by using four input-one output data set. It is found that all the defection, acceleration and velocity data significantly contribute to the performance of the neuro-fuzzy model. Figure 4-8 shows a selected set of the input-output signals for training the neuro-fuzzy model. The deflection, acceleration, velocity and current signals are used as the inputs while the high impact load applied on the MR damper is used as an output signal.

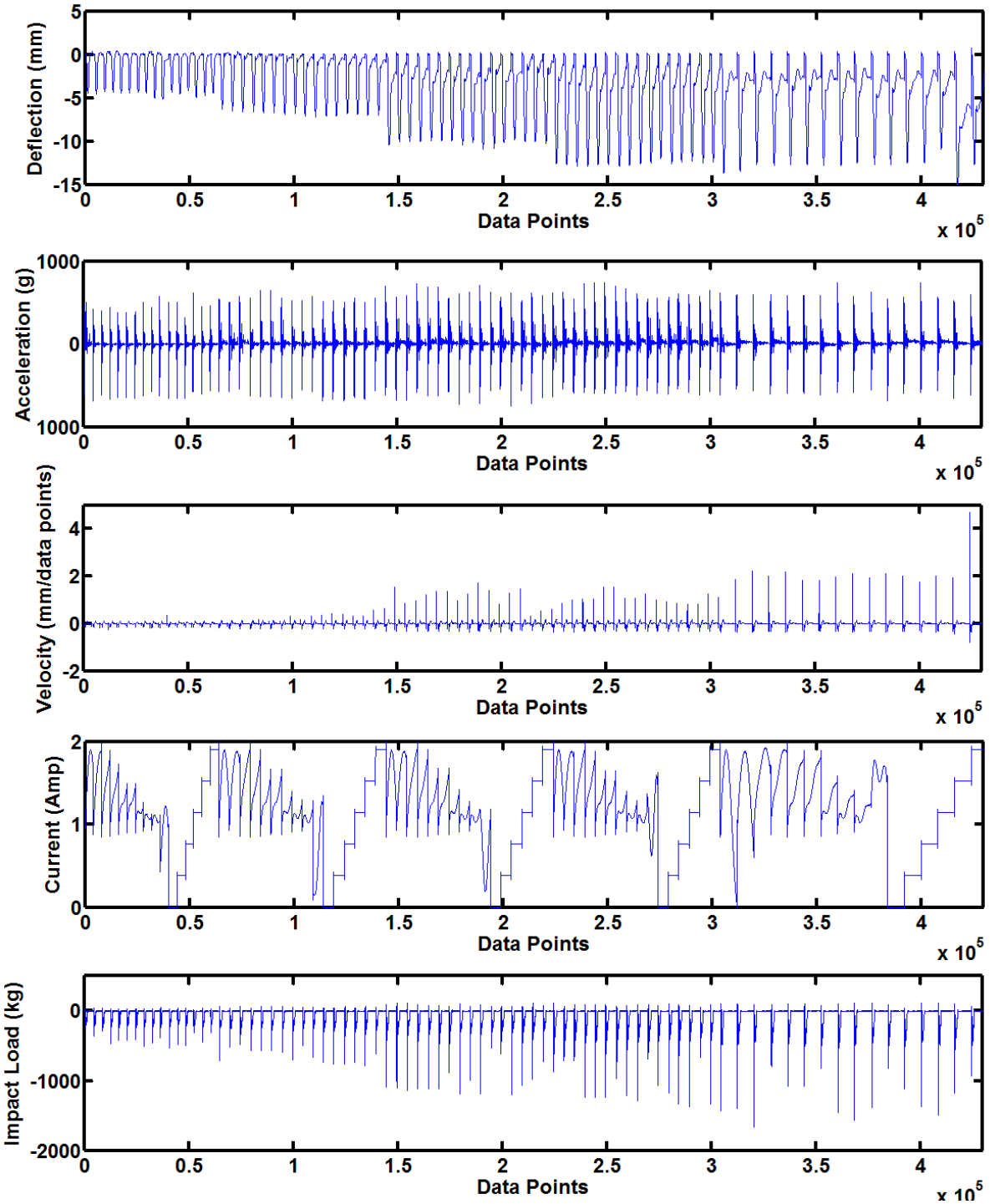

Figure 4-8. Input-output data sets to train the neuro-fuzzy models

4.4.1.4. The OF neuro-fuzzy model

The same parametric studies are performed to investigate the effect of the input-output data set on the performance of the OF neuro-fuzzy model. The performance of the models for different input data sets are evaluated in Table 4-6.

Table 4-6. Simulation parameter studies for the OF neuro-fuzzy models

		Input				
Model #		Deflection	Acceleration	Velocity	Current	Accuracy (%)
1	1 in 1 out	+				85.66
2			+			86.16
3				+		85.68
4					+	85.67
5	2 in 1 out	+	+			91.05
6		+		+		91.05
7		+			+	92.02
8			+	+		91.13
9			+		+	91.35
10				+	+	91.08
11	3 in 1 out	+	+	+		99.81
12		+	+		+	99.78
13		+		+	+	99.79
14			+	+	+	99.81
15	4 in 1 out	+	+	+	+	**99.84**

It is seen that the accuracy of the OF neuro-fuzzy model is over 85% for all input-output data sets. In order to be persistent in the evaluation of the results, the same input-output data set was used to train the OF neuro-fuzzy model with the bare neuro-fuzzy model.

4.4.2. System identification results

4.4.2.1. Bouc-Wen model

The time history responses of the Bouc-Wen model employing various currents and different drop release heights are depicted in Figure 4-9.

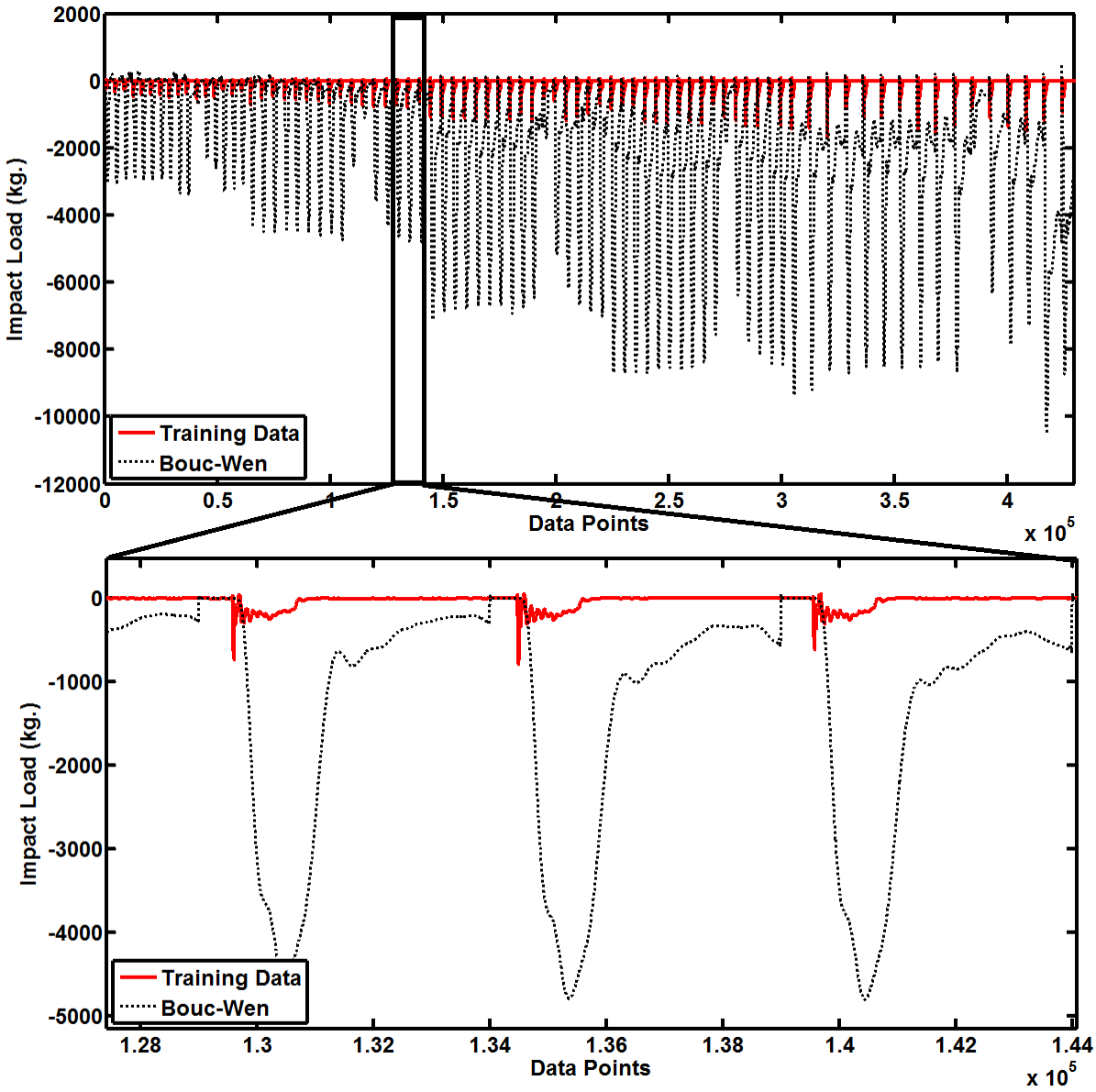

Figure 4-9. Comparison of the impact load measurements with the Bouc-Wen model for various currents and drop release heights

It is shown from Figure 4-9 that the Bouc-Wen model does not capture the nonlinear behavior of the MR damper system under a variety of impact loads and current signals. The fitting rates of models are about 3 %. This could be inferred from two facts: (1) the parameters of the Bouc-Wen model (Hengo et al. 2008) are determined using a single current level. Thus, the model may not accurately predict the experimental data for other currents levels. (2) the model only uses one auxiliary nonlinear differential equation to describe the hysteretic behavior of the MR damper, which makes it very challenging to incorporate different impact load cases with variety of current signals.

4.4.2.2. Bingham model

Figure 4-10 compares the real measured impact load with the estimates from the Bingham models.

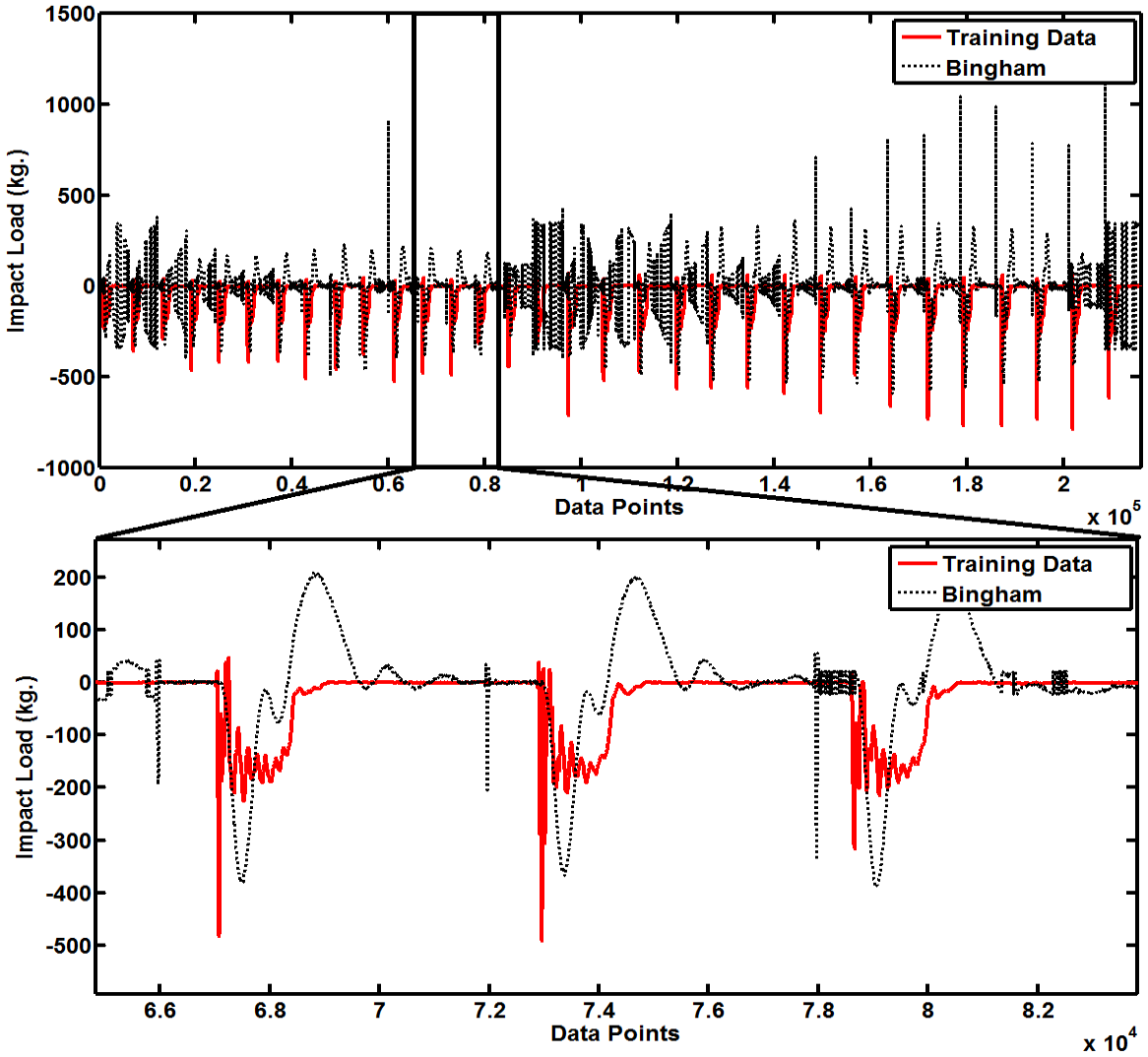

Figure 4-10. Comparison of the impact load measurements with Bingham plastic model for various currents and drop release heights

As seen in Figure 4-10, the predicted results of the Bingham model are not in an agreement with the measurements of the actual impact loads. Only the 5% of the MR damper behavior under a variety of impact loadings and control inputs are accurately predicted. As previously discussed, it is difficult to predict the complicated behavior of the MR dampers under

a variety of impact forces and current signals. The reason is that the Bingham model is implemented with constant parameters.

4.4.2.3. Neuro-fuzzy modeling

A variety of the neuro-fuzzy model architectures have been considered, including various combination of input and output data sets. Figure 4-11 represents a selected architecture of the neuro-fuzzy model.

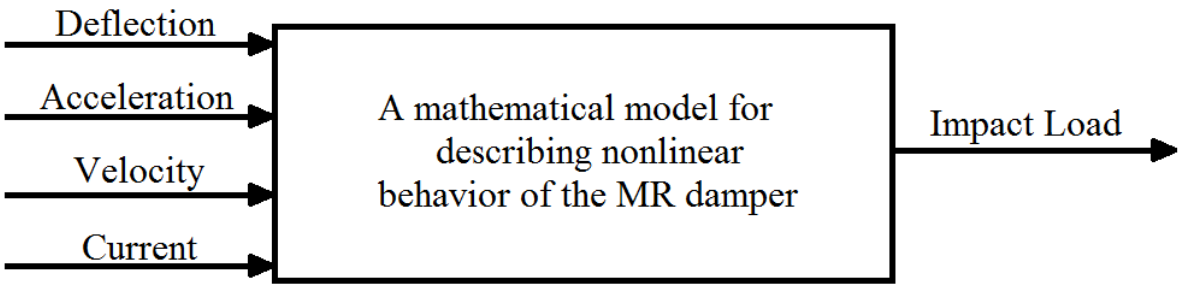

Figure 4-11. Configuration of the neuro-fuzzy model: Impact load prediction

Figure 4-12 compares the real measured impact load data with the estimations of the neuro-fuzzy model for five different force levels under various current levels,

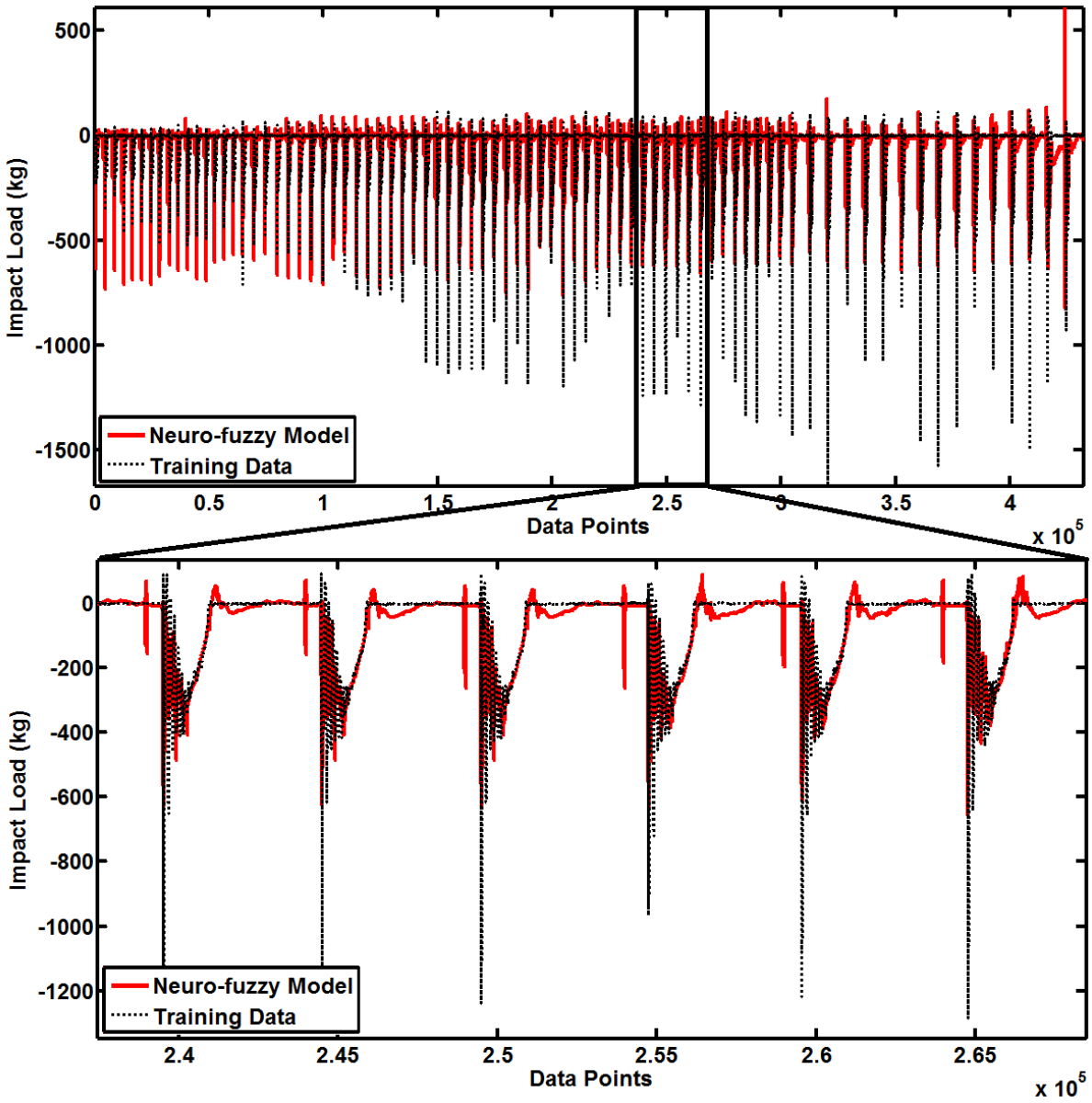

Figure 4-12. Neuro-fuzzy training results: constant, sinusoidal and random currents for different drop release heights

The results show that the neuro-fuzzy predictions give reasonable match between the trained and actual test data. The fitting rate of the model for the four input-one output data set is about 75%. However, as mentioned in the previous sections, the performance of the neuro-fuzzy model to capture the peak impact values decreases as the impact loads increase. The underestimation of the impact load in the control system design can reduce the effectiveness of the MR damper to dissipate the impact energy. For this reason, the OF neuro-fuzzy model is used to increase the accuracy of the predictions.

4.4.2.4. The OF neuro-fuzzy modeling

Figure 4-13 represents the conceptual configuration of the propsed OF neuro-fuzzy models.

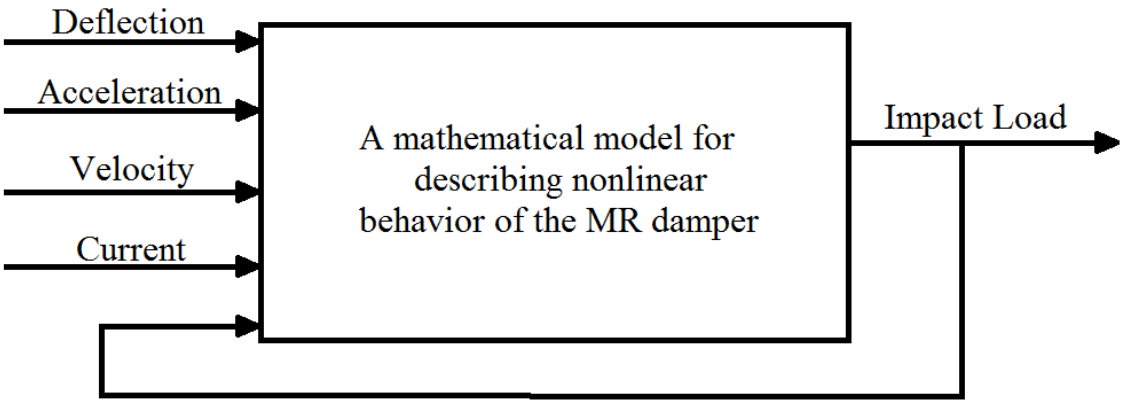

Figure 4-13. Configuration of the OF neuro-fuzzy model: Impact load prediction

The selected MFs of the OF neuro-fuzzy model are presented in Figure 4-14. Left column shows the initial MFs values, while the right column represents the optimally tuned MFs.

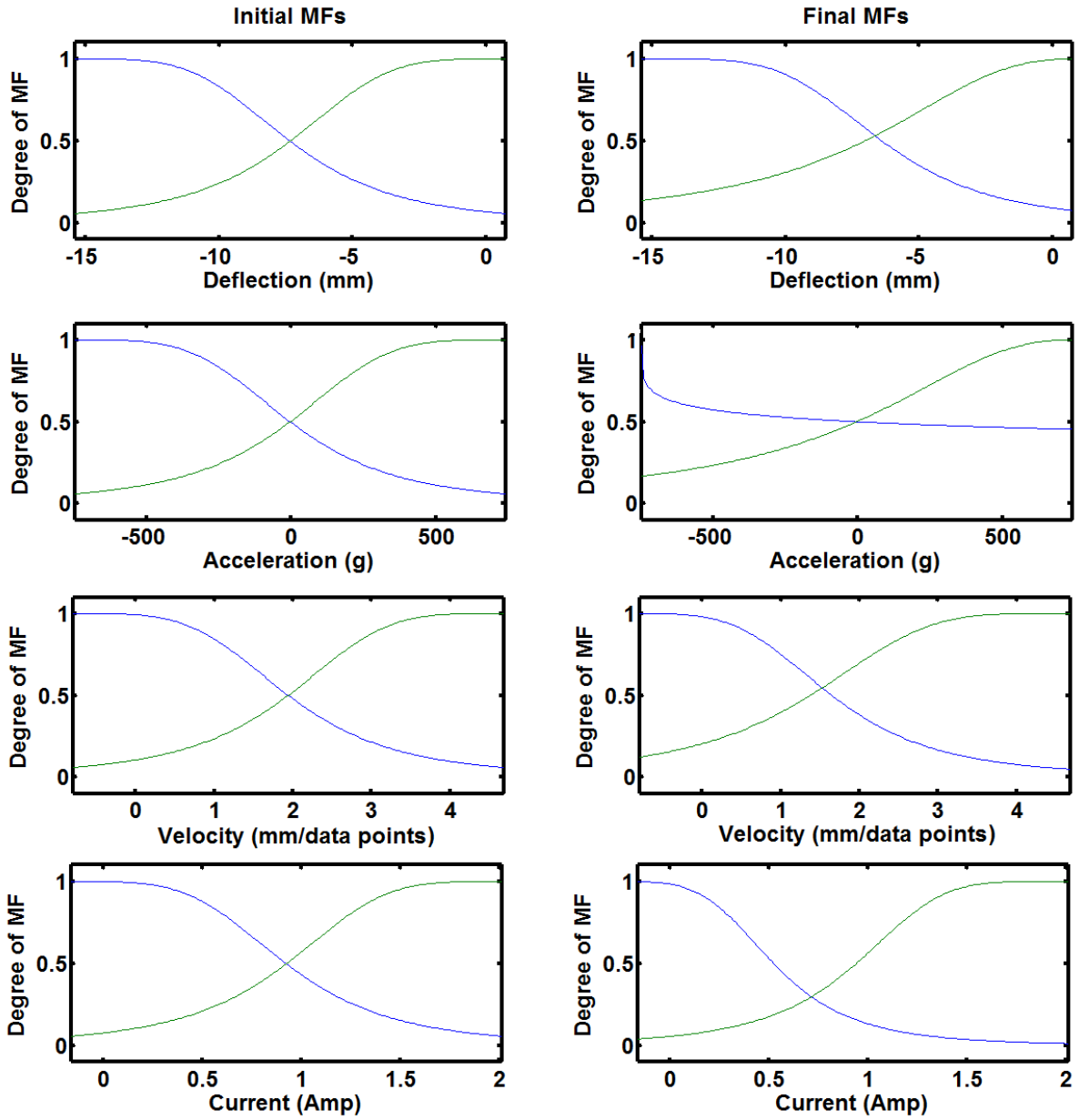

Figure 4-14. Initial and final membership functions

Figure 4-15 depicts the time steps and the iteration of the OF neuro-fuzzy model. For the model, a total of iterations of 10 are assumed adequte since the the modeling performance is satisfied with the 10 iterations.

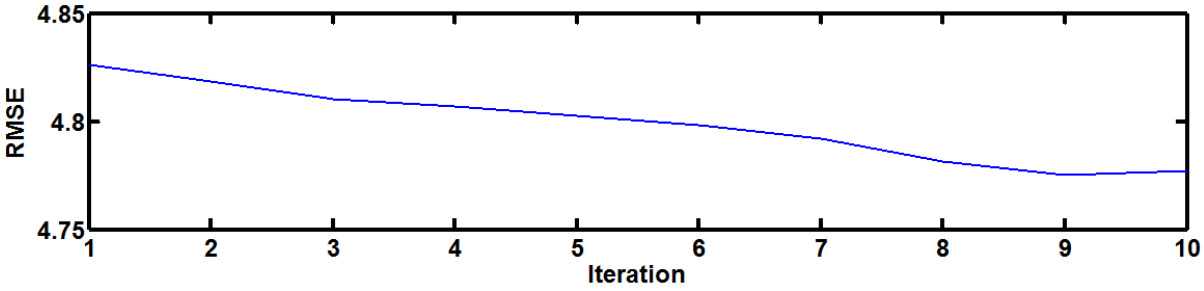

Figure 4-15. Iteration

With these parameter settings, Figure 4-16 compares the real measured impact force the MR damper employing the sinusoidal, random and constant currents under different drop release heights with the estimates from the OF neuro-fuzzy model.

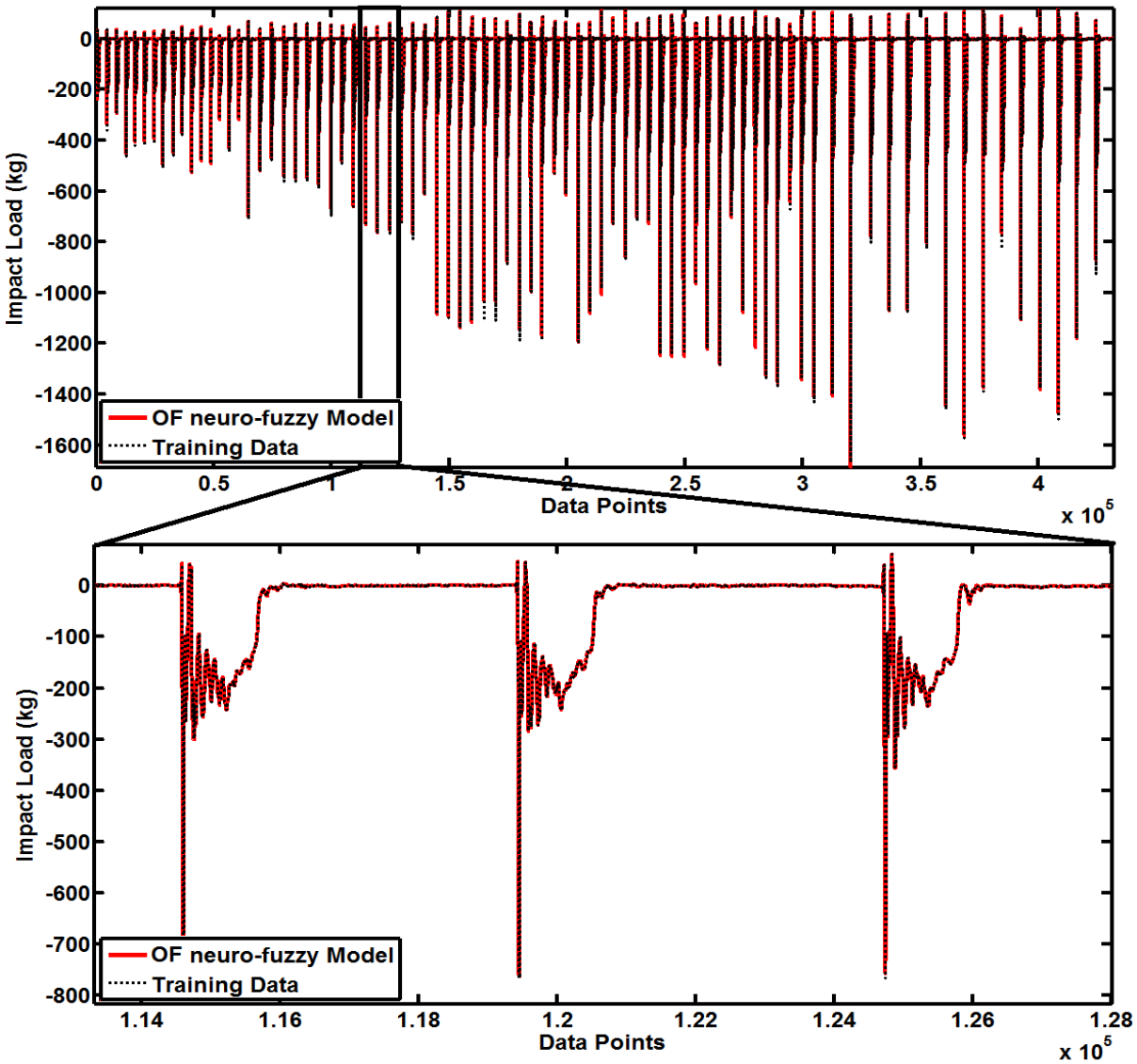

Figure 4-16. OF neuro-fuzzy training results: constant, sinusoidal and random currents for different drop release heights

As can be seen from the figure, there is a great agreement between the fuzzy estimates and the original measurements. It is expected that the identified model that incorporates a variety of control signals such as the constant, sinusoidal, and random current signals will be useful to smart control system design to effectively dissipate the high impact energy (Mikułowski and Holnicki-Szulc, 2007).

To generalize the trained model, different data sets that not used for the training process are used for testing the trained fuzzy model. Figure 4-17 and Figure 4-18 exhibit the graphs of validated data sets.

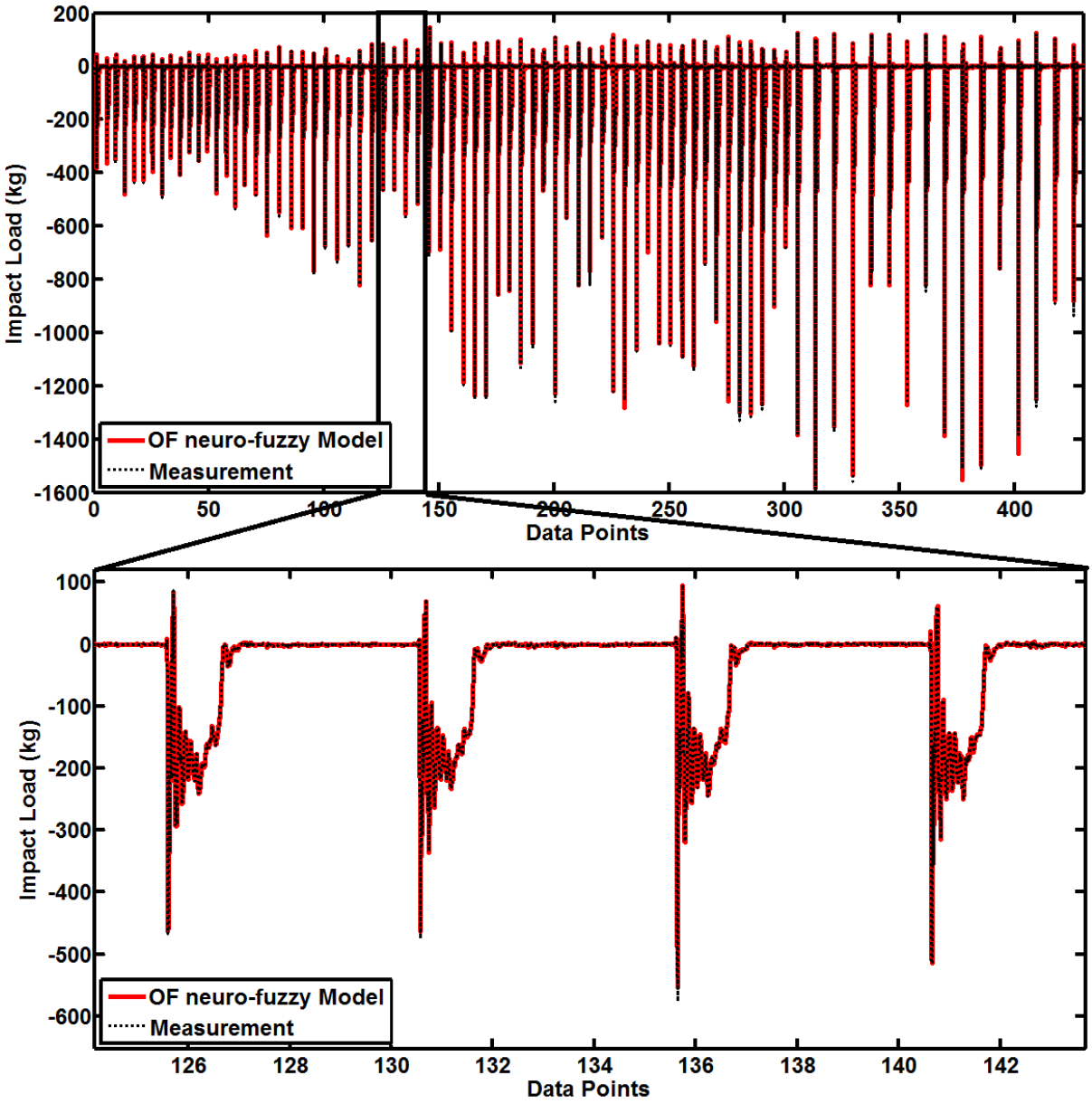

Figure 4-17. 1st validation

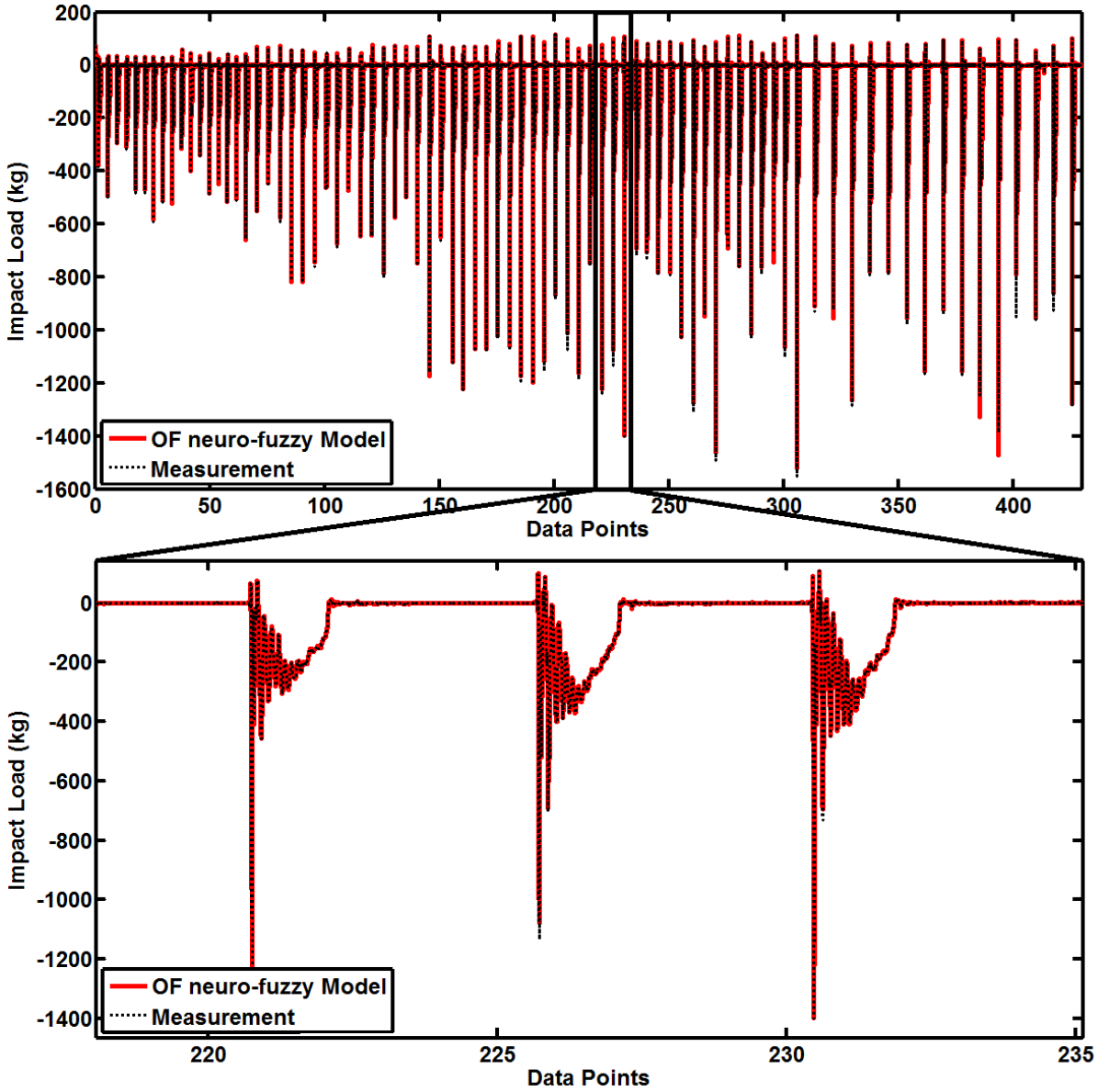

Figure 4-18. 2nd validation

As shown in figures, OF neuro-fuzzy models have precisely predicted the impact force on MR damper. To investigate the constitutive relationship of the proposed model, hysteric response behaviors such as impact load-displacement or impact load-velocity curves are also modeled. Figure 4-19, Figure 4-20 and Figure 4-21 depict the comparison of measured impact load-displacement and impact load-velocity curves with the predictions of OF neuro-fuzzy models. Figure 4-19 shows the impact load-displacement and impact load-velocity curves for the MR damper subjected to different impact loads and sinusoidal current signal, while Figure 4-20 and Figure 4-21 show the same curves for random and constant current signals, respectively.

Results demonstrated that OF neuro-fuzzy model is very effective to predict the hysteric response behaviors of MR dampers under high impact loads.

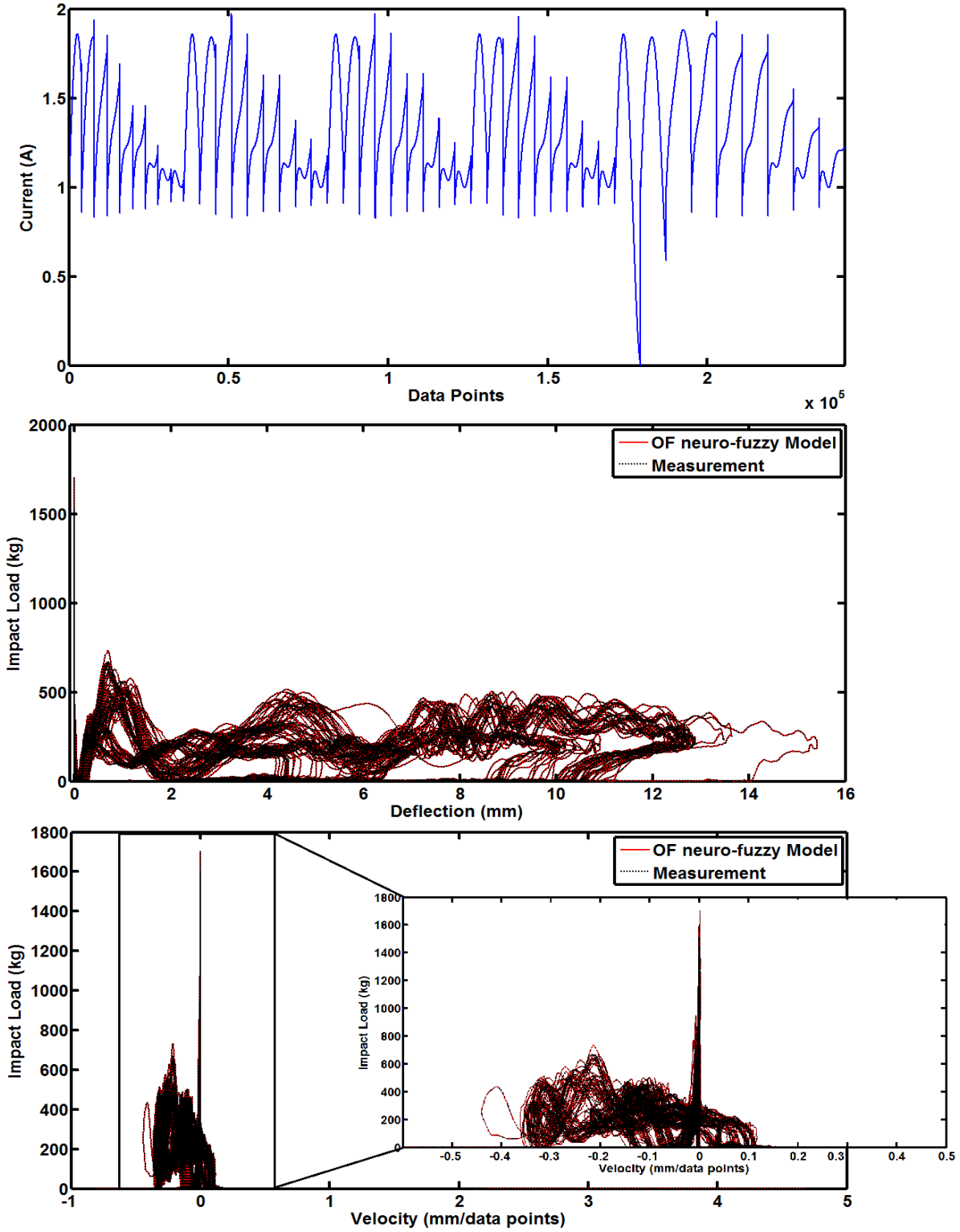

Figure 4-19. Impact Load-Displacement and Impact Load-Velocity curves: Different drop release heights and sinusoidal current signal

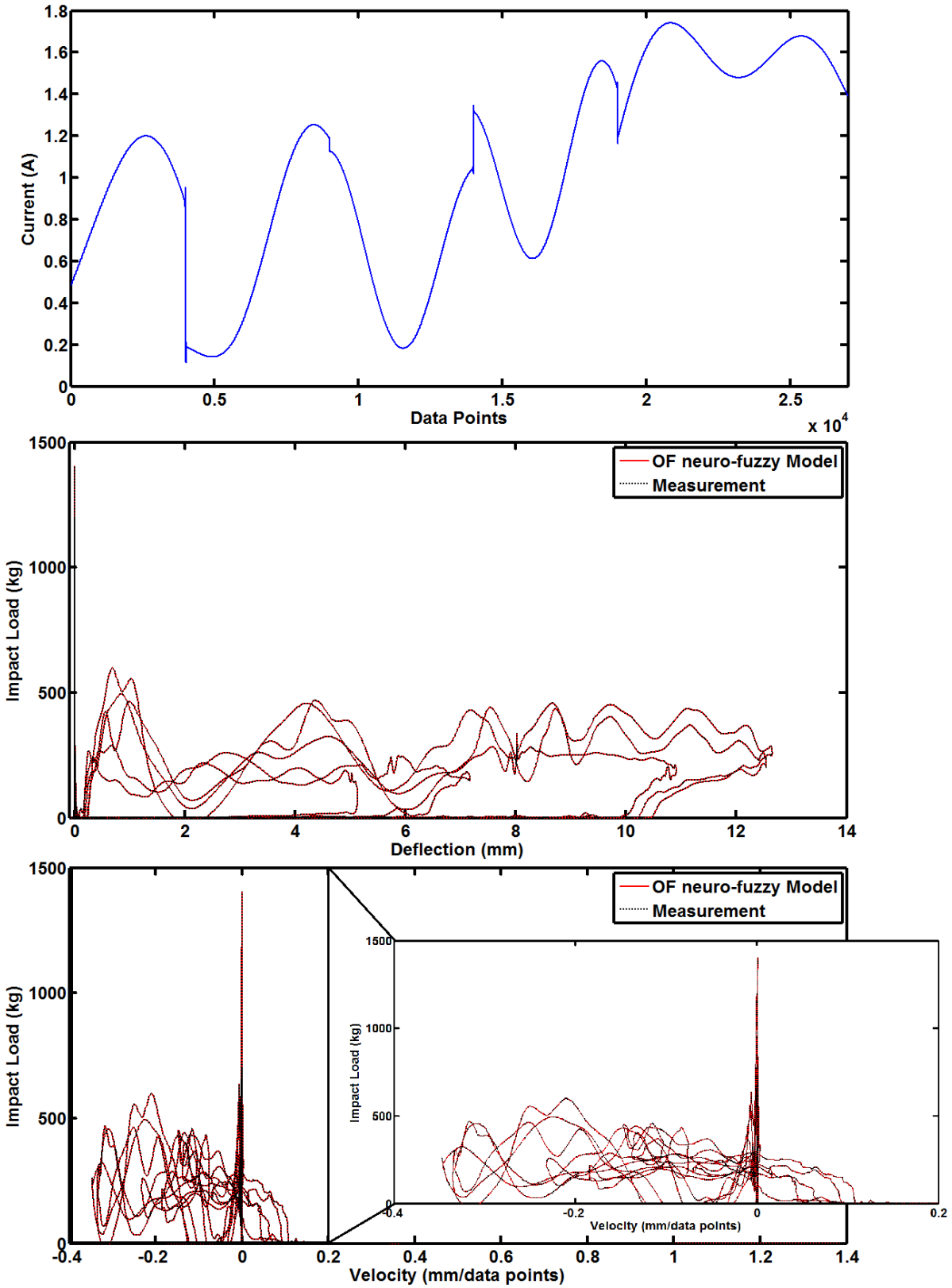

Figure 4-20. Impact Load-Displacement and Impact Load-Velocity curves: Different drop release heights and random current signal

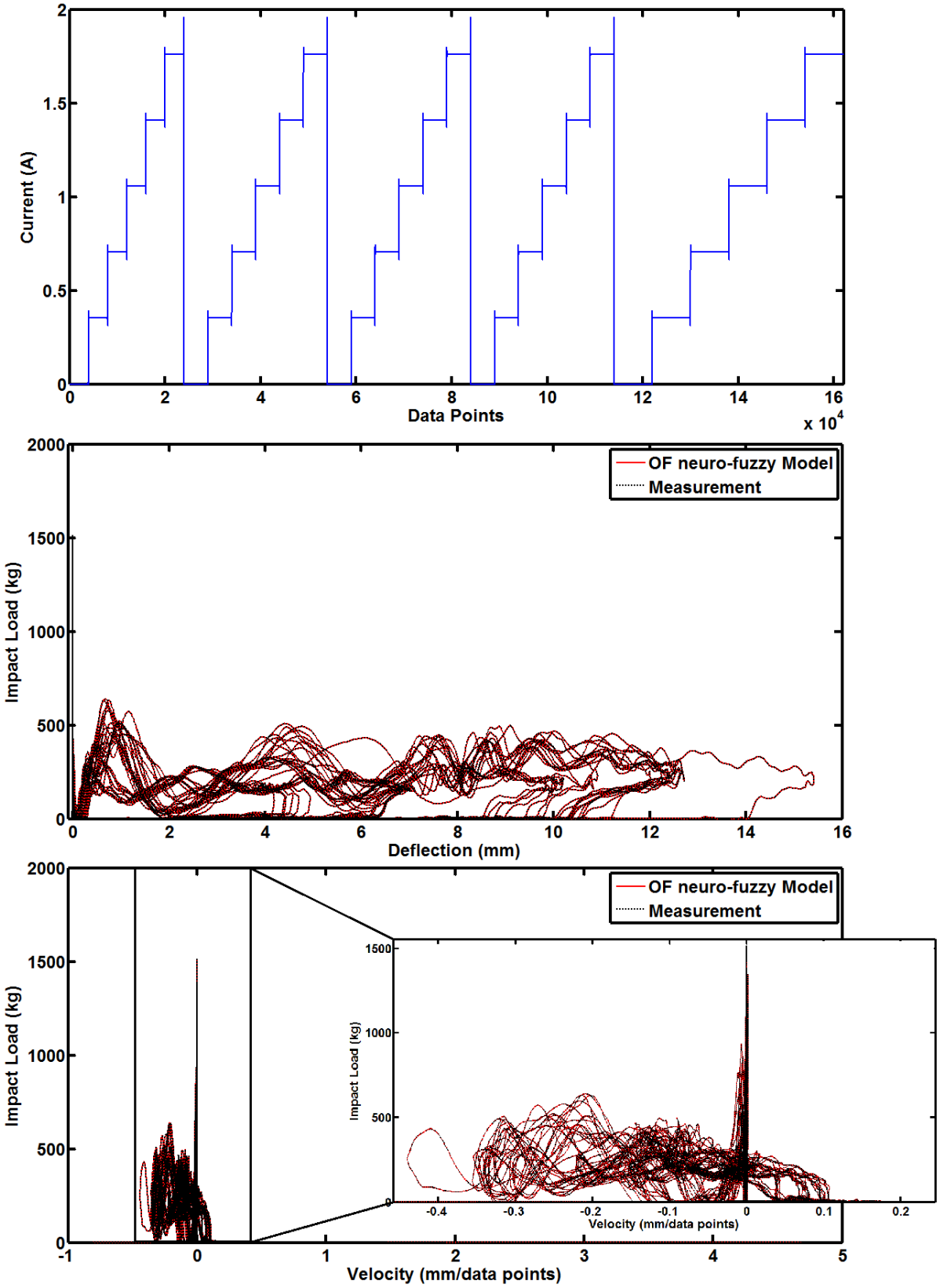

Figure 4-21. Impact Load-Displacement and Impact Load-Velocity curves: Different drop release heights and constant current signal

4.4.3. Evaluation of results

Several evaluation indices are also used to quantify the performance of the proposed neuro-fuzzy models. As a first evaluation index, the maximum absolute error is calculated as

$$J_1 = \max\left|\hat{y} - \tilde{y}\right| \tag{4-28}$$

where $\hat{y}$ is the trained data and $\tilde{y}$ is the actual measurements. Second evaluation criterion is defined as the mean of absolute error

$$J_2 = \text{mean}\left|\hat{y} - \tilde{y}\right| \tag{4-29}$$

Third criterion index is minimum absolute error

$$J_3 = \min\left|\hat{y} - \tilde{y}\right| \tag{4-30}$$

The fourth evaluation index is formulated as follows

$$J_4 = \left[1 - \frac{\text{var}(\hat{y} - \tilde{y})}{\text{var}(\hat{y})}\right] \times 100 \tag{4-31}$$

where *var* represent the variance of data. The fitting rate of index J_4 shows the accuracy of the predictions of the models. The better the trained model predicts the measurement results accuratly, the more the fitting rate of index J_4 will become close to 100.

Table 4-7 shows the results of the error analysis between the trained and actual data for the different SI approaches.

Table 4-7. Error Quantities of the SI Models

		J_1 (Unit)	J_2 (Unit)	J_3 (Unit)	J_4 %
Training	Bouc-Wen	1.532e+4	1.996e+3	1.083e-5	**2.27**
	Bingham	1.663e+3	55.138	1.836e-5	**5.70**
	Neuro-fuzzy	**1.1193e+3**	**26.216**	**1.957e-5**	**74.67**
	OF neuro-fuzzy	**131.55**	**1.028**	**1.605e-7**	**99.84**
Validation	Bouc-Wen -1	1.032e+4	2.125e+3	1.083e-5	**2.09**
	Bouc-Wen -2	1.032e+4	2.120e+3	1.083e-5	**2.10**
	Bingham -1	1.668e+3	55.715	7.594e-5	**5.42**
	Bingham -2	1.668e+3	55.722	4.556e-5	**5.43**
	Neuro-fuzzy -1	**1.054e+3**	**26.241**	**8.089e-6**	**74.28**
	Neuro-fuzzy -2	**1.008e+3**	**26.111**	**7.594e-5**	**73.59**
	OF neuro-fuzzy -1	**184.59**	**1.027**	**2.966e-8**	**99.76**
	OF neuro-fuzzy -2	**240.38**	**1.045**	**4.093e-7**	**99.72**

It is observed from both training and validation processes that the fuzzy models achieved a great performance. But the performance of the OF neuro-fuzzy model, in terms of accuracy and peak impact load predicitons, is better than the conventional neuro-fuzzy model. The accuracy of the OF neuro-fuzzy model is about 99% for both training and validation in terms of the evaluation index J_4 , which means that the OF neuro-fuzzy is very effective in predicting the dynamic responses of the MR damper under high impact loads. It is also found that J_1, J_2 and J_3 of the OF neuro-fuzzy model are better than the benchmark models. For example, in the training of the OF neuro-fuzzy model, the maximum difference between the estimate and the measurement is 131.55 kg, which is 8% of the measurement (1557.6 kg) for the trained model.

4.5. Conclusion

Various parametric and nonparametric SI approaches for estimating the nonlinear impact response of MR dampers under a variety of high impact loadings and current signals are studied in this paper. The Bingham, Bouc-Wen and two Takagi-Sugeno fuzzy models are investigated. To obtain the input-output data set, a series of experimental studies are performed. The MR damper fluids are controlled with constant, sinusoidal, and random currents under different impact loads. A large number of drop release testing is performed three times to train and validate the models. In the training of the fuzzy models, the deflection, acceleration, velocity and current signals are used as input signals to predict the applied high impact force of the MR damper. Various input-output data combinations with different types of membership function (MF) are considered in this study. It is confirmed from the extensive testing and modeling that

the appropriate selections of current levels, the training data set and the MF types are very important in improving the performance of the neuro-fuzzy models. Although the benchmark parametric models were effective in estimating the behavior of MR dampers when the velocity of the applied forces is low and/or the applied currents are constant, they do not produce the reasonable match for random current signals under a variety of high impact loads. The conventional neuro-fuzzy model gives reasonable match between the predicted and actual test data. However the peak impact value predictions, which is essential in design of a control system to dissipate the impact energy, is not accurate. In conclusion, it is demonstrated from both the training and validation results that the OF neuro-fuzzy model is very effective in modeling the nonlinear behaviors of an MR damper employing random current signals under a variety of high impact loads.

5. Smart Fuzzy Control for Impact Response Mitigation of Reinforced Concrete Structures

5.1. Introduction

In recent years, there has been a growing interest to understand the behavior of reinforced concrete structures exposed to high impact loads (Wang and Li 2006; Ahmadian and Norris 2008; Ravindrarajah and Lyte 2008; Hongsheng and Suxiang 2009; Wiklo and Holnicki-Szulc 2009a-b; Consolazio et al. 2010; Arsava et al. 2013b). For example, extreme events such as vehicle collisions, construction accidents, gas explosions, terrorist attacks or barge-bridge pier collisions may create severe dynamic loads. Although the occurrences of these kinds of events are rare, the intense dynamic stresses produced by the impact can result with structural failure. Thus, understanding the behavior and mitigating the response of structures under extreme loading conditions has a great importance for people's safety. As a promising strategy, application of smart control system in the field of civil engineering has become an attractive topic due to its effectiveness to absorb and dissipate the external energy in real time (Arsava et al. 2013a).

In particular, Magnetorheological (MR) dampers, which can be both operated as passive or active dampers, have received great attention for use in large-scale civil infrastructural systems (Spencer et al. 1997b; Mikułowski and Holnicki-Szulc 2007). Fast response, reliable operation and low manufacturing cost are the most distinguishing attributes of the MR dampers (Dyke et al. 1996 a, 1998, 2001; Yi et al. 1998, 1999; Kim et al. 2009, 2010). The MR dampers consist of the hydraulic cylinder filled with magnetic coils and MR fluid. In active cases, the efficiency of the MR damper to absorb and dissipate the energy can be optimized by changing the magnetic field on the MR fluid. However, developing a control algorithm is very challenging due to nonlinear impact behavior of the time-varying smart structures equipped with nonlinear MR dampers (Arsava et al. 2013 a-b).

Several control algorithms have been developed for use with the MR dampers: Dyke et al. (1996 b-c) proposed a clipped-optimal control to reduce dynamic response of the structure under seismic loads. The control algorithm uses the acceleration feedbacks to adjust the voltage on the MR dampers. The effectiveness of the proposed algorithm was demonstrated on a numerical model that considers a 3-story smart building equipped with an MR damper. In another study of Dyke and Spencer (1997a), a decentralized bang-bang controller, a lyapunov

controller, clipped-optimal controller and a modulated homogeneous friction algorithm were discussed and compared. It was shown from extensive simulations that the performance of the control system was highly dependent on the choice of algorithm employed. Ying et al. (2002) and Ni et al. (2002) focused on the stochastic optimal control strategy for randomly excited nonlinear systems. As a distinguishing feature, Ni et al. (2002) also focused on installation position of the MR damper. A 1:15 scaled structural system was used in the experimental studies. A 12-story building and an 8-story building model were constructed and subjected to seismic load. It was demonstrated that the proposed semi-active controller provided efficient structural response reduction but the control efficiency was influenced by the location of the MR dampers. Zhang and Roschke (1999) have used a linear quadratic Gaussian with loop transfer recovery control to mitigate the acceleration response of tall structures under wind loads.

However, all of the aforementioned controllers were designed based on predefined parameters and require a full understanding of the dynamics of the structure (Zhao et al. 2003). In other words, these controllers require the properties of the structure (e.g. mass, damping and stiffness) and disturbance (magnitude, location and frequency) in the optimization process. Due to uncertainty of the high impact loads and complexity of smart structures, it is difficult to implement the aforementioned conventional controllers into the smart structures under high impact loads. Thus, this study proposes a fuzzy logic controller for energy dissipation and damage mitigation of smart structures equipped with MR dampers subjected to high impact loading.

Due to their simplicity and being more robust, fuzzy controllers attracted the attention from many investigators (Kim and Clark 1999; Zhou and Chang 2000). Liu et al. (2001) proposed a closed-loop control system based on fuzzy logic to suppress the bridge deck motion under random excitation. From the results, it was demonstrated that the proposed fuzzy logic control system significantly reduced the deck displacement, while the absolute deck acceleration remained practically unchanged. Wilson and Abdullah (2005a) developed a fuzzy controller to regulate the damping properties of the structure-MR damper system under four different earthquake loads. They demonstrated that both floor displacement and acceleration responses were successfully reduced in terms of root mean square. Although fuzzy control system design is straightforward, the tuning of fuzzy controllers is a difficult and sophisticated procedure due to the large number of parameters that define the membership functions and inference mechanisms (Wilson and Abdullah 2005b). In this context, different approaches were proposed such as genetic algorithms (GA) (Arslan and Kaya 2001), neural networks (Lin and Lee 1991), self-

tuning (Maeda et al. 1990), gain scheduling (Jang and Gulley 1994) and manual-tuning (Driankov et al. 1993).

However, the aforementioned studies were focused on the application of fuzzy controllers to structural systems subjected to seismic or wind loads. As of yet, there is no studies on development of a smart fuzzy control model for large civil structures employing MR dampers under high impact forces. Therefore, this paper proposes the application of fuzzy logic theory to the high impact response mitigation of large civil structures employing MR damper technology.

The fuzzy control system design procedure is described in Section 5.2. Section 5.3 provides information about the experimental setup, equipment and procedures. In Section 5.4, the results and evaluations of the proposed controller including training and validation are presented. Concluding remarks are presented in Section 5.5.

5.2. Smart impact response mitigation

5.2.1. Smart control systems

A smart control system can be described as a system containing multifunctional parts that can sense, control and actuate (Nestorović and Trajkov 2010). Smart control systems employing devices such as variable-office dampers, variable-friction dampers, shape memory alloy actuators, piezo-electrics, etc., have been applied to various structures (Hurlebaus and Gaul 2006). Implementing the smart control technology into the structures has attracted a great deal of attention in the field of civil engineering because smart structures provide a great improvement in the dynamic performance of the structural systems without increasing the structural member sizes or requiring high cost of control power (Hurlebaus and Gaul 2006; Kim et al. 2009).

This study specifically focused on the impact response mitigation of structures using MR dampers. Some of the distinguishing characteristics of MR dampers are can be listed as: (i) MR dampers require low power sources when they operated as active controllers. (ii) Their performance is stable in a broad temperature range. (iii) They have a very fast response time. (iv) They have a high yield stress level (Kim et al., 2009). An integrated structure-MR damper system is depicted in Figure 5-1.

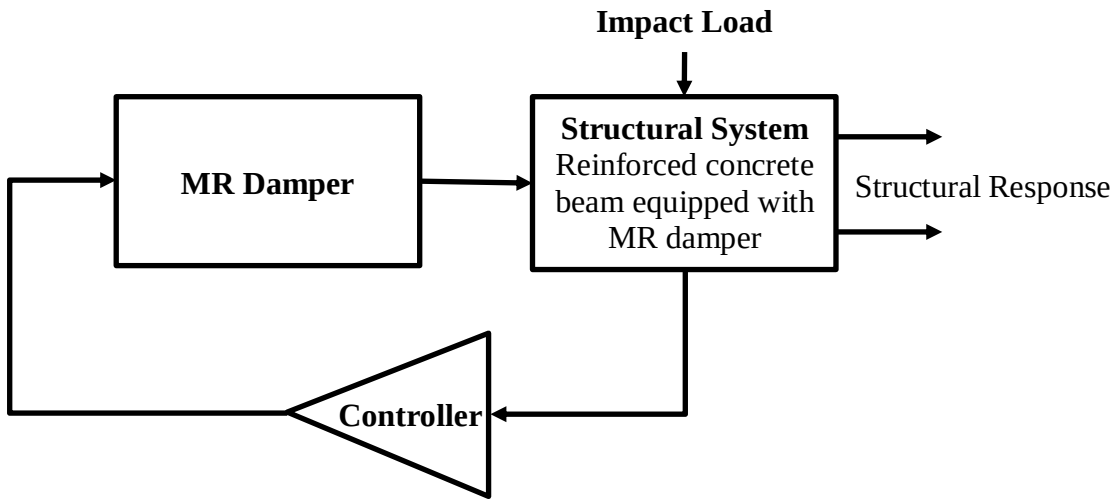

Figure 5-1. Integrated building structure-MR damper system

To fully use the MR damper technology in mitigating the dynamic response of the structure under high impact loads, a robust computational model is required. However, developing such a mathematical model considering the interaction effects between the structural system and the nonlinear MR damper control devices under high impact loads is challenging. As an example, Figure 5-2 and Figure 5-3 depict the maximum deflection and acceleration responses obtained from smart reinforced concrete structure, respectively. High impact responses are collected from a smart reinforced concrete beam equipped with an MR damper. It is expected that MR dampers with high current value will reduce the structural response more effectively. However, there is a nonlinear relationship between the dynamic responses and the current on the MR damper. For 60 mm drop release height, the optimal structural responses are obtained with the current of 0 A (Passive control), while an optimum control is achieved with 1.9 A for 120 mm drop release height. Thus, it becomes challenging to optimize the current level on the MR damper to mitigate the dynamic responses for different drop release heights.

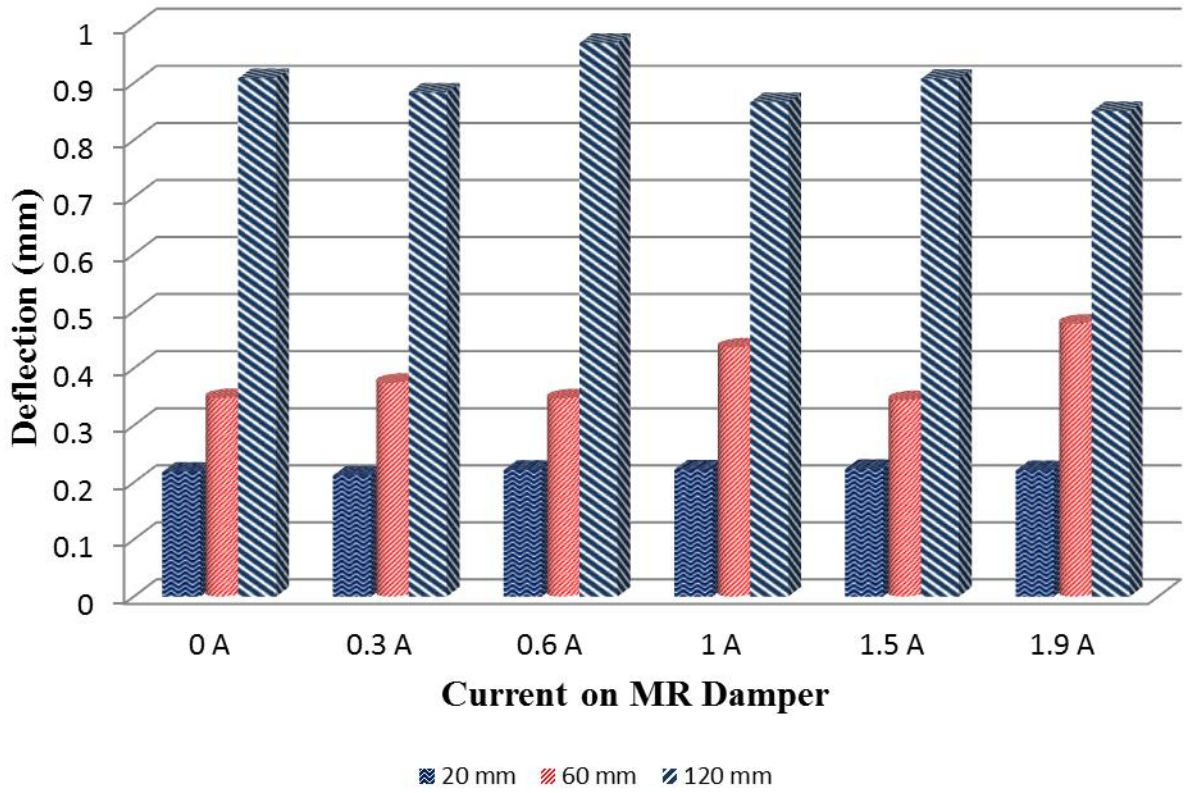

Figure 5-2. Deflection response- Various currents and different drop release heights

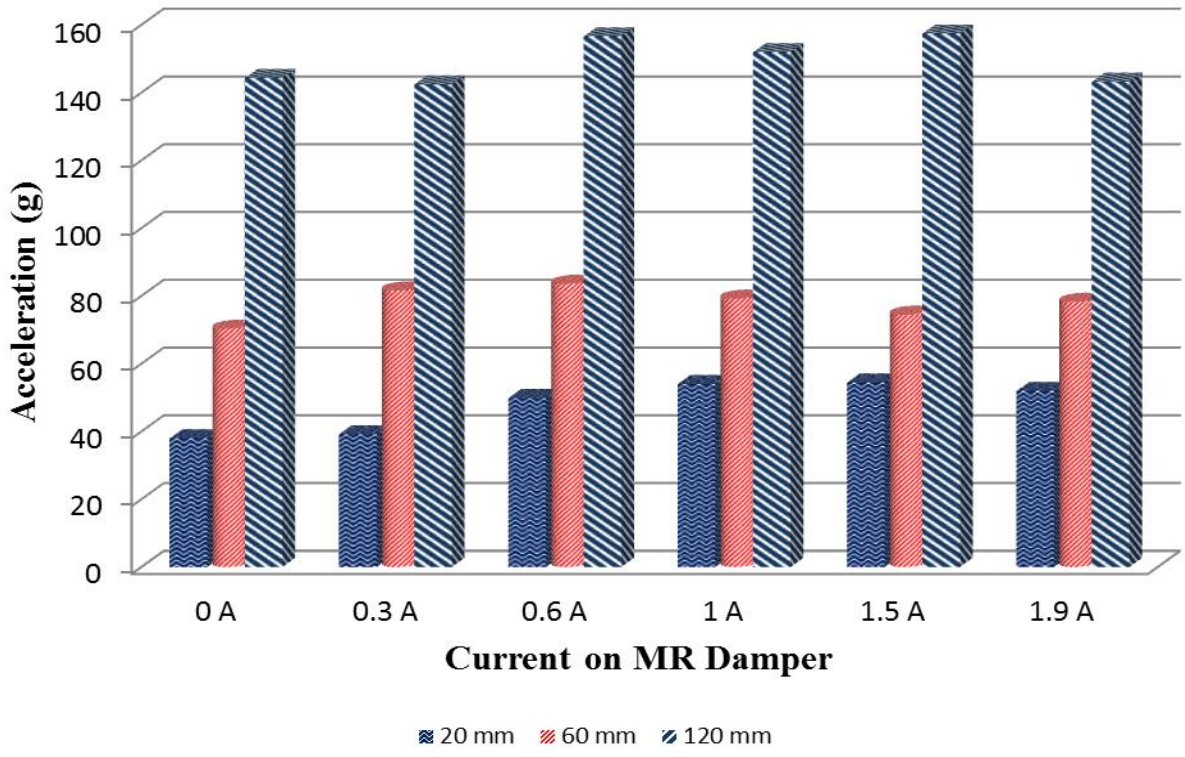

Figure 5-3. Acceleration response- Various currents and different drop release heights

In this context, a fuzzy control system is proposed in this paper to address the complex nonlinear behavior of smart structure under high impact loads.

5.2.2. Time-delayed fuzzy logic

A fuzzy logic controller can be described as an input-output map that uses 'if-then' rules to solve the complex problems. It uses fuzzy rules and an inference engine to anticipate the response of structures. Fuzzy controllers can be divided into three steps: fuzzification, evaluation of rules and collection of the outputs. (1) In the fuzzification step, the given crisp inputs are transferred to fuzzy values. (2) The fuzzy rules are applied to fuzzified inputs to determine the linguistic value of the output. (3) Membership functions of all rules are collected and combined as a single fuzzy set. In this paper, the parameters of the fuzzy controller are optimized using artificial neural network. The integrated fuzzy-neural network control model is depicted in Figure 5-4.

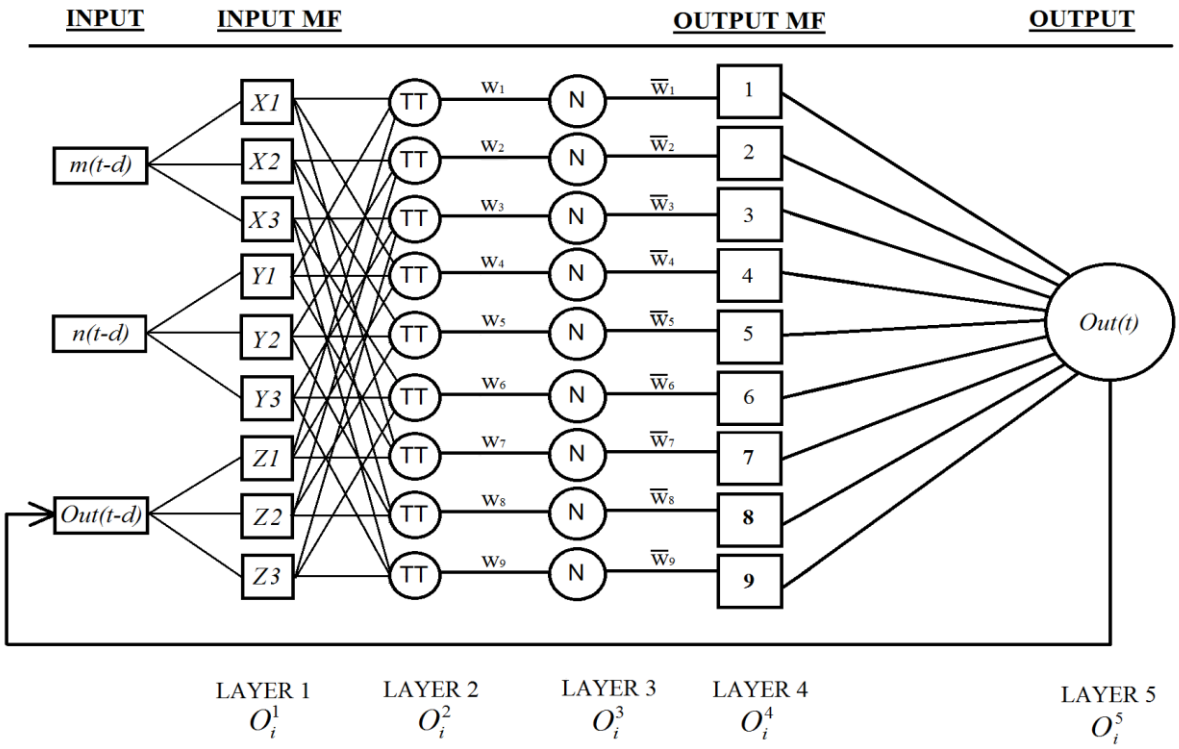

Figure 5-4. Proposed fuzzy-neuro controller

A typical three rule fuzzy model is as follows

Rule 1: If m is X_1, n is Y_1 and o is Z_1, then $Out_1^{\,t} = p_1 m^{t-d} + q_1 n^{t-d} + k_1 Out_1^{\,t-d} + re_1$ (5-1)

Rule 2: If m is X_2, n is Y_2 and o is Z_2, then $Out_2^{\,t} = p_2 m^{t-d} + q_2 n^{t-d} + k_2 Out_2^{\,t-d} + re_2$ (5-2)

Rule 3: If m is X_3, n is Y_3 and o is Z_3, then $Out_3^{\,t} = p_3 m^{t-d} + q_3 n^{t-d} + k_3 Out_3^{\,t-d} + re_3$ (5-3)

where m^{t-d}, n^{t-d} are inputs at time t-d and Out^{t-d} is the input from the previous iteration, while d represents the time delay term. Output of the fuzzy system at time t is defined as Out^t. In the model consequent parameters are represented as p_i, q_i, k_i and re_i. The functions of Layer 1 is presented as

$$O_i^1 = \mu \begin{bmatrix} X_i\left(m^{t-d}\right) \\ Y_i\left(n^{t-d}\right) \\ Z_i\left(Out^{t-d}\right) \end{bmatrix} \tag{5-4}$$

where μ is the appropriate parameterized membership function (MF), and O_i^1 (i = 1,2,3) is the output that specifies the degree to which the given input m^{t-d} satisfies the quantifier X.

Layer 2 combines the input that are fuzzified in Layer 1. The product of Layer 2 is the combination of all incoming outputs that is called 'firing strength' of a fuzzy control rule

$$w_i^t = \mu X_i(m^{t-d}) \times \mu Y_i(n^{t-d}) \times \mu Z_i(Out^{t-d}),\ i = 1,2,3 \tag{5-5}$$

In Layer 3 the output of Layer 2 is normalized by taking the ratio of the firing strength

$$\overline{w}_i^t = \frac{w_i^t}{w_1^t + w_2^t + w_3^t},\ i = 1,2,3 \tag{5-6}$$

As a next step, node functions ($Out_i^t = p_i m^{t-d} + q_i n^{t-d} + k_i Out^{t-d} + re_i, i = 1,2,3$) are applied to output of Layer 3

$$O_i^4 = \overline{w}_i^{\,t} \times Out_i^t = \overline{w}_i \times \left(p_i m^{t-d} + q_i n^{t-d} + k_i Out^{t-d} + re_i \right),\ i = 1,2,3 \tag{5-7}$$

In the last step, Layer 5 summates the layer inputs

$$O_i^5 = overall\ \ output + \sum_i \overline{w}_i^t \times Out_i^t = \frac{\sum_i w_i^t \times Out_i^t}{\sum_i w_i^t},\ i = 1,2,3 \tag{5-8}$$

In the optimization of the results, the fuzzy controller uses adjustable parameters such as number of MF, type of MF, iteration and size of the step.

5.2.3. Smart fuzzy controller

Fuzzy control theory is one of the recent smart control strategies to improve the dynamic performance of the structures (Casciati et al., 1994; Casciati, F., 1997; Choi et al., 2004; Dounis et al., 2007; Nomura et al., 2007, Pourzeynali et al., 2007; Gu and Oyadiji, 2008; Shook et al., 2008; Kim et al., 2011). The reason is that it can be applied to ill-defined dynamic systems with the robust performacne and high adaptabiltiy (Jang 1993; Keskar and Asanare 1997; Aware et al. 2000). A number of design methodologies for fuzzy logic controllers have been successively applied to a variety of large-scale civil building structures (Kim et al., 2009). They include trial-and-errors-based methodologies (Subramaniam et al. 1996; Battaini et al., 1998, 2004; Symans and Kelly, 1999; Loh et al., 2003; Park et al., 2003); a self-organizing approach (Al-Dawod et al. 2004); training using linear quadratic Gaussian (LQG) data (Al-Dawod et al. 2001); neural networks-based learning (Faravelli and Rossi, 2002; Faravelli and Yao, 1996; Tani et al., 1998); adaptive fuzzy (Zhou et al., 2003); genetic algorithms-based training (Ahlawat and Ramaswamy, 2000, 2002, 2004; Kim and Roschke, 2006; Yan and Zhou, 2006); fuzzy sliding mode (Alli and Yakut, 2005; Kim et al., 2004; Wang and Lee, 2002); etc. However, no study on systematic design framework has been conducted to design a nonlinear fuzzy controller for building structures equipped with a nonlinear semiactive control device.

Hence this paper propses a nonlinear smart fuzzy controller that can optimize the damping force of the MR damper control device under a variety of impact loading. As previously explained, finding an optimal current level to mitigate structural responses with various impact velocities is very challenging. Under an unexpected circumstances, such as the exceedance of the

designed impact velocity, conventional contollers might not be able to balance the damper force and dynamic response.

The proposed fuzzy controller is operated as: i) When the structure collides with a movable object, sensors measure the rapidly varying structural responses such as accelerations, deflections and strains. ii) Using an A/D converter, the obtained data are transformed to digital inputs that the computer can use. iii) The voltage signal from the proposed fuzzy controller is converted into the current signals so that the magnetic field on the MR fluids is activated. iv) The current signals adjust the force level on the MR damper in real time. v) The optimized MR damper effectively absorbs and dissipates the external energy. Figure 5-5 depicts the configuration of the fuzzy controller.

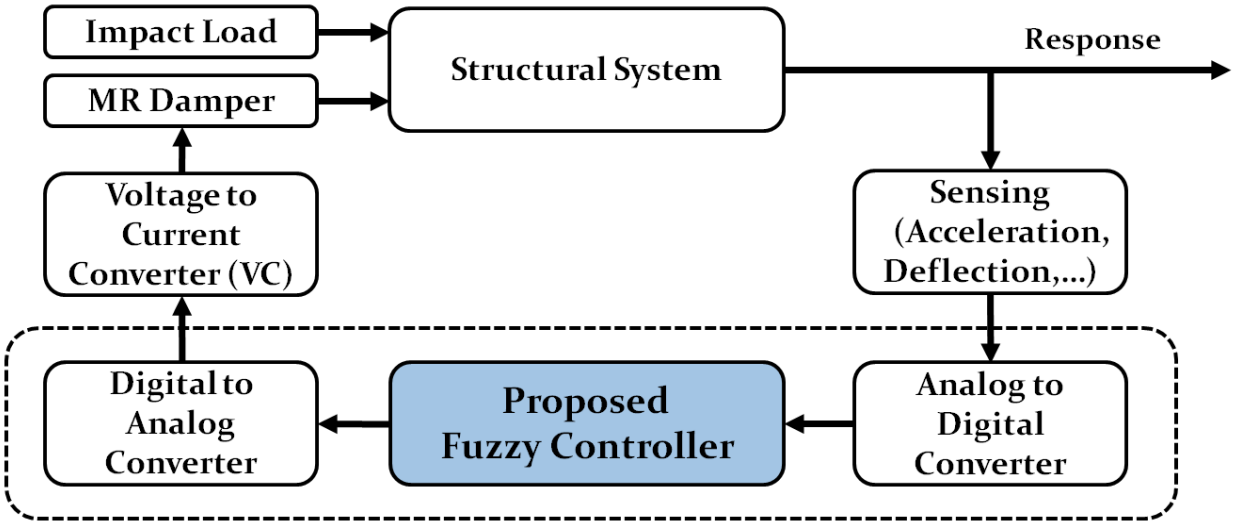

Figure 5-5. Configuration of fuzzy controller

In order to implement the fuzzy controller models into structural systems, experimental studies are performed (Section 5.3). Impact loads, currents on MR damper, accelerations and deflections are measured.

5.2.4. Proportional integral derivative controller (PID)

As a baseline model, a proportional integral derivative (PID) controller is used in the study. A mathematical description of PID controller is (Kim et al. 2010)

$$Cu(t) = K_P Out(t) + K_I \int_0^t Out(t)dt + K_D \frac{dOut(t)}{d(t)}, \quad (5\text{-}9)$$

where *Cu(t)* is the current value on MR damper at time *t*, and K_p, K_I and K_D are the weight factors of the PID controller. The weight factors are determined via many trial and errors.

5.3. Experimental studies

To demonstrate the effectiveness of the proposed approach, a reinforced concrete beam structure equipped with an MR damper is investigated under various impact loads. The experimental setup includes a drop tower impact test facility, a reinforced concrete beam, an MR damper, a data acquisition system and sensors.

5.3.1. Drop tower test facility

Dynamic response of the smart structure under high impact loads was investigated by the drop tower test facility in Structural Impact Mechanics and Mitigation Laboratory in the Civil and Environmental Engineering Department at Worcester Polytechnic Institute, as shown in Figure 5-6. The maximum impact load capacity of the facility is 22,500 kilogram. The applied impact loads and velocities were adjusted by changing the drop release height and drop mass.

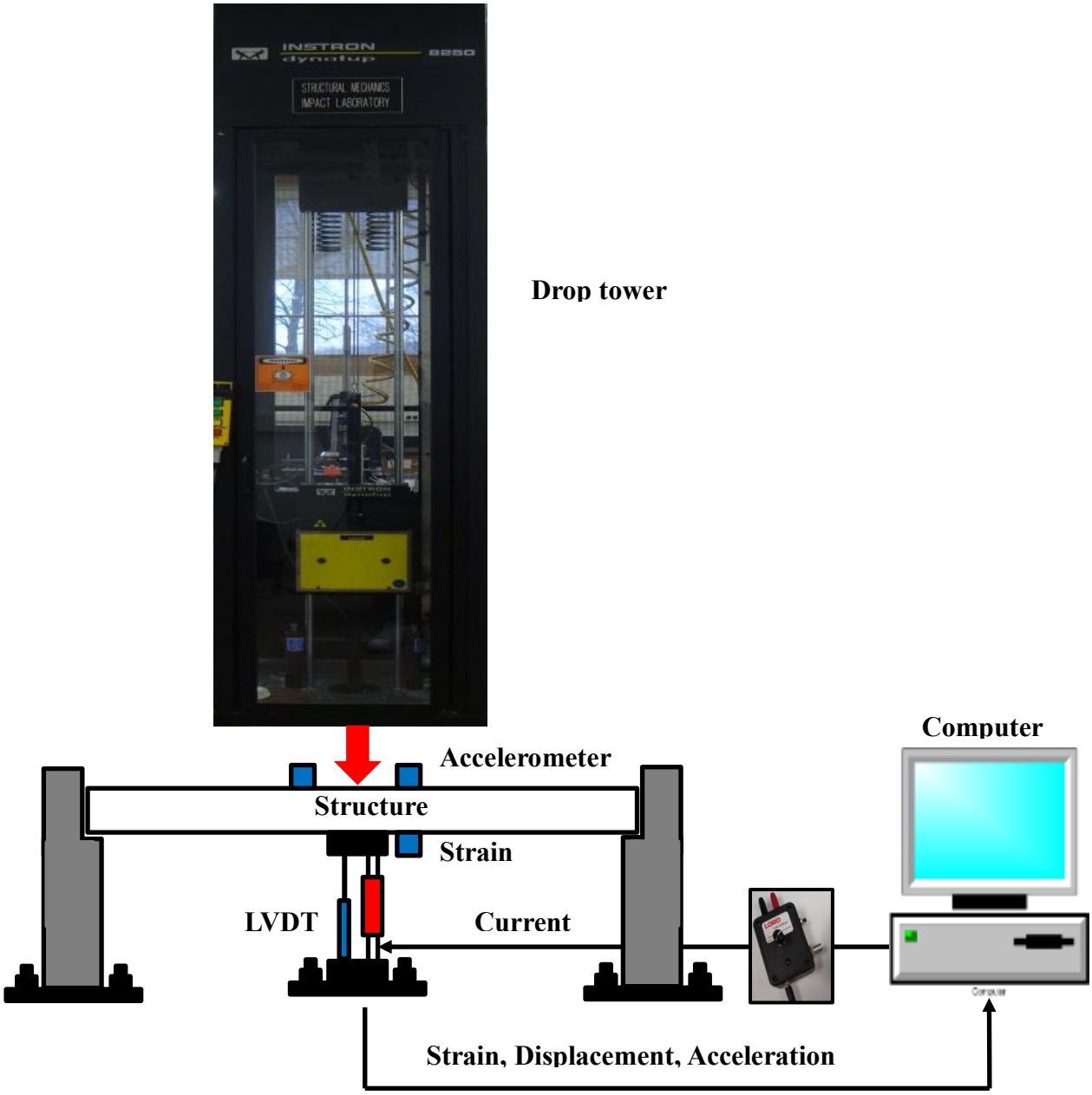

Figure 5-6. Drop-tower testing facility and experimental test setup

5.3.2. Reinforced concrete beam equipped with MR dampers

A simply supported reinforced concrete beam is selected to obtain input-output data to train the fuzzy controller. In this context, the reinforced concrete beams with a size of 10*x*10*x*100 cm is designed and constructed (Figure 5-7a). A total of 6 longitudinal deformed steel bars are placed within the concrete beams. The yield strength of longitudinal steel bars with 7.5 cm in diameter was measured as 248 MPa. As stirrups, 0.25 cm steel wires are placed with 7.5 cm spacings. Portland cement concrete mixtures with a maximum aggregate size of 6.5 mm are used (Figure

5-7b). The poured concrete beams were cured over three weeks in a curing room (Figure 5-7c). At the time of testing, the compressive strength and modulus of elasticitiy of the concrete was calculated as 26 MPa and 15 GPa, respectively.

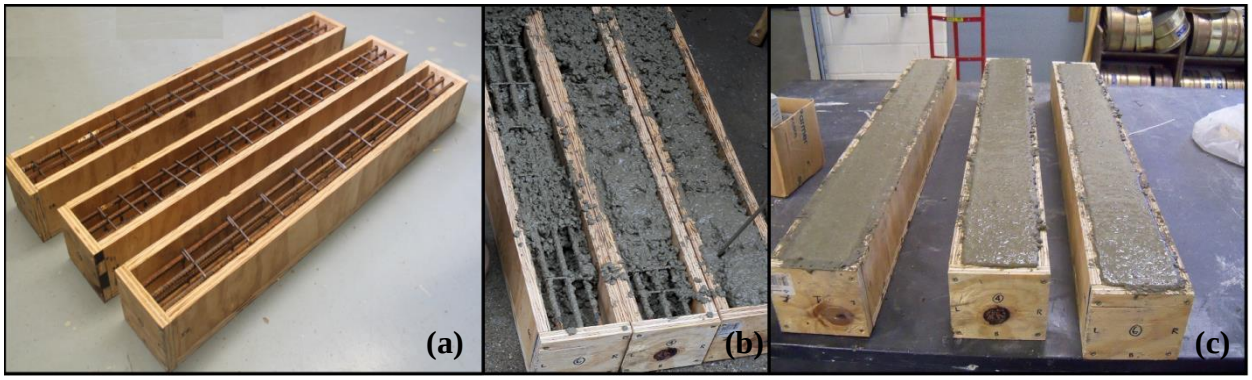

Figure 5-7. Preparation of concrete beams

In order to investigate the performance of the passive and active controlled structure, an MR damper is placed under mid-span of the simply supported beam (Figure 5-8). The reinforced concrete beam was tested under different impact loads and different current levels on the MR damper.

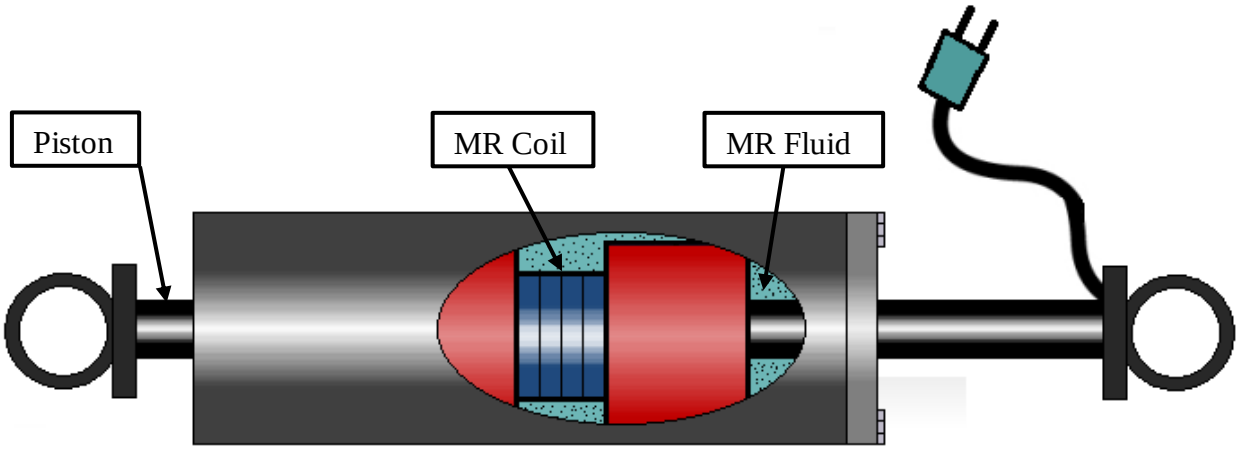

Figure 5-8. Schematic of RD-8040-1 MR damper

5.3.3. Data acquisition

Acceleration, deflection, strain and impact force data are collected in the experimental tests. All sensors are connected to the National Instrument (NI) labview data acquisition system. The acceleration data is measured by two PCB type 302A accelerometers with a capacity of 500 g, while an N2A series strain gauge is used to measure the strain. A R.D.P product ACT1000A type

LVDT is used in the displacement measurements. Impact load data is measured by a 4,500 kg capacity Central HTC-10K type load cell. Placement of the sensors is depicted in Figure 5-9. As a sampling rate of the data acquisition system, 10,000 data points per second is selected.

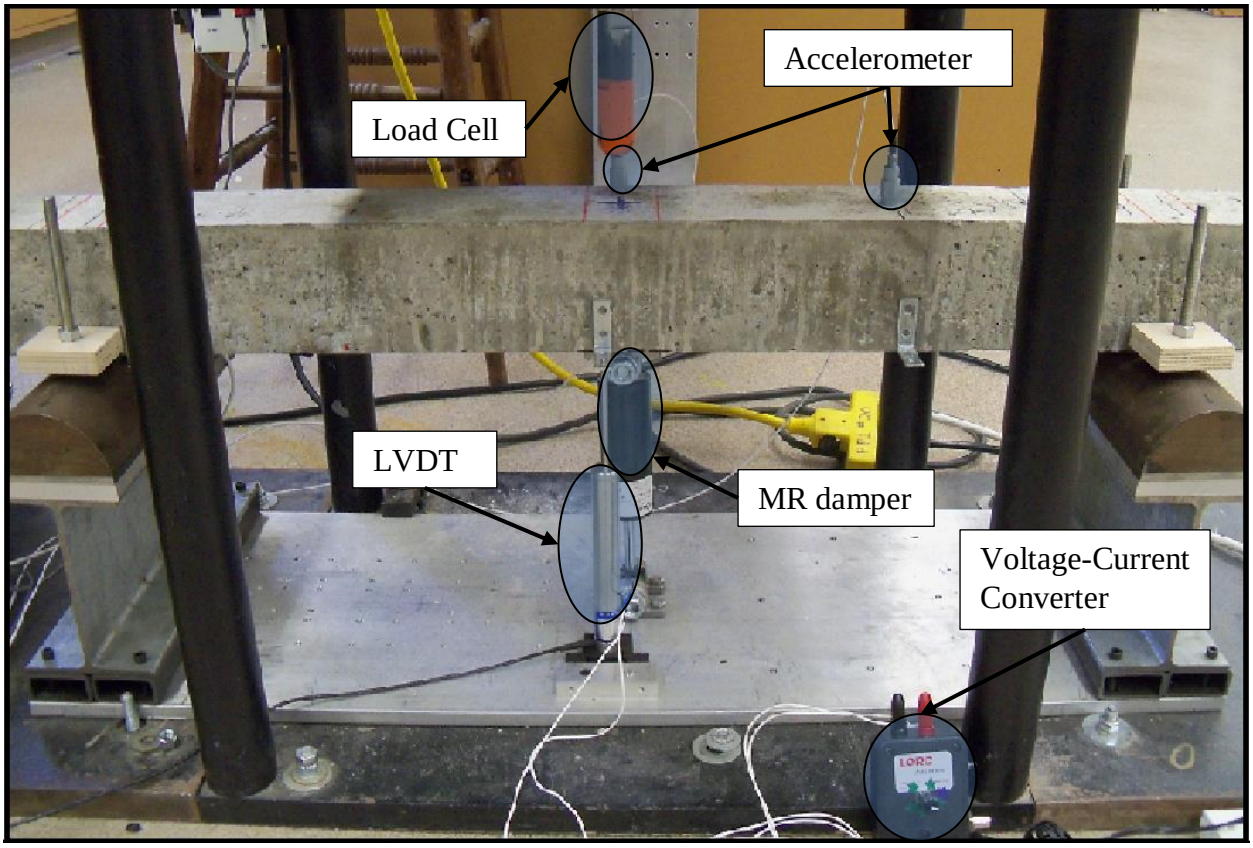

Figure 5-9. Configuration of the sensors and data acquisition system

5.3.4. Test details

The objective of the experimental test is to investigate the performance of the smart structure under a variety of impact loads and different constant signals. For each drop release height, the impact test is performed 21 times with various constant current signals. Details of the performed tests can be found in Table 5-1

Table 5-1. Experimental Test Details

Case Studies	Current on MR Damper (A)	Drop Release Height (mm)	Impact Velocity (mm/s)
Case 1 - Case 21	Uncontrolled 0-1.9 (20 different cases)	20	775
Case 22 - Case 43	Uncontrolled 0-1.9 (20 different cases)	40	885
Case 44 - Case 65	Uncontrolled 0-1.9 (20 different cases)	60	1025
Case 66 - Case 87	Uncontrolled 0-1.9 (20 different cases)	80	1375
Case 88 - Case 109	Uncontrolled 0-1.9 (20 different cases)	100	1695
Case 110 - Case 131	Uncontrolled 0-1.9 (20 different cases)	120	2058

A total of 131 impact tests are performed to investigate the structure with and without an MR damper. Six different impact force levels were applied to structure-MR damper system. The collected data is used to find the optimum current signal for each drop release height.

5.4. Results

5.4.1. Fuzzy controller design

Based on the identified model (Arsava et al. 2013a), an effective control system is developed to optimize the magnetic field on MR fluid. The proposed fuzzy controller adjusts the current on MR damper using the structural response feedbacks. The conceptual configuration of the fuzzy controller is shown in Figure 5-10.

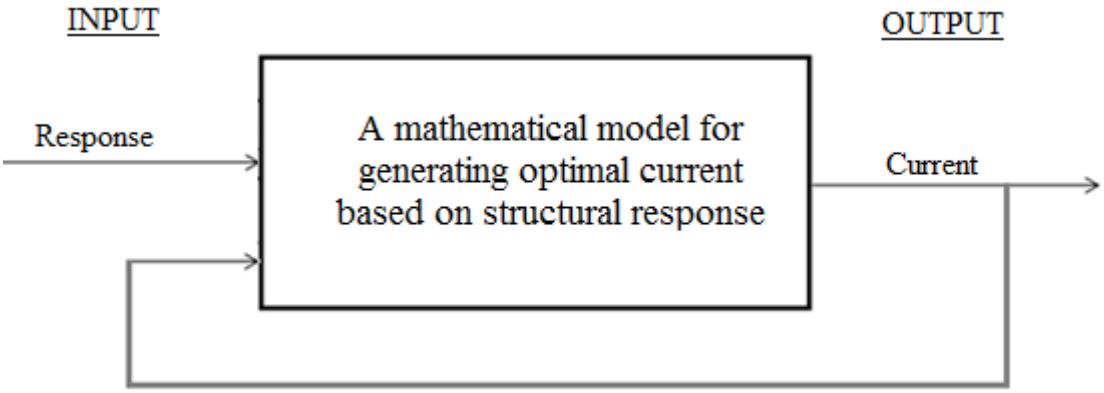

Figure 5-10. Configuration of the fuzzy controller

To develop the proposed fuzzy controller, sets of input and output data are collected. Figure 5-11 shows the input-output data signals for training the fuzzy controller. Deflection, acceleration and strain values are used as the inputs to predict the optimized current signal.

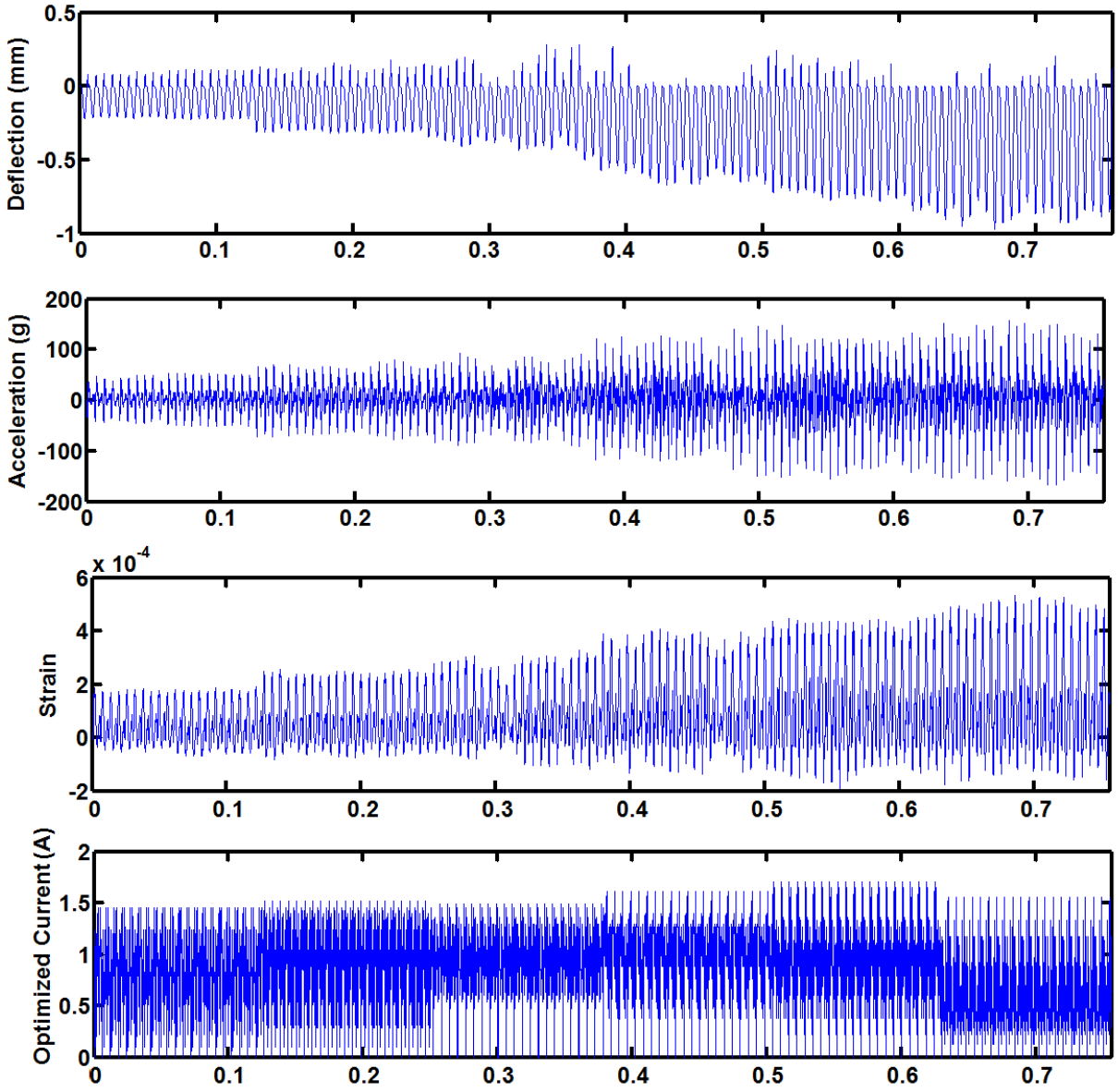

Figure 5-11. Input–output data sets to train the fuzzy controller

As previously discussed, experimental test was repeated 21 times for each drop release height to investigate the performance of the passive controller with different current signals. Figure 5-12 to Figure 5-14 compare the deflection, acceleration and strain responses of the smart beam for uncontrolled, fuzzy controlled, passive controlled (21 different current signals) and PID controlled scenarios under different impact loads. Figure 5-12 depicts the comparison of the uncontrolled-controlled system for 80 mm drop release heights, while Figure 5-13 and Figure 5-14 show the same comparison for 100 mm and 120 mm, respectively.

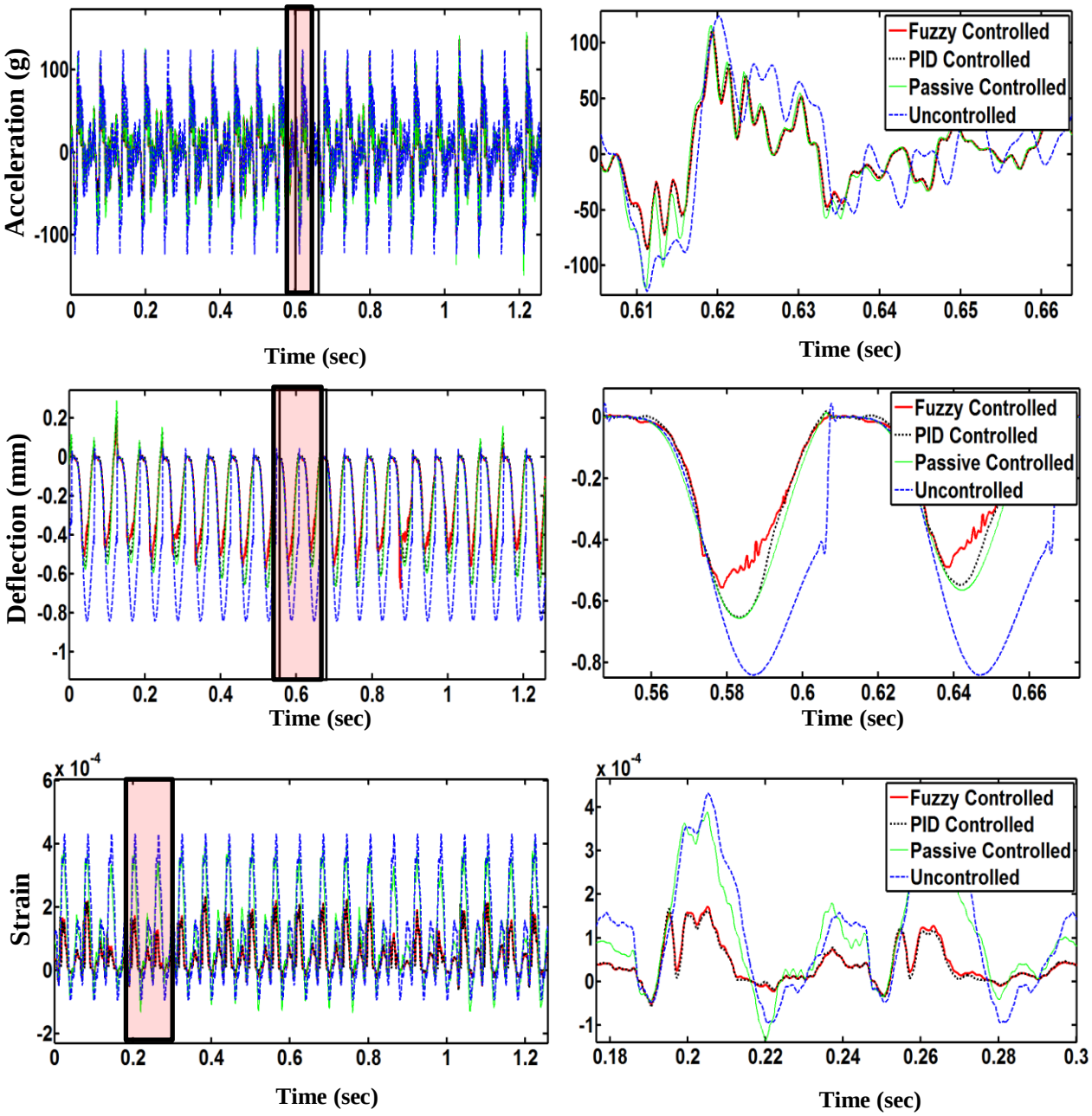

Figure 5-12. Comparison of structural responses for 80 mm drop release height

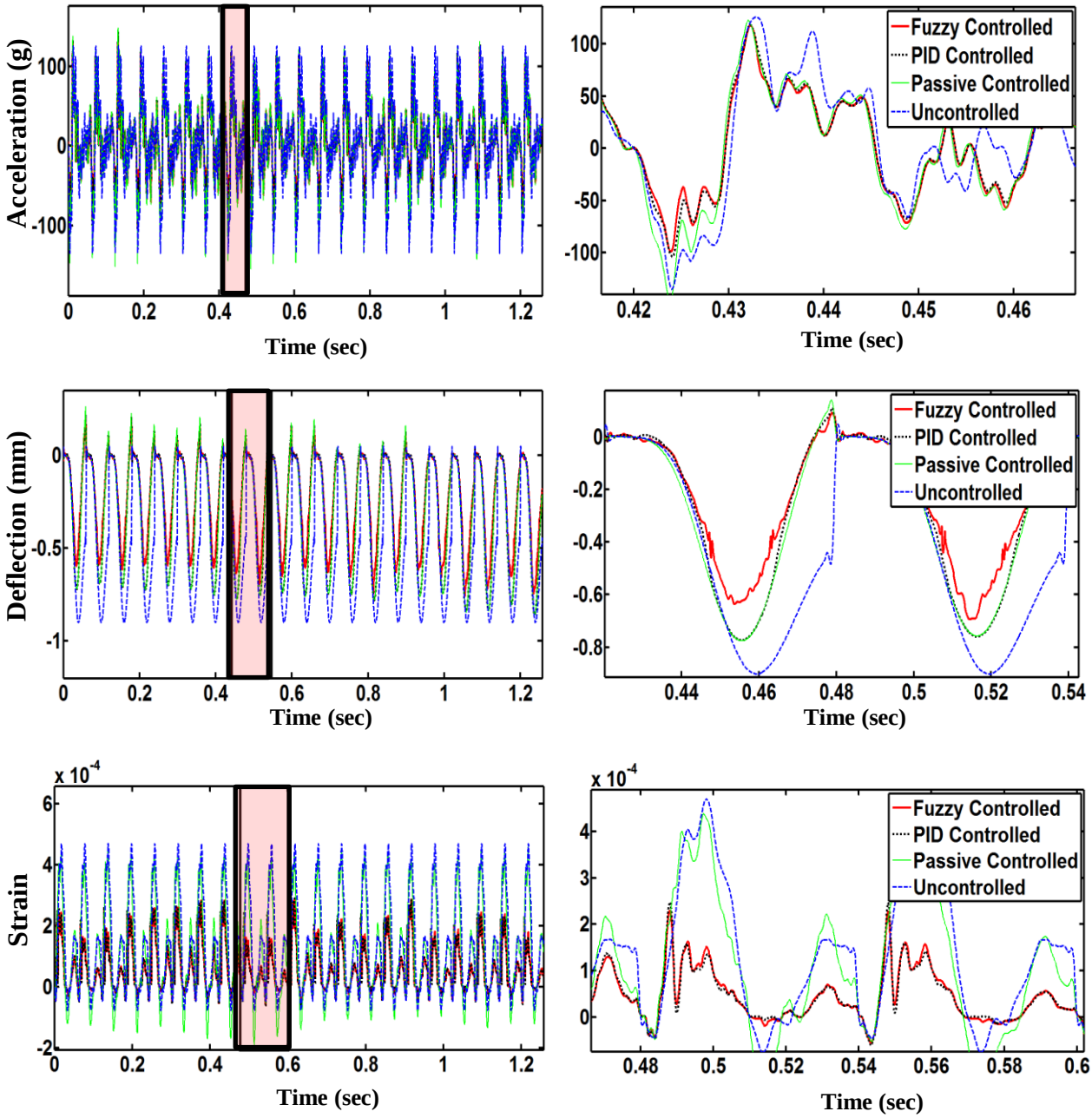

Figure 5-13. Comparison of structural responses for 100 mm drop release height

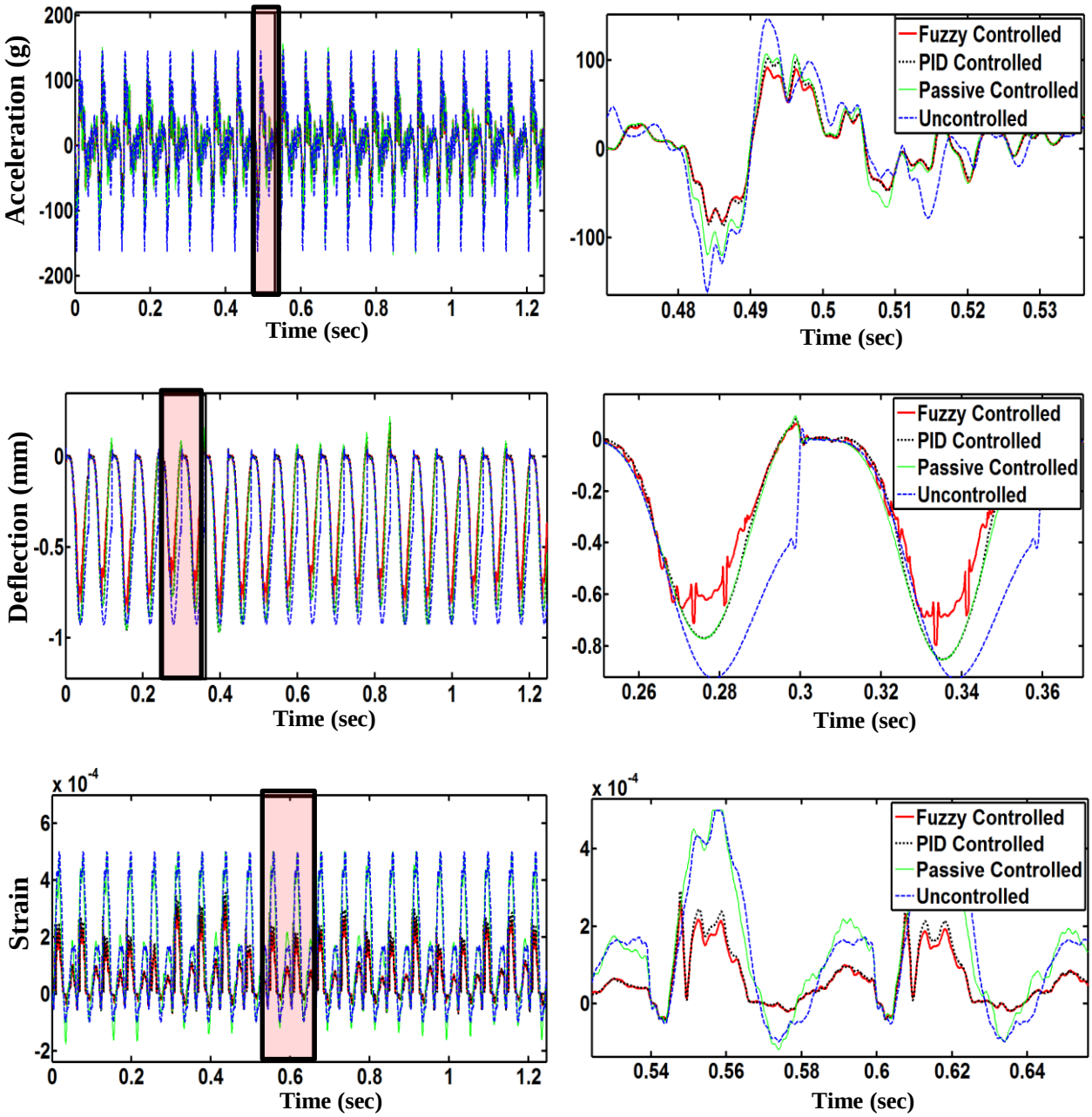

Figure 5-14. Comparison of structural responses for 120 mm drop release height

It is observed that the fuzzy controller is very effective in mitigating the dynamic response of the smart structures equipped with an MR damper under high impact loads. The following sections quantitatively evaluate the performances of the proposed control approach.

5.4.2. Evaluation of results

To further evaluate the performance of the proposed fuzzy control approach, several evaluation indices are used. Table 5-2 shows the evaluation results of the fuzzy controller: J_1, J_2 and J_3 are the max, mean and norm values of the deflection response in units of mm, respectively. J_4, J_5 and J_6 are the max, mean and norm values of the acceleration response in units of g. J_7, J_8 and J_9 are the same indeces for strain. Table 5-2 is prepared by as follows: i) Averaga value of the 21 tests are calculted for fuzzy controlled and PID controlled case. ii) For passive controller, current signal that optimally mitigates the all three responses is selected. iii) Average values of the fuzzy controller and PID controller are compared with the optimum passive controller.

Table 5-2. Evaluation of Fuzzy Controller

		Drop Release Heights					
		20 mm	40 mm	60 mm	80 mm	100 mm	120 mm
J1 (mm)	Fuzzy	0.2058	0.3110	0.3638	**0.5303**	**0.6469**	**0.8023**
	PID	**0.2008**	0.2982	0.3634	0.6012	0.7576	0.8745
	Constant	0.2083	**0.2884**	**0.3405**	0.5422	0.6898	0.8823
	Uncont.	0.3453	0.5035	0.6598	0.8403	0.9014	0.9255
J2	Fuzzy	0.0737	**0.1061**	**0.1329**	**0.2022**	**0.2404**	**0.2927**
	PID	**0.0735**	0.1078	0.1375	0.2266	0.2831	0.3397
	Constant	0.0803	0.1132	0.1332	0.2139	0.2629	0.2950
	Uncont.	0.1517	0.2382	0.3103	0.3954	0.4279	0.4297
J3	Fuzzy	**2.4814**	**3.6242**	**4.4882**	**6.7102**	**8.0570**	**9.7197**
	PID	2.4886	3.6761	4.6203	7.7129	9.7204	11.4476
	Constant	2.6617	3.7682	4.8664	7.1152	8.9036	10.0162
	Uncont.	4.9918	7.5151	9.7017	12.3583	13.3166	13.3380
J4 (g)	Fuzzy	**43.1210**	**62.6290**	**69.6912**	105.9594	**113.3196**	**118.2632**
	PID	46.4868	64.1127	70.6925	**105.8904**	114.6854	129.8054
	Constant	48.7880	68.7154	77.6009	112.3156	136.1696	147.9068
	Uncont.	43.5579	74.0918	102.5360	123.7852	134.7998	161.3505
J5	Fuzzy	**12.3497**	17.2963	**20.1864**	**27.2016**	**32.2482**	**32.8535**
	PID	12.9568	17.8828	20.5751	27.6501	32.9003	33.9469
	Constant	12.5644	**17.2643**	23.4565	31.7676	37.8026	36.4895
	Uncont.	14.5272	19.386	31.6845	40.2154	42.5226	45.7377
J6	Fuzzy	**398.2899**	**551.2982**	**622.5683**	**860.7699**	**1007.5449**	**1026.4737**
	PID	420.7748	570.2542	635.7409	879.4364	1035.7980	1079.8712
	Constant	412.6260	577.4205	739.9685	1025.0073	1111.9199	1146.1574
	Uncont.	494.9671	655.2607	1034.2256	1268.3519	1354.4695	1494.8402
J7	Fuzzy	**$6.459E^{-5}$**	$9.332E^{-5}$	**$1.136E^{-4}$**	$1.846E^{-4}$	**$2.391E^{-4}$**	**$2.492E^{-4}$**
	PID	$6.735E^{-5}$	**$9.086E^{-5}$**	$1.176E^{-4}$	**$1.843E^{-4}$**	$2.463E^{-4}$	$2.757E^{-4}$
	Constant	$1.681E^{-4}$	$2.223E^{-4}$	$1.981E^{-4}$	$4.124E^{-4}$	$4.060E^{-4}$	$4.683E^{-4}$
	Uncont.	$1.653E^{-4}$	$2.531E^{-4}$	$3.653E^{-4}$	$4.317E^{-4}$	$4.706E^{-4}$	$5.000E^{-4}$
J8	Fuzzy	**$1.842E^{-5}$**	$2.758E^{-5}$	$3.423E^{-5}$	$5.441E^{-5}$	**$6.907E^{-5}$**	**$7.098E^{-5}$**
	PID	$1.914E^{-5}$	**$2.734E^{-5}$**	**$3.404E^{-5}$**	**$5.301E^{-5}$**	$6.912E^{-5}$	$7.696E^{-5}$
	Constant	$5.643E^{-5}$	$7.350E^{-5}$	$7.477E^{-5}$	$1.024E^{-4}$	$1.372E^{-4}$	$1.518E^{-4}$
	Uncont.	$5.318E^{-5}$	$8.457E^{-5}$	$1.190E^{-4}$	$1.420E^{-4}$	$1.566E^{-4}$	$1.747E^{-4}$
J9	Fuzzy	**$6.073E^{-4}$**	$9.337E^{-4}$	**$1.138E^{-3}$**	$1.845E^{-3}$	**$2.364E^{-3}$**	**$2.390E^{-3}$**
	PID	$6.359E^{-4}$	**$9.280E^{-4}$**	$1.158E^{-3}$	**$1.813E^{-3}$**	$2.373E^{-3}$	$2.643E^{-3}$
	Constant	$1.840E^{-3}$	$2.476E^{-3}$	$2.411E^{-3}$	$3.442E^{-3}$	$4.484E^{-3}$	$4.985E^{-3}$
	Uncont.	$1.834E^{-3}$	$2.822E^{-3}$	$3.903E^{-3}$	$4.632E^{-3}$	$5.163E^{-3}$	$5.644E^{-3}$

Both fuzzy and PID controllers gave the lowest values for almost all indexes, which means that the models are very effective in mitigating the dynamic responses of the smart

systems under a variety of impact loadings. However, the performance of the fuzzy controller for high impact loads is much better than the PID and passive controller. For 120 mm drop release height, fuzzy controller reduced the deflection response about 13%, while PID and passive controller reduced the deflection about 5.5% and 5%, respectively, over the uncontrolled case. In low impact forces, although the J_1 values of the fuzzy controller is worse than the others, J_2 and J_3 values gave the best results for all cases except 20 mm. When J_7, J_8, J_9 are evaluated, it is seen that there is a slight difference between the values for low impact cases. The good performance of fuzzy controller becomes significant with the increase of the impact load.

Table 5-3 compares the performance of controllers, in terms of a percentage reduction in impact response, over the uncontrolled case. For 100 mm drop release height, the fuzzy controller resulted in a reduction of the maximum acceleration almost by 9% and 20 % over the best PID and passive case, respectively. With this in mind, fuzzy controller can be considered as the best model for mitigating impact response of the smart structures under ambient excitations in this paper due to the similar J_7, J_8, J_9 but better J_2, J_3, J_4, J_5 and J_6 values.

Table 5-3. Evaluation of Percentage Reduction in Impact Response

		Drop Release Heights					
		20 mm	40 mm	60 mm	80 mm	100 mm	120 mm
Def. (%)	Fuzzy	40.3997	38.2324	44.8621	**36.8916**	**28.2339**	**13.3117**
	PID	**41.8477**	40.7746	44.9227	28.4541	15.953	5.51053
	Constant	39.6756	**42.721**	**48.3935**	35.4754	23.4746	4.66775
Acc. (%)	Fuzzy	**1.00303**	**15.4711**	**32.0325**	14.4006	**15.9349**	**26.7042**
	PID	-6.7242	13.4686	31.0559	**14.4563**	14.9217	19.5507
	Constant	-12.007	7.2564	24.3184	9.26573	-1.0162	8.33199
Strain (%)	Fuzzy	**60.9256**	63.1292	**68.9023**	57.2388	**49.1925**	**50.16**
	PID	59.2559	**64.1011**	67.8073	**57.3083**	47.6626	44.86
	Constant	-1.6939	12.1691	45.7706	4.4707	13.7272	6.34

In fuzzy contol, there is a decreasing trend in the deflection dissipation with the increase of the impact force. The rule base structure of the fuzzy controller produces this phenomenon. As explained in the previous sections the fuzzy control process is a chain of rules, which are functions of input-output data set, number of iterations and type and quantity of membership functions. Each input has a weight on the development of the fuzzy rules. There should be a dominant fuzzy if-then rule to account for the final output, instead of multiple rules with similar firing strengths (Jang, 1993). This minimizes the uncertainty and makes the rule set more informative. For the proposed fuzzy controller, acceleration and strain responses are found to be

dominant input factors influencing the output current signal. Due to their dominant frequency, they have a strong influence on the creation of the fuzzy rules. Their weight values are greater than the group threshold level. In this context, for high impact load cases, fuzzy controller optimizes the current on MR damper by giving priority to dissipation of acceleration and strain responses. The performace of the defection mitigation can be improved by using gain factors to increse the weight of the input. However, this improvement can cause deterioration in the acceleration and strain dissipation.

5.5. Conclusion

This paper represents the application of a fuzzy controller to the mitigation of the high impact response in smart structures. To demonstrate the effectiveness of the proposed fuzzy control system, a reinforced concrete (RC) beam structure is investigated. The RC beam employs an MR damper whose fluids are controlled with currents. To train the fuzzy controller, deflection and acceleration responses of the smart structure under different collision scenarios are used as inputs while the current on the MR damper is used as outputs. As a baseline model, a proportional integral derivative controller (PID) is used. The structural responses of the uncontrolled, PID controlled, passive controlled and fuzzy controlled systems are compared under a variety of loading conditions. It is demonstrated that the proposed fuzzy controller is effective in mitigating high impact responses of smart structures.

6. Smart Control of Reinforced Concrete Bridge Piers under a Variety of Impact Loads

6.1. Introduction

Bridge piers, which are designed to resist destructive forces such as wind, vehicle and seismic loads, are very susceptible to collision loads. The excessive force due to collision can affect the structural integrity of the bridge by causing fracture or excessive deformations. Although, a great deal of interest has been generated to use structural control systems in the protection of bridge structures subjected to dynamic environmental hazards, such as earthquakes and strong winds, smart structural systems under impact loads is a new topic in literature (Das and Dey 1992, Wilde and Fujino 1993, Shelley et al. 1995, Patten et al. 1996).

In recent years, magnetorheological (MR) dampers, which uses a magnetic fluid that can change its rheological properties with the application of a magnetic field, has attracted a great deal of attention in the area of vibration control (Yang et al. 2002, Duan et al. 2003, Carlson 2005, Hu et al. 2012). The MR damper can be operated either as a passive or as an active damper. In active cases, the MR fluids are changed into a semi-solid state in a few milliseconds with the application of a magnetic field. This unique aspect allows the MR damper remain operable as passive damper even when the control feedback components are not functioning properly. Other distinguishing properties of the MR damper are its mechanical simplicity, fast response, high dynamic range, low manufacturing cost, large force capacity and robustness (Dyke et al. 1996a, 1998, 2001; Yi et al. 1998, 1999; Kim et al. 2009, 2010). However, developing a control algorithm is very challenging due to nonlinear impact behavior of the time-varying smart structures equipped with nonlinear MR dampers (Arsava et al. 2013a).

In this study, fuzzy logic controllers are used to optimize the magnetic field on the MR fluid due to their simplicity and being more robust according the conventional controllers (Kim and Clark 1999; Zhou and Chang 2000). Many investigators have demonstrated that fuzzy controlled MR damper system shows great deal of promise for civil engineering applications in recent years (Kim and Clark 1999; Zhou and Chang 2000, Jansen and Dyke 2000, Liu et al. 2001, Zhou et al. 2003, Yan and Zhou 2006). Liu et al. (2001) proposed a closed-loop control system based on fuzzy logic to suppress the bridge deck motion under random excitation. It was demonstrated that the proposed fuzzy logic control system significantly reduced the deck displacement, while the absolute deck acceleration remained practically unchanged. Wilson and

Abdullah (2005a) developed a fuzzy controller to regulate the damping properties of the structure-MR damper system under four different earthquake loads. They demonstrated that both floor displacement and acceleration responses were successfully reduced in terms of root mean square. However, most of the studies on fuzzy controlled MR damper technology has focused on seismic or wind load dissipation while relatively little research has been carried out on the under high impact forces (Liu and Chen 2011, Hu et al. 2012). Liu and Chen (2011) proposed developing a time delayed fuzzy-PID controller to optimize the damping force of MR dampers under high impact loads. Displacement, the impact force and the damper chamber pressure were used as inputs to obtain the optimum current signal. Experimental studies were performed on a single bar long-stroke MR damper. It was demonstrated that the performance of the proposed time delay fuzzy PID algorithm is better than the fixed current control in terms of improving the damping force and enhancing the stability. Another study was performed by Hu et al. (2012). In the study, an MRD50 type of large-scale magnetorheological shock absorber was designed and manufactured to control the recoil dynamics of a gun. To control the applied current in the piston coil by MR damper, three kinds of control algorithms, including on–off control, PID control, and fuzzy control algorithm, were designed. The results showed that the fuzzy control reduced the stroke and pressure peak of the MR shock absorber. The main focus of the aforementioned studies was on the control of the MR damper itself under impact loads, not specifically a large structure employing MR dampers. As of yet, there is no studies on development of a smart fuzzy control model for large bridge structures employing MR dampers under high impact forces. Therefore, this paper proposes the application of fuzzy logic theory to the high impact response mitigation of reinforced concrete bridge structures employing MR damper technology.

In this context, a reinforced concrete bridge pier equipped with MR damper subjected to high impact loads is investigated. The main part of a bridge superstructure (concrete deck and steel girders) and a single bridge pier in the center of the bridge span is designed. The bridge pier is scaled down linearly making sure the pier's stiffness had the same scaled down ratio as the full model. This scaled down model is then tested using an drop tower test facility.

Section 6.2 provides information about the experimental setup, equipment and procedures. In Section 6.3, design procedure of the controllers is described. The results and evaluations of the proposed controller are presented in Section 6.4. Concluding remarks are presented in Section 6.5.

6.2. Experimental studies

This research experimentally evaluated the proposed fuzzy logic control approach for its impact response mitigation via passive and PID control. In this context, a scaled down bridge pier structure equipped with an MR damper is investigated under various impact loads.

6.2.1 Drop tower test facility

The drop tower test facility in Structural Impact Mechanics and Mitigation Laboratory in the Civil and Environmental Engineering Department at Worcester Polytechnic Institute is used to apply impact loads to the bridge pier (Figure 6-1). The impact load is applied by a 6.8 kg free falling drop-mass. The magnitude of the impact load, which can be maximum 22.5 ton, can be adjusted by changing the drop release height and drop mass.

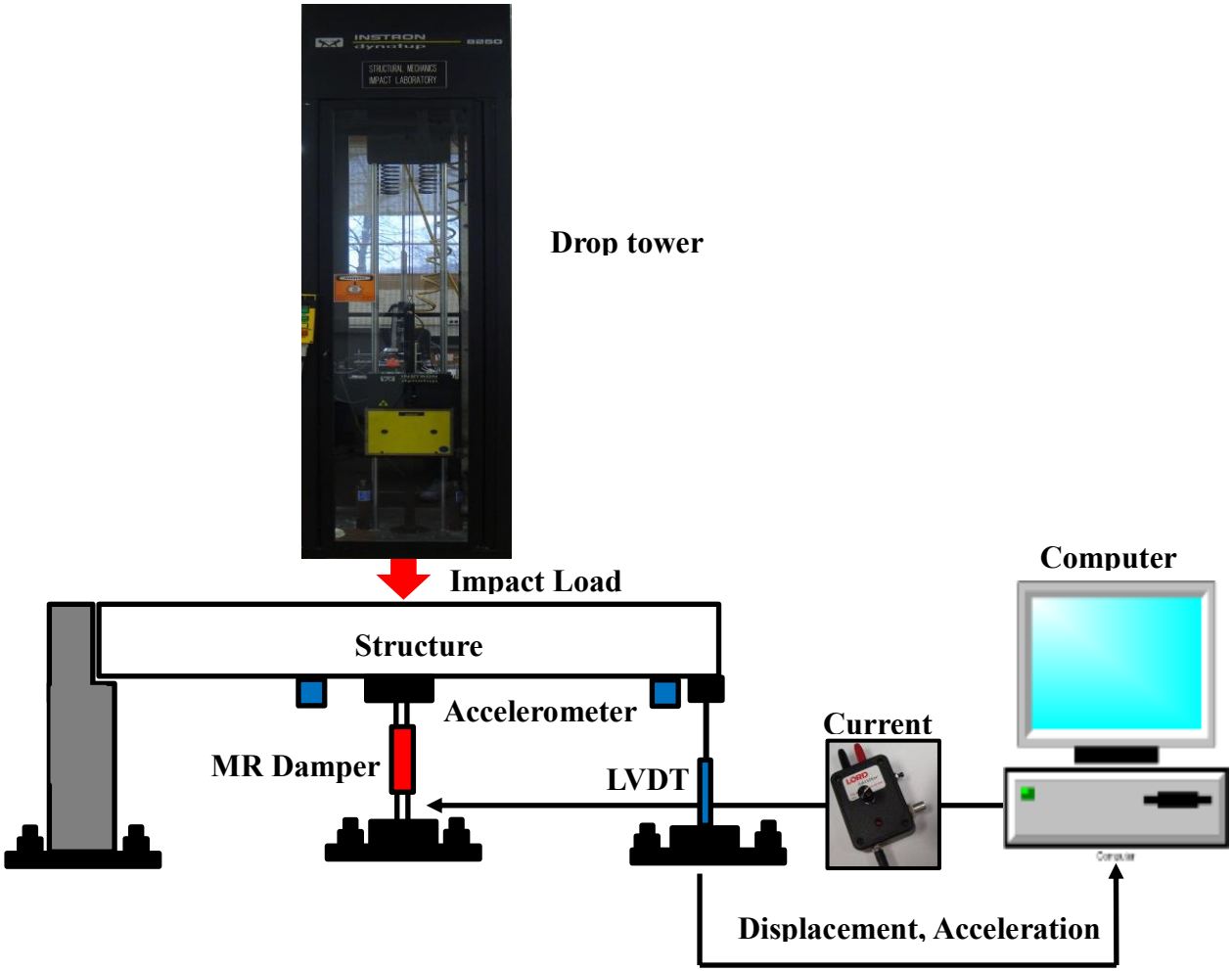

Figure 6-1. Drop-tower testing facility and experimental test setup

6.2.2 Reinforced concrete bridge pier equipped with MR dampers

A reinforced concrete bridge pier is selected to obtain input-output data to train the proposed fuzzy logic controller. An equivalent single cantilever beam structure is designed to have the same stiffness of the full scale pier, which had three columns and a pier cap, in accordance with The American Association of State Highway and Transportation Officials (AASHTO, 2012) specifications. This single structure is then scaled down to fit in the drop tower test facility. The 1/150 scale is used for the dimensions of the pier.

A scaled down bridge pier with a size of 15*x*25*x*100 cm is constructed (Figure 6-2). One end of the member is clamped in order to act as a fixed end while the other end is left free just like a real bridge pier. After the beam is placed the final cantilever length is measured as 56 cm. At the time of testing, the modulus of elasticitiy and the compressive strength of the concrete was calculated as 15 Gpa and 26 MPa, respectively.

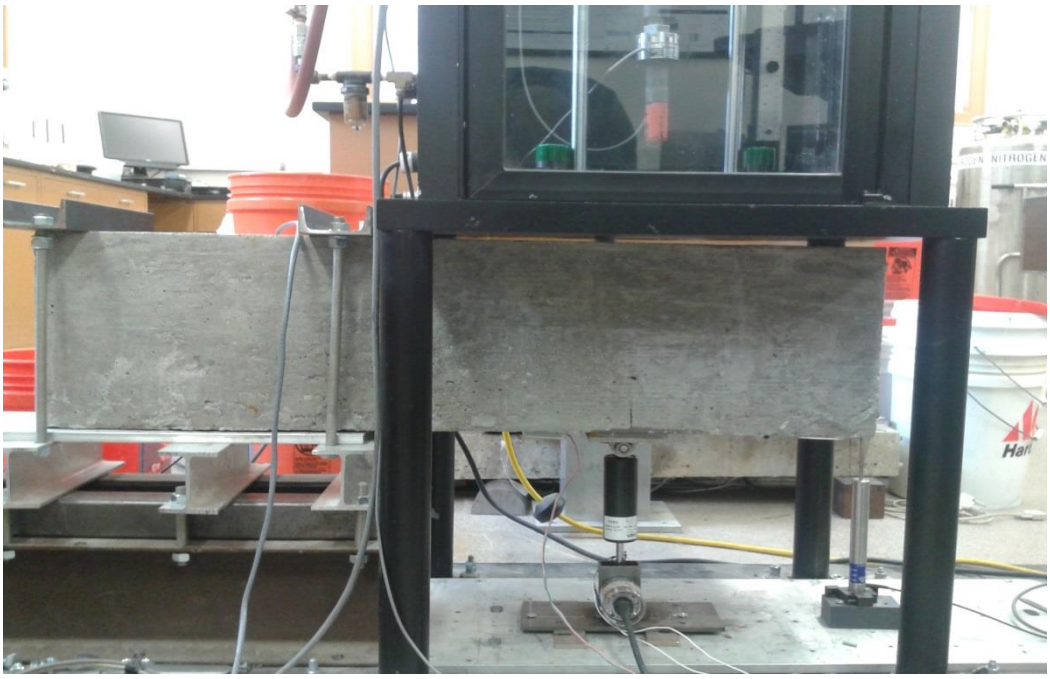

Figure 6-2. Reinforced concrete bridge pier

An MR damper is placed under mid-span of the cantilever beam in order to investigate the performance of the passive and active controlled structure (Figure 6-3). The scaled down bridge pier is tested under various impact loads and different current levels on the MR damper.

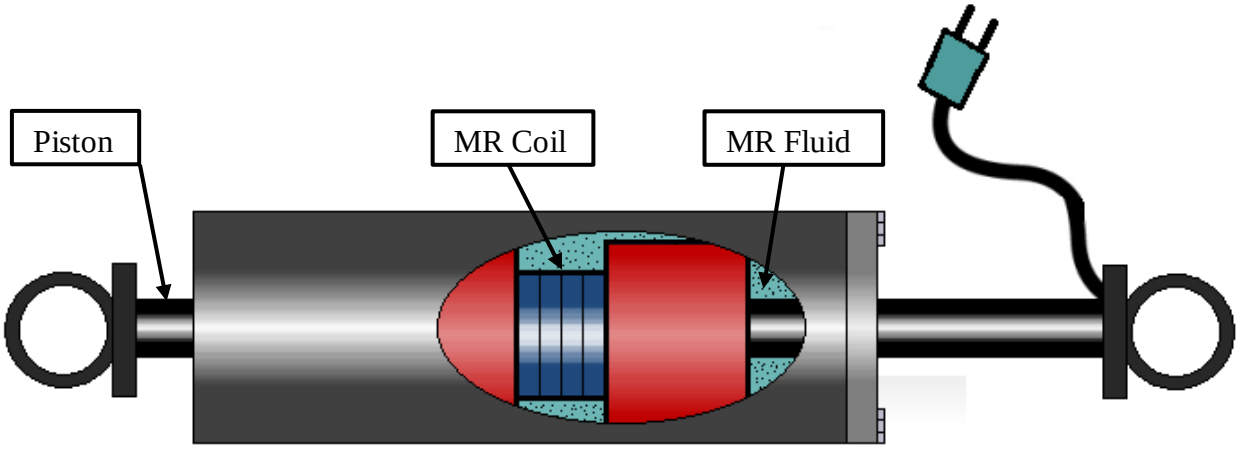

Figure 6-3. Schematic of RD-8040-1 MR damper

6.2.3 Data acquisition

During impact testing on the cantilever test specimen, which represents a scaled down bridge pier, dSPACE data acquisition system is used to collect the structural responses and sending

voltage signals. dSPACE integrates three different software packages that are Matlab, Simulink and dSPACE controldesk. Matlab and Simulink are used to develop the controller and perform analytical tests, while dSPACE controldesk is used to execute the mathematical model in real-time. Acceleration, deflection, impact force and voltage data are collected in the experimental tests. Two PCB type 302A accelerometers with a capacity of 500 g are used to measure the acceleration. A R.D.P product ACT1000A type LVDT is used in the displacement measurements. Impact load data is measured by a 4,500 kg capacity Central HTC-10K type load cell. As a sampling rate of the data acquisition system, 10,000 data points per second is selected. Placement of the sensors is depicted in Figure 6-4Figure 2-7.

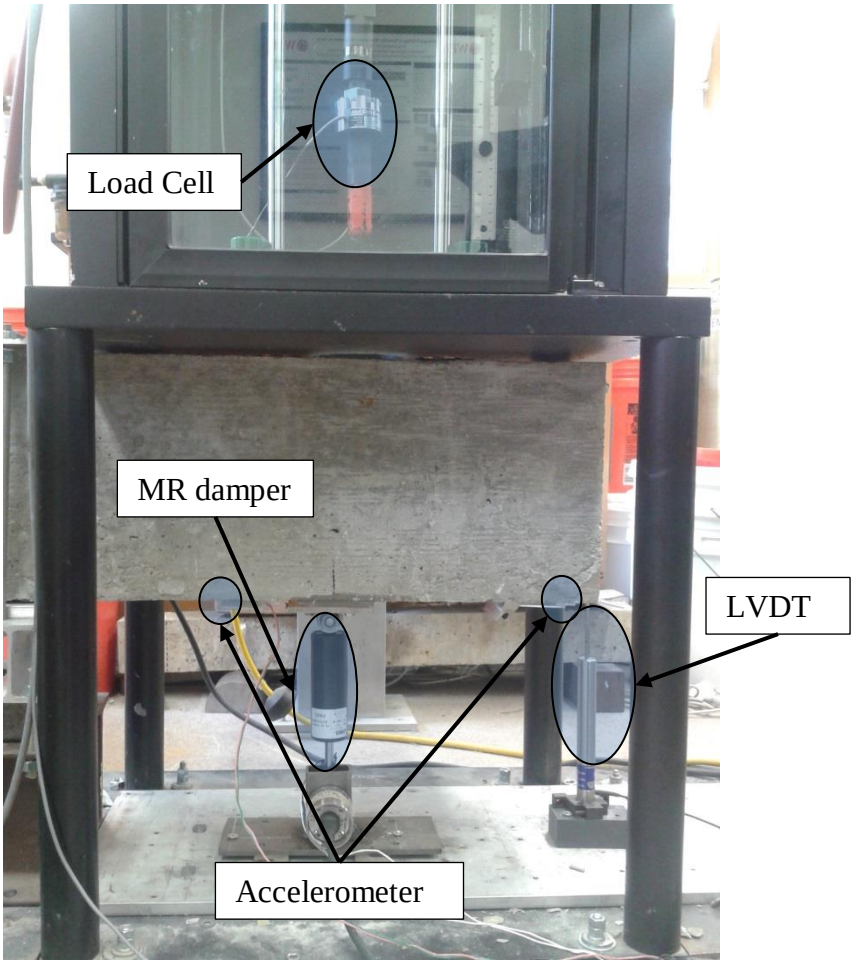

Figure 6-4. Configuration of the sensors and data acquisition system

6.2.4 Test details

The objective of the experimental test is to investigate the performance of the smart structure under a variety of impact loads and different voltage signals. For each drop release height, the

impact test is performed 14 times for various cases such as uncontrolled, passive, PID and fuzzy logic control. For each drop release height and current on the MR damper, the drop release test is performed three times to validate the impact response. Average values of the tests are used in the evaluation of the control models. Details of the performed tests can be found in Table 6-1.

.

Table 6-1. Experimental Test Details

Case Studies	Current on MR Damper (V)	Drop Release Height (mm)	Impact Velocity (mm/s)
Case 1 - Case 14	Uncontrolled 0-5 (10 different constant current) PID Control Fuzzy Logic Control	30	775
Case 15 - Case 28	Uncontrolled 0-5 (10 different cases) PID Control Fuzzy Logic Control	60	885
Case 29 - Case 42	Uncontrolled 0-5 (10 different cases) PID Control Fuzzy Logic Control	80	1025
Case 43 - Case 56	Uncontrolled 0-5 (10 different cases) PID Control Fuzzy Logic Control	110	1375
Case 57 - Case 70	Uncontrolled 0-5 (10 different cases) PID Control Fuzzy Logic Control	130	2058

A total of 210 impact tests are performed to investigate the structure with and without an MR damper. Five different impact force levels are evaluated under different control signals. Average values of the fuzzy controller and PID controller are compared with the optimum passive controller.

6.3. Impact Response Mitigation

Various impact forces (i.e. a number of drop release heights) and numerous counter acting control forces (i.e. a variety of levels of current signals) are investigated in the experimental study.

6.3.1. Passive Control

Passive control can be simply described as an energy dissipation mechanism, which is designed to modify the stiffness of the structure without requiring an external power supply. Passive controllers do not use a real-time structural response feedback and adjust the damping of the structure without developing an opposite control force. This non-optimal behavior of passive systems results with an uncertainty about the response in unexpected large events such as collisions. In the study, passive control is simulated by applying a constant voltage (0-5 V) to the MR damper. Figure 6-5 depicts the input-output data set obtained from the experimental study with passive control.

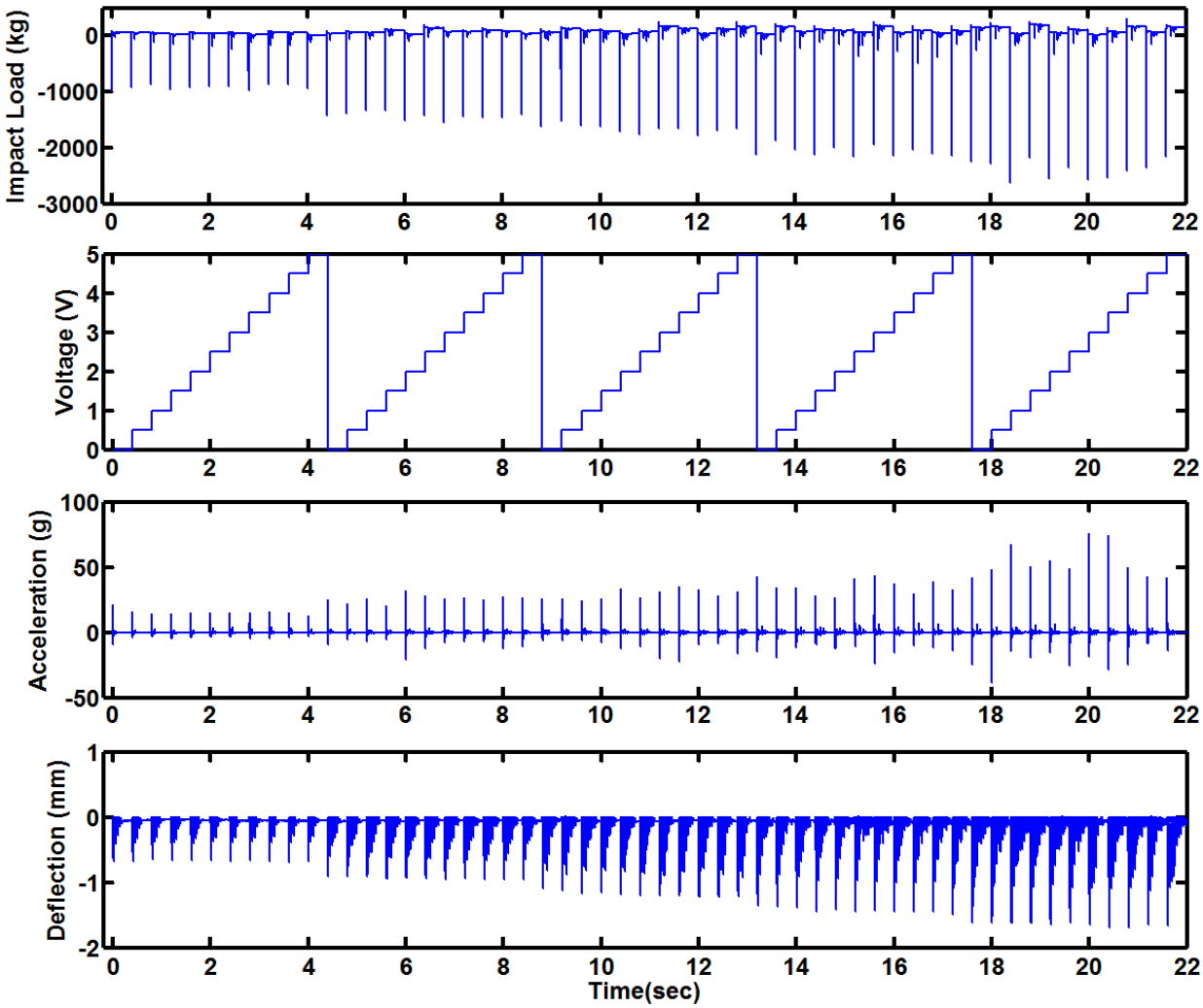

Figure 6-5. Input-output data set - Passive controlled

A computer algorithm is developed in dSPACE to collect structural responses and send control signals to MR damper simultaneously. For passive control, the program sends the

previously defined current signals to the MR damper, while collecting the structural responses. Then the collected data set is processed and evaluated by using MATLAB software.

Figure 6-6 and Figure 6-7 show the detailed comparison between the uncontrolled and the passive controlled structure (11 different current signals). Figure 6-6 depicts the comparison of the acceleration responses for five different drop release heights, while Figure 6-7 makes the same comparison for deflection responses.

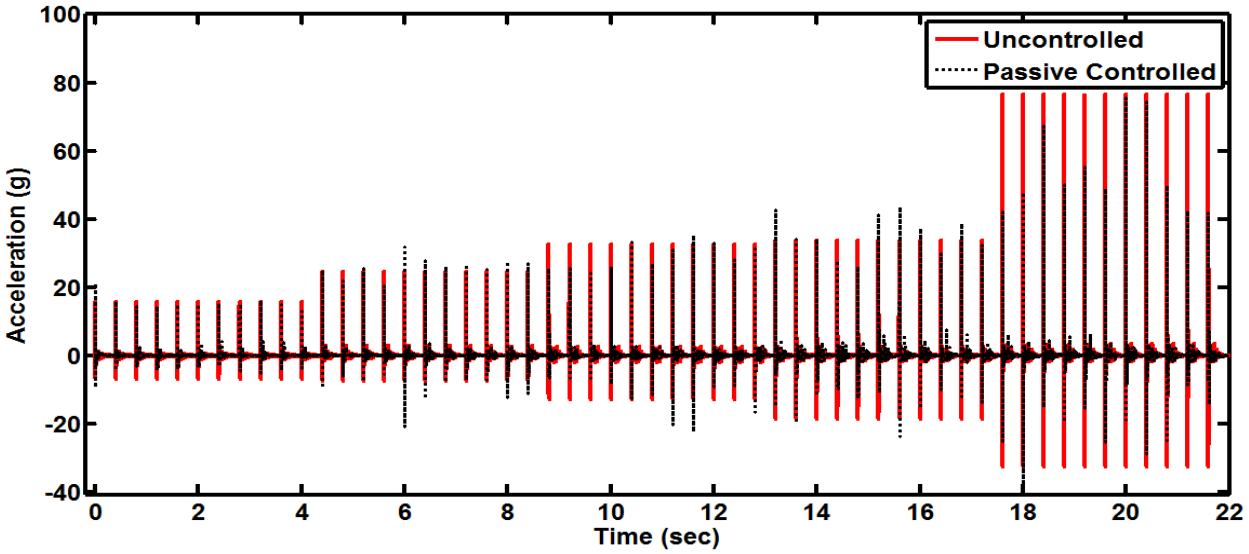

Figure 6-6. Acceleration responses – passive control and different drop release heights

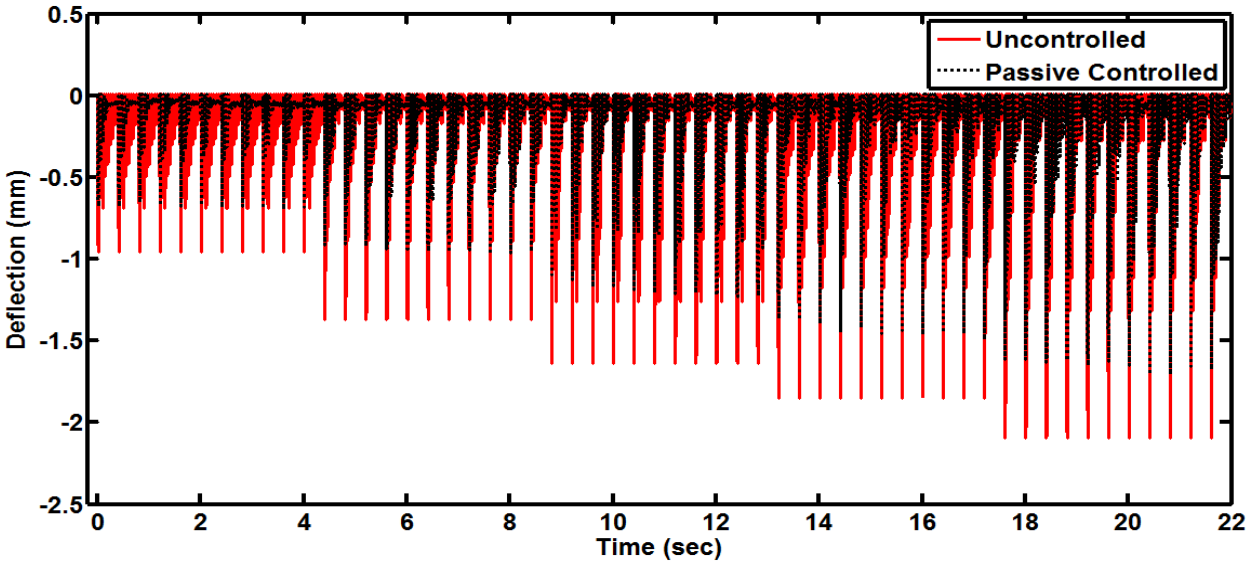

Figure 6-7. Deflection responses – passive control and different drop release heights

Results show that there is a nonlinear relationship between the dynamic responses and the voltage on the MR damper. As an example, for 30 mm drop release height, the optimal structural responses are obtained with the voltage of 5 V, while an optimum control is achieved with 2 V

for 110 mm drop release height. Optimum voltage signals for 60, 80 and 130 mm drop release heights are found as 1.5, 1 and 5 V respectively. The challenge to optimize the current level on the MR damper to mitigate the dynamic responses for different drop release heights is demonstrated by the experimental study.

6.3.2. PID Control

In the study, a proportional integral derivative (PID) controller is also used as a benchmark. A mathematical description of PID controller is as follows. (Kim et al. 2010)

$$Cu(t) = K_P Out(t) + K_I \int_0^t Out(t)dt + K_D \frac{dOut(t)}{d(t)}, \tag{6-1}$$

where *Cu(t)* is the current value on MR damper at time *t*, and K_p, K_I and K_D are the weight factors of the PID controller. The weight factors are determined via many trial and errors. Structure-MR damper model is build in Matlab-Simulink toolbox and then integrated to dSPACE. In the optimization of the voltage signal, acceleration response is used as the control parameter. Figure 6-8 shows the input output data set of the PID controlled structure-MR damper system.

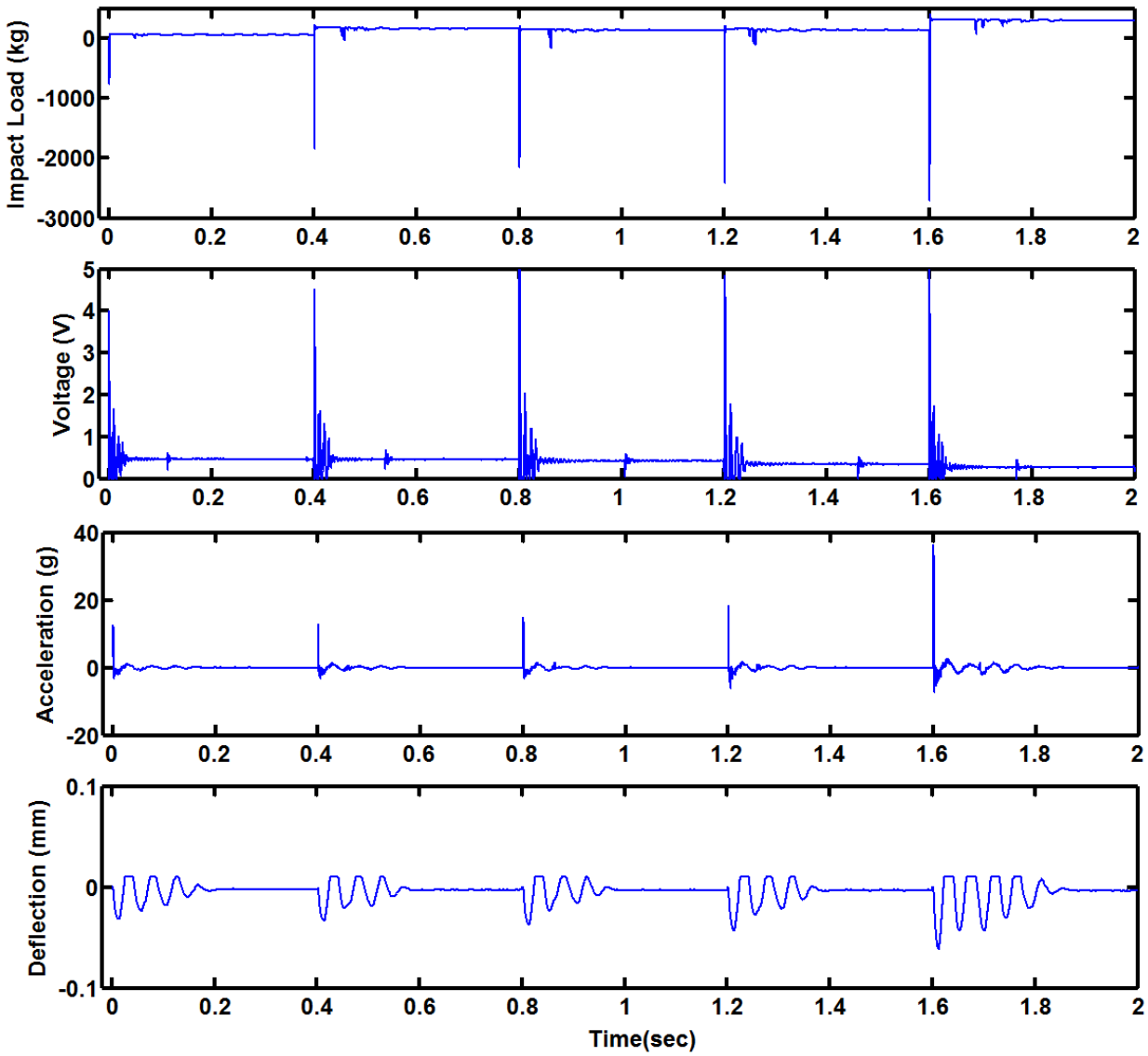

Figure 6-8. Input-output data set – PID controlled

The superior behavior of PID controller over passive controller is expected, due to its ability to reduce the steady state error and increases the stability by tuning the parameters in the minimal time delays. Figure 6-9 compares the acceleration response of the uncontrolled- PID controlled structure, while Figure 6-10 shows the deflection responses.

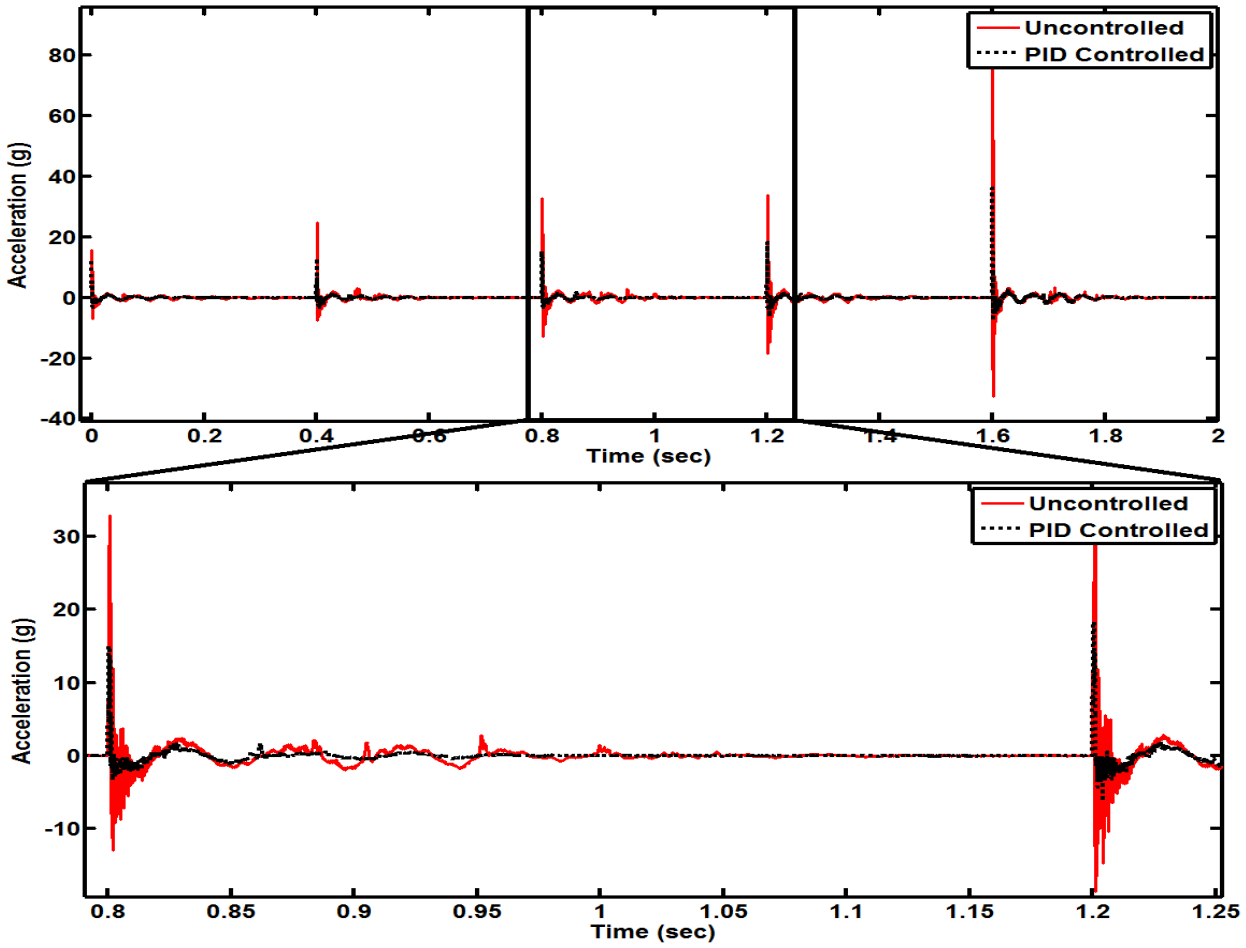

Figure 6-9. Acceleration responses – PID control and different drop release heights

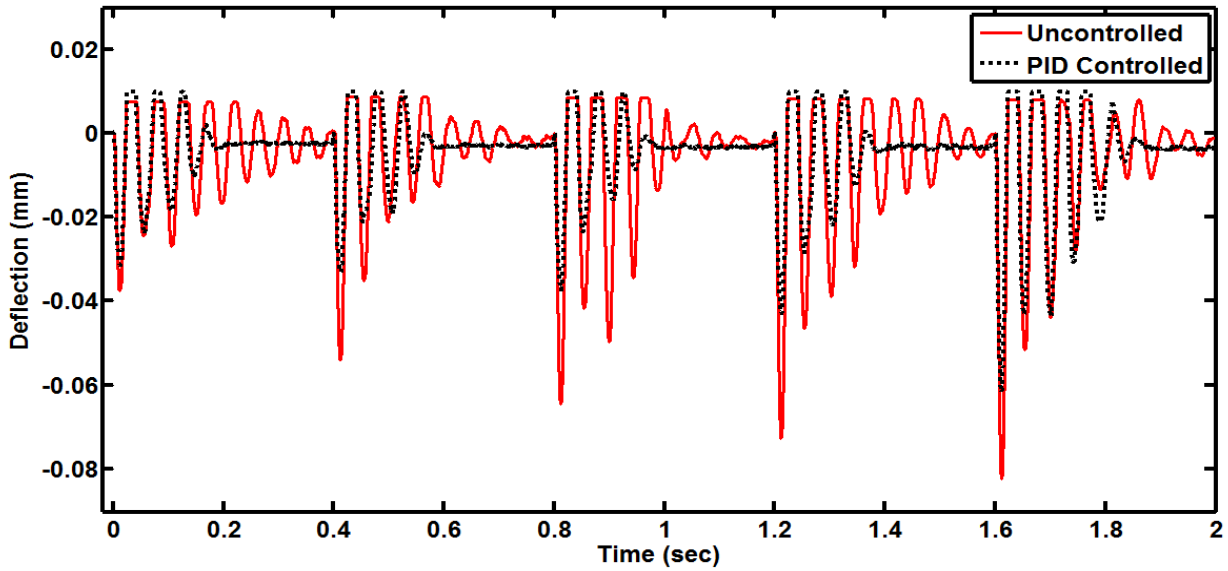

Figure 6-10. Deflection responses – PID control and different drop release heights

It is shown from the figures that the PID controller is effective in mitigating the nonlinear dynamic response of the bridge pier employing an MR damper under impact loads. For

example, for 30 mm drop release height, the maximum acceleration response of the PID controlled structure model is 12.5 g, which is about 20% less than the uncontrolled case. PID control decreased the maximum uncontrolled deflection of the smart bridge pier about 45% for 110 mm drop release height. Although, PID controller has a great performance in mitigating the impact response of bridge pier, there is lack of adaptability. In other words, PID weight factors have to be recalculated and optimized for each impact load scenario, which is a time consuming and labor intensive process. In this context, a fuzzy logic control algorithm is proposed to improve the reliability and robustness of the controlled system.

6.3.3. Fuzzy Logic Control

Fuzzy control theory is one of the recent smart control strategies to improve the dynamic performance of the structures (Casciati et al. 1994; Casciati, F. 1997; Choi et al. 2004; Dounis et al. 2007; Nomura et al. 2007, Pourzeynali et al. 2007; Gu and Oyadiji 2008; Kim et al. 2011).

Based on the identifed model of Arsava et al. (2013a), a control algorithm is developed to optimize the magnetic field on MR fluid. In the taining process of the model, acceleration responses obtained from the sensors are used as input to predict the optimum voltage signal. The conceptual configuration of the proposed model is shown in Figure 6-11.

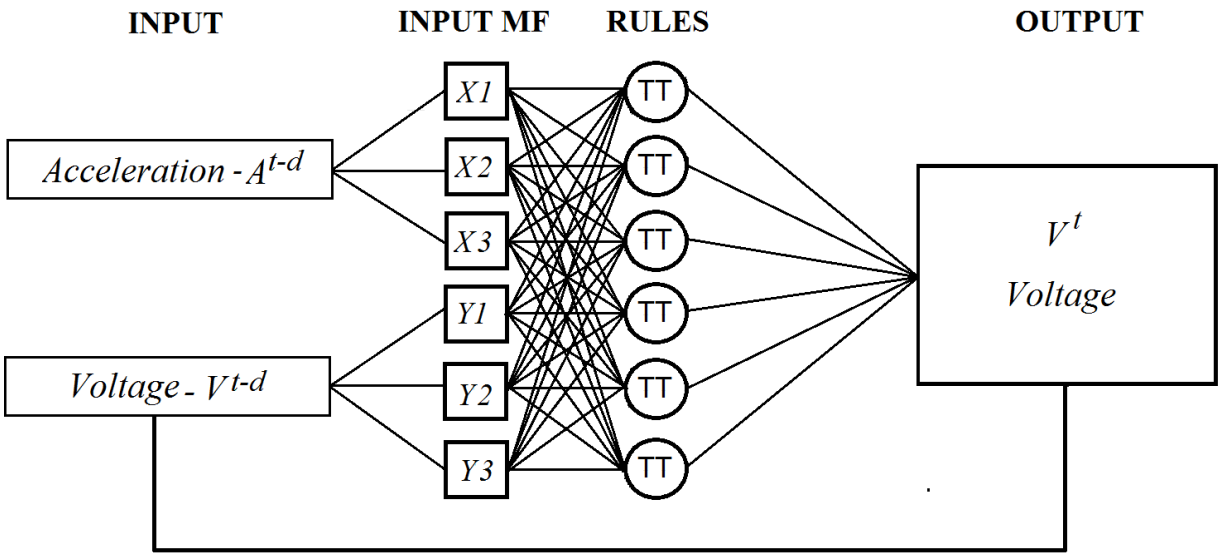

Figure 6-11. Configuration of the TANFIS model

The mathematical model of the fuzzy model is as follows.

For rule *c*: If $A^{t-d}(u)$ is X_{c1}, $A^{t-d}(u\text{-}1)$ is X_{c2}, $A^{t-d}(u\text{-}2)$ is X_{c3}, …, and $A^{t-d}(u\text{-}h+1)$ is X_{ch} then

$$\tilde{A}^{t-d}(u+1) = A_c \tilde{A}^{t-d}(u) + B_c g(u) \tag{6-2}$$

where

$$\tilde{A}^{t-d}(u) = \left[A^{t-d}(u) \;\; A^{t-d}(u-1) \;\; A^{t-d}(u-2) \;\; A^{t-d}(u-h+1)\right]^T \tag{6-3}$$

and $g(u)$ denotes the input variable. c= 1,2,…,h and h is the number of rules. The delay term is represented by d. $\tilde{A}^{t-d}(u+1)$ is the output of the c'th rule, while A_c and B_c are the state and input matrices of the system as correlated with the c'th rule. The behavior of the system can be described as

$$\tilde{V}^t(u+1) = \left[\frac{\sum_{c=1}^{h} w_c^{t-d}(u)\left(A_c \tilde{A}^{t-d}(u) + B_c g(u)\right) + \sum_{c=1}^{h} w_c^{t-d}(u)\left(D_c \tilde{V}^{t-d}(u) + E_c g(u)\right)}{\sum_{c}^{h} w_c^{t-d}(u)}\right] \tag{6-4}$$

where $w_c^{t-d}(u)$ is the combination of all incoming outputs that is called 'firing strength' of a fuzzy control rule.

Figure 6-12 shows the input output data obtained for fuzzy logic controlled bridge pier. As described in Section 6-2, the average values of the three tests are used in the evaluation of the models.

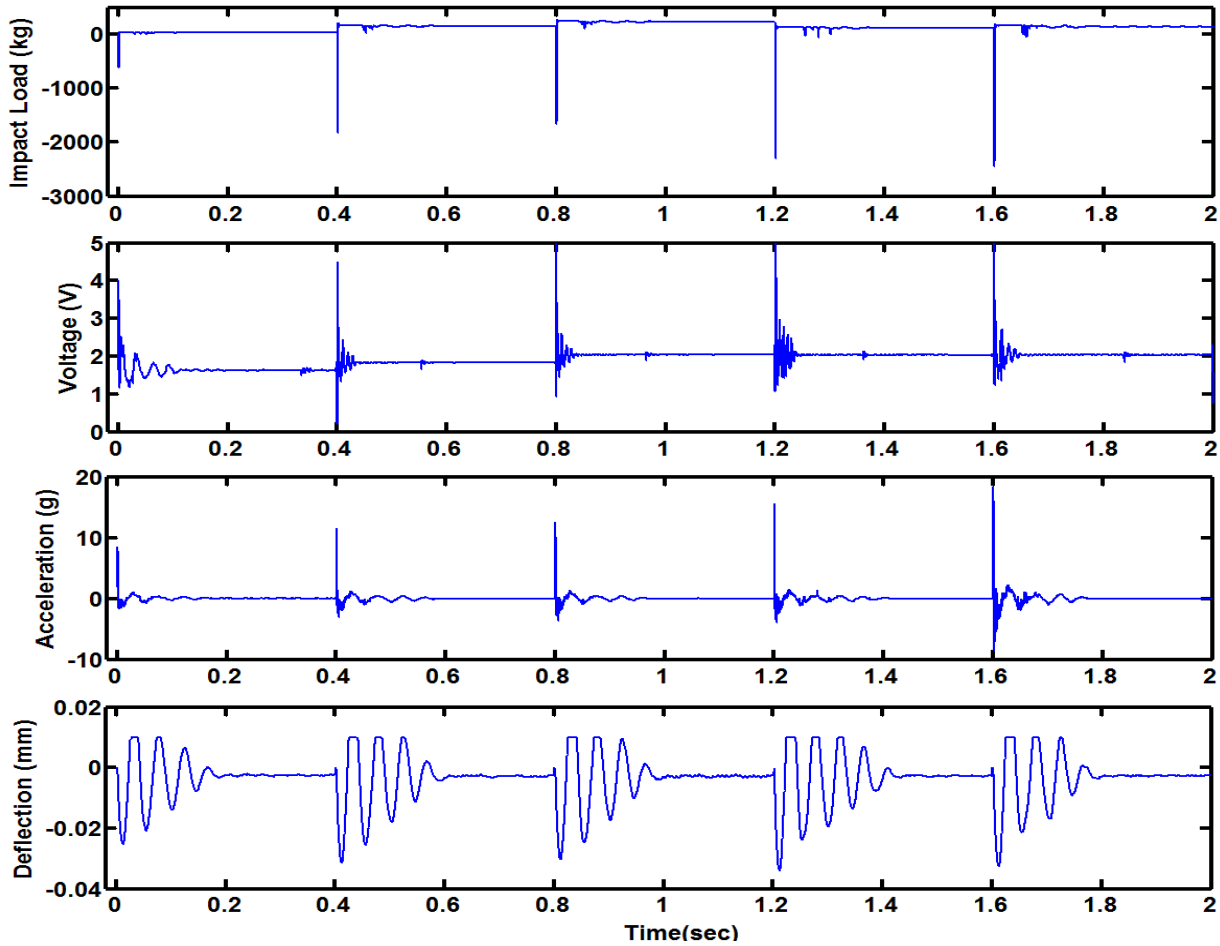

Figure 6-12. Input-output data set – Fuzzy logic controlled

Figure 6-13 and Figure 6-14 shows the acceleration and deflection response of the fuzzy logic controlled bridge pier-MR damper system under impact loads.

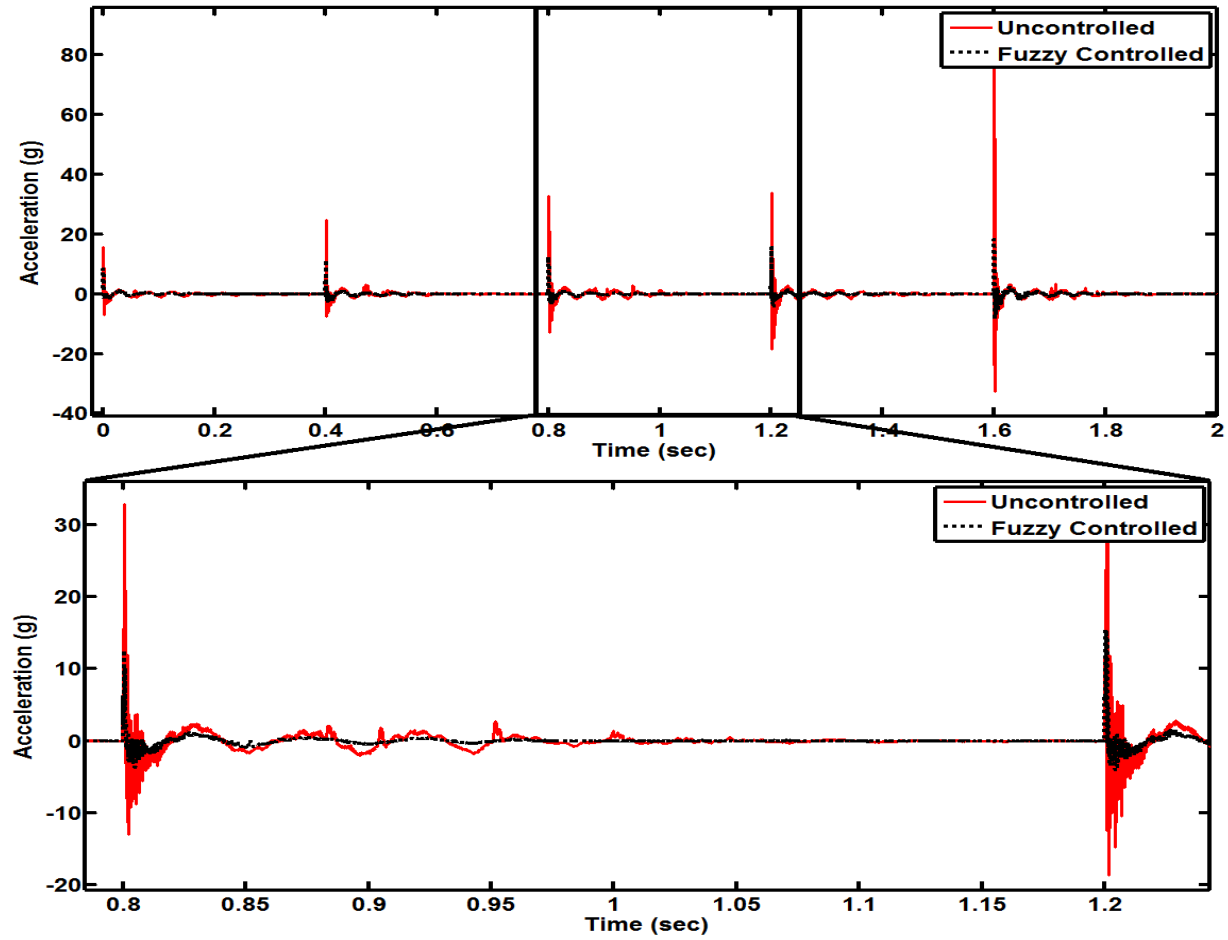

Figure 6-13. Acceleration responses – Fuzzy logic control and different drop release heights

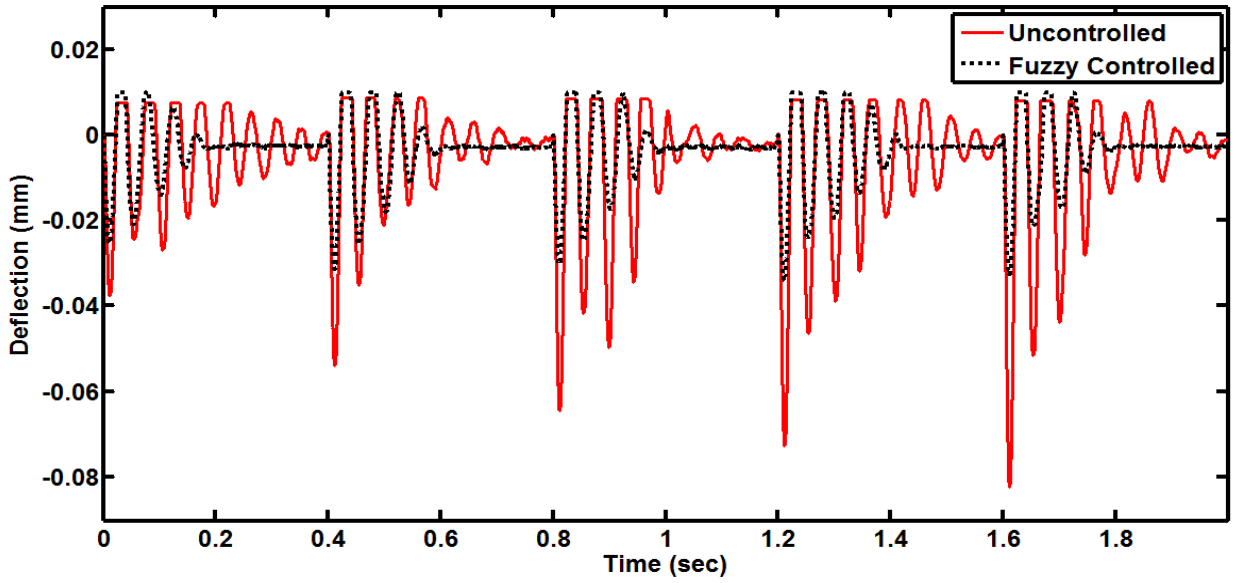

Figure 6-14. Deflection responses – Fuzzy logic control and different drop release heights

It is observed that fuzzy logic controller significantly improved the dynamic behavior of the smart bridge pier under impact load. For 130 mm, the maximum acceleration response of the

fuzzy controlled structure is about 18 g, which is 76%, 49% and 56% and less than the uncontrolled, PID controlled and passive controlled (with optimum current) structure, respectively. When the deflection responses are evaluated, fuzzy controller decreased the maximum uncontrolled deflection about 58%, which is 44% and 47% better than the PID and passive controllers. The quantitative evaluation of the proposed model is presented in detail in the following section.

6.4. Evaluation of results

To evaluate the performance of the proposed fuzzy control approach, several evaluation indices are used. J_1, J_2 and J_3 are the max, mean and norm values of the acceleration response in units of g, respectively. J_4, J_5 and J_6 are the max, mean and norm values of the deflection response in units of mm.

Table 6-2 shows a detailed comparison between the studied controllers. As discussed in the Section 2.4, optimum voltage signals are used in the evaluation of the passive control.

Table 6-2. Evaluation of Fuzzy Controller

		Drop Release Heights				
		30 mm	60 mm	80 mm	110 mm	130 mm
J1 (g)	Fuzzy	**8.5450**	**11.4811**	**12.5462**	**15.6323**	**18.3340**
	PID	12.5830	12.9873	15.0557	18.3337	36.3676
	Constant	12.8674	20.5250	24.1537	26.2165	41.7610
	Uncont.	15.7589	24.7759	32.8513	33.9016	76.8240
J2 (g)	Fuzzy	**0.1576**	**0.1951**	**0.1829**	**0.2253**	**0.3425**
	PID	0.1930	0.1964	0.2068	0.2611	0.5044
	Constant	0.2207	0.3519	0.4381	0.4859	0.5768
	Uncont.	0.3698	0.3955	0.5673	0.6093	0.6839
J3 (g)	Fuzzy	**25.8503**	**34.1772**	**33.6442**	**40.1765**	**63.9279**
	PID	34.2712	36.3477	40.0007	48.4878	84.7655
	Constant	40.4374	57.8880	68.7813	85.0856	96.2351
	Uncont.	47.8073	65.5764	86.2201	102.0797	155.6425
J4 (mm)	Fuzzy	**0.0254**	**0.0315**	**0.0304**	**0.0339**	**0.0344**
	PID	0.0336	0.0347	0.0373	0.0433	0.0618
	Constant	0.0268	0.0372	0.0461	0.0558	0.0660
	Uncont.	0.0376	0.0539	0.0646	0.0729	0.0824
J5 (mm)	Fuzzy	0.0054	0.0069	**0.0066**	**0.0075**	**0.0065**
	PID	0.0067	0.0069	0.0069	0.0083	0.0145
	Constant	**0.0040**	**0.0066**	0.0078	0.0077	0.0108
	Uncont.	0.0082	0.0075	0.0097	0.0113	0.0109
J6 (mm)	Fuzzy	0.4976	0.6359	**0.6092**	**0.6866**	**0.6249**
	PID	0.6397	0.6466	0.6590	0.7960	1.3272
	Constant	**0.3832**	**0.6090**	0.7420	0.7885	1.0672
	Uncont.	0.6958	0.7687	1.0349	1.1003	1.1715

Fuzzy controller gave the lowest values for almost all indices, which means that the model is very effective in mitigating the dynamic responses of the smart bridge pier under variety of impact loadings. Figure 6-15 and Figure 6-16 depict the detailed comparison of the studied controllers for diferent drop release heights.

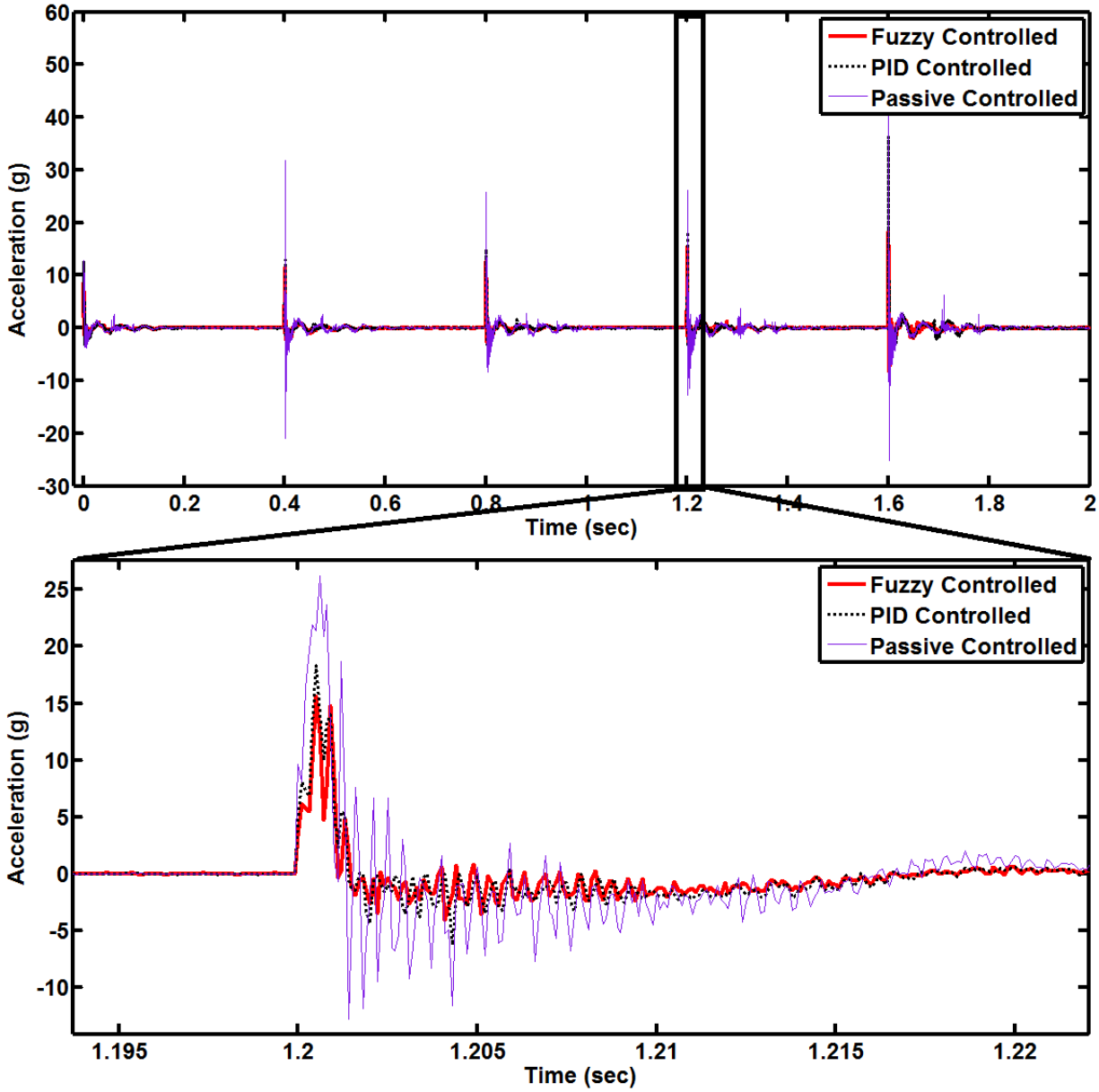

Figure 6-15. Comparison of controllers – Acceleration

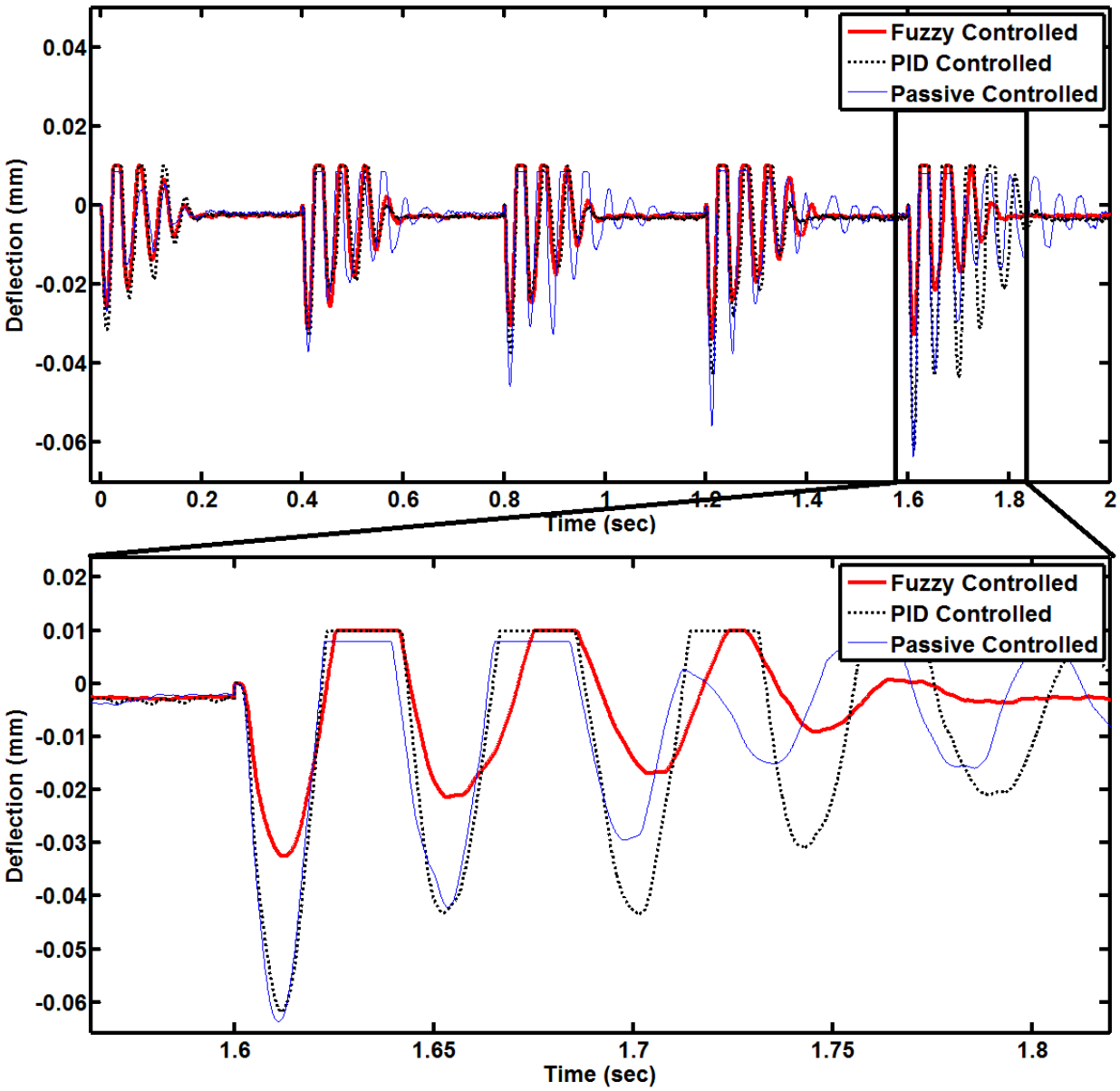

Figure 6-16. Comparison of controllers – Deflection

As previously discussed, six indices are used to evaluate the experimental results. The first evalaution index, J_1, represents the maximum acceleration response obtained from the impact tests. The low value in J_1 represents the good acceleration response mitigation. As an example, in 110 mm drop release height, the J_1 value of fuzzy controller is about 15 g, which is about 53%, 40% and 14% less than the unctonrolled, passive controlled and PID controlled cases, respectively. When the models are evaluated in terms of max deflection, J_4, it is seen that fuzzy controller performed better than the PID and passive contollers. J_4 of fuzzy controller is about 39% and 21% less than the passive and PID controllers.

J_2 and J_5 indeces show the mean value of the acceleration and deflection responses. Small J_2 and J_5 values imply the better performance. For instance, for 130 mm drop release height, J_2 index of fuzzy controller is 50%, 59% and 67% of the unctonrolled, passive controlled and PID controlled cases, respectively. J_5 value of fuzzy controlled structure is about 1.67, 1.66 and 2.23 times smaller than the unctonrolled, passive controlled and PID controlled structure.

The norm values of the acceleration, J_3, and , J_6, deflection are used to measure the value of the response vectors. The low value in J_3 and J_6 represent the good response mitigation. For 80 mm drop release heihgt, J_3 value of fuzzy controlled structure is about 1.18, 2.04 and 2.56 times smaller than the unctonrolled, passive controlled and PID controlled structure. Both PID and passive controllers gave the J_5 index about 0.65 mm and 0.74 mm, which are 7% and 22% higher than the fuzzy contoller.

Table 6-3 compares the performance of the controllers in terms of impact response mitigation, over the uncontrolled case. As an example, for 80 mm drop release height, fuzzy controller reduced the maximum uncontrolled acceleration and deflection responses about 61% and 52%, respectively.

Table 6-3. Evaluation of Control Models in Terms of Uncontrolled Impact Response Mitigation

		Drop Release Heights				
		30 mm	60 mm	80 mm	110 mm	130 mm
Acceleration (%)	Fuzzy	**45.7764**	**53.6603**	**61.8092**	**53.889**	**76.1351**
	PID	20.1530	47.5807	54.1702	45.9208	52.6612
	Constant	18.3484	17.1574	26.4756	22.6686	45.6408
Deflection (%)	Fuzzy	**32.3894**	**41.5196**	**52.9850**	**53.4722**	**58.1992**
	PID	10.6041	35.6976	42.1894	40.5902	24.9884
	Constant	28.6912	31.0440	28.5691	23.3828	19.9585

6.5. Conclusion

This paper represents a smart fuzzy logic controller for bridge piers equipped with magnetorheological (MR) dampers in order to mitigate the nonlinear structural responses due to collision loads and reduce the risk of collapse. To demonstrate the effectiveness of the proposed fuzzy logic controller an equivalent single cantilever beam structure was manufactured to have the same stiffness of the full scale pier, which had three columns and a pier cap, in accordance with the American Association of State Highway and Transportation Officials (AASHTO, 2012) specifications. Then the scaled down smart bridge pier was tested under a variety of impact loads to generate sets of input data for training the proposed fuzzy controller. To train the fuzzy controller, acceleration response is used as input while the optimum voltage on the MR damper is output. After the fuzy controller is trained, the test speciment is subjected to impact forces from a variety of drop release heights, and the effectiveness of the fuzzy controller is investigated in real time. As baseline models, passive controller and a proportional integral derivative controller (PID) are used. Study showed that there is a nonlinear relationship between the dynamic responses and the voltage on the MR damper, which makes it challenging to optimize the voltage level on the MR damper for different impact loads. It is also seen that the weight factors of PID controller have to be recalculated and optimized for each impact load scenario, which is a time consuming and labor intensive process. The performances of controllers are compared against that of the uncontrolled system in order to determine which system effectively reduces the impact response of the bridge pier. It is demonstrated that the proposed fuzzy controller is an effective model in mitigating the nonlinear dynamic responses of smart bridge structure under various impact loads.

7. A Novel Health Monitoring Scheme for Smart Structures

7.1. Introduction

Structural health monitoring (SHM) systems have received a lot of attention in the civil engineering field (Bulut et al 2005, Kim et al. 2013, Huang 2011, Mita and Hagiwara 2003, Worden and Lane 2001). In particular, SHM assists engineers to detect structural damage proactively with non-destructive testing by providing real-time monitoring systems (Farrar and Worden 2007). For example, when the structure is excited by a natural or man-made hazard, the properties of structural system such as stiffness and damping may change. The measured changes that are observed by sensors may alert the SHM system. Then, the SHM provides real-time information to identify location and severity of damage which can work as a proactive warning mechanism (Figueiredo et al. 2012). However, it would be challenging for such damage detection approaches to be applied to smart structures due to the highly complicated nonlinear behavior of integrated structure-smart control systems.

One of the promising methods to classify and evaluate the highly nonlinear structural responses obtained from integrated structure-control systems would be to use the support vector machine (SVM) framework (Kim et al. 2013). In general, SVM uses the statistical learning theory to transform the data to a higher dimensional feature space and find the optimal hyperplane in the space that maximizes the margin between classes (Burges 1998; Mohammadnejad et al. 2011; Hou et al. 2011). SVM has recently been applied to the civil engineering field. Worden et al. (2001) applied SVM in the investigation of the vibration-based damage of truss structures. Another application was performed by Mita et al. (2003) in the damage detection of shear-type building structures. In the study, the changes in the model frequency of the structure were observed and SVM was adopted to determine the local damages. Shimada and Mita (2005) applied a SVM framework to a damage assessment system of bending structures. They verified the performance of the SVM using analytical models and experiments. It was demonstrated that SVM is effective in detecting damage in bending structures. Oh and Sohn (2009) evaluated the effectiveness of an SVM in structural damage detection in the presence of an unmeasured operational variation. It has also been demonstrated from previous studies that SVM can be effective in classifying the damage on bridge structures (Bulut et al. 2005, Park et al. 2006, Vines-Cavanaugh et al. 2010). Bulut et al. (2005) focused on the damage detection of the Humboldt Bay Middle Channel Bridge by using a SVM classifier. Another

study was performed on detection of abnormality on a cable-stayed bridge structure (Vines-Cavanaugh et al. 2010). Damage statuses of the expension joints were classified by SVM. Park et al. (2006) proposed a nonlinear SVM-based binary classification for damage detection of small-scale steel bridge components. The maximum peak values at a specific frequency were compared to show the efficiency of SVM.

However, the main focus of all of the aforementioned studies was on the linear behavior of uncontrolled linear dynamic systems, not highly nonlinear behavior of complex structure-smart control systems. Although SVM is one of the most effective classification processes, Tipping (2001) stated that the accuracy of the SVM classification can decrease significantly when it is trained using small data sets. Furthermore, since SVM considers optimal selection for penalty term and kernel parameters (Foody 2008), finding optimal parameters is computationally expensive (Tipping 2001).

On the other hand, the relevance vector machine (RVM), which is a Bayesian extension of SVM, can be considered as an alternative method. There are previous studies that used RVM as an alternative to SVM. The study of Xiang-min et al. (2007) in bioengineering field was mainly focused on the comparison of SVM and RVM models. They demonstrated that the performance of RVM in terms of generalization and decision speed was better, while the training efficiency and classification accuracy of RVM was similar to that of SVM. Foody (2008) used RVM in the multi-class classification of an agricultural test site. However, there is only one study about RVM in the civil engineering field (Huang et al. 2011). The study was focused on a Bayesian formalism, which was based on the relevance vector machine (RVM), to compress the data obtained from SHM systems. They proposed diagnostic tools to investigate whether the compressed representation of the signal was optimal. However, the main purpose of the study was to decrease the data transfer cost by compressing the signals obtained from SHM systems, not the damage classification of highly nonlinear smart structure systems. As of yet, there is no research on RVM that has proposed to classify the damage of smart structures. With this in mind, an RVM-based structural health monitoring framework for damage detection of structures equipped with time-varying hysteretic control devices is proposed so that the nonlinear behavior of integrated structure-smart control systems is effectively classified in this paper.

This paper is organized as follows: Section 7.2 discusses the SVM and RVM in detail. Discrete wavelet transforms (DWT), autoregressive (AR) model and damage-sensitive feature are also discussed in Section 7.2. In Section 7.3, the case study and its procedures are described. The binary and multi-class classification results, including comparison of SVM and RVM, are given in Section 7.4. Concluding remarks are given in Section 7.5.

7.2. Multiclass nonlinear relevance vector machine (MNRVM)

The data generation, regression and classification process is depicted in Figure 7-1. For the classification process, multiclass nonlinear relevance vector machine (MNRVM) is considered in this paper. In order to obtain data for training and validating the RVM, a scaled three-story smart building equipped with an MR damper is studied. The properties of the three story building structure are adopted from a scaled building model (Dyke et al. 1996b) of a prototype building structure that was developed by Chung et al. (1989). The structural system is subjected to random excitation and random current values on the MR damper. Acceleration, velocity and displacement of the smart structure are obtained. First, DWT is applied to selected data sets in order to compress and denoise them. As a second step, the AR model estimates the filtered response and constructs wavelet-based AR (WAR). As a third step, MNRVM classifies the WAR data into either healthy or damaged status. In MNRVM classification, one part of the WAR data is used to train the data, while the other part is applied to the validation process.

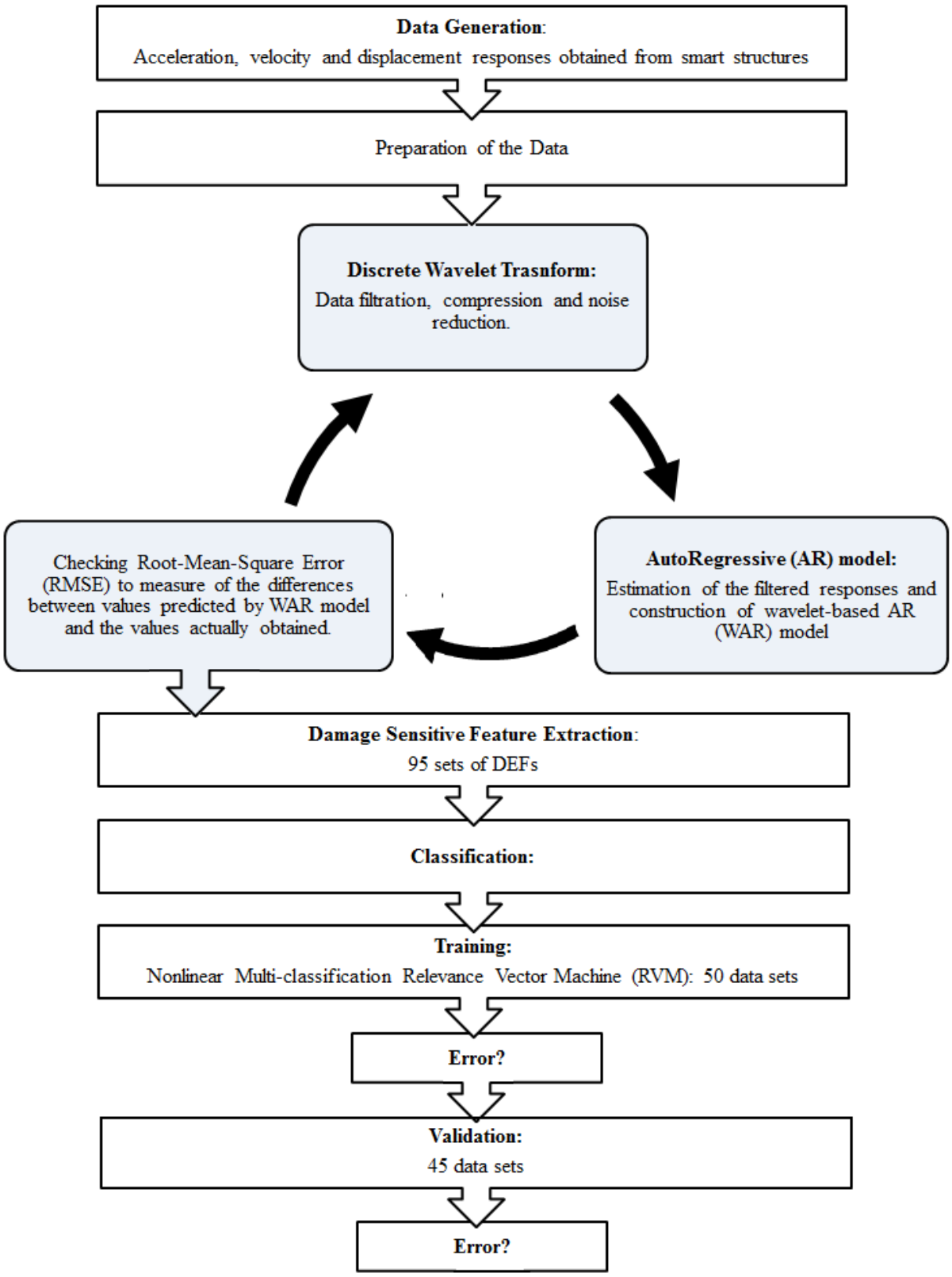

Figure 7-1. Architecture of the proposed RVM scheme for smart structures

The support vector machine that will be used as a benchmark is described first in the following section and then the proposed RVM is present.

7.2.1. Support vector machine (SVM)

In general, SVM classifier finds the support vectors which maximize the margin (or the distance) by using training data. Linear SVM can be categorized into soft-margin SVM and hard-margin SVM. Soft-margin SVM is for the data sets which are mixed and cannot be separated into classes. On the other hand, hard-margin SVM is usually applied to the situation where the data points are separable. Hard-margin SVM uses the following equation to find the support vectors.

$$\textit{Minimize} \quad d(\mathbf{w}_s) = \frac{1}{2}\langle \mathbf{w}_s, \mathbf{w}_s \rangle, \tag{7-1}$$

$$\text{Subject to} \quad T_{sv}\left(\langle \mathbf{w}_s, \mathbf{y}_{sv} \rangle + b_s\right) \geq 1, \text{ for } sv = 1, 2, \ldots, N, \tag{7-2}$$

where $\mathbf{w}_s$ and $\mathbf{y}_{sv}$ are the weight vector and the sv^{th} input vector data respectively. T_{sv} is the sv^{th} target variable and b_s is the bias and $\langle \mathbf{w}_s, \mathbf{y}_{sv} \rangle$ is the inner product operation of $\mathbf{w}_s$ and $\mathbf{y}_{sv}$. The decision boundary F_{sv} is derived as

$$F_{sv} = \langle \mathbf{w}_s^*, \mathbf{y} \rangle + b_s^* = 0, \tag{7-3}$$

where $\mathbf{w}_s^*$ is the weight factor and b_s^* is bias obtained from the Eqn. (7-1). $\mathbf{y}$ is the input point.

In the soft-margin SVM algorithm, *slack variables* are introduced to minimize the error and maximize the margin. To determine the decision boundary of soft-margin SVM, following equations are used

$$\textit{Minimize} \quad d(\mathbf{w}_s) = \frac{1}{2}\langle \mathbf{w}_s, \mathbf{w}_s \rangle + C_s \sum \delta_{sv}, \tag{7-4}$$

$$\textit{Subject to} \quad T_{sv}\left(\langle \mathbf{w}_s, \mathbf{y}_{sv} \rangle + b_s\right) \geq 1 = \delta_{sv}, \text{ for } sv = 1,2,\ldots,N, \text{ for } \delta_{sv} \geq 0. \tag{7-5}$$

where δ_{sv} is the slack parameter and C_s is the margin parameter. By transforming the $\mathbf{y}_{sv}$ term to $\mathbf{y}_{sv} \rightarrow \Phi(\mathbf{y}_{sv})$ non-linear SVM can be transformed to a linear SVM. For nonlinear SVM the Eqn. (7-1) is modified as

$$T_{sv}\left(\left\langle \mathbf{w}_s, \Phi(\mathbf{y}_{sv})\right\rangle + b_s\right) \geq 1, \quad \text{for } sv=1,2,\ldots,N. \tag{7-6}$$

To facilitate the operation in nonlinear SVM, a kernel function K_s, which is a dot-product in the transformed feature space as follows, is used

$$K_s\left(\mathbf{y}_{sv}, \mathbf{y}_{sv'}\right) = \left\langle \Phi(\mathbf{y}_{sv}), \Phi(\mathbf{y}_{sv'})\right\rangle, \tag{7-7}$$

where $sv' = 1, 2, ..., N$. The Gaussian radial basis function is used in both classification and regression. The parameter set of Gaussian kernel affects the formation of the decision boundaries (Kim et al. 2013). Optimization of the kernel variance, σ, reduces the misclassification errors, provides smoother decision surface and more regular decision boundary. The associated kernel (Guo and Li 2009) is expressed as

$$K_s\left(\mathbf{y}_{sv}, \mathbf{y}_{sv'}\right) = exp\left(-\frac{\left\|\mathbf{y}_{sv} - \mathbf{y}_{sv'}\right\|^2}{2\sigma^2}\right). \tag{7-8}$$

Using appropriate kernel function that satisfies the Mercer's condition and non-probabilistic estimations are drawbacks of SVM. Furthermore, the usage of error/margin tradeoff parameters (δ_{sv} and C_s) during cross-validation process results in data loss and increased computation time. Thus, in order to decrease the computation time and prevent data loss, an RVM approach is adopted that decreases the computation time while maintaining accuracy.

7.2.2. Relevance vector machine (RVM)

RVM estimates the class of given input by calculating the probability of membership for pre-defined classes. The RVM can overcome the limitation of SVM whose outputs are deterministic values. Since the uncertain nature of data is not expressed in SVM, the complexity parameter is necessary to be found by checking all possible value of C, and kernel function must be satisfied the semi-positive definite condition (Nguyen et al. 2013). On the other hand, since RVM does

not require defining the parameter C, it reduces sensitivity to the hyperparameter settings. It has a probabilistic output (Mahesh 2009). Thus a new RVM approach, which is much sparse and fast when compared to SVM, is proposed to classify the damage on smart structures in this paper. Linear form of an RVM classifier is considered as

$$\mathbf{y}_{rv} = \mathbf{w}_s{}^T K_s, \text{ for } rv=1,2,\ldots,N. \tag{7-9}$$

The process starts by training the RVM classifier. The RVM is trained with an input data set to obtain the optimum parameters for the RVM classifier. In our case, the RVM classifier separates the input data into the healthy and damaged (5%, 10%, 15%, 30% and 50%) signals.

Similar to the SVM, the training data set consists of the training input data and its target variables, which are defined as $\mathbf{y}_{rv}$ and T_{rv}, respectively. T_{rv} can be also defined as the identification of $\mathbf{y}_{rv}$ vector with M feature elements. In the study one-versus-the-others approach is used, where a single classifier is trained per class to distinguish that class from all other classes. For example, $T_{rv}=0$ represents the healthy case, while $T_{rv}=1$ is used to describe the 5%, 10%, 15%, 30% and 50% damaged cases. The distribution of the weight vector $\mathbf{w}_s$ is considered to be a zero-mean Gaussion prior as

$$f_{\mathbf{w}}(\mathbf{w}_s) = \prod_{s=0}^{N} \frac{1}{\sqrt{2\pi\alpha_s}} \exp\left\{-\frac{\mathbf{w}_s{}^2}{2\alpha_s}\right\}, \tag{7-10}$$

where α_s is defined as the variance of the $(s+1)^{\text{th}}$ component of $\mathbf{w}$. As an example, the posterior probability of health strucuture ($T_{rv}=0$) can be written as a logistic sigmoid function of $\mathbf{y}_{rv}$ as follows

$$P\{T_{rv}=0|K_s\} = h(\mathbf{y}_{rv}) = h(\mathbf{w}_s{}^T K_s), \tag{7-11}$$

where $h(a)=1/(1+e^{-a})$ is the logistic sigmoid fuction

$$a = \log \frac{P\{K_s[T_{rv}=0]P[T_{rv}=0]\}}{P\{K_s[T_{rv}=1]P[T_{rv}=1]\}}. \tag{7-12}$$

The likelihood function of training data for two class classification can be written as

$$f_{T_{rv}|\mathbf{w}_S}(T_{rv}|\mathbf{w}_s) = \prod_{rv=1}^{N} h(\mathbf{y}_{rv})^{T_{rv}}[1-h(\mathbf{y}_{rv})]^{1-T_{rv}}. \tag{7-13}$$

Since $f_{T_{rv}|\mathbf{w}_S} \alpha \; f_{T_{rv}|\mathbf{w}_S} \; f_{\mathbf{w}}(\mathbf{w}_s)$, the optimum $\mathbf{w}_S^{\star}$ is calculated by solving the following equation

$$\text{argmax} \;\; \mathbf{w}_s \sum_{rv=1}^{N}\left[T_{rv}\log\xi_{rv} + (1-T_{rv})\log(1-\xi_{rv})\right] - \frac{1}{2}\mathbf{w}_s{}^T \Delta \mathbf{w}_s. \tag{7-14}$$

where $\xi_{rv} = h(\mathbf{y}_{rv})$ and $\Delta = diag(\alpha_0^{-1}, \alpha_1^{-1}, \ldots \alpha_N^{-1})$. When the RVM classifier is trained, the RVM classifier applies $\mathbf{w}_S^{\star}$ to Eqn. (7-9). The validation data is separated to the class with which the likelihood of membership is greatest. For multi-class classification with a *U* class Equation (7-13) is extended as

$$f_{T_{rv}|\mathbf{w}_S}(T_{rv}|\mathbf{w}_s) = \prod_{n=1}^{N}\prod_{u=1}^{U}\sigma\{h(\mathbf{y}_{rv_u})\}^{T_{rv_u}}, \tag{7-15}$$

where T_{rv_u} is the indicator variable for case *n* to be a member of class *U* and $h(\mathbf{y}_{rv_u})$ is the predictor for class *U*.

The RVM is trained and validated with the WAR coefficients, which is the integration of DWT and AR. Both DWT and AR model is described in detail in the following sections.

7.2.3. Discrete wavelet transforms (DWT)

The DWT decomposes the given signal into several levels of subcomponents and then reconstruct them into to the original signal to compress the data and reduce the noise (Thuillard 2001). A continuous WT can be represented as

$$W_{S_1,S_2} = 1/\sqrt{S_1}\int_{-\infty}^{\infty} f(n)\times\psi\times\left(\frac{x-S_2}{S_1}\right)dt, \tag{7-16}$$

where S_1 and S_2 are the scaling factor and translation parameter, respectively, and $f(n)$ is the discrete time signals. The derived DWT is defined as

$$W_{S_1,S_2} = 2^{-\frac{s}{2}}\sum_{S_1}\sum_{S_2} f(n)\psi\left(2^{-S_1}n - S_2\right). \tag{7-17}$$

As a time frequency analysis method, DWT isolates the high frequency components from the original signal. In order to investigate both high and low frequency signals, DWT can be utilized for multi-resolution analysis (MRA). The MRA decomposes the time-series signals obtained from the smart structure into both low and high frequency components at different resolutions (Kim et al. 2013). The scaling function ϕ and the corresponding wavelet ψ are defined as follows

$$\phi_{S_1,S_2} := 2^{-\frac{S_1}{2}}\times\phi\times\left(2^{-S_1}n - S_2\right), \tag{7-18}$$

$$\psi_{S_1,S_2} := 2^{-\frac{S_1}{2}}\times\psi\times\left(2^{-S_1}n - S_2\right). \tag{7-19}$$

The scaling function acts as a low pass filter for filtering the data from high frequencies, while the corresponding wavelet filters the lower frequencies. As a useful tool to filter the data and decompose the time series in terms of time and frequency, DWT is applied to AR model in order to increase the modeling efficiency.

7.2.4. Autoregressive (AR) model

The objective of the AR model is to estimate the behaviour of structural dynamic system by using the obtained responses from the smart structure. In particular, AR model is given by

$$\mathbf{y}_t = \sum_{k_r}^{P} a_{k_r} y_{t-k_r} + \mathbf{e}_t, \tag{7-20}$$

where *P* presents the maximum order of the AR model and e_t is a noise source or prediction-error term. The term y_{t-k_r} is defined as candidate vector and can be arranged as the matrix shown below

$$\begin{bmatrix} \mathbf{y}(0) & \mathbf{y}(-1) & \mathbf{y}(-2) & \cdots & \mathbf{y}(1-P) \\ \mathbf{y}(1) & \mathbf{y}(0) & \mathbf{y}(-1) & \cdots & \mathbf{y}(2-P) \\ \vdots & \vdots & \vdots & \cdots & \vdots \\ \mathbf{y}(t-1) & \mathbf{y}(t-2) & \mathbf{y}(t-3) & \cdots & \mathbf{y}(t-P) \\ \vdots & \vdots & \vdots & \cdots & \vdots \\ \mathbf{y}(N-1) & \mathbf{y}(N-1) & \mathbf{y}(N-1) & \cdots & \mathbf{y}(N-P) \end{bmatrix} \tag{7-21}$$

where *N* is described as the number of the data points. In the estimation of the a_{k_r} coefficient, least-squares analysis is performed

$$\mathbf{y}_t = \boldsymbol{\theta}_l^T \mathbf{H} + \mathbf{e}_t , \tag{7-22}$$

where $\boldsymbol{\theta}_l$ is the coefficient matrix and $\mathbf{H}$ is the vectors.

$$\boldsymbol{\theta}_l^T = \begin{bmatrix} g_0 & g_1 & g_2 & \dots & g_R \end{bmatrix}, \tag{7-23}$$

$$\mathbf{H} = \begin{bmatrix} h_0 & h_1 & h_2 & \dots & h_R \end{bmatrix}, \tag{7-24}$$

where *R* and g_i are the number of selected linearly independent vectors and optimal estimates of the AR model coefficients respectively. In order to minimize the error, e_t, in the least-squares sense, the criterion function is defined as

$$J_N(\boldsymbol{\theta}_l) = \left[\mathbf{y}_t - \boldsymbol{\theta}_l^T \mathbf{H}\right]^2. \tag{7-25}$$

Minimization of the criterion function with respect to $\boldsymbol{\theta}_g$ is as

$$\hat{\boldsymbol{\theta}}_l = \left[\mathbf{H}\mathbf{H}^T\right]^{-1}\mathbf{H}\mathbf{y}_t \,. \tag{7-26}$$

From the obtained coefficients, $\left|\overline{g_m^2 h_m^2}\right|$ is calculated and the h_m is rearranged in descending order. In order to reduce the error significantly, the number of the candidate vectors, h_m, needs to be optimized. This iterative approach is just applicable only when the h_m reduces the error significantly. For example, if h_m that is added in the least square framework results in a negligible decrease or increase in the error, it is removed from the model. As previously mentioned, DWT is integrated with the AR model to enhance the efficiency of AR modeling. It is observed that the new WAR model requires less CPU time and is effective to reducing the amount of data noise.

7.2.5. Wavelet-based AR model (WAR)

In the classification process of the RVM, WAR models are used. As discussed in previous sections, the DWT is an effective tool to decompose time series into subseries in terms of time and frequency. Thus, it increases the efficiency of the time-series modeling, by integrating DWT with the AR model. The WAR can be derived by modifying the Equation (7-20) as

$$\hat{\mathbf{y}}_t = \sum_{k_r=0}^{P} a_{k_r} W^1_{S_1,S_2,t-k_r} + \mathbf{e}_t \,. \tag{7-27}$$

The WAR model uses level 2 wavelet-filtered signals. The WAR coefficients are transformed into a set of poles to perform structural damage detection of smart structures.

7.2.6. Pole location identification

Using Z-transform, the WAR coefficients can be transformed into a set of poles (Nair et al. 2006).

$$W_z = \sum_{L=0}^{P} a_L z^{-L} W_z + \sum_{L=0}^{P} b_L z^{-L} X_z \,, \tag{7-28}$$

where W_z is Z-transforms of response output y_t, X_z is the prediction-error term, and P and L represent the maximum AR and MA model orders, respectively. The transfer function of an ARMA model is as follows

$$G_z = \frac{W_z}{X_z} = \frac{b_0 + b_1 z^{-1} + b_2 z^{-2} + b_3 z^{-3} + \ldots + b_L z^{-L}}{1 - a_1 z^{-1} - a_2 z^{-2} - a_3 z^{-3} + \ldots - a_p z^{-p}}. \quad (7\text{-}29)$$

The denominator of the transfer function G_z is a characteristic equation of order P. By solving the root of the denominator, the system poles can be obtained as

$$\left[z^p - a_1 z^{-1} - a_2 z^{-2} - a_3 z^{-3} + \ldots - a_p \right] = 0. \quad (7\text{-}30)$$

When a structure has changes on the properties of structural systems, they can be quantitatively measured by the migration patterns of the transfer function poles (Nair et al. 2006). To this end, a damage-sensitive feature (DSF) is proposed to capture the changes of the AR coefficients obtained from an undamaged to damaged structural systems.

7.2.7. Damage-sensitive feature extraction

In the discrimination between healthy and damaged structures, a new DSF is used. In particular, DSF is extracted by normalizing the WAR coefficients. In this study the DSF is obtained by normalizing the WAR coefficients using a pseudo energy expression with velocity responses. Thus, the proposed DSF is determined as follows

$$DSF = \frac{\sum_{q}^{P} \frac{1}{2} m \left| V_q^E \right|^2}{\max\left\{ \sum_{q}^{P} \frac{1}{2} m \left| V_q^E \right|^2 \right\}}, \quad (7\text{-}31)$$

where m and V_q^E are the structural mass and the q^{th} WAR coefficient obtained from the velocity responses, respectively. It was demonstrated that it is difficult to construct the accurate DSF using only the first few WAR coefficients (Nair et al. 2006; Kim et al. 2013). Hence, in this

study, a total of 95 DSF are extracted from 95 WAR coefficients for different scenarios including healthy smart structure and smart structures with 5%, 10%, 15%, 30%, 50% damages. To demonstrate the effectiveness of the proposed multiclass nonlinear relevance vector machine (MNRVM), status of the measured data is classified into the healthy and damaged ones (5%, 10%, 15%, 30% and 50%). It is shown that RVM is effective in classifying various damage statuses of the smart structures using reduced computation load.

7.3. Case study: smart structures

7.3.1. Magnetorheological (MR) damper

In recent years, magnetorheological (MR) dampers have received great attention with the increase of smart structure applications in many engineering fields as shown in Figure 7-2. MR dampers combine the best features of both passive and active control systems (Spencer et al. 1997b; Kim et al. 2009). In particular, MR dampers work as a semi-active system with the application of a magnetic field to the MR fluid. The magnetic field affects the rheological and flow properties of the MR fluid to absorb and dissipate energy effectively. On the other hand, without any current on the system, MR dampers turn to a passive damper. The integration of the MR damper technology with the structure is described in the following section.

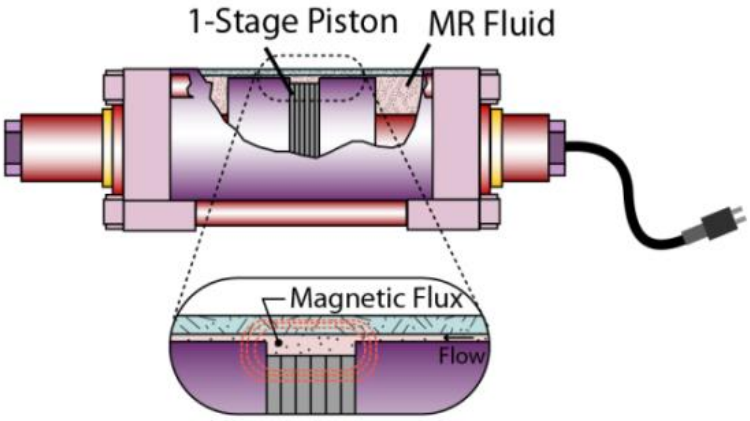

Figure 7-2. Schematic of MR damper

7.3.2. A building equipped with an MR damper

A typical example of an integrated structure-MR damper is shown in Figure 7-3.

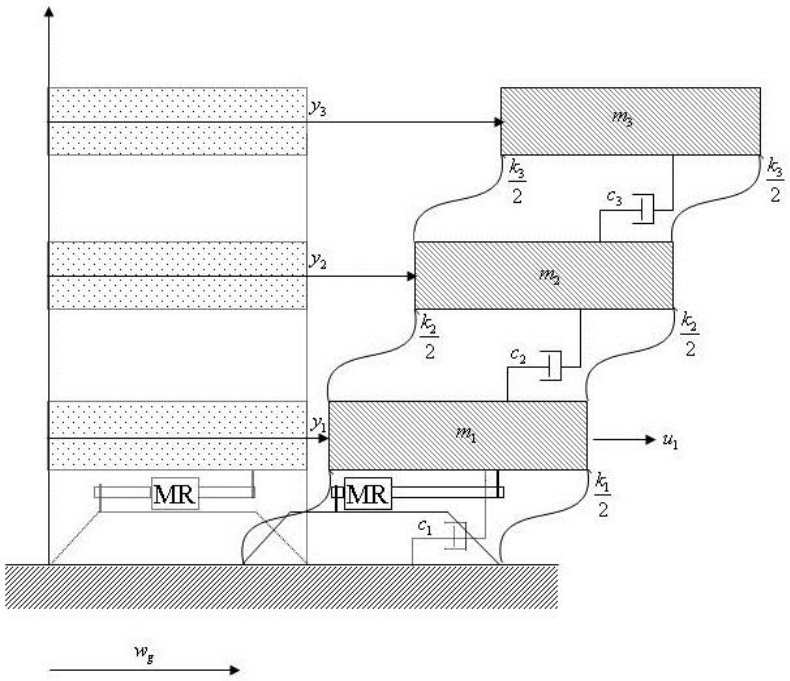

Figure 7-3. Smart building equipped with MR dampers

The equation of motion of the integrated smart structure is

$$M\ddot{y}_s + C\dot{y}_s + Ky_s = \Gamma f_{MR}(ti, y_{si}, \dot{y}_{si}, v_1) - M\Lambda\ddot{w}_g, \tag{7-32}$$

where $\ddot{w}_g$, v_1, Γ and Λ are defined as the earthquake disturbance, voltage level to be applied, location vector of control forces and location vector of disturbance signal at time *ti*, respectively. The system matrices are

$$M = \begin{bmatrix} m_1 & 0 & 0 \\ 0 & m_2 & 0 \\ 0 & 0 & m_3 \end{bmatrix} \tag{7-33}$$

is the mass matrix,

$$C = \begin{bmatrix} c_1 + c_2 & -c_2 & 0 \\ -c_2 & c_2 + c_3 & -c_3 \\ 0 & -c_3 & c_3 \end{bmatrix} \tag{7-34}$$

is the damping matrix,

$$K = \begin{bmatrix} k_1 + k_2 & -k_2 & 0 \\ -k_2 & k_2 + k_3 & -k_3 \\ 0 & -k_3 & k_3 \end{bmatrix} \tag{7-35}$$

is the stiffness matrix, while the MR damper force vector is

$$f_{MR}(ti, y_{si}, \dot{y}_{si}, v_1) = \begin{bmatrix} f_{MR}(ti, y_{si}, \dot{y}_{si}, v_1) \\ 0 \\ 0 \end{bmatrix}, \tag{7-36}$$

where y_{si} is displacement, $\dot{y}_{si}$ is velocity and $\ddot{y}_{si}$ is acceleration at the i^{th} floor level relative to the ground. A conceptual configuration of the integrated building-MR damper system is depicted in Figure 7-4.

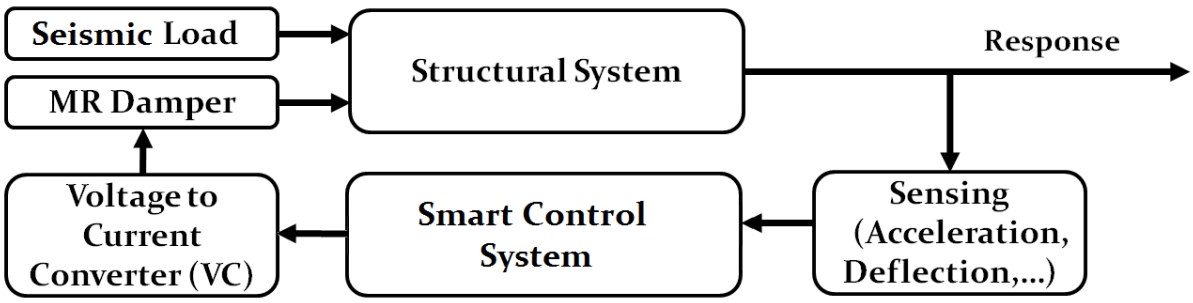

Figure 7-4. Integrated structure-MR damper system

The state-space model can be obtained by converting the second order differential equation as

$$\dot{z}_s = A^* z_s + B^* f_{MR}(ti, z_{s1}, z_{s4}, v_1) - E^* \ddot{w}_g, \tag{7-37}$$

$$ov = C^* z_s + D^* f_{MR}(ti, z_{s1}, z_{s4}, v_1) - no, \tag{7-38}$$

where

$$A^* = \begin{bmatrix} 0 & I \\ -M^{-1}K & -M^{-1}C \end{bmatrix}, \tag{7-39}$$

$$B^* = \begin{bmatrix} 0 \\ -M^{-1}F \end{bmatrix}, \tag{7-40}$$

$$C^* = \begin{bmatrix} I & 0 \\ 0 & I \\ -M^{-1}K & -M^{-1}C \end{bmatrix}, \tag{7-41}$$

$$D^* = \begin{bmatrix} 0 \\ 0 \\ M^{-1}F \end{bmatrix}, \tag{7-42}$$

$$E^* = \begin{bmatrix} 0 \\ F_l \end{bmatrix}, \tag{7-43}$$

where F_l is the location matrix that represents the Chevron braces, while n is the noise vector. The structural properties of a three-story building structure are given in Table 7-1.

Table 7-1. The structural properties of a three-story building structure

Floor	Mass (M)	Damping (C)	Stiffness (K)
1	m_1= 98.3 kg	c_1 = 125 Ns/m	k_1 = 516,000 N/m
2	m_2= 98.3 kg	c_2 = 50 Ns/m	k_2 = 684,000 N/m
3	m_3= 98.3 kg	c_3 = 50 Ns/m	k_3 = 684,000 N/m

The properties of the three story building structure are adopted from a scaled building model (Dyke et al. 1996b) of a prototype building structure that was developed by Chung et al.

(1989). The MR damper is implemented using a modified Bouc-Wen model because it is commonly adopted in the field of large-scale civil structures (Spencer et al. 1997b)
The properties of the SD-1000 MR damper are given as in Table 7-2.

Table 7-2. Parameters for SD-1000 MR damper model

Parameter	Value	Parameter	Value
c_{0a}	21.0 Nscm^{-1}	α_a	140 Ncm^{-1}
c_{0b}	3.50 Nscm^{-1} V^{-1}	α_b	695 Ncm^{-1} V^{-1}
k_0	46.9 Ncm^{-1}	γ	363 cm^{-2}
c_{1a}	283 Nscm^{-1}	β	363 cm^{-2}
c_{1b}	2.95 Nscm^{-1} V^{-1}	A_{MR}	301
k_1	5.00 Ncm^{-1}	N_{MR}	2
x_0	14.3 cm	η	190 s^{-1}

In order to develop the WAR model, a set of dynamic responses are collected from the smart structure model. The damage scenarios are discussed in the following section.

7.3.3. Damage scenario

In the study, damage on the structure is measured in terms of stiffness reduction. The stiffness values on the 1st and 2nd levels are examined under ambient excitations and random voltage signals.

Table 7-3 shows the damage scenarios. The healthy structure is assigned to case 0 and case 6, i.e., Case 0 represents the undamaged situation for the first floor, while Case 6 is the healthy situation for the second floor. The damage measure is related with the percentage in the stiffness reduction. As an example, 10% damage on the 1nd floor level implies the 10% stiffness decrease in the 1st floor.

Table 7-3. Damage scenarios

Damage case	Damage location	Damage severity
0	N/A	N/A
1	1st floor	5%
2		10%
3		15%
4		30%
5		50%
6	N/A	N/A
7	2nd floor	5%
8		10%
9		15%
10		30%
11		50%

7.4. Classification results

To demonstrate the effectiveness of the proposed RVM approach, binary and multi-class classifications are considered in the paper. To quantify the performance, several evaluation indices are used. As a first evaluation index, sensitivity is calculated as

$$J_1 = \frac{TP}{TP + FN} \times 100, \tag{7-44}$$

where *TP* and *FN* represent the true positive and false negative, respectively. Sensitivity parameter is used to measure the proportion of actual positives such as the percentage of healthy data which is truly classified as healthy. Second evaluation index is defined as the specificity

$$J_2 = \frac{TN}{TN + FP} \times 100, \tag{7-45}$$

where *TN* is the true negative and *FP* is false positive. Specificity measures the proportion of negative such as the percentage of healthy data which are correctly classified as not damaged. Third evaluation index is accuracy

$$J_3 = \frac{(TP + TN)}{(TP + FN + TN + FP)} \times 100. \quad (7\text{-}46)$$

Numbers of the used support and relevance vectors are defined as the fourth evaluation index.

J_4= Number of vectors. (7-47)

The last evaluation index J_5 is assigned as the CPU time to evaluate the duration of the training time.

J_5=CPU time. (7-48)

Following sections evaluates the performances of binary and multi-class classification of SVM and RVM. It is seen that RVM classifies the status of the structure accurately with significantly reduced load of computation compared to SVM model.

7.4.1. Two-class classification

In binary classification, the measured data is classified into either healthy or damaged status. In order to obtain input data for training and validating the SVM and RVM models, 95 DSF are collected for healthy case and each damaged cases. To train the models, 100 data points are used. First 50 data of the healthy case and first 10 data from each 5%, 10%, 15%, 30% and 50% damaged statuses are used for training. Then, the models are validated by using 270 data points, which are different form the training data. The models are evaluated by using the last 45data of the healthy case and last 45 data of the 5%, 10%, 15%, 30% and 50% damaged statuses. In other words, models are trained with 100 data points (50 for healthy case, 50 for damaged case) and then validated with 270 data (45 for healthy case, 225 for damaged case). Figure 7-5 and Figure 7-6 represent the training results while Figure 7-7 and Figure 7-8 show the validation of binary SVM and RVM classifications for different floor levels.

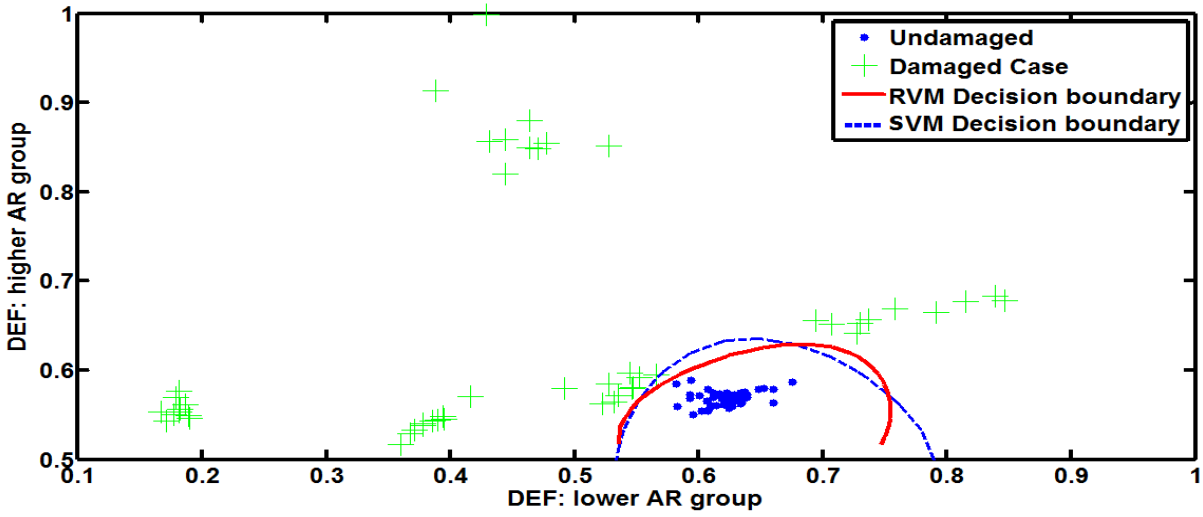

Figure 7-5. Training of RVM and SVM: case 0 through case 5

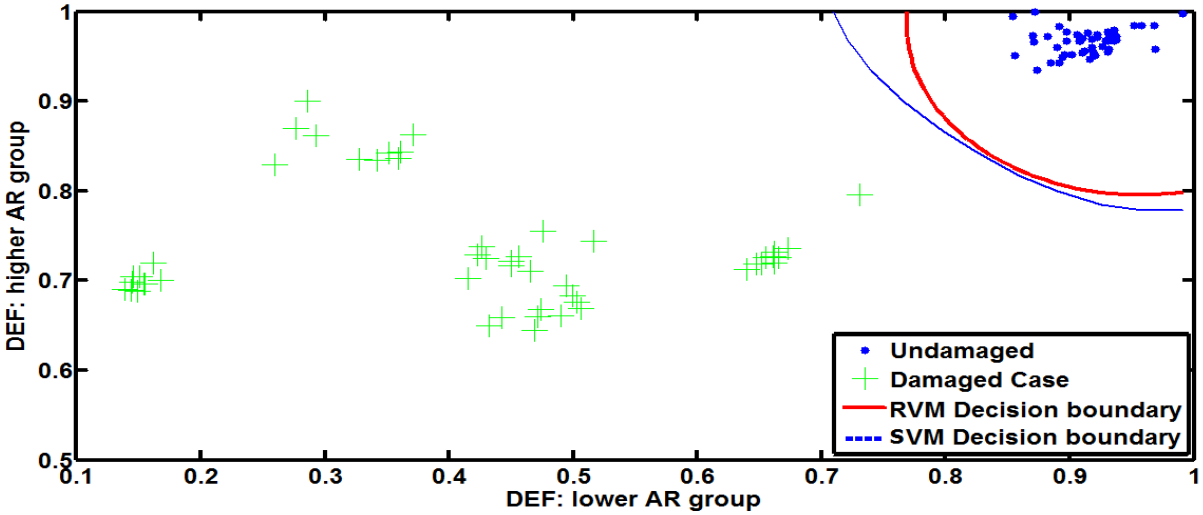

Figure 7-6. Training of RVM and SVM: case 6 through case 10

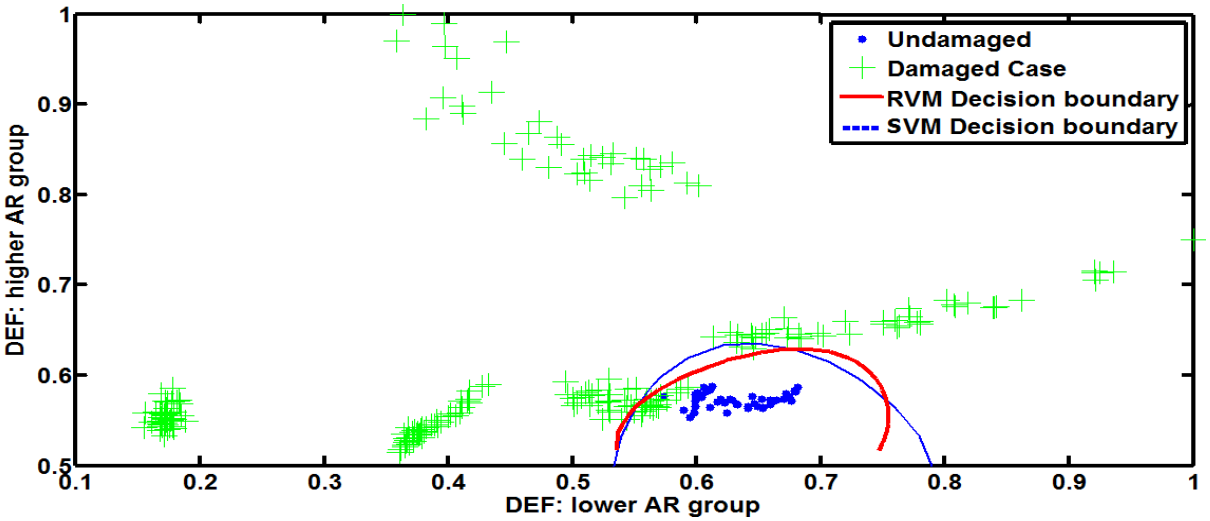

Figure 7-7. Validation of RVM and SVM binary classifications: case 0 through case 5

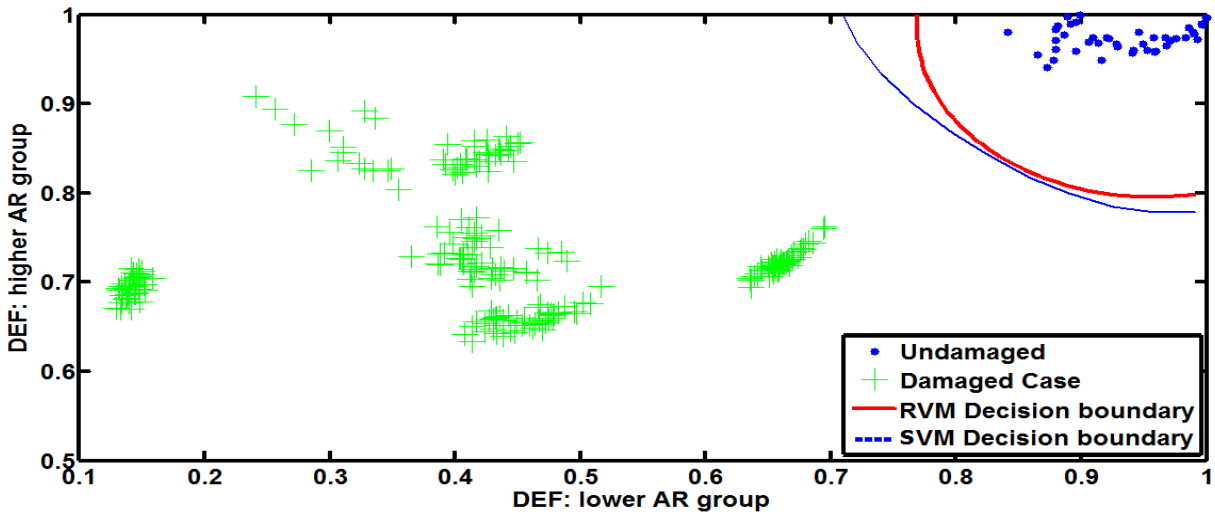

Figure 7-8. Validation of RVM and SVM binary classifications: case 6 through case 10

Table 7-4 compares SVM and RVM binary classifications in term of aforementioned evaluation indexes.

Table 7-4. Evaluation indexes of SVM and RVM binary classification

			*J*1 (%)	*J*2 (%)	*J*3 (%)	*J*4	*J*5 (sec.)
SVM	1st Floor	Healthy	70.42	100.00	92.36	0	3.08
		Damaged	100.00	70.42		26	
	2nd Floor	Healthy	100.00	100.00	100.00	0	2.37
		Damaged	100.00	100.00		9	
RVM	1st Floor	Healthy	72.46	100.00	93.10	1	1.53
		Damaged	100.00	72.46		2	
	2nd Floor	Healthy	100.00	100.00	100.00	3	1.21
		Damaged	100.00	100.00		0	

It is observed that both SVM and RVM are effective in the classification of the data into healthy and damaged statuses. However, when the two frameworks are compared in terms of the number of required vectors, the number of required vectors of RVM is much less than that of SVM.

7.4.2. Multi-class classification

In the training of the multi-class classification, the same training set, which is used in the binary classifications, is used. The measured data is classified into the healthy and damaged (5%, 10%,

15%, 30% and 50%). Models are evaluated by 270 data points (45 for healthy and 45 for each 5%, 10%, 15%, 30% and 50% damaged cases). Figure 7-9 to Figure 7-12 represent the training and validation results of SVM.

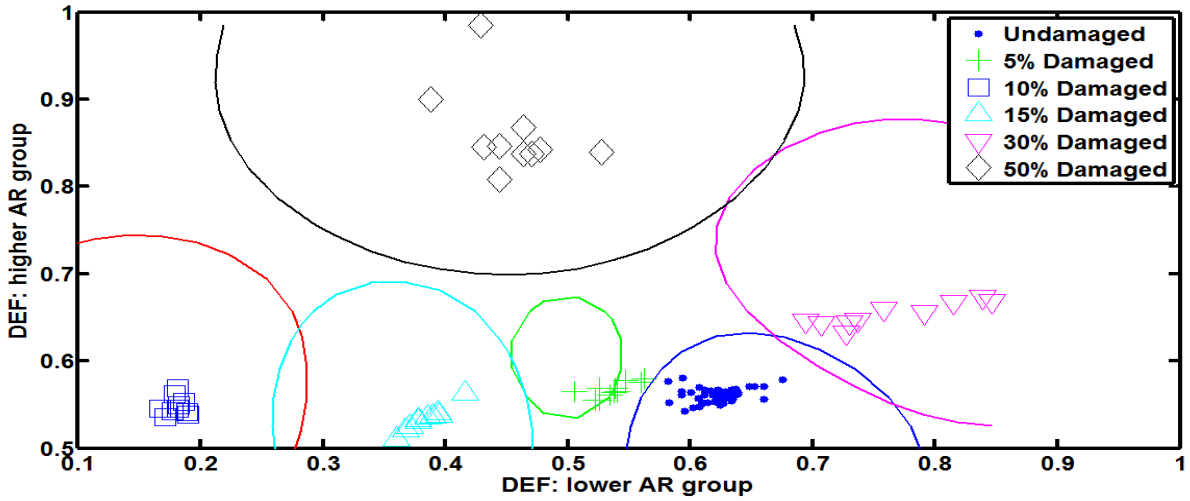

Figure 7-9. Training of SVM multi-class classification: case 0 through case 5

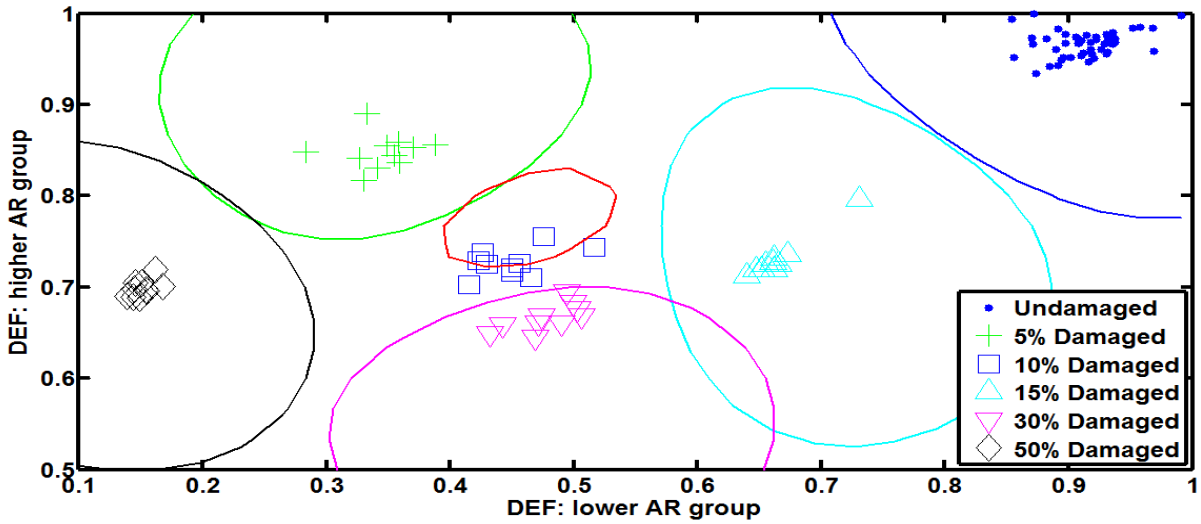

Figure 7-10. Training of SVM multi-class classification: case 6 through case 10

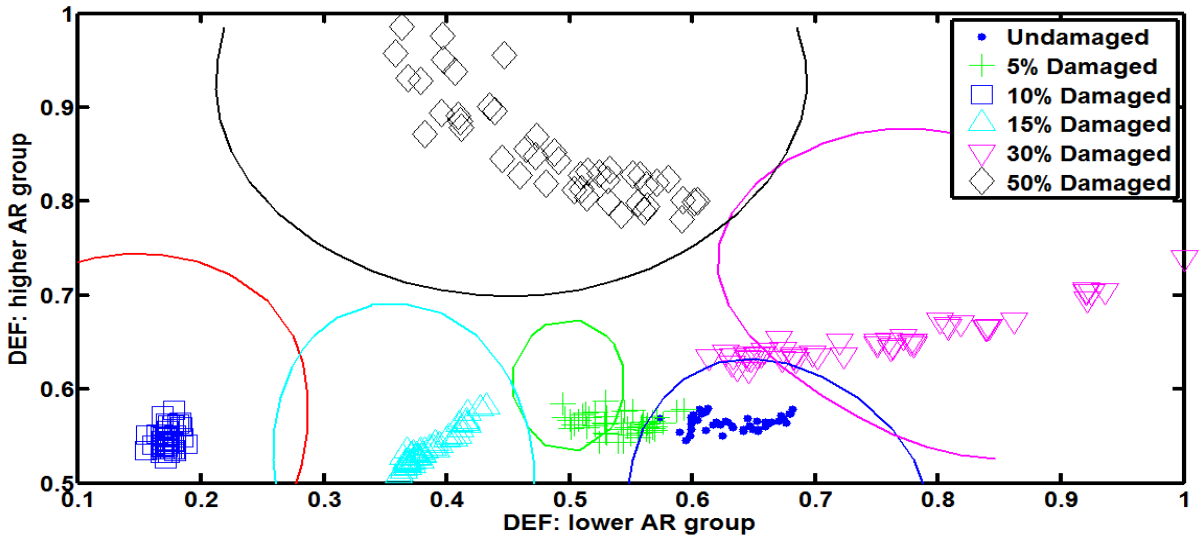

Figure 7-11. Validation of SVM multi-class classification: case 0 through case 5

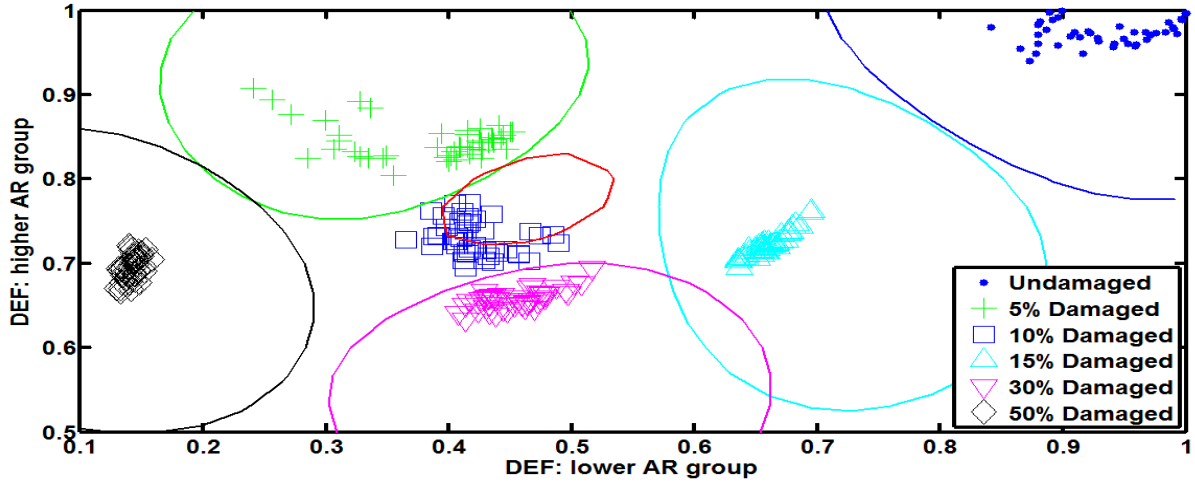

Figure 7-12. Validation of SVM multi-class classification: case 6 through case 10

Figure 7-13 to Figure 7-16 show the results of RVM classification.

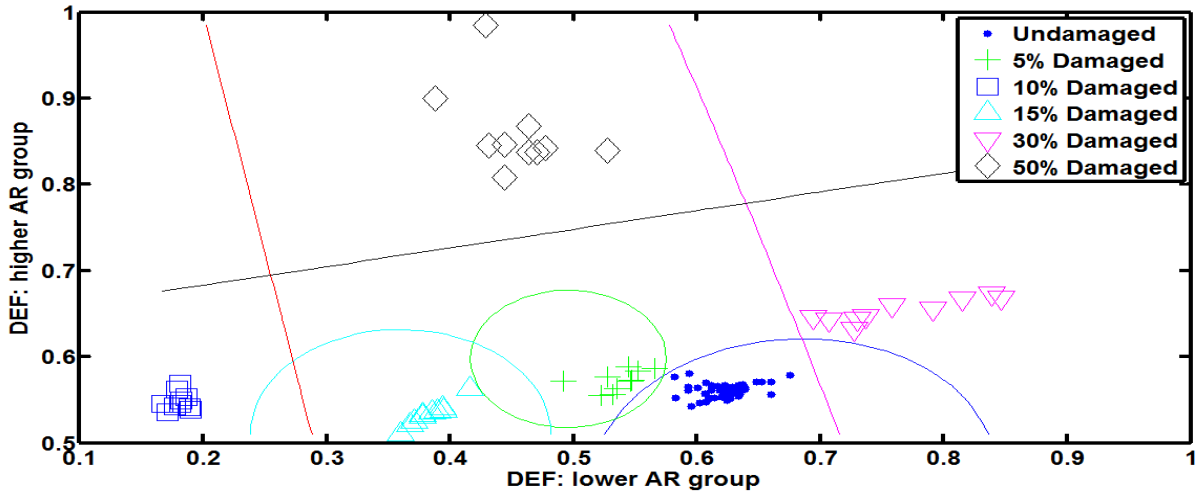

Figure 7-13. Training of RVM multi-class classification: case 0 through case 5

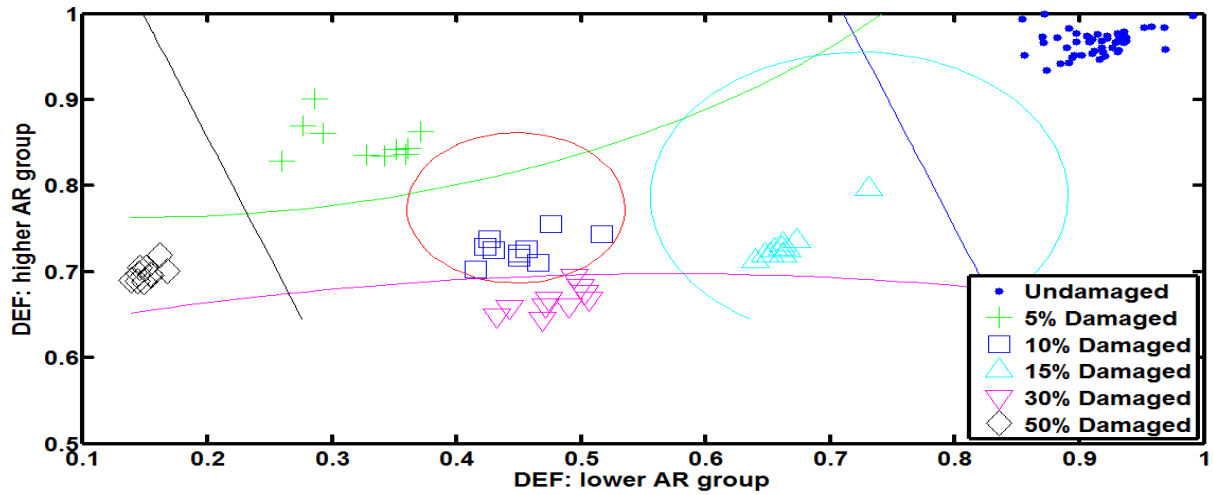

Figure 7-14. Training of RVM multi-class classification: case 6 through case 10

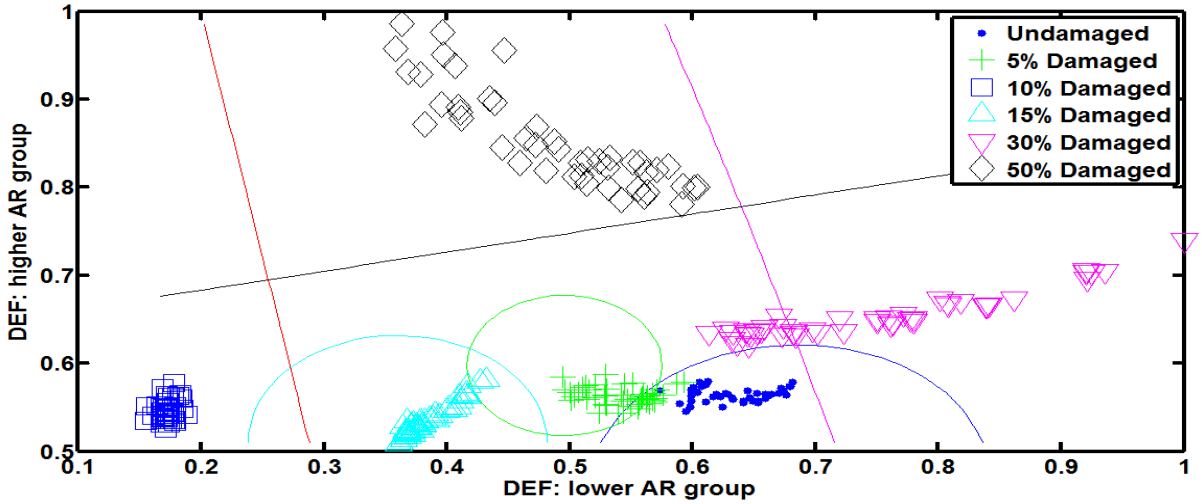

Figure 7-15. Validation of RVM multi-class classification: case 0 through case 5

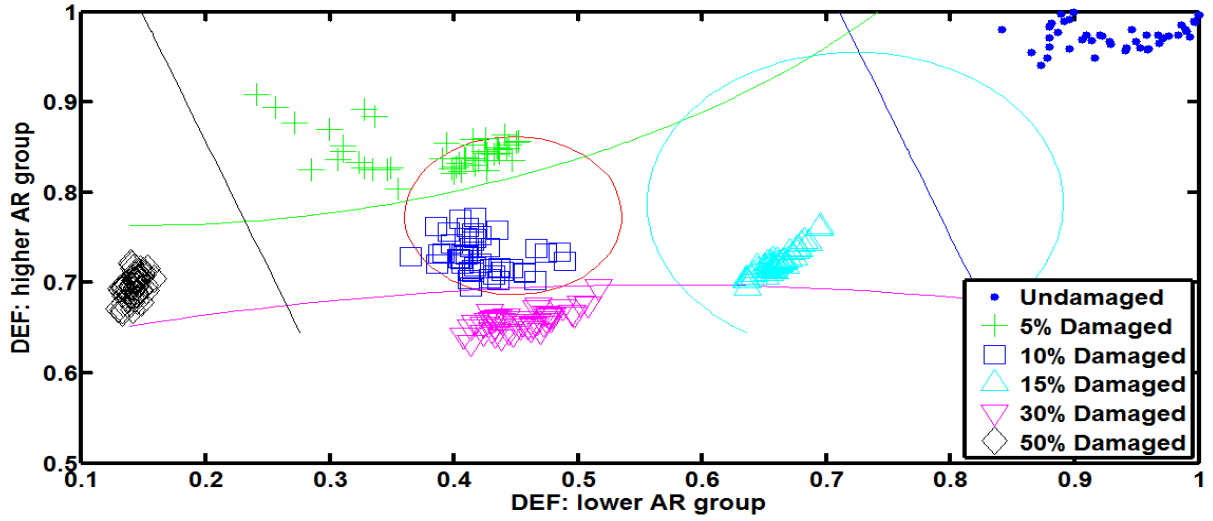

Figure 7-16. Validation of RVM multi-class classification: case 6 through case 10

Figure 7-17 depicts the comparison of SVM and RVM in terms of number of vectors used in training, while Figure 7-18 compares the training errors of both approaches. Figure 7-19 shows the number of validation error for each damaged statuses.

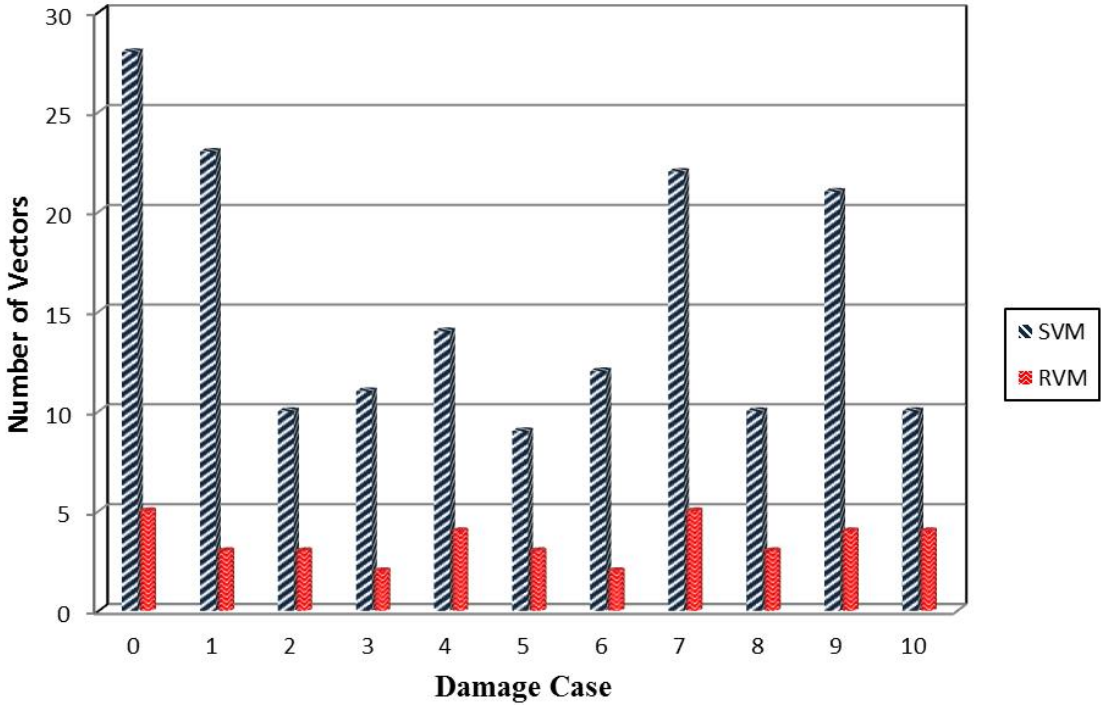

Figure 7-17. Comparison of number of support and relevance vectors for each damage statuses

Figure 7-18. Comparison of training errors vectors for each damage statuses

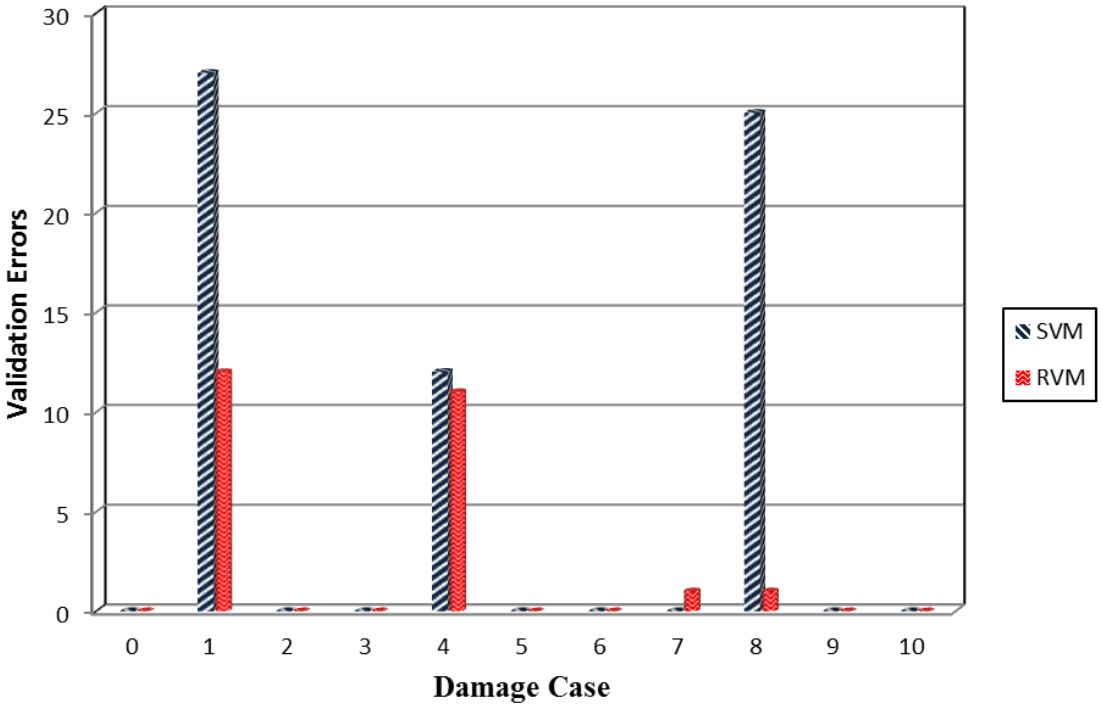

Figure 7-19. Comparison of validation errors vectors for each damage statuses

Table 7-5 evaluates the multi-class classification of SVM and RVM.

Table 7-5. Evaluation of SVM and RVM multi-class classification

	Damage Case	J_1 (%)	J_2 (%)	J_3 (%)	J_4	J_5 (sec.)
SVM	0	100.00	92.89	94.07	28	23.09
	1	37.78	100.00	89.63	23	
	2	100.00	100.00	100.00	10	
	3	100.00	100.00	100.00	11	
	4	73.33	100.00	95.56	14	
	5	100.00	100.00	100.00	9	
	6	100.00	100.00	100.00	28	
	7	100.00	100.00	100.00	12	
	8	44.44	100.00	90.74	22	8.48
	9	100.00	100.00	100.00	10	
	10	100.00	100.00	100.00	21	
	11	100.00	100.00	100.00	10	
RVM	0	100.00	91.56	92.96	5	5.59
	1	82.22	99.11	96.30	3	
	2	100.00	100.00	100.00	3	
	3	100.00	100.00	100.00	2	
	4	66.67	100.00	94.44	4	
	5	100.00	100.00	100.00	3	
	6	100.00	100.00	100.00	5	
	7	100.00	100.00	100.00	2	
	8	97.78	88.89	90.37	5	4.83
	9	100.00	100.00	100.00	3	
	10	100.00	99.56	99.63	4	
	11	100.00	100.00	100.00	4	

It is observed from the simulations that both RVM and SVM models effectively classify most damage cases, except 5% damage scenario (SVM Case 1), 30% damage scenario (SVM Case 4, RVM Case 4) in the 1st floor level and 10% damage (SVM Case 8) in the 2nd floor level. As previously discussed, five indices are used to evaluate the simulation results. To calculate J_1, J_2 and J_3, four statistical parameters TP, TN, FP, FN are used. TP, TN, FP and FN define the correctly identified, incorrectly identified, correctly rejected and incorrectly rejected data,

respectively. As an example, in the Case 1 (5% damage) of the first floor level, the SVM system correctly classified 17 of 45 data points as the 5% damaged case (i.e. TP=17), which gives sensitivity of 37.78%. The remaining 28 data is classified as "Not 5% damaged" (i.e. FN=28). None of the "Not 5% damaged" data set (i.e. healthy, 10%, 15%, 30% and 50% damaged data) is classfied as the 5% damaged case (i.e. FP=0). In other words, all the data on the "Not 5% damaged" are correctly classified (i.e. TN=225), which gives specificity of 100%.

The first evalaution index, sensitiviy (J_1), demonstrates the performance on damage detection of the monitoring scheme . The small value in J_1 represents the poor damage detection. For both SVM and RVM models, the J_1 is 100 for almost all damage cases, which means both models are very effective in damage classification of the smart structures under ambient excitations. However, the RVM model has higher values of J_1 than the SVM for the 5% damage case in the 1st floor level and 10% damage in the 2nd floor level.

Specifity (J_2) index shows the ability of the monitoring schemes to identify the TN. For instance, for the 2nd floor-Case 8 (10% damage), 44 data are correctly classified as the 10% damaged class (TP=44, FN=1), while 200 data are truly classified as "not 10% damaged case" (TN=200, FP=25) using the RVM, and thus J_2 value becomes 88.89%. On the other hand, the main data set (10% damaged) is correctly classified by 97.78%.

When both sensitivity and specificity are simultanously considered (i.e., J_3), the accuracy of both SVM and RVM models is over 90%. Note that although the J_1 has a small value, the J_3 can be high values for some damage cases. This can be explained by the number of data points of TN. In the calculation of J_3, the TN value becomes dominant due to its large number of data points.

It is observed that the proposed RVM scheme outperforms over the SVM approach using less decision vectors (i.e. reduced computation). For example, in the validation of the multi-class RVM model, the total required vector (J_4) that creates the decision boundaries for the first floor is 20, which is 16% of the SVM model. It is also noted that the computation performance of the RVM is better than the SVM. With this in mind, the RVM approach can be considered as the better model for classifying damages of the smart structures under ambient excitations in this paper due to the similar J_2, J_3 but better J_1, J_4 and J_5 values.

7.5. Conclusion

This paper presents the application of the relevance vector machine (RVM) framework to the damage classification of smart buildings equipped with magnetorheological (MR) dampers.

Responses of the smart structure under ambient excitations are measured and used as input data sets. Using discrete wavelet transform (DWT), the input data are filtered and then estimated by autoregressive (AR) models. Finally, the RVM is applied to the AR coefficient data to classify them with respect to the damage statuses. It is aimed to classify the data into undamaged structure and damaged structure with 5%, 10%, 15%, 30%, and 50%.

In the study, the support vector machine (SVM) is selected as a baseline. Both binary and multi-class classification performance of the SVM frameworks is compared with the one of the proposed RVM. Sensitivity, specificity, accuracy, and number of vectors used for training and computation time of the framework are used as the evaluation indexes. It is demonstrated that RVM is very effective in classifying various levels of damage status. It is also shown that the training process of RVM is shorter than SVM. In near future, the authors intend to test the performance of the proposed health monitoring scheme using a more complicated numerical example.

8. Summary

8.1. Summary and concluding remarks

This dissertation proposes usage of smart control technology to mitigate impact hazard on structures. In this context, novel algorithms are developed for identification, control and monitoring of smart structures under high impact forces. Focus is first laid on the identification of smart structures equipped with magnetorheological (MR) dampers subjected to high impact forces. The aim is to develop mathematical models to predict the structural responses for different collision scenarios. As a benchmark model, a traditional adaptive neuro fuzzy inference system (ANFIS) is used due to its effectiveness to solve the ill-defined systems. To train the ANFIS model, high impact loads and current signals are used as input while the acceleration and deflection responses are used as output signals. The results demonstrated that although the ANFIS model is effective in the system identification (SI) of seismically excited building-MR damper systems (Mitchell et al., 2012), it is not effective to identify the features of high frequency impact loads. In order to preserve the dynamics of time series and increase sensitivity for high frequency signals, a time-delay framework is employed in ANFIS model. The proposed time-delayed adaptive neuro-fuzzy inference system (TANFIS) combines aspects of fuzzy logic theory and neural networks. It uses the outputs of the previous steps to predict the features of the following output. The additional time-delayed input data, which involves the important features of the output data, increases the sensitivity of the SI model. Same input-output data set is used in the training of the proposed TANFIS model. It is demonstrated that the TANFIS model is able to adequately and efficiently model the nonlinear behavior of the integrated structure-MR damper systems under high impact loads. Although the TANFIS model is robust against uncertainties and high frequency signals, a second study is performed to reduce the computation time.

With this in mind, the wavelet transform is integrated to the previously developed TANFIS model. The objective of the wavelet transform is to extract the important features of the input data by filtering and compressing it. To obtain the necessary input-output data set to train the proposed W-TANFIS model, a simply supported reinforced concrete beam structure is investigated. W-TANFIS gave the fitting rate almost 100%, which means that the model is accurate in estimating the dynamic responses of the smart reinforced concrete structures under impact loading. When the ANFIS, TANFIS, and W-TANFIS models are evaluated in terms of

computation time, it is observed that W-TANFIS is much better than the ANFIS and TANFIS. For the W-TANFIS models, the computation time is almost 70 and 27 times smaller than the ones of ANFIS and TANFIS models, respectively. As a conclusion, the proposed SI models are effective to understand and predict how the smart concrete structure will act under various impact loads. Based on the identified models, a smart control algorithm is designed to optimize the current level of MR dampers for the dissipation of the structural impact energy.

A fuzzy logic control algorithm is developed to improve the impact performance of control system used on high-rise buildings and highway bridge structures. A simply supported reinforced concrete beam equipped with MR damper is tested under different impact loads and different current levels. Obtained data is used in the training of the fuzzy logic controller. Acceleration, deflection, and strain responses are used as input to predict the optimized current signal. Analytical studies demonstrated the proposed fuzzy controller is effective to mitigate all three responses for high impact cases. A second study is performed to validate the effectiveness of the fuzzy logic controller through experimentally. An equivalent single cantilever beam structure is designed, which has the same stiffness of the full-scale bridge pier, and then subjected to impact forces from a variety of drop release heights. In the training of the fuzzy controller, acceleration response is used to optimize the current signal. Then the specimen is tested under various impact loads, and the effectiveness of the fuzzy controller is obtained in real time. Experimental studies showed that, for high impact load cases, the proposed fuzzy controller reduced the uncontrolled acceleration and deflection responses of a reinforced concrete bridge pier by about 76% and 58%, respectively. It is also seen that the fuzzy controller outperforms the benchmark PID and passive controllers.

In the last study, a relevance vector machine (RVM) framework is presented for the damage classification of smart buildings equipped with MR dampers. As a benchmark model, a support vector machine (SVM) framework is used. Stiffness values of a three-story smart structure equipped with MR damper are examined under random excitations and random voltage signals. The models are trained to classify the data into undamaged structure and damaged structure with 5%, 10%, 15%, 30%, and 50%. Both binary and multi-class classification performance of the SVM frameworks is compared with the one of the proposed RVM. It is seen that SVM requires a large number of data set in the development of the decision boundaries, which increases the computation time and computational complexity. The proposed RVM scheme outperforms the SVM approach using less decision vectors (i.e. reduced computation). For example, in the validation of the multi-class RVM model, the total required vector to create

the decision boundaries for the first floor is 84% less than the SVM model. It is also noted that the computational performance of the RVM is better than the SVM.

As a conclusion, it has been demonstrated from the analytical and experimental study that: 1) the proposed system identification model is accurate and fast to understand and predict how the smart concrete structure will act under various impact loads, 2) the proposed fuzzy logic controller is effective in mitigating high impact responses of the smart structures, 3) the developed structural health monitoring algorithm has low computational complexity and it is effective in identifying damage in time-varying nonlinear dynamic systems under ambient excitations.

8.2. Future research

It is recommended that the proposed smart control framework be applied to seismic or wind-excited structures equipped with MR dampers. When compared with the high frequency impact loads, seismic or wind-excited smart structures have lower frequency (USGS, 2014), lower computational complexity, and less statistical variance. It is predicted that the proposed time-delay based system identification and control models, which uses the important features of the output as an input, would be effective for less complex systems. In near future, the authors intend to test the performance of the proposed smart control framework on seismically excited smart structures.

Further research is recommended to apply the proposed smart control framework into large-scale structures employing MR dampers. In addition, it is recommended to improve the proposed structural health monitoring system for identifying the location of the damage.

9. References

Adeli H. and Jiang X. 2006 "Dynamic Fuzzy Wavelet Neural Network Model for Structural System Identification."*Journal of Structural Engineering*, 132:102-111.

Ahlawat A.S. and Ramaswamy A. 2000 "Multi-Objective Optimal Design of FLC Driven Hybrid Mass Damper for Seismically Excited Structures." *Earthquake Engineering & Structural Dynamics*, 31:1459–1479.

Ahlawat A.S. and Ramaswamy, A. 2002 "Multiobjective Optimal FLC Driven Hybrid Mass Damper System for Torsionally Coupled, Seismically Excited Structures." *Earthquake Engineering & Structural Dynamics*, 31:2121–2139.

Ahlawat A.S. and Ramaswamy A. 2004 "Multiobjective Optimal Fuzzy Logic Control System for Response Control of Wind-Excited Tall Buildings." *Journal of Engineering Mechanics (ASCE)*, 130:524–530.

Ahmadian M. and Norris J.A. 2008 "Experimental Analysis of Magneto Rheological Dampers when Subjected to Impact and Shock Loading." *Communications in Nonlinear Science and Numerical Simulation*, 13:1978-1985.

Al-Dawod M., Samali B., Naghdy F. and Kwok K.C.S. 2001 "Active Control of Along Wind Response of Tall Building Using A Fuzzy Controller." *Engineering Structures*, 23:1512–1522.

Al-Dawod M., Samali B., Naghdy F. and Kwok K.C.S. 2004 "Fuzzy Controller for Seismically Excited Nonlinear Buildings." *Journal of Engineering Mechanics (ASCE)*, 130:407–415.

Alhanafy T.E. 2007 "A Systematic Algorithm to Construct Neuro-fuzzy Inference System." *16th International Conference on Software Engineering and Data Engineering*, 1:137-142.

Alli H. and Yakut O. 2005 "Fuzzy Sliding-Mode Control of Structures." *Engineering Structures*, 27:277–284.

Allison S.H. and Chase J.G. 1994 "Identification of Structural System Parameters Using the Cascade-Correlation Neural Network." *Journal of Dynamic Systems, Measurement, and Control,* 116:790-792.

American Association of State Highway and Transportation Officials (2012). *AASHTO LRFD Bridge Design Specifications: Customary U.S. Units 2012.* Washington D.C.

Arsava K.S., Kim Y. and El-Korchi T. 2013a "Nonlinear System Identification of Smart Structures under High Impact Loads." *Journal of Smart Materials and Structures,* Paper ID: 055008.

Arsava K.S., Kim Y. and El-Korchi T. 2013b "Nonlinear System Identification of Smart Reinforced Concrete Structures under İmpact Loads" *Journal of Vibration and Control,* In Press.

Arsava K.S. and Kim Y. 2014a "Modeling of Magnetorheological Dampers under Various Impact Loads." *Smart Materials and Structures,* In Review.

Arsava K.S. and Kim Y. 2014b "Smart Fuzzy Control for Impact Response Mitigation of Reinforced Concrete Structures." *Smart Materials and Structures,* In Review.

Arsava K.S. and Kim Y. 2014c "Smart Control of Reinforced Concrete Bridge Piers under a Variety of Impact Loads." In Preparation.

Arsava K.S., Chong J.W. and Kim Y. 2014d "A Novel Health Monitoring Scheme for Smart Structures." *Journal of Vibration and Control,* 1-19:DOI: 10.1177/1077546314533716.

Arslan A. and Kaya M. 2001 "Determination of Fuzzy Logic Membership Functions Using Genetic Algorithms." *Fuzzy Sets and Systems,* 118:297-306.

Aware M.V., Kqthari A.G. and Choube S.O. 2000 "Application of Adaptive Neuro-Fuzzy Controller (ANFIS) For Voltage Source Inverter Fed Induction Motor Drive." *Power Electronics and Motion Control Conference,* Beijing, China, 935-939.

Aydin A.C., Tortum A. and Yavuz A. 2006 "Prediction of Concrete Elastic Modulus Using Adaptive Neuro-Fuzzy Inference System." *Civil Engineering and Environmental System*, 23:295-309.

Bani-Hani K., Ghaboussi J. and Schneider S.P. 1999 "Experimental Study of Identification and Control of Structures using Neural Network Part 1: Identification." *Earthquake Engineering and Structural Dynamics*, 28:995-1018.

Balasubramaniam V., Raghunath P.N. and Suguna K. 2012 "An Adaptive Neuro-Fuzzy Inference System Based Modeling for Corrosion-Damaged Reinforced HSC Beams Strengthened with External Glass Fibre Reinforced Polymer Laminates." *Journal of Computer Science*, 8:879-890.

Battaini M., Casciati F. and Faravelli L. 1998 "Fuzzy Control of Structural Vibration. An Active Mass System Driven by a Fuzzy Controller." *Earthquake Engineering & Structural Dynamics*, 27:1267–1276.

Battaini M., Casciati F. and Faravelli L. 2004 "Controlling Wind Response through a Fuzzy Controller." *Journal of Engineering Mechanics (ASCE)*, 130:486–491.

Bulut A., Singh A.K., Shin P, Fountain T., Jasso H., Yan L, and Elgamal A. 2005 "Real-time Nondestructive Structural Health Monitoring Using Support Vector Machines and Wavelets." *Proceeding of SPIE*, 5770: 180-189.

Burges C.J.C. 1998 "A Tutorial on Support Vector Machines for Pattern Recognition." *Data Mining and Knowledge Discovery*, 2: 121-167.

Carlson J.D. 2005. "MR Fluids and Devices in the Real World." *International Journal of Modern Physics B*, 19:1463-1470.

Casciati F., Faravelli L. and Yao T. 1994 "Application of Fuzzy Logic to Achieve Structural Control." *Proceedings of the Second European Conference on Smart Strucutres and Materials*, San Antonio, TX, USA, 206-209.

Casciati F. 1997 “Checking the Stability of A Fuzzy Controller for Nonlinear Structures.” *Microcomputers in Civil Engineering*, 12:205–215.

Choi K.M., Cho S.W., Jung H.J. and Lee I.W. 2004 “Semi-Active Fuzzy Control for Seismic Response Reduction using Magneto-rheological Dampers.” *Earthquake Engineering & Structural Dynamics*, 33:723-736.

Chung L.L., Lin R.C., Soong T.T. and Reinhorn A.M. 1989 “Experiments on Active Control for MDOF Seismic Structures.” *ASCE Journal of Engineering Mechanics*, 115: 1609-1627.

Consolazio G.R., Cook R.A. and McVay M.C. 2006 “Barge Impact Testing of The St. George Island Causeway Bridge Phase III: Physical Testing and Data Interpretation.” *Structures Research Report, Department of Civil and Coastal Engineering,* University of Florida.

Consolazio G.R., and McVay M.C. 2008 “Development of Improved Bridge Design Provisions for Barge Impact Loading.” *Structures Research Report, Department of Civil and Coastal Engineering,* University of Florida.

Consolazio G.R., Davidson M.T. and Getter D.J. 2010 “Vessel Crushing and Structural Collapse Relationships for Bridge Design.” *Structures Research Report, Department of Civil and Coastal Engineering,* University of Florida, USA, Aug 2010.

Das A.K. and Dey S.S. 1992. “Effects of Tuned Mass Dampers on Random Response of Bridges.” *Computers and Structures*, 43:745-750.

Dominguez A., Sedaghati R. and Stiharu I. 2004 “Modeling the Hysteresis Phenomenon of Magnetorheological Dampers.” *Smart Materials and Structures*, 13:1351–61.

Dominguez A., Sedaghati R. and Stiharu I. 2006 “A New Dynamic Hysteresis Model for Magnetorheological Dampers.” *Smart Materials and Structures*, 15:1179-1189

Dounis A.I., Tiropanis P., Syrcos G.P. and Tseles D. 2007 “Evolutionary Fuzzy Logic Control of Base-Isolated Structures in Response to Earthquake Activity.” *Structural Control and Health* Monitoring, 14:62–82.

Driankov D., Hellendoorn H. and Reinfrank M. 1993 "An Introduction to Fuzzy Control." *Published by Springer*, Heidelberg, Berlin.

Duan Y.F., Ni Y.Q., Ko J.M. and Chen Z.Q. 2003. "Amplitude-Dependent Frequency and Damping Identification of Bridge Cables with MR Shock Absorbers in Different Setups." *Smart Structures and Materials 2003: Smart Systems and Nondestructive Evaluation for Civil Infrastructures*, 5057:218-228.

Dyke S.J. and Spencer B.F.Jr. 1996a "Seismic Response Control Using Multiple MR Dampers." *Proceedings of the 2nd International Workshop on Structural Control*, Hong Kong, China, 163-173.

Dyke S.J., Spencer B.F.Jr., Sain M.K. and Carlson J.D. 1996b "Modeling and Control of Magnetorheological Dampers for Seismic Response Reduction." *Smart Materials and Structures*, 5:565-575.

Dyke S.J., Spencer B.F.Jr., Sain M.K. and Carlson J.D. 1996c "Experimental Verification of Semi-Active Structural Control Strategies Using Acceleration Feedback." *3rd International Conference on Motion and Vibration Control*, Chiba, Japan, 291-296.

Dyke S.J. and Spencer B.F.Jr. 1997 "A Comparison of Semi-Active Control Strategies for the MR Damper." *International Conference on Intelligent Information Systems*, Grand Bahama Island, Bahamas, 580-584.

Dyke S.J., Spencer B.F.Jr., Sain M.K. and Carlson J.D. 1998 "An Experimental Study of MR Dampers for Seismic Protection." *Smart Materials and Structures*, 7:693-703.

Dyke S.J., Yi F., Caicedo J.M. and Carlson J.D. 2001 "Experimental Verification of Multinput Seismic Control Strategies for Smart Dampers." *ASCE Journal of Engineering Mechanics*, 127:1152-1164.

Faravelli L. and Yao T. 1996 "Use Of Adaptive Networks in Fuzzy Control of Civil Structures." *Microcomputers in Civil Engineering*, 11:67–76.

Faravelli L. and Rossi R. 2002 "Adaptive Fuzzy Control: Theory Versus Implementation." *Journal of Structural Control*, 9:59–73.

Farrar C.R. and Worden K. 2007 "An Introduction to Structural Health Monitoring." *Philosophical Transactions of the Royal Society*, 365: 303-315.

Figueiredo E., Park G., Farinholt K.M., Farrar C.R. and Lee J. 2012 "Use of Time-Series Predictive Models for Piezoelectric Active-Sensing in Structural Health Monitoring Applications." *Journal of Vibration and Acoustics*, 134: 1-10.

Filev D.P. 1991 "Fuzzy Modeling of Complex Systems." *International Journal of Approximate Reasoning*, 5:281-290.

Fonseca E.T., Vellasco P.C.G.S., Vellasco M.M.B.R. and Andrade S.A.L. 2008 "A Neuro-Fuzzy Evaluation of Steel Beams Patch Load Behavior." *Advances in Engineering Software*, 39:558-572.

Foody G.M. 2008 "RVM-based Multi-class Classification of Remotely Sensed Data." *International Journal of Remote Sensing*, 29: 1817-1823.

Gencoglu M. and Mobasher B. 2007 "Static and Impact Behavior of Fabric Reinforced Cement Composites in Flexure." *High Performance Fiber Reinforced Cement Composites - HPFRCC 5*, Mainz, Germany 53:463-470.

Graczykowski C. and Holnicki-Szulc J. 2009 "Protecting Offshore Wind Turbines Against Ship Impacts By Means Of Adaptive Inflatable Structures." *Shock and Vibration*, 16: 335-353.

Graczykowski C., Sekuła K. and Holnicki-Szulc J. 2011 "Real-Time Identification of Impact Load Parameters." *Proceedings of the 5th ECCOMAS Thematic Conference on Smart Structures and Materials*, 544-551.

Gopalakrishnan K. and Khaitan S.K. 2010 "Finite Element Based Adaptive Neuro-Fuzzy Inference Technique for Parameter Identification of Multi-Layered Transportation Structures." *Transport*, 25:58-65.

Gu Z.Q. and Oyadiji O. 2008 "Application of MR Damper in Structural Control Using ANFIS Method." *Computers and Structures*, 86:427–436.

Guo L. and Li X. 2009 "Rolling Bearing Fault Classification Based On Envelope Spectrum And Support Vector Machine." *Journal of Vibration and Control*, 15: 1349-1363.

Hengbo X., Qin F., Ziming G. and Hao W. 2008 "Experimental Investigation into Magnetorheological Damper Subjected to Impact Loads." *Transactions of Tianjin University*, 14:540-544.

Holnicki-Szulc J., Graczykowski C., Mikulowski G., Mróz A. and Pawłwski P. 2009 "Smart Technologies for Adaptive Impact Absorption." *Solid State Phenomena*, 154:187-194.

Hongsheng H. and Suxiang Q. 2009 "Performance Simulation and Experimental Evaluation for a Magnet-rheological Damper under Impact Load." *Proceedings of the 2008 IEEE International Conference on Robotics and Biomimetics*, Bangkok, Thailand, 1538-1543.

Hou J., Jiang W. and Lu W. 2011 "Application of a Near-Field Acoustic Holography-Based Diagnosis Technique in Gearbox Fault Diagnosis." *Journal of Vibration and Control*, 19: 3-13.

Hu H., Jiang X., Wang J. and Li Y. 2012. "Design, Modeling, and Controlling of a Large-Scale Magnetorheological Shock Absorber under High Impact Load." *Journal of Intelligent Material Systems and Structures*, 23:635-645.

Huang Y., Beck J.L., Li H., and Wu S. 2011 "Robust Diagnostics for Bayesian Compressive Sensing with Applications to Structural Health Monitoring." *SPIE Smart Structures and Materials + Nondestructive Evaluation and Health Monitoring*, 7982: 79820J-1 - 79820J-9.

Hung S.L., Huang C.S., Wen C.M. and Hsu Y.C. 2003 "Nonparametric Identification of a Building Structure from Experimental Data using Wavelet Neural Network." *Computer-Aided Civil and Infrastructure Engineering*, 18:356-368.

Hurlebaus S. and Gaul L. 2006 "Smart Structure Dynamics." *Mechanical Systems and Signal Processing*, 20:255-281.

Jang J.S.R. 1993 "ANFIS: Adaptive-Network-Based Fuzzy Inference System." *IEEE Transactions on Systems, Man, and Cybernetics*, 23:665-685.

Jang J.S.R. and Gulley N. 1994 "Gain Scheduling Based on Fuzzy Controlled Design." *Industrial Fuzzy Control and Intelligent Systems Conference, and the NASA Joint Technology Workshop on Neural Networks and Fuzzy Logic*, San Antonio, TX, USA, 101-105.

Jansen L.M. and Dyke S.J. 2000. "Semiactive Control Strategies for MR Dampers: Comparative Study." *Journal of Engineering Mechanics*, 126:795-803.

Jung H.J., Choi K.M., Spencer B.F.Jr. and Lee I.W. 2006 "Application of some Semi-Active Control Algorithms to a Smart Base-Isolated Building Employing MR Dampers." *Structural Control and Health Monitoring*, 13:693–704.

Kerber F., Hurlebaus S., Beadle B.M. and Stobener U. 2007 "Control Concepts for an Active Vibration Isolation System." *Mechanical Systems and Signal Processing*, 21:3042– 3059.

Keskar A.G. and Asanare K. L. 1997 "Floating Membership Fuzzy Controller for Adaptive Control of AC Drive." *IEEE Conf. lSIE'97*, Guimaraes, Portugal, 1216-1221.

Kim H.S. and Roschke P.N. 2006 "Design of Fuzzy Logic Controller for Smart Base Isolation System Using Genetic Algorithm." *Engineering Structures*, 28:84–96.

Kim S. and Clark W.W. 1999 "Fuzzy Logic Semi-Active Vibration Control." *Adaptive Structures and Material Systems*, 59:367-372.

Kim Y. and Langari R. 2007 "Nonlinear Identification and Control of A Building Structure with A Magnetorheological Damper System." *American Control Conference*, New York-NY, USA, 3353 - 3358.

Kim Y., Langari R. and Hurlebaus S. 2009 "Semiactive Nonlinear Control of a Building with a Magnetorheological Damper System." *Mechanical Systems and Signal Processing*, 23: 300-315.

Kim Y., Langari R. and Hurlebaus S. 2010 "Control of Seismically Exited Benchmark Building using Linear Matrix Inequality-based Semiactive Nonlinear Fuzzy Control." *ASCE Journal of Structural Engineering*, 136:1023-1026.

Kim Y., Langari R. and Hurlebaus S. 2011 "MIMO Fuzzy Identification of Building-MR Damper System." *International Journal of Intelligent and Fuzzy Systems*, 22:185-205.

Kim Y., Chong J.W., Chon K.H., Kim J.M. 2013 "Wavelet-Based AR-SVM for Health Monitoring of Smart Structures." *Journal of Smart Materials and Structures*, 22: 1-12.

Lee D.Y., Choi Y.T. and Wereley N.M. 2002 "Performance Analysis of ER/MR Impact Damper Systems using Herschel-Bulkley Model." *Journal of Intelligent Material Systems and Structures*, 13:4525–4531.

Li F., Li-ping L. and Xin-he X. 2012 "Research on Modeling and Fuzzy Control of Magneto-Rheological Intelligent Buffer System for Impact Load." *Journal of Shanghai Jiaotong University*, 17:567-572.

Lin C-T. and Lee C.S.G. 1991 "Neural-Network-Based Fuzzy Logic Control and Decision System." *IEEE Transactions on Computers*, 40:1320-1336.

Lin J.W., Betti R., Smyth A.W. and Longman R.W. 2001 "On-line Identification of Non-linear Hysteretic Structural Systems using a Variable Trace Approach." *Earthquake Engineering and Structural Dynamics*, 30:1279-1303.

Lin J.W. and Betti R. 2004 "On-line Identification and Damage Detection in Non-linear Structural Systems using a Variable Forgetting Facto Approach." *Earthquake Engineering and Structural Dynamics*, 33:419-444.

Liu Y., Gordaninejad F., Evrensel C.A. and Hitchcock G. 2001 "An Experimental Study on Fuzzy Logic Vibration Control of a Bridge Using Fail-Safe Magneto-Rheological Fluid Dampers." *Smart Structures and Materials - Smart Systems for Bridges, Structures, and Highways*, Newport Beach, CA, USA, 281-288.

Liu B. and Chen J. 2011. "Control System Design of Magneto-rheoloical Damper under High-Impact Load." *Modern Applied Science*, 5:253-258.

Loh C.H., Wu L.Y. and Lin P.Y. 2003 "Displacement Control of Isolated Structures with Semi-Active Control Devices." *Journal of Structural Control*, 10:77–100.

Luca S-G., Chira F. and Rosca V-O. 2005 "Passive, Active and Semi-Active Control Systems in Civil Engineering." *Bulletin of the Polytechnic Institute of Jassy, Constructions, Architecture Section*, 3:23-31.

Lynch P.J. 2002 "Decentralization of Wireless Monitoring and Control Technologies for Smart Civil Structures." *A Dissertation Submitted to the Department of Civil and Environmental Engineering and the Committee on Graduate Studies of Stanford University*, Stanford-CA, USA.

Maeda M., Sato T. and Murakami S. 1990 "Design of the Self-Tuning Fuzzy Controller." *International Conference on Fuzzy Logic & Neural Networks*, Iizuka, Japan, 393-396.

Mahesh P. 2009 "Kernel Methods in Remote Sensing: A Review." *ISH Journal of Hydraulic Engineering*, 15: 194-215.

Mao M., Hu W., Wereley N.M., Browne A.L. and Ulicny J. 2007 "Shock Load Mitigation Using Magnetorheological Energy Absorber with Bifold Valves." *Proceedings of SPIE*, 6527:652710.1-652710.12.

Martin M.T. and Doyle J.F. 1996 "Impact Force Identification from Wave Propagation Responses." *International Journal of Impact Engineering* 18:65–77.

Masri S.F., Smyth A.W., Chassiakos A.G., Caughey T.K. and Hunter N.F. 2000 "Application of Neural Networks for Detection of Changes in Nonlinear Systems." *ASCE Journal of Engineering Mechanics,* 126:666-676.

Mikułowski G. and Holnicki-Szulc J. 2007 "Adaptive Landing Gear Concept - Feedback Control Validation." *Smart Materials and Structures,* 16:2146-2158.

Mita A. and Hagiwara H. 2003 "Damage Diagnosis of a Building Structure Using Support Vector Machine and Modal Frequency Patterns." *The International Society for Optical Engineering,* 5057: 118-125.

Mitchell R., Kim Y. and El-Korchi T. 2012 "System Identification of Smart Structures using Wavelet Neuro-Fuzzy Model." *Journal of Smart Materials and Structures,* Paper ID: 115009.

Mohammadnejad M., Gholami R., Ramezanzadeh A. and Jalali M.E. 2011 "Prediction of Blast-Induced Vibrations in Limestone Quarries Using Support Vector Machine." *Journal of Vibration and Control,* 18: 1322-1329.

Muzzammil M. 2010 "ANFIS Approach to the Scour Depth Prediction at A Bridge Abutment." *Journal of Hydroinformatics,* 12:474-485.

Na U.J., Park T.W., Feng M.Q. and Chung L. 2009 "Neuro-Fuzzy Application for Concrete Strength Prediction Using Combined Non-Destructive Tests." *Magazine of Concrete Research,* 64:245-256.

Nair K.K., Kiremidjian A.S. and Law K.H. 2006 "Time Series-based Damage Detection and Localization Algorithm with Application to the ASCE Benchmark Structure." *Journal of Sound and Vibration,* 291: 349-368.

Nestorović T. and Trajkov M. 2010 "Active Control of Smart Structures–An Overall Approach." *Facta Universitatis Series: Architecture and Civil Engineering,* 8:35-44.

Nguyen T.V., Chong J.W., and Shin H. 2012 “Indoor Localization with Relevance Vector Machine.” In Review.

Ni Y.Q., Liu H.J. and Ko J.M. 2002 “Experimental Investigation on Seismic Response Control of Adjacent Buildings Using Semi-Active MR Dampers.” *Smart Systems and Materials - Smart Systems for Bridges, Structures, and Highways*, San Diego, CA, USA, June 2002, 334-344.

Nomura Y., Furuta H. and Hirokane M. 2007 “An Integrated Fuzzy Control System for Structural Vibration.” *Computer-Aided Civil and Infrastructure Engineering*, 22:306–316.

Oh C.K. and Sohn H. 2009 “Damage Diagnosis under Environmental and Operational Variations Using Unsupervised Support Vector Machine.” *Journal of Sound and Vibration*, 325: 224-239.

Ostrowski M., Griskevicius P. and Holnicki-Szulc J. 2007 “Pyro-Adaptive Impact Energy Absorber.” *Journal of Kones,* 14:303-309.

Ozbulut O.E. and Hurlebaus S. 2010 “Neuro-fuzzy modeling of temperature- and strain-rate-dependent behavior of NiTi shape memory alloys for seismic applications.” *Journal of Intelligent Materials and Structures*, 21, 837-849.

Park K.S., Koh H.M. and Seo C.W. 2003 “Independent Modal Space Fuzzy Control of Earthquake-Excited Structures.” *Engineering Structures*, 26:279–289.

Park S., Yun C.B., Roh Y. and Lee J.J. 2006 “PZT-Based Active Damage Detection Techniques for Steel Bridge Components.” *Journal of Smart Materials and Structures*, 15: 957-966.

Patten W.N., Sack R.L. and He Q. 1996. “Controlled Semiactive Hydraulic Vibration Absorber for Bridge.” *Journal of Structural Engineering*, 122:187-192.

Pourzeynali S., Lavasani H.H. and Modarayi A.H. 2007 “Active Control of High Rise Building Structures Using Fuzzy Logic and Genetic Algorithms.” *Engineering Structures*, 29:346–357.

Ravindrarajah S.R. and Lyte M.C. 2008 "Energy Absorbing Concrete for Impact Loading. " *Proceedings of the Int. Conf. on Advances in Concrete Construction*, India, Hyderabad.

Schurter K.C. and Roschke P.N. 2000 "Fuzzy Modeling of a Magnetorheological Dampers Using ANFIS." *The Ninth IEEE International Conference on Fuzzy Systems*, San Antonio-TX, USA, 1:122-127.

Scruggs J. 1999 "Active, Regenerative Control of Civil Structures." *A Master of Science Thesis Submitted to the Department of Electrical and Computer Engineering of Faculty of the Virginia Polytechnic Institute and State University*, Blacksburg-VA, USA.

Scruggs J. and Lindner D.K. 1999 "Active Energy Control in Civil Structures." *Smart Structures and Materials: Smart Systems for Bridges, Structures, and Highways*, Newport Beach-CA, USA, 3671:194-205.

Sekuła K., Graczykowski C. and Holnicki-Szulc J. 2013 "On-Line Impact Load Identification." *Journal of Shock and Vibration*, 20:123-141.

Sharma H., Hurlebaus S., and Gardoni P. 2008 "Development of a Bridge Bumper to Protect Bridge Girders from Overheight Vehicle Impact." *Computer-Aided Civil and Infrastructure Engineering*, 23: 415-426.

Sharma H., Hurlebaus S., and Gardoni P. 2012 "Performance-based Response Evaluation of Reinforced Concrete Columns subject to Vehicle Impact." *International Journal of Impact Engineering*, 43: 52-62.

Shelley S.J., Lee K.L., Aksel T. and Aktan A.E. 1995. "Active-control and Forced-vibration Studies of Highway Bridge." *Journal of Structural Engineering*, 121:1306-1313.

Shimada M. and Mita A. 2005 "Damage Assessment of Bending Structures Using Support Vector Machine." *Proceeding of SPIE*, 5765: 923-930.

Shook D.A., Roschke P.N., Lin P.Y. and Loh C.H. 2008 "GA-Optimized Fuzzy Logic Control of A Large-Scale Building for Seismic Loads." *Engineering Structures*, 30:436–449.

Spencer B.F.Jr. and Soong T.T. 1997a "New Applications and Development of Active, Semi-Active and Hybrid Control Techniques for Seismic and Non-Seismic Vibration in the USA." *Proceedings of International Post-SMiRT Conference Seminar on Seismic Isolation, Passive Energy Dissipation and Active Control of Vibration of Structures*, Cheju, Korea.

Spencer B.F.Jr., Dyke S.J., Sain M.K. and Carlson J.D. 1997b "Phenomenological Model for Magnetorheological Dampers." *ASCE Journal of Engineering Mechanics*, 123: 230-238.

Spencer B.F.Jr. and Nagarajaiah S. 2003 "State of the Art of Structural Control." *ASCE Journal of Structural Engineering*, 129:845-856.

Subramaniam R.S., Reinhorn A.M., Riley M.A. and Nagarajaiah S. 1996 "Hybrid Control of Structures Using Fuzzy Logic." *Microcomputers in Civil Engineering*, 11:1–17.

Suresh K., Deb S.K. and Dutta A. 2008 "Parametric System Identification of Multistoreyed Buildings with Non-uniform Mass and Stiffness Distribution." *Proceedings of 14th WCEE*, Beijing, China, Paper ID: 05-01-0053.

Symans M. and Kelly S.W. 1999 "Fuzzy Logic Control of Bridge Structures Using Intelligent Semi-Active Seismic Isolation Systems." *Earthquake Engineering & Structural Dynamics*, 28:37–60.

Tahmasebi P. and Hezarkhani A. 2010 "Application of Adaptive Neuro-Fuzzy Inference System for Grade Estimation; Case Study, Sarcheshmeh Porphyry Copper Deposit, Kerman, Iran." *Australian Journal of Basic and Applied Sciences*, 4:408-420.

Tani A., Kawamura H. and Ryu S. 1998 "Intelligent Fuzzy Optimal Control of Building Structures." *Engineering Structures*, 20:184–192.

Tesfamariam S. and Najjaran H. 2007 "Adaptive Network–Fuzzy Inferencing to Estimate Concrete Strength Using Mix Design." *Journal of Materials in Civil Engineering*, 19:7 550-560.

Thuillard M. 2001 "Wavelets in Soft Computing." *World Scientific Series in Robotics and Intelligent Systems*, World Scientific Publishers.

Tipping E.M. 2001 "Sparse Bayesian Learning and the Relevance Vector Machine." *Journal of Machine Learning Research*, 1: 211-244.

United States Geological Survey, http://www.usgs.gov/, accessed 5/25/2014

Vines-Cavanaugh D., Cao Y. and Wang M.L. 2010 "Support Vector Machine for Abnormality Detection on a Cable-Stayed Bridge." *Proceeding of SPIE*, 7647: 1-11.

Wang, A.P. and Lee, C.D. 2002. "Fuzzy Sliding Mode Control for A Building Structure Based on Genetic Algorithms", *Earthquake Engineering & Structural Dynamics*, 31:881–895.

Wang J. and Li Y. 2006 "Dynamic Simulation and Test Verification of MR Shock Absorber under Impact Load." *Journal of Intelligent Material Systems and Structures*, 17:309-314.

Wang H. and Hu H. 2009 "The Neuro-Fuzzy Identification of MR Damper." *Sixth International Conference on Fuzzy Systems and Knowledge Discovery*, 6:464-468.

Wang H. 2009 "Modeling of Magnetorheological Damper Using Neuro-Fuzzy System." *Advances in Intelligent and Soft Computing*, 62:1157-1164.

Wang H. 2010 "Hierarchical ANFIS Identification of Magneto-Rheological Dampers." *Applied Mechanics and Materials*, 29:32:343-348.

Wiklo M. and Holnicki-Szulc J. 2009a "Optimal Design of Adaptive Structures: Part I. Remodeling For Impact Reception." *Structural and Multidisciplinary Optimization*, 37:305–318.

Wiklo M. and Holnicki-Szulc J. 2009b "Optimal Design of Adaptive Structures: Part II. Adaptation to Impact Loads." *Structural and Multidisciplinary Optimization*, 37:351–366.

Wilde K. and Fujino Y. 1993. "Aerodynamic Control of Bridge Deck Flutter by Active Surfaces." *Journal of Engineering Mechanics*, 124:718-727.

Wilson C.M.D. and Abdullah M.M. 2005a "Structural Vibration Reduction Using Fuzzy Control of Magnetorheological Dampers." *ASCE Structures Congress*, New York, USA, April 2005, 1-12.

Wilson C.M.D. and Abdullah M. 2005b "Fuzzy Control of Magnetorheological Dampers in Civil Structures." *6th European Conference on Structural Dynamics*, Paris, France Sep 2005.

Worden K., and Lane A.J. 2001 "Damage Identification Using Support Vector Machines." *Smart Materials and Structures*, 10: 540-547.

Xiang-min X., Yun-feng M., Jia-ni X., and Feng-le Z. 2007 "Classification Performance Comparison between RVM and SVM." In: *IEEE International Workshop on Anti-counterfeiting, Security, Identification*, Xiamen, Fujian, China, 208-211.

Yan G. and Zhou L.L. 2006 "Integrated Fuzzy Logic and Genetic Algorithms for Multi-Objective Control of Structures Using MR Dampers." *Journal of Sound and Vibration*, 296:368–382.

Yan G. and Zhou L.L. 2009. "Impact Load Identification of Composite Structure Using Genetic Algorithms." *Journal of Sound and Vibration*, 319:869–884.

Yang G., Spencer B.F., Carlson J.D. and Sain M.K. 2002. "Large-scale MR fluids dampers: modeling and dynamic performance consideration." *Engineering Structures*, 24:309-323.

Yang Y.N. and Lin S. 2004 "On-line Identification of Non-linear Hysteretic Structures using Adaptive Tracking Technique." *International Journal of Non-Linear Mechanics*, 39:1481-1491.

Yi F., Dyke S.J., Frech S. and Carlson J.D. 1998 "Investigation of Magnetorheological Dampers for Earthquake Hazard Mitigation." *Proceedings of the 2nd World Conference on Structural Control*, Kyoto, Japan, June 1998, 349-358.

Yi F., Dyke S.J., Caicedo J.M. and Carlson J.D. 1999 "Seismic Response Control Using Smart Dampers." *Proceedings of the 1999 American Control Conference*, San Diego, CA, USA, 1022-1026.

Ying Z. G., Ni Y. Q. and Ko J. M. 2002 "Non-Clipping Optimal Control of Randomly Excited Nonlinear Systems Using Semi-Active ER/MR Dampers." *Smart Systems and Materials: Smart Systems for Bridges, Structures, and Highways*, San Diego, CA, USA, 209-218.

Zeinali M., Mazlan S.A, Fatah A.Y.A., and Zamzuri H. 2013 "A Phenomenological Dynamic Model of A Magnetorheological Damper Using A Neuro-Fuzzy System." *Journal of Smart Materials and Structures*, Paper ID: 125013.

Zhang J. and Roschke P.N. 1999 "Active Control of a Tall Structure Excited by Wind." *Journal of Wind Engineering and Industrial Aerodynamics*, 83:209-223.

Zhao Y., Collins E.G.Jr., and Dunlap D. 2003 "Design of Genetic Fuzzy Parallel Parking Control Systems." *American Control Conference*, Denver, CO, USA, 4107-4112.

Zhou L. and Chang C.C. 2000 "Adaptive Fuzzy Control for a Structure-MR Damper System." *Smart Structures and Materials: Smart Systems for Bridges, Structures, and Highways*, Newport Beach, CA, USA, 105-115.

Zhou L., Chang C.C. and Wang L.X. 2003 "Adaptive Fuzzy Control for Nonlinear Building–Magnetorheological Damper System." *Journal of Structural Engineering (ASCE)*, 129:905–913.